Pure

Bangor University

DOCTOR OF PHILOSOPHY

Advanced Optical OFDM transceivers for Optical Access Networks

Zheng, Xing

Award date:
2011

Awarding institution:
Bangor University

Link to publication

General rights
Copyright and moral rights for the publications made accessible in the public portal are retained by the authors and/or other copyright owners and it is a condition of accessing publications that users recognise and abide by the legal requirements associated with these rights.

- Users may download and print one copy of any publication from the public portal for the purpose of private study or research.
- You may not further distribute the material or use it for any profit-making activity or commercial gain
- You may freely distribute the URL identifying the publication in the public portal ?

Take down policy
If you believe that this document breaches copyright please contact us providing details, and we will remove access to the work immediately and investigate your claim.

Download date: 10. Jul. 2024

Advanced Optical OFDM Transceivers for Optical Access Networks

Xing Zheng

PRIFYSGOL
BANGOR
UNIVERSITY

A thesis submitted for the degree of
Doctor of Philosophy

School of Electronic Engineering
Bangor University

February 2011

LLYFRGELL PRIFYSGOL BANGOR UNIVERSITY LIBRARY

Abstract

Intensity Modulation and Direct Detection (IMDD) Optical Orthogonal Frequency Division Multiplexing (OOFDM) is considered as one of the most competitive candidates for high-speed, cost-effective and flexible Next Generation Passive Optical Networks (NG-PONs). For practical implementation of the technique, five technical challenges originating from inherent OFDM properties and/or IMDD system characteristics have to be solved successfully. The challenges include: i) insufficient utilization of Multi-Mode Fibre (MMF) frequency response; ii) improvement in IMDD OOFDM transmission capacity in Single-Mode Fibre (SMF)-based systems; iii) simplification of OOFDM transceiver configurations; iv) the employment of low-cost transceiver components to achieve the desired system performance; v) effective compensation of directly modulated DFB laser (DML)-induced positive frequency chirp. The present PhD dissertation research is dedicated to addressing the aforementioned challenges.

For fully utilizing the system frequency response of a MMF transmission link, an Adaptively Modulated OOFDM (AMOOFDM) modem using Subcarrier Modulation (SCM) (AMOOFDM-SCM) is proposed, which consists of two AMOOFDM modems in parallel with one operating at the baseband and the other being modulated onto an intermediate Radio Frequency (RF) carrier. Extensive investigations show that, compared with AMOOFDM, AMOOFDM-SCM not only enhances the transmission capacity versus reach performance by a factor of approximately 2, but also considerably improves the system flexibility and performance robustness.

When use is made of the AMOOFDM-SCM technique in SMF-based transmission links, the intermixing effect induced by direct detection in the receiver is identified to be a dominant factor limiting the maximum achievable AMOOFDM-SCM performance. To maximize the link performance through mitigating the intermixing effect, three AMOOFDM-SCM modem designs of different complexity levels are proposed by applying Single Sideband (SSB) modulation and/or spectral gapping in AMOOFDM-SCM. It is shown that these AMOOFDM-SCM designs can support >60Gb/s signal transmission over at least 20km, which is >1.5 times higher than that supported by the AMOOFDM modems.

In the above-mentioned three AMOOFDM-SCM modems, two Inverse Fast Fourier Transform (IFFT)/ Fast Fourier Transform (FFT) operations are required in the transmitter/receiver. To reduce the transceiver complexity and system cost, three simplified AMOOFDM-SCM modems are proposed, each of which requires a single IFFT/FFT operation. These designs not only significantly simplify the AMOOFDM-SCM modem configurations but also offer extra network features such as input/output reconfigurability without compromising the transmission performance.

To relax the requirements on parameters of key transceiver components such as Digital-to-Analogue Converters (DACs) and Analogue-to-Digital Converters (ADCs), a reduction in Peak-to-Average Power Ratio (PAPR) associated with an OFDM signal is necessary. To achieve such an objective, AMOOFDM using Phase Modulation (PM) (AMOOFDM-PM) is proposed and explored in IMDD SMF systems. AMOOFDM-PM utilises an electrical OFDM signal to modulate the phase of a RF carrier prior to performing optical intensity modulation. Compared to AMOOFDM, AMOOFDM-PM can considerably reduce the PAPRs of OFDM signals and simultaneously lower the minimum requirements on quantization bits and sampling rates of DACs/ADCs.

To effectively compensate the DML frequency chirp effects, detailed investigations of dynamic negative power penalty characteristics of OOFDM signal transmission are undertaken in DML-based IMDD systems incorporating MetroCor fibres with negative dispersion parameters. Excellent agreement between numerical simulations and real-time experimental measurements is obtained over a wide diversity of system conditions. The physical mechanism underpinning the occurrence of negative power penalties is the reduction in subcarrier intermixing impairments due to the compensation between DML positive frequency chirp and MetroCor negative chromatic dispersion. It is also shown that the negative power penalty is independent of both cyclic prefix and signal modulation format, and, more importantly, controllable when adaptive modulation and/or appropriate adjustments of DML operating conditions are applied.

Finally, for reducing the DML frequency chirp, a simple and effective chirp compensation technique is also proposed, which utilizes an electrical analogue circuit and an optical phase modulator. The electrical analogue circuit produces a phase signal mimicking the original phase of the DML-modulated optical signal, and the optical phase modulator driven by the generated phase signal compensates the DML frequency chirp. In DML-

based IMDD AMOOFDM PON systems, the technique can almost completely alleviate the DML frequency chirp effect and simultaneously improve the transmission capacity by approximately 25% for transmission distances in a range of 30-80km. In addition, the technique is also robust to variations in DML operating conditions.

The results presented in the thesis can provide valuable technical solutions for further improving the OOFDM transmission capacity, performance robustness and system flexibility, as well as simultaneously reducing the transceiver complexity and system cost for cost-sensitive NG-PONs.

Acknowledgements

First of all, I am especially grateful to my supervisor, Dr. Jianming Tang, for his continuous guidance, encouragement and strong support during my PhD research and study at Bangor University in the past years.

My sincere gratitude also extends to Dr. Yanhua Hong for her constructive comments and suggestions on my papers and the thesis, as well as her kind care about my life in Bangor.

I would like to express my sincere thanks to Prof. Kun Qiu in University of Electronic Science and Technology of China who brought me into the field of optical communications and recommended me to study in Bangor University.

I would also like to thank the colleagues I worked with, for constructive suggestions, discussions and encouragement over the last several years. They include Prof. Baojian Wu, Dr. Xianqing Jin, Dr. Jinlong Wei, Dr. Xuelin Yang, Roger P. Giddings, Dr. Emilio Hugues-Salas, Elias Giacoumidis, Muttsam A. Jarajreh, Jakobus Groenewald, Muthusamy Kamalanathan as well as Christian S. Costa who was a visiting PhD student from Spain and his supervisor Beatriz. O. Tamant, both of whom have contributed to the dissertation work described in Chapter 10.

Also, my acknowledgements also extend to other people who have helped me with my work in Bangor University.

Last but not least, I would like to sincerely appreciate my parents who always believe in me well beyond what I deserve from being their son, and always remind me what the word "Home" means.

Abbreviation

ADC	Analogue-to-Digital Converter
ADSL	Asymmetric DSL
AMOOFDM	Adaptively Modulated OOFDM
AMOOFDM-SCM	AMOOFDM modem using SCM
AMOOFDM-PM	AMOOFDM using PM
APON	ATM PON
ATM	Asynchronous Transfer Mode
BER	Bit Error Rate
BL	Bit Loading
BPF	Band-Pass Filter
BPL	Bit-and-Power Loading
BPON	Broadband PON
CO	Central Office
CTF	Channel Transfer Function
CW	Continuous Waveform
DAC	Digital-to-Analogue Converter
DFB	Distributed Feedback
(I)DFT	(Inverse) Discrete Fourier Transform
DMD	Differential Mode Delay
DML	Directly Modulated Laser
DSB	Double Sideband
DQPSK	Differential Quadrature Phase Shift Keying
DSL	Digital Subscriber Line
DSLAM	DSL Access Multiplexer
DSP	Digital Signal Processing
E/O	Electrical-to-Optical
EPON	Ethernet PON

FDM	Frequency Division Multiplexing
FEC	Forward Error Correction
FPGA	Field-Programmable Gate Array
(I)FFT	(Inverse) Fast Fourier Transform
FTTH/B/C	Fiber-To-The-Home/Building/Curb
FWM	Four-Wave Mixing
GPON	Gigabit PON
GVD	Group-Velocity Dispersion
ICI	Inter-Carrier Interference
IMDD	Intensity Modulation and Direct Detection
IPTV	Internet Protocol Television
ISI	Inter-Symbol Interference
LAN	Local Area Network
LD	Laser Diode
LPF	Low-Pass Filter
MAC	Media Access Control
MAN	Metropolitan Area Network
MMF	Multi-Mode Fibre
MZM	Mach-Zehnder Modulator
NG-PON	Next Generation Passive Optical Network
ODN	Optical Distribution Network
O/E	Optical-to-Electrical
OLT	Optical Line Termination
ONU	Optical Network Unit
OFDM	Orthogonal Frequency Division Multiplexing
OOFDM	Optical OFDM
PAPR	Peak-to-Average Power Ratio
PL	Power Loading
PM	Phase Modulation

PMD	Physical Media Dependent
PON	Passive Optical Network
PSK	Phase Shift Keying
QAM	Quadrature Amplitude Modulation
R&D	Research and Development
RF	Radio Frequency
RS	Reconfigurable Scheme
(N)RZ	(Non-) Return to Zero
SBS	Stimulated Brillouin Scattering
SCM	Subcarrier Modulation
SMF	Single-Mode Fibre
SSMF	Standard SMF
SNR	Signal-to-Noise Ratio
SOA	Semiconductor Optical Amplifier
QD-SOA	Quantum Dot SOA
SPM	Self-Phase Modulation
SRS	Stimulated Raman Scattering
SSB	Single Sideband
TDM	Time Division Multiplexing
VDSL2	Very-high-speed DSL 2nd Generation
WDM	Wavelength Division Multiplexing
XPM	Cross-Phase Modulation

Contents

1 Introduction

Over the past several decades, telecommunication technologies and networks have experienced tremendous advances in terms of transmission capacity and network functionality. Today, core networks can provide enormous transmission bandwidth of approximately 100 Pb/s·km [1], existing access networks, however, only support data rates of <60 Mb/s per user over limited transmission distance [2]. Driven by exponentially growing highly bandwidth-hungry services such as high-quality Internet Protocol Television (IPTV) and peer-to-peer multimedia services, access networks are major obstacles to satisfy end-users' needs in the near future. Therefore, exploring advanced technologies capable of addressing the challenges associated with present access networks is one of the hottest research and development topics of today [3-5].

To access various Internet services, the majority of broadband users world-wide currently rely on copper cable-based techniques and/or wireless access techniques. The major disadvantage associated with these available techniques is their limited bandwidth [2]. As optical fibres have almost infinite bandwidth, optical access networks such as Fiber-To-The-Home/Building/Curb (FTTH/B/C) have been considered to be one of the most promising technical strategies for satisfying the ever increasing end-users' bandwidth demands [6,7]. To massively deploy FTTH/B/C in practice, Passive Optical Networks (PONs) have become one of the most attractive solutions, as PONs provide, using cheap components, not only high transmission capacities but also required flexible and scalable operation functions such as dynamic bandwidth allocation [7,8]. The existing PONs can support signal line rates of 2.488Gb/s for downstream and 1.244Gb/s for upstream (ITU-T G.984 Gigabit PON (GPON)) or 1.244Gb/s bidirectional transmission (IEEE 802.3ah Ethernet PON(EPON)) [9,10], which are, however, expected to reach their specified capacity limits within the next three years [3]. Therefore, the IEEE and ITU-T are actively developing Next Generation PONs (NG-PONs) targeting transmission speeds of 10 Gb/s or beyond [3]. In addition to transmission capacity, a number of other crucial issues should also be considered to enable the achievements of the aforementioned targets [3]. These issues include, for example, spectral efficiency, chromatic dispersion tolerance, optical power budget, network complexity and system cost, as well as compatibility with the current deployed PON infrastructures.

In recent years, a large number of novel techniques have been proposed and investigated with an aim of achieving high-speed, cost-effective, flexible and "future-proof" NG-PONs [5,8,11-14]. These techniques include, for example, Wavelength Division Multiplexing (WDM), static WDM/Time Division Multiplexing (TDM) and dynamic WDM/TDM. In particular, Optical Orthogonal Frequency Division Multiplexing (OOFDM), first proposed in 2005 [15], has attracted extensive research and development interest world-wide and is considered as one of the most competitive candidates for practical implementation in NG-PONs. This is because of its inherent and salient advantages including significant cost-effectiveness due to the use of advanced Digital Signal Processing (DSP) technology, excellent resistance to linear system impairments, highly efficient utilization of channel spectral characteristics, relatively high transmission speed, great performance robustness and system flexibility, as well as the capability of supporting hybrid dynamic allocation of broadband services among various end-users in both the frequency and time domains [16-21].

In addition, for NG-PON applications, Intensity Modulation and Direct Detection (IMDD) OOFDM has demonstrated more competitiveness in comparison with other OOFDM techniques such as coherent OOFDM, as IMDD OOFDM can offer a further reduction in both the network complexity and installation and maintenance cost without strongly compromising the transmission performance [14,16,17]. Furthermore, IMDD OOFDM using adaptive Bit Loading (BL), referred to as Adaptively Modulated OOFDM (AMOOFDM) throughout this thesis, has demonstrated significant improvements in transmission performance, system flexibility and performance robustness compared to the IMDD OOFDM technique based on an identical signal modulation format across all subcarriers. In AMOOFDM, for a specific transmission system, through negotiations between the transmitters and the receivers, the maximum transmission performance is always achievable regardless of electrical/optical component imperfections, fibre types, launching conditions and transmission distances [16, 17].

Recently, significant IMDD OOFDM research achievements have been made: in 2009, world-first real-time OOFDM transceivers were experimentally demonstrated, which support end-to-end transmission of 1.5Gb/s Differential Quadrature Phase Shift Keying (DQPSK)-encoded signals over 500m Multi-Mode Fibre (MMF)-based IMDD transmission systems incorporating Directly Modulated Distributed Feedback (DFB)

Lasers (DMLs) [22]. In 2010, the highest ever end-to-end real-time OOFDM transmission of 11.25Gb/s over 25km Single-Mode Fibres (SMFs) was experimentally demonstrated in DML-based IMDD PON systems using low-cost, off-the-shelf electrical/optical components [14]. More recently, in similar systems, end-to-end real-time symbol synchronization of 128 Quadrature Amplitude Modulation (QAM)-encoded OOFDM signals has also been experimentally achieved [20]. These "proof-of-concept" experimental demonstrations have paved a solid path leading to practical implementations of IMDD OOFDM in NG-PON systems.

However, for practical deployment, IMDD OOFDM NG-PONs still have five challenges originating from inherent OFDM properties and/or IMDD system characteristics. These challenges are summarised as follows:

i) Insufficient utilization of frequency response beyond baseband. It is well known [23,24] that the frequency response of an IMDD MMF link consists of two major spectral regions: a steadily decaying narrow baseband region in the vicinity of the optical carrier frequency, as well as a broad and flat passband region at frequencies beyond the baseband. The AMOOFDM technique is capable of utilizing the baseband frequency response property of a MMF-based transmission link; however it is not able to transmit signals over the broad passband frequency response region. This drawback considerably limits its maximum achievable transmission capacity in IMDD MMF systems. Therefore, to further improve the OOFDM transmission performance, innovative technical solutions should be explored by making full use of the link frequency response.

ii) Significant improvement in SMF-based IMDD OOFDM system transmission capacity by Subcarrier Modulation (SCM). Unlike the above-mentioned MMF link, a SMF-based IMDD transmission link has a Gaussian-shaped frequency response with its peak occurring at the optical carrier frequency and the frequency response is much wider and flatter compared to those associated with the MMF links. To fully utilise such link frequency response, the SCM technique can be explored, in which an entire baseband signal is modulated onto an intermediate Radio Frequency (RF) carrier that drives directly an optical intensity modulator. By appropriately detuning the RF carrier frequency, use can be made of any region of the frequency response of an arbitrary transmission link. By introducing SCM into AMOOFDM, an AMOOFDM-SCM technique has been proposed in MMF/SMF-based IMDD links, as described in Section 1.1 [25,26]. However, the strong

intermixing effect due to direct detection in the receiver is a crucial factor limiting the maximum achievable transmission performance of the AMOOFDM-SCM technique in SMF IMDD systems, as shown in Chapter 6 [26]. Therefore, it is important to investigate the feasibility of mitigating the intermixing effects in SMF links to maximize the transmission performance.

iii) Simplification of AMOOFDM-SCM transceiver design: Each of the aforementioned AMOOFDM-SCM modems requires two separate Inverse Fast Fourier Transform (IFFT)/ Fast Fourier Transform (FFT) operations. As the IFFT and FFT are the most computationally intense functions in the AMOOFDM-SCM modems, the AMOOFDM-SCM modem designs may increase the transceiver complexity and cost. Therefore, simplified AMOOFDM-SCM modem design incorporating a single IFFT/FFT is of great importance.

iv) Relaxed requirements on key transceiver components: To further reduce the transceiver cost with the desired transmission performance being maintained, opportunities should also be explored to utilise low-cost optical/electrical components. To achieve such an objective, the minimum requirements on key components such as Digital-to-Analogue Converters (DACs) and Analogue-to-Digital Converters (ADCs) should be relaxed. An OFDM signal waveform has high amplitude fluctuations that produce large Peak-to-Average Power Ratios (PAPRs) [27]. A high PAPR may cause nonlinear distortions associated with the DACs/ADCs, because occasional peaks having amplitudes of higher than the average value may exceed the dynamic range of the DACs/ADCs. This inevitably increases the minimum requirements on quantization bits and sampling rates of the DACs/ADCs. Therefore, it is very crucial to investigate an effective technique to reduce the PAPRs of OFDM signals.

v) DML-induced positive frequency chirp: in cost-effective OOFDM NG-PON systems, the use of DMLs is preferable due to their major advantages namely low cost, compactness, low power consumption, relatively small driving voltage and high output power [28]. However, in DML-based IMDD OOFDM PONs utilizing Standard SMFs (SSMFs) with positive chromatic dispersion, positive frequency chirp associated with typical DMLs significantly limits the maximum achievable OOFDM transmission performance [16].

Clearly, the above-mentioned five challenges raise significant barriers for practically implementing high-speed and cost-effective OOFDM NG-PON systems. Addressing these challenges is vital for maximizing the achievable transmission performance, considerably simplifying the transceiver design and simultaneously reducing installation and maintenance cost. These activities can also provide valuable technical solutions to network designers for upgrading the existing PONs toward NG-PONs.

1.1 Major Achievements of the Dissertation Research

To address the aforementioned five challenges in IMDD OOFDM PON systems, in my PhD dissertation research work, several novel techniques have been proposed and investigated. The major achievements of the research work are summarized as follows:

- **AMOOFDM-SCM over worst-case MMF links**

For fully utilizing the frequency response beyond baseband of a MMF transmission link, an AMOOFDM-SCM modem is proposed, which consists of two AMOOFDM modems in parallel with one operating at the baseband and the other being modulated onto an intermediate RF carrier. For simplicity, throughout the thesis, the AMOOFDM signal produced by each of the above-mentioned AMOOFDM modems is referred to as a SCM subcarrier. Clearly, AMOOFDM-SCM offers major opportunities of not only manipulating the signal modulation format taken on each individual AMOOFDM subcarrier involved in a SCM subcarrier, but also positing each individual SCM subcarrier at an optimum link frequency response region. Detailed investigations of the transmission performance of the AMOOFDM-SCM modems are undertaken in single-channel, optical amplifier-free, worst-case IMDD MMF links. It is shown that, based on commercially available RF components, at least 64 Gb/s over 500 m and 37 Gb/s over 1000 m AMOOFDM-SCM signal transmission is feasible in the aforementioned MMF links having 3-dB bandwidths as small as 292.5 MHz·km. In comparison with AMOOFDM, the technique can not only almost double the capacity versus reach transmission performance but also reveal significantly relaxed requirements on key component parameters, improved flexibility and robustness and more efficient use of MMF link spectral properties.

- **AMOOFDM-SCM using Single Sideband (SSB) modulation over IMDD SMF links**

For fully exploiting the frequency response of an IMDD SMF link, detailed explorations of the maximum achievable transmission performance of the AMOOFDM-SCM technique are undertaken in SMF-based IMDD transmission links without incorporating optical amplification and fibre chromatic dispersion compensation. The intermixing effect induced by beatings between subcarriers of various types upon direct detection in the receiver is identified to be a crucial factor limiting the maximum achievable AMOOFDM-SCM performance. To maximize the link performance through mitigating such an effect, three AMOOFDM-SCM designs of different complexity levels are proposed, by applying SSB modulation and/or spectral gapping to AMOOFDM-SCM. These designs are referred to as AMOOFDM-SCM scheme I, AMOOFDM-SCM scheme II and AMOOFDM-SCM scheme III. The configuration of AMOOFDM-SCM scheme I is identical to that presented in Chapter 5, whilst the configuration of AMOOFDM-SCM scheme II is similar to AMOOFDM-SCM scheme I, except that, in AMOOFDM-SCM scheme II, a spectral gap in the electrical domain is introduced between the optical carrier and the first SCM subcarrier. The only configuration difference between AMOOFDM-SCM scheme III and AMOOFDM-SCM scheme II is that the two SCM subcarriers in AMOOFDM-SCM scheme III are real-valued SSB electrical signals generated using the phase-shift method [29]. It is shown that the SSB modulation and/or spectral gapping can effectively reduce the impact of the intermixing effect. As a direct result, these AMOOFDM-SCM designs can support >60Gb/s signal transmission over 20km, 40km and 60km, which are >1.5 times higher than those supported by AMOOFDM modems.

- **Simplified AMOOFDM-SCM with added input/output reconfigurability**

In the above-mentioned three AMOOFDM-SCM modem designs, two IFFT/FFT operations are required in each transmitter/receiver. For the purpose of simplifying the transceiver architectures, three novel designs of AMOOFDM-SCM modems configurations, referred to as Reconfigurable Scheme (RS) I, II and III, are proposed, each of which requires a single IFFT/FFT operation only. The general structures of the three proposed RS modems are similar to those corresponding to the AMOOFDM-SCM schemes. The considerable differences between these two sets of modems are the signal processing approaches used in distributing the encoded incoming data prior to the IFFT

operation in the transmitter and those adopted in recovering the received data after the FFT operation in the receiver, as presented in Chapter 7. These designs not only significantly simplify the AMOOFDM-SCM modem configurations but also offer extra unique features such as input/output reconfigurability without compromising the transmission performance. In addition to the above-mentioned advantages, these RS modems also have a number of major advantages including cost reduction, doubled number of end-users, system flexibility and performance robustness to variations in transmission link conditions and compatibility with the current deployed PON infrastructures due to the provision of a number of network functionalities such as dynamic bandwidth allocation, broadcasting and network monitoring functionalities.

- **Phase Modulation (PM)-enabled OOFDM transmission performance improvement in IMDD SMF systems incorporating parameter-relaxed DACs/ADCs.**

To lower the minimum requirements on key parameters of DACs/ADCs through reducing high PAPRs associated with OFDM signals, AMOOFDM using PM (AMOOFDM-PM) is proposed and theoretically explored in IMDD SMF systems. AMOOFDM-PM utilises an electrical OFDM signal to modulate the phase of a RF carrier prior to performing optical intensity modulation. Compared to AMOOFDM, AMOOFDM-PM can considerably reduce the PAPRs of OFDM signals and simultaneously relax the minimum requirements on both the quantization bits and sampling rates of DACs/ADCs. Simulations show that when small DAC/ADC quantization bits and/or low DAC/ADC sampling rates are adopted, AMOOFDM-PM can double the transmission capacity, compared to AMOOFDM. In addition, AMOOFDM-PM also shows excellent system flexibility and performance robustness to variations in transmission link characteristics. Furthermore, AMOOFDM-PM can be implemented directly using DSP without considerably increasing the transceiver complexity.

- **Negative power penalties of OOFDM signal transmissions in DML-based IMDD systems incorporating negative dispersion fibres**

The use of DMLs imposes positive frequency chirp onto modulated signals. To compensate for the DML frequency chirp effect, use can be made of negative dispersion SMFs such as MetroCor fibres and negative power penalties have been observed

experimentally at specific Bit Error Ratios (BERs) [30,31]. In the thesis, detailed investigations of dynamic negative power penalty characteristics of OOFDM signal transmissions are undertaken in DML-based IMDD systems incorporating MetroCor fibres. Excellent agreement between numerical simulations and real-time experimental measurements is obtained over a wide diversity of transmission conditions of the aforementioned systems. The physical mechanism underpinning the occurrence of negative power penalties is the reduction in subcarrier intermixing impairment due to the compensation between positive DML frequency chirp and MetroCor negative chromatic dispersions. It is also shown that the negative power penalty is independent of both cyclic prefix and signal modulation format, and, more importantly, controllable when adaptive modulation and/or appropriate adjustments of DML operating conditions are applied. This work verifies a promising approach for compensating the DML frequency chirp effects in the IMDD OOFDM transmission systems and the resulting negative power penalty can ultimately increase the system optical power budget. More importantly, it offers effective means for further maximizing the transmission performance of the systems considered here.

- **Compensation of DML frequency chirps in existing fibre infrastructures**

In addition to the employment of negative dispersion fibres, a simple and effective DML frequency chirp compensation technique is also proposed, which allows the reuse of existing PON architectures. This technique utilizes an electrical analogue circuit and an optical phase modulator. The electrical analogue circuit produces a phase signal mimicking the original phase of the DML-modulated optical signal, and the optical phase modulator driven by the phase signal compensates for the DML frequency chirp. The proposed technique can almost completely alleviate the DML frequency chirp effect. In particular, compared to uncompensated AMOOFDM IMDD PON systems incorporating DMLs, the proposed technique can not only significantly increase the transmission capacity by approximately 25% for transmission distances ranging from 30km to 80km, but also considerably improve the system performance tolerance to variation in DML operating condition, thus leading to enhanced performance robustness. In addition, optimum electrical analogue circuit design parameters have also been identified, which enable the present technique to offer the system operating condition-independent transmission performance. It is also worth pointing out that the electrical analogue circuit required can be easily integrated with other electrical components incorporated in the AMOOFDM

transceivers, and the integration between the DMLs and optical phase modulators is also practically feasible.

The above-mentioned work has resulted in 3 papers published in world-leading professional journals, 6 papers presented in international/national conferences, and 3 full journal papers submitted to major international journals. These papers were completed by the author of the thesis and form the main content of the dissertation work presented here.

1.2 Thesis Structure

The thesis consists of eleven chapters. Overviews of OFDM and OOFDM techniques, PONs and IMDD OOFDM PON systems are presented in Chapters 2-4, and detailed research work are presented and discussed in Chapters 5-10.

In Chapter 2, to enable a better understanding of the work presented in the thesis, fundamentals of OFDM are described in detail. Two categories of OOFDM including coherent OOFDM and IMDD OOFDM are outlined. In the IMDD OOFDM category, AMOOFDM is described in detail. Moreover, the major differences between coherent OOFDM and IMDD OOFDM are summarized to highlight the importance of IMDD OOFDM in PON application scenarios.

In Chapter 3, the background of access networks is discussed briefly with special attention being focussed on different PON architectures. In addition, the advantages of utilizing IMDD OOFDM in NG-PONs are also discussed.

Chapter 4 deals with cost-effective IMDD OOFDM systems. Following the detailed review of OFDM modems in Chapter 2, Chapter 4 discusses IMDD links in detail, with effort being given to describing key optical components. These optical components include optical fibres, photodetectors and intensity modulators. In addition, the five challenges associated with IMDD OOFDM systems are explained in detail.

In Chapter 5, AMOOFDM-SCM is proposed and investigated in a single-channel, optical amplifier-free MMF link. When compared with AMOOFDM, AMOOFDM-SCM not only enhances the capacity versus reach performance by a factor of about 2, but also

considerably lowers the requirements on key transceiver components as well as improving the robustness of the MMF link performance.

In Chapter 6, detailed investigations of the AMOOFDM-SCM transmission performance are undertaken in SMF-based transmission links without optical amplification and chromatic dispersion compensation. The intermixing effect is identified to be a crucial physical factor limiting the maximum achievable transmission performance of the AMOOFDM-SCM technique. For mitigating such an effect, three AMOOFDM-SCM designs of different complexity are proposed and explored theoretically.

In Chapter 7, three simplified AMOOFM-SCM modem configurations are proposed and investigated, each of which requires a single IFFT/FFT only. Simulations show that these architectures can retain the transmission performance and simultaneously offer input/output reconfigurability. Moreover, the optimum RF frequencies of the SCM subcarriers are identified for each of these simplified modems.

In Chapter 8, AMOOFDM-PM is proposed and investigated theoretically in SMF-based transmission links. Due to the use of AMOOFDM-PM, the PAPR of an OFDM signal can be significantly reduced and the minimum requirements on key transceiver components can also be relaxed. Moreover, AMOOFDM-PM-enabled improvements in transmission capacity for different link configurations are explored theoretically.

In Chapter 9 and 10, detailed explorations of effective approaches are undertaken to reduce the frequency chirp effects induced by DMLs. In Chapter 9, use is made of negative dispersion fibre such as MetroCor fibres in IMDD OOFDM systems. Dynamic negative power penalty characteristics of OOFDM signal transmissions are obtained over DML-based IMDD MetroCor systems. Comparisons are also made between numerical simulations and our real-time experimental measurements, based on which the physical mechanism underpinning the negative power penalties is identified. In addition, for a given DML-based IMDD OOFDM MetroCor SMF system, discussions are made of the impacts of cyclic prefix, adaptive modulation, signal modulation format and DML operating conditions on the negative power penalty effect. In Chapter 10, a simple and effective DML frequency chirp compensation technique is presented and theoretically explored in similar OOFDM systems. The physical mechanism underpinning the effectiveness of the proposed technique is explored in detail. The optimum values of circuit design parameters

are identified for different transmission distances. In addition, detailed explorations are made of the sensitivity of the system performance to DML operating conditions.

Finally, the thesis is summarized in Chapter 11.

References

[1] "Alcatel-Lucent Bell Labs announces new optical transmission record and breaks 100 Petabit per second kilometer barrier," available at http://www.alcatel-lucent.com.

[2] Leonid G. Kazovsky, Wei-Tao Shaw, D. Gutierrez, N. Cheng, and Shing-Wa Wong, "Next-generation optical access networks," J. Lightw. Technol., vol. 25, no. 11, pp. 3428-3442, Nov. 2007.

[3] F. J. Effenberger, J-I Kani and Y. Maeda, "Standardization trends and prospective views on the next generation of broadband optical access systems," IEEE J. Select. Area. Comm., vol. 28, no. 6, pp. 773-780, Aug. 2010.

[4] H. Song, B-W Kim, and B. Mukherjee, "Long-reach optical access networks: a survey of research challenges, demonstrations, and bandwidth assignment mechanisms," IEEE Comm. Surveys & Tutorials, vol. 12, no. 1, First Quarter 2010.

[5] M. Cvijetic, "Advanced technologies for next-generation fiber networks," Optical Fibre Communication/National Fibre Optic Engineers Conference (OFC/NFOEC), (OSA, 2010), Paper OWY1.

[6] H. Shinohara, "Broadband access in Japan: Rapidly growing FTTH market," IEEE Comm. Magazine., vol. 43, no. 9, pp. 72–78, Sep. 2005.

[7] P. W. Shumate, "Fiber-to-the-home: 1977-2007," J. Lightw. Technol., vol. 26, no. 9, pp. 1093-1103, May. 2008.

[8] J-I Kani, "Enabling technologies for future scalable and flexible WDM-PON and WDM/TDM-PON systems," IEEE J. Select. Top. Quantum. Electron. vol. 16, no. 5, pp. 1290-1297, Sept./Oct. 2010.

[9] IEEE Standard 802.3ah, "Carrier sense multiple access with collision detection (CSMA/CD) access method and physical layer specifications amendment: media access control parameters, physical layers, and management parameters for subscriber access networks," 2004.

[10] ITU-T Recommendation G.984.1, "Gigabit-capable passive optical networks (G-PON): general characteristics," 2003.

[11] IEEE Standard 802.3av, "Carrier sense multiple access with collision detection (CSMA/CD) access method and physical layer specifications-amendment: physical layers specifications and management parameters for 10 Gb/s passive optical networks," 2009.

[12] ITU-T Recommendation G.987.1, "10Gigabit-capable passive optical networks (XG-PON): general requirements," 2009.

[13] N. Cvijetic, D. Y. Qian, J. Q. Hu, and T. Wang, "Orthogonal frequency division multiple access PON (OFDMA-PON) for colorless upstream transmission beyond 10 Gb/s," IEEE J. Select. Area. Comm., vol. 28, no. 6, pp. 781-790, Aug. 2010.

[14] R. P. Giddings, X. Q. Jin, E. Hugues-Salas, E. Giacoumidis, J. L. Wei, and J. M. Tang, "Experimental demonstration of a record high 11.25Gb/s real-time optical OFDM transceiver supporting 25km SMF end-to-end transmission in simple IMDD systems," Opt. Express., vol. 18, no. 6, pp. 5541-5555, Mar. 2010.

[15] J. M. Tang, P. M. Lane and K. A. Shore, "High-speed transmission of adaptively modulated optical OFDM signals over multimode fibres using directly modulated DFBs," J. Lightw. Technol., vol. 24, no. 1, pp. 429–441, Jan. 2006.

[16] J. M. Tang and K. A. Shore, "30Gb/s signal transmission over 40-km directly modulated DFB-laser-based single-mode-fiber links without optical amplification and dispersion compensation," J. Lightw. Technol., vol. 24, no. 6, pp. 2318-2327, June. 2006.

[17] T-N. Duong, N. Genay, M. Ouzzif, J. L. Masson, B. Charbonnier, P. Chanclou and J. C. Simon, "Adaptive loading algorithm implemented in AMOOFDM for NG-PON system integrating cost-effective and low bandwidth optical devices," IEEE Photon. Technol. Lett., vol. 21, no. 12, pp. 790-792, Jun. 2009.

[18] D. Qian, N. Cvijetic, J. Hu and T. Wang, "108 Gb/s OFDMA-PON with polarization multiplexing and direct detection," J. Lightw. Technol., vol. 28, no. 4, pp. 484-493, Feb. 2010.

[19] J. L. Wei, C. Sánchez, R. P. Giddings, E. Hugues-Salas, and J. M. Tang, "Significant improvements in optical power budgets of real-time optical OFDM PON systems," Opt. Express., vol. 18, no. 20, pp. 20732-20745, Sep. 2010.

[20] X. Q. Jin, R. P. Giddings, E. Hugues-Salas and J. M. Tang, "Real-time experimental demonstration of optical OFDM symbol synchronization in directly modulated DFB laser-based 25km SMF IMDD systems," Opt. Express., vol. 18, no. 20, pp. 21100-21110, Sep. 2010.

[21] X. Zheng, X. Q. Jin, R. P. Giddings, J. L. Wei, E. Hugues-Salas, Y. H. Hong and J. M. Tang, "Negative power penalties of optical OFDM signal transmissions in directly modulated DFB laser-based IMDD systems incorporating negative dispersion fibres," IEEE Photonics J., vol. 2, no. 4, pp. 532-542, Aug. 2010.

[22] R. P. Giddings, X. Q. Jin, H. H. Kee, X. L. Yang, and J. M. Tang, "Real-time implementation of optical OFDM transmitters and receivers for practical end-to-end optical transmission systems," Electron. Lett., vol. 45, no.15, pp. 800-802, July. 2009.

[23] E. J. Tyler, P. Kourtessis, M. Webster, E. Rochart, T. Quinlan, S. E. M. Dudley, S. D. Walker, R. V. Penty, and I. H. White, "Toward terabitper-second capacities over multimode fibre links using SCM/WDM techniques," J. Lightw. Technol., vol. 21, no. 12, pp. 3237–3243, Dec. 2003.

[24] X. Q. Jin and J. M. Tang, "Effectiveness of the use of 3-dB bandwidths of multimode fibres for estimating the transmission performance of adaptively modulated optical OFDM Signals over IMDD links," J. Lightw. Technol., vol. 27, no. 18, pp. 3992-3998, Sep. 2009.

[25] X. Zheng, J. M. Tang and P. S. Spencer, "Transmission performance of adaptively modulated optical OFDM modems using subcarrier modulation over worst-case multimode fibre links," IEEE Comm. Lett., vol. 12, no. 10, pp. 788-790, Oct. 2008.

[26] X. Zheng, J. L. Wei and J. M. Tang, "Transmission performance of adaptively modulated optical OFDM modems using subcarrier modulation over SMF IMDD links for access and metropolitan area networks," Opt. Express., vol. 16, no. 25, pp. 20427-20440, Dec. 2008.

[27] S. C. Thompson, A. U. Ahemd, J. G. Proakis, J. R. Zeidler, M. J. Geile, "Constant envelope OFDM," IEEE Trans. Comm., vol. 56, no. 8, pp. 1300-1312, Aug. 2008.

[28] J. J. Yu, Z. S. Jia, M. F. Huang, M. Haris, P. N. Ji, T. Wang and G. K. Chang, "Applications of 40-Gb/s chirp managed laser in access and metro networks," J. Lightw. Technol., vol. 27, no. 3, pp. 253-265, Feb. 2009.

[29] A. B. Carlson, P. B. Crilly and J. C. Rutledge, *Communication Systems: An Introduction to Signals and Noise in Electrical Communication*, McGraw-Hill Higher Education, 2002.

[30] X. Q .Jin, R. P. Giddings and J. M .Tang, "Real-time transmission of 3Gb/s 16-QAM encoded optical OFDM signals over 75km SMFs with negative power penalties," Opt. Express. vol. 17, no. 17, pp. 14574-14585, Aug. 2009.

[31] X. Q. Jin, R. P. Giddings, E. Hugues-Salas and J. M. Tang, "Real-time demonstration of 128-QAM-encoded optical OFDM transmission with a 5.25bit/s/Hz spectral efficiency in simple IMDD systems utilizing directly modulated DFB lasers," Opt. Express. vol. 17, no. 22, pp. 20484-20493, Oct. 2009.

2 OFDM Principles and OOFDM

Contents

This chapter introduces the fundamentals of OFDM and OOFDM, which forms the foundation of the work presented in the thesis.

2.1 Basic Concept of OFDM

OFDM proposed by R. W. Chang in 1966 [1] is a technique capable of combating the multipath fading effect. It has widely been adopted in wireless communications. As OFDM is a special case of Frequency Division Multiplexing (FDM) [2,3], a typical FDM system is shown in Fig.2.1, which transmits data by dividing a stream into several parallel bit streams with low bit rates and modulating each of these data streams onto different subcarriers with different RF frequencies. The RF frequency of each individual subcarrier is chosen appropriately to ensure a sufficiently wide frequency gap between the adjacent subcarriers' spectra, as shown in Fig.2.2 (a). Moreover, the parallel data streams can be recovered by down-converting each of these subcarriers with an identical RF frequency and finally using low pass filtering.

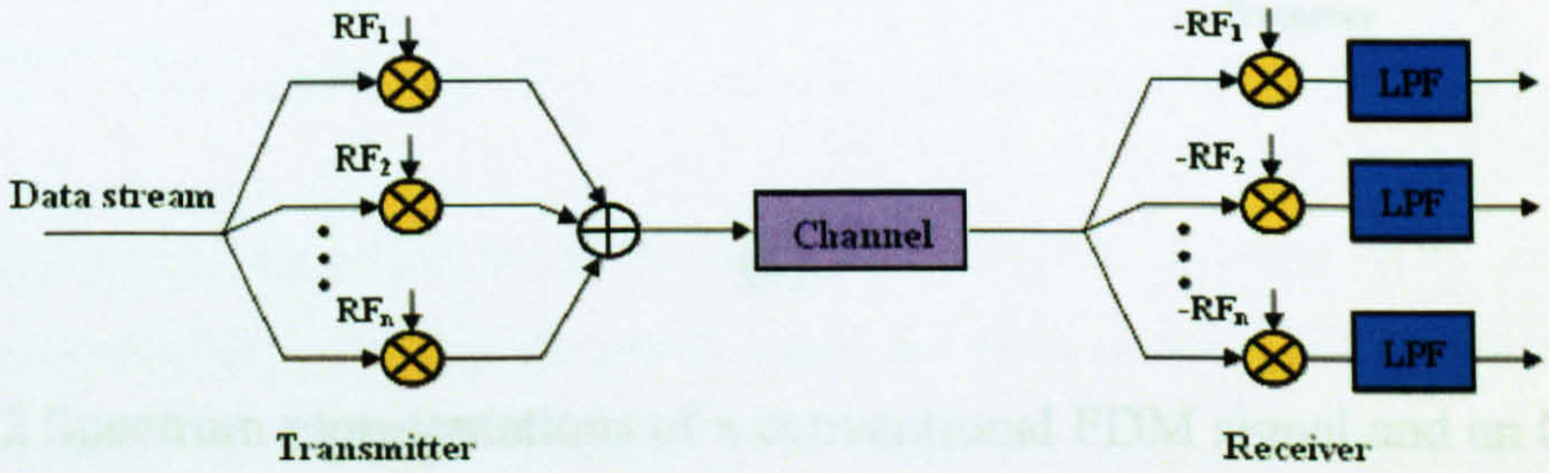

Fig.2.1 Schematic diagram of a typical FDM system. RF: radio frequency; LPF: low-pass filter.

Compared with conventional FDM, OFDM precisely chooses the RF frequencies to ensure that all these subcarriers are orthogonal to each other. The orthogonality amongst all the subcarriers can be realized by separating the subcarriers by integer multiples of the inverse of the symbol duration of the parallel bit streams. This causes the spectrum of each subcarrier to overlap other subcarriers' spectra and the resulting spectral efficiency of the OFDM system is much higher than that of the conventional FDM system, as shown in Fig. 2.2 [2].

In practice, modulation/demodulation in an OFDM system can be realized simply by Inverse Discrete Fourier Transform (IDFT)/ Discrete Fourier Transform (DFT) [4] or more efficient IFFT/ FFT [5]. As IFFT/FFT can be practically implemented by modern DSP technology, the OFDM technique requires much lower system complexity and thus reduces the system cost compared to conventional FDM [5]. Apart from that, OFDM also has advantages including robustness against channel dispersion and ease of phase and channel estimation in a time-varying environment [5].

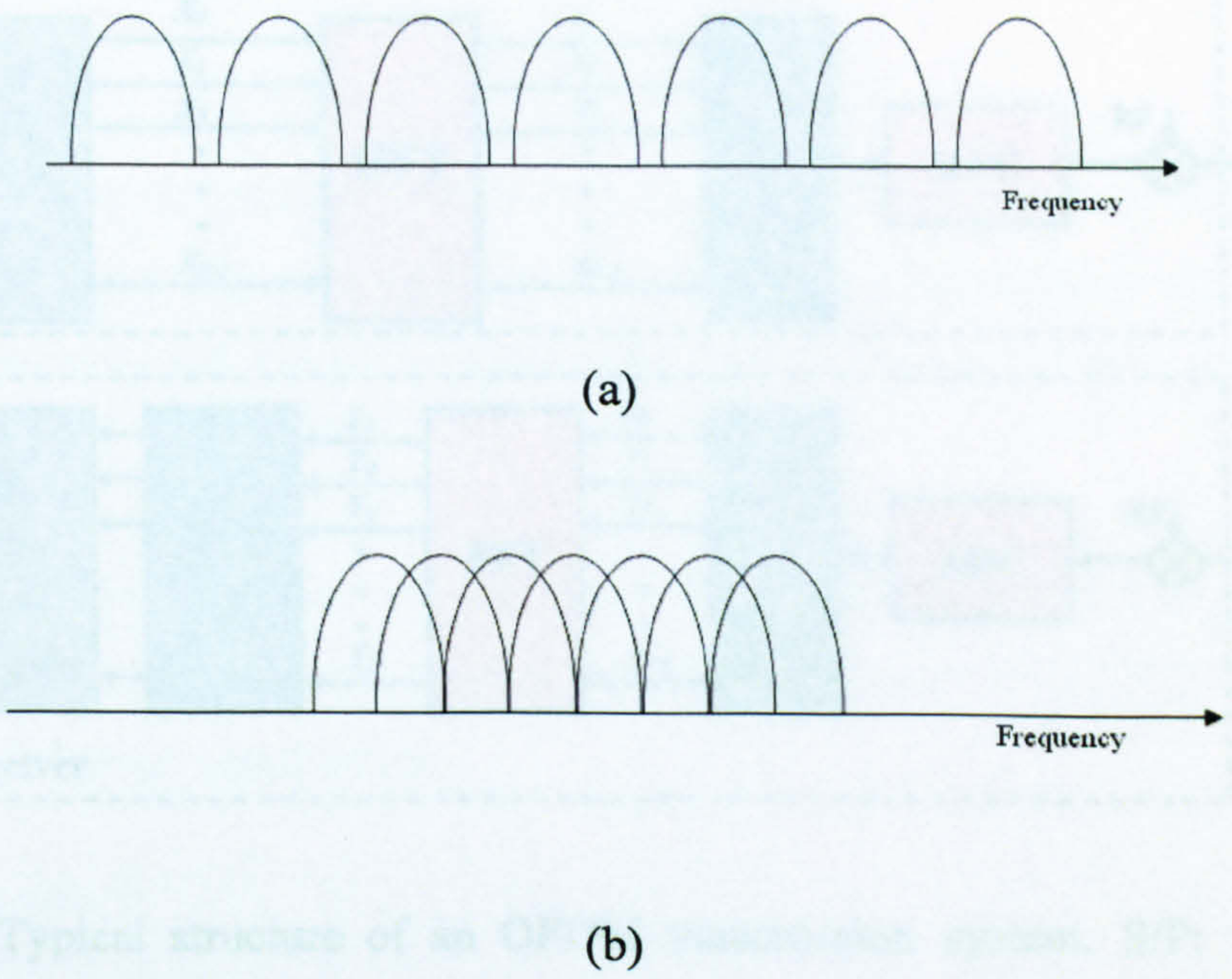

Fig. 2.2 Spectrum representations of a conventional FDM signal and an OFDM signal. (a) Conventional FDM; (b) OFDM.

2.2 Typical Configurations of OFDM Transceivers

A typical OFDM system consists of a transmitter, a receiver and a transmission link in between, as shown in Fig.2.3. In the transmitter, an incoming binary data sequence is encoded to serial complex numbers using different signal-modulation formats such as Phase Shift Keying (PSK) and QAM. A serial-to-parallel converter truncates the encoded complex data sequence into a large number of sets of closely and equally spaced narrowband data and each set contains the same number of subcarriers. An IFFT is then applied to each set of subcarriers to generate parallel OFDM symbols. To combat the dispersion effect, a cyclic prefix is added to the front of each OFDM symbol [3,6]. The

cyclic prefix is essentially a copy of the last fraction of each OFDM symbol and does not carry any useful information. After that, these OFDM symbols are serialized to form a long digital signal sequence, to which signal clipping is applied to limit the OFDM signal power within a pre-determined dynamic range. After passing through a DAC which converts the digital data sequence into an analogue signal waveform, the generated analogue OFDM signal is up-converted with a RF carrier and launched into a transmission link.

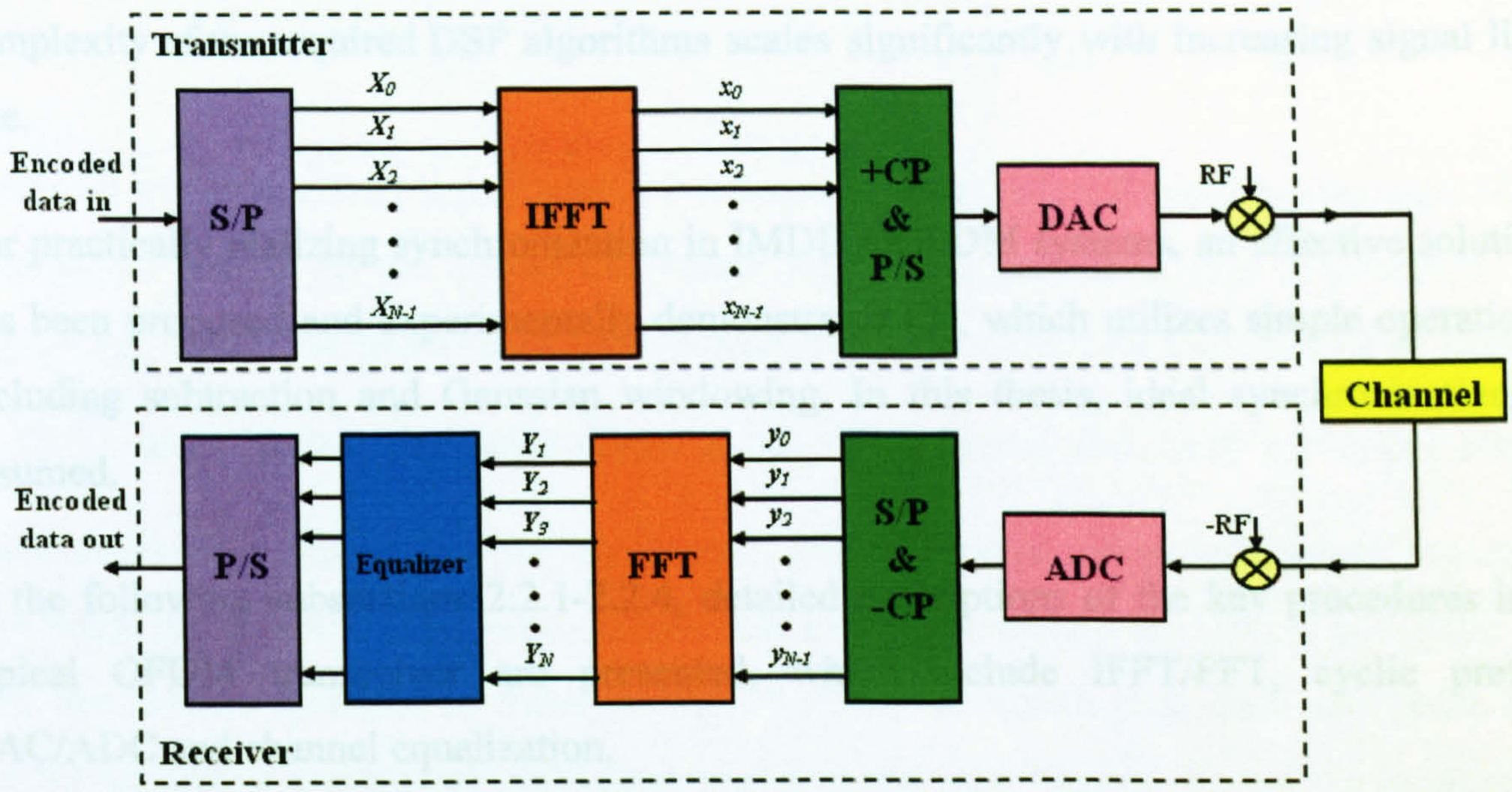

Fig.2.3 Typical structure of an OFDM transmission system. S/P: serial-to-parallel converter; +CP: cyclic prefix insertion; P/S: parallel-to-serial converter; DAC: digital-to-analogue converter; RF: radio frequency; ADC: analogue-to-digital converter; -CP: cyclic prefix removing.

In the receiver, the received signal is processed in an inverse procedure of the transmitter including down-conversion utilising a RF carrier with a frequency identical to that of the transmitter, digitalization in an ADC, serial to parallel conversion, cyclic prefix removing, FFT, equalization and decoding.

It should be mentioned that the above descriptions of the OFDM transceiver are based on the assumption that the OFDM transmission system is synchronized precisely. However, in practice, synchronization errors may occur due to sampling clock offsets induced by the clock mismatch between the transmitter and the receiver, symbol timing offsets induced by the time delay of a transmission link, and carrier frequency offsets induced by the frequency mismatch between oscillators involved in the transmitter and the receiver [3].

In wireless OFDM systems, a conventional autocorrelation synchronization technique has been widely adopted, which is based on sophisticated autocorrelation of incoming signals at signal sampling or over-sampling speeds [7], i.e., a sequence of samples is multiplied by a time-shifted copy of the same sequence. By altering the time shift, the multiplication and sum operations are performed and repeated to produce a time dependent autocorrelation profile, which is then employed for synchronization. Clearly, such a technique is not suitable for end-to-end real-time high-speed OOFDM transmission systems, as the complexity of the required DSP algorithms scales significantly with increasing signal line rate.

For practically realizing synchronization in IMDD OOFDM systems, an effective solution has been proposed and experimentally demonstrated [7], which utilizes simple operations including subtraction and Gaussian windowing. In this thesis, ideal synchronization is assumed.

In the following subsections 2.2.1-2.2.4, detailed descriptions of the key procedures in a typical OFDM transceiver are presented, which include IFFT/FFT, cyclic prefix, DAC/ADC and channel equalization.

2.2.1 IFFT/FFT

In the transmitter, for the k-th subcarrier in the n-th OFDM symbol, the encoded complex number denoted as $X_{k,n}$ is used to modulate the k-th subcarrier waveform and the resulting waveform [3] can be written as

$$x_{k,n}(t) = X_{k,n} e^{j2\pi f_k t} \prod(\frac{t - nT}{T}) \tag{2.1}$$

where

$$\Pi(\frac{t}{T}) = \begin{cases} 1, & -T/2 \le t \le T/2 \\ 0, & otherwise \end{cases} \tag{2.2}$$

T is the time period of the OFDM symbol, f_k is the frequency of the k-th subcarrier. f_k satisfies

$$f_k = f_c + \frac{k}{T} \qquad k=0,1,\ldots,N\text{-}1 \tag{2.3}$$

with f_c being the central frequency and N being the number of the subcarriers, the frequency difference Δf between adjacent subcarriers is then fixed at $\frac{1}{T}$. Therefore, the correlation between any two subcarriers in the n-th symbol is given by

$$\delta_{kl} = \frac{1}{T}\int_{(n-1)T}^{nT} x_{k,n}x_{l,n}^{*}dt = \frac{X_{k,n}X_{l,n}^{*}}{T}\int_{(n-1)T}^{nT} e^{j2\pi(f_k-f_l)t}dt = X_{k,n}X_{l,n}^{*}e^{j\pi(f_k-f_l)T}\frac{\sin\left[\pi(f_k-f_l)T\right]}{\pi(f_k-f_l)T} = \begin{cases}0, & k\neq l\\ 1, & k=l\end{cases} \tag{2.4}$$

where all the subcarriers' amplitudes are normalized. Eq.(2.4) indicates that orthogonality is achieved among all the subcarriers when Eq.(2.3) is satisfied. This is illustrated in Fig.2.4 (a), where the spectrum of each subcarrier is represented by the function of $sinc(x)$ as $\prod(\frac{t}{T})$ has a rectangular pulse shape. It should be noted that each subcarrier has a spectrum with a zero value at the central frequencies of other subcarriers' spectra. Moreover, the corresponding time-domain subcarriers waveforms are plotted in Fig.2.4 (b) with the colours identical to those in Fig.2.4 (a). It is shown that each subcarrier has exactly an integer number of oscillating cycles in the time interval T, and the number of oscillating cycles between adjacent subcarriers differs exactly by one. Due to the orthogonality properties, the Inter-Carrier Interference (ICI) effect can be overcome even if the spectra of the subcarriers overlap.

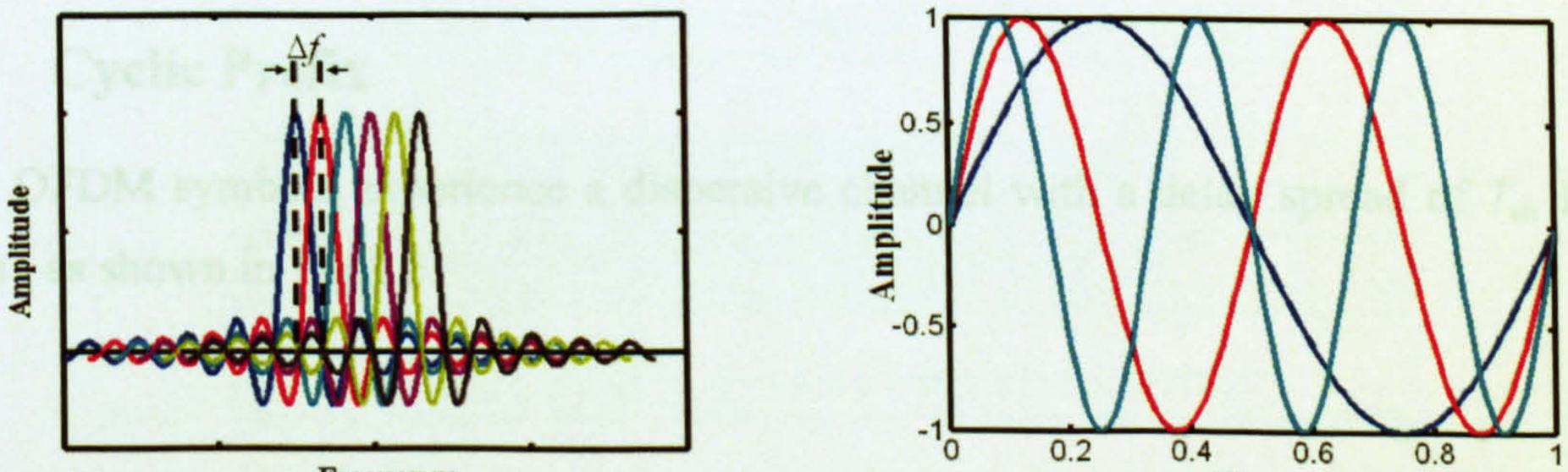

(a) (b)

Fig. 2.4 OFDM signal spectrum and time-domain waveform. (a) OFDM signal spectrum; (b) time-domain waveforms for the first three normalized subcarriers shown in Fig. 2.4. (a).

When all the subcarrier waveforms are combined, the time-domain *n*-th OFDM symbol within a time duration of [(*n*-1)*T*, *nT*] can be expressed as :

$$x_n(t) = \frac{1}{N}\sum_{k=0}^{N-1} X_{k,n} e^{j2\pi f_k t} \tag{2.5}$$

Assuming $x_n(t)$ is sampled at an interval of *T*/*N*, then the *m*-th sample within [(*n*-1)*T*, *nT*] can be rewritten as:

$$x_n(m) = \frac{1}{N}\sum_{k=0}^{N-1} X_{k,n} e^{j2\pi f_k \frac{Tm}{N}} = \frac{1}{N}\sum_{k=0}^{N-1} X_{k,n} e^{j\frac{2\pi km}{N}} \tag{2.6}$$

where *m*=0,1,...*N*-1. It is interesting to note that Eq.(2.6) has a form identical to IFFT and thus the OFDM signal can be directly produced by IFFT. Similarly, for an ideal OFDM system without suffering from any dispersive effects, in the receiver, the complex data for the *k*-th subcarrier $Y_{k,n}$ can be recovered from the received symbol $y_n(m)$ using FFT:

$$Y_{k,n} = \frac{1}{N}\sum_{m=0}^{N-1} y_n(m) e^{j\frac{-2\pi km}{N}} \tag{2.7}$$

For practical transmission systems with dispersive effects, the insertion of cyclic prefix and the use of equalization are required for combating Inter-Symbol Interference (ISI) and frequency dependent loss induced by the channel [3].

2.2.2 Cyclic Prefix

When OFDM symbols experience a dispersive channel with a delay spread of T_d, ISI [5] occurs , as shown in Fig.2.5.

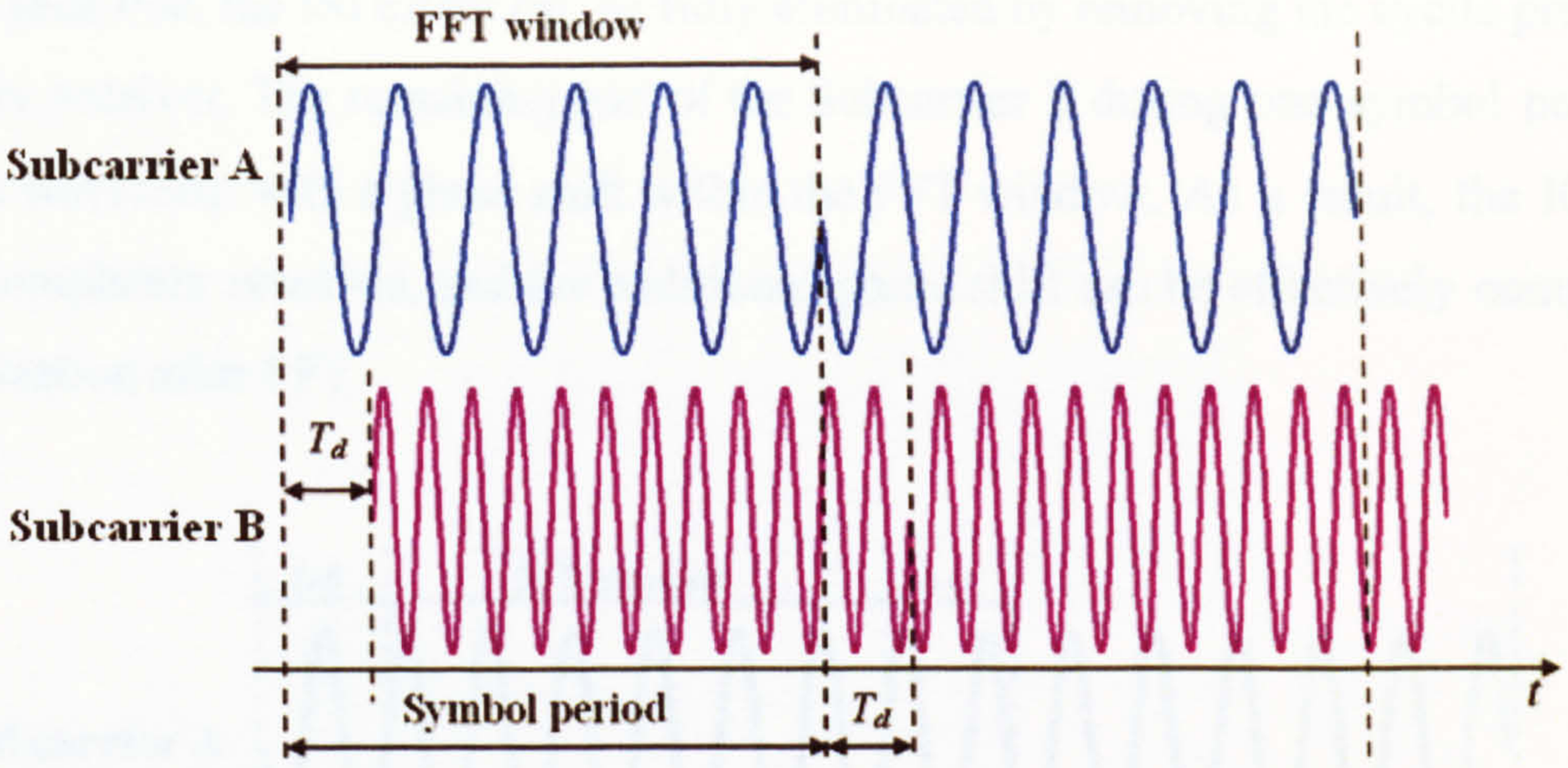

Fig.2.5 ISI and ICI caused by a dispersive channel.

For simplicity, each OFDM symbol has only two subcarriers represented by "Subcarrier A" and "Subcarrier B" and the fast and slow delay spread is T_d. Within an OFDM symbol, Subcarrier B is delayed by T_d against Subcarrier A. If a FFT window containing a complete OFDM symbol for Subcarrier A is selected, Subcarrier B crosses the symbol boundary, this leads to interference between neighboring OFDM symbols. Moreover, the OFDM waveform in the FFT window for Subcarrier B is incomplete, which destroys the orthogonality as mentioned in Eq. (2.4) and causes the ICI effect. To solve the ISI and ICI effects, a cyclic prefix can be used in front of each OFDM symbol, as shown in Fig.2.6. In this figure, ΔG is the time duration of the cyclic prefix.

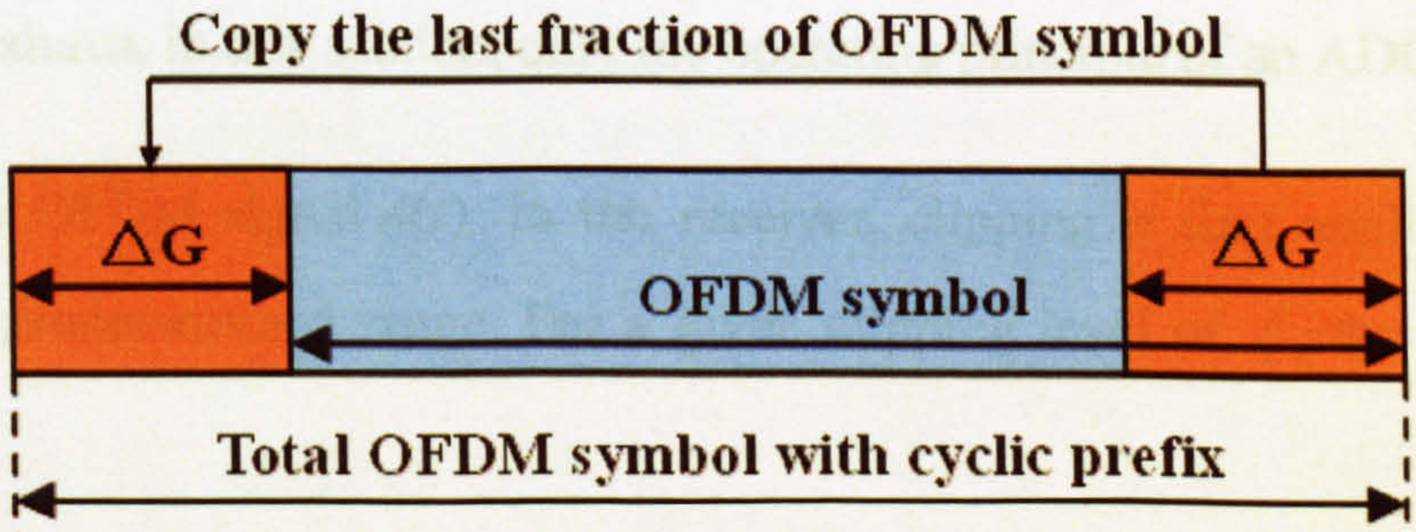

Fig.2.6 Use of cyclic prefix

The effectiveness of using a cyclic prefix in compensating for both the ISI and ICI effects is shown in Fig.2.7, where ΔG is chosen to satisfy

$$\Delta G > T_d \tag{2.8}$$

It can be seen that, the ISI effect can be fully eliminated by removing the cyclic prefix after FFT in the receiver. The remaining part of the Subcarrier B during one symbol period is a complete waveform with a phase shift within the FFT window. As a result, the ICI effect can be completely resolved, and the additional phase shift can be effectively compensated by equalization after FFT.

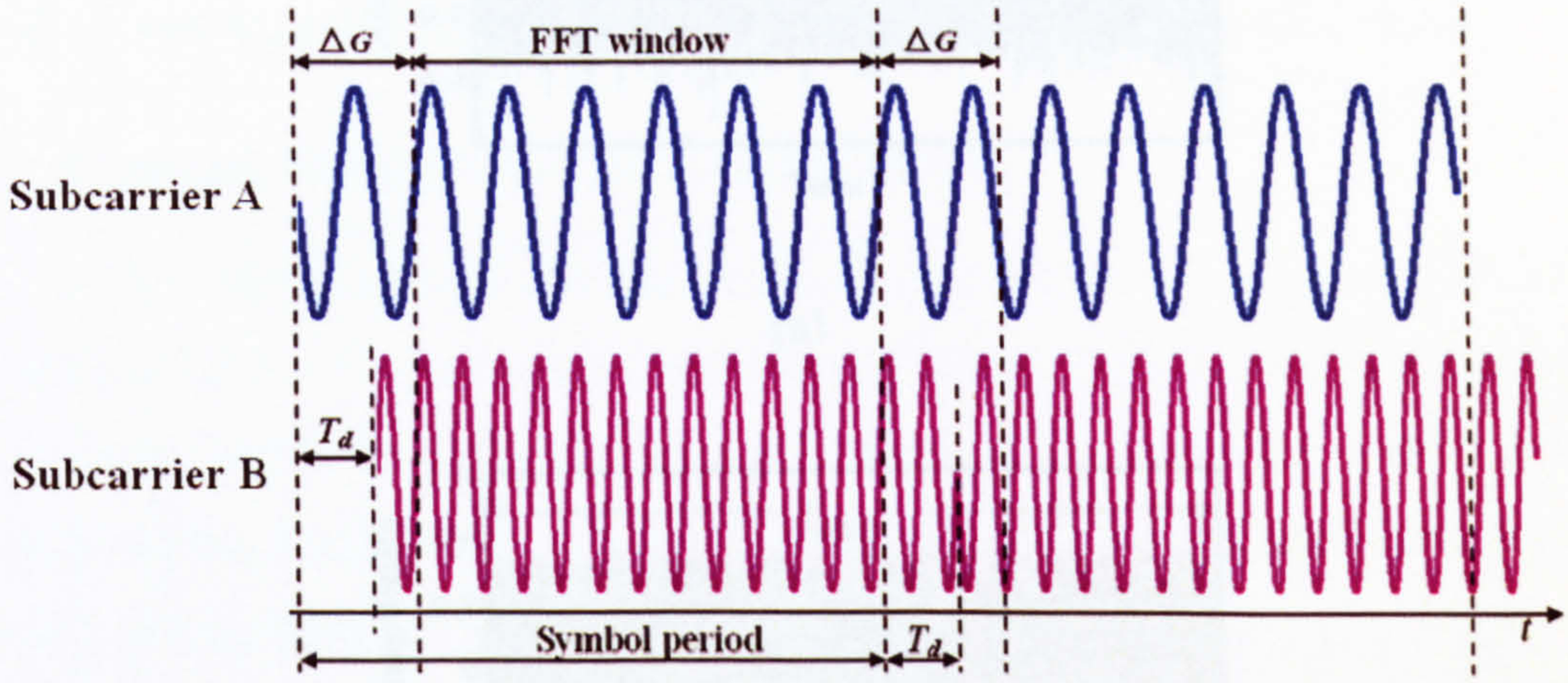

Fig.2.7 Compensation for ISI and ICI by cyclic prefix.

2.2.3 DAC/ADC

To convert a digital OFDM signal into an analogue OFDM waveform, a DAC is utilised after parallel-to-serial conversion in the transmitter. Correspondingly, an ADC is required to recover the received signal in the receiver. As the DAC and ADC have the similar signal processing procedures, in this section, only the operating principle of an ADC is described.

For an analogue OFDM signal $A(t)$ in the receiver, clipping is first applied to limit its power within a predetermined range. For a given clipping level of ξ, the clipped signal has the form [8]

$$A_{clip}(t) = \begin{cases} A(t), & |A(t)| \le \Lambda \\ \Lambda e^{j\arg[A(t)]}, & |A(t)| > \Lambda \end{cases} \tag{2.9}$$

where Λ is defined as $\Lambda = \sqrt{\xi P_m}$ with P_m being the mean signal power. From Fig.2.8, it can be seen that signal clipping also introduces waveform distortions, which become more

severe with reducing ξ. In practice, ξ is appropriately chosen at an optimum value to mitigate the clipping distortions.

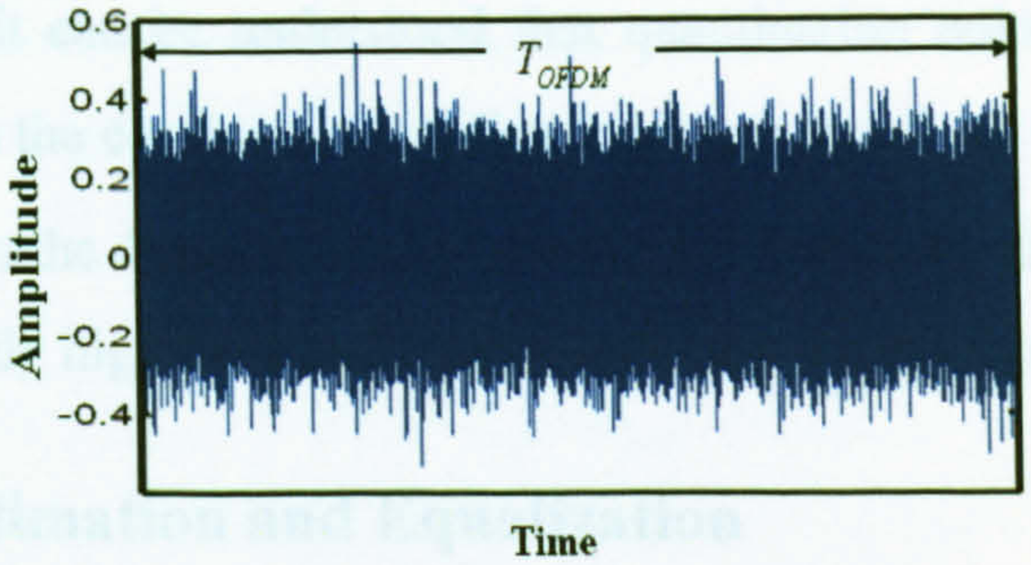

(a)

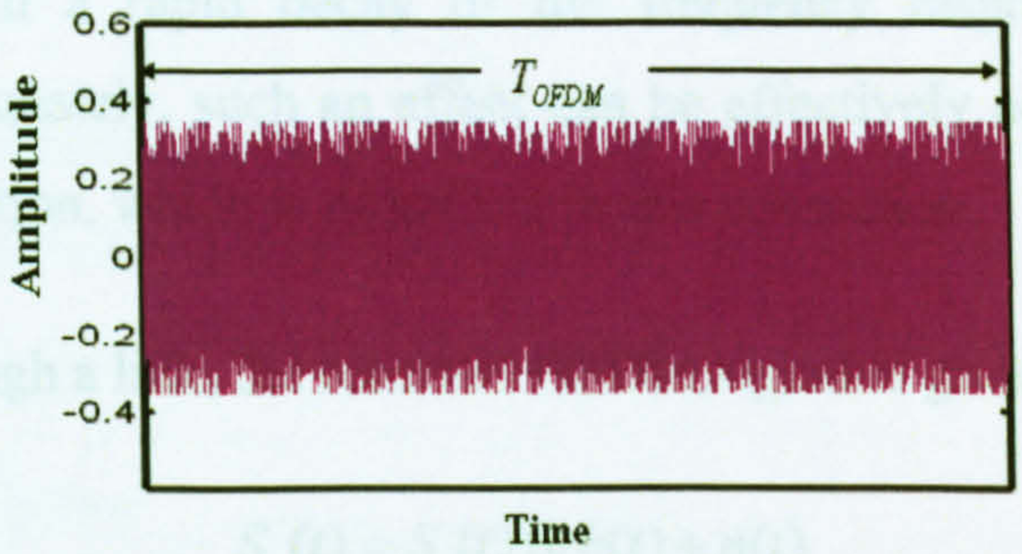

(b)

Fig.2.8 Comparisons of the signal clipping effect on the OFDM signal between different clipping levels; (a) a 13dB clipping level; (b) a 9 dB clipping level.

After clipping, $A_{clip}(t)$ is sampled and linearly quantized into a set of equally distributed quantization levels within a range of $[-\Lambda, \Lambda]$. The quantization process can be described as follows,

$$A_Q = \sum_{i=-L/2+1}^{L/2} \frac{A_i + A_{i-1}}{2} g(A_s, A_i, A_{i-1}) \tag{2.10}$$

where A_Q is the quantized value, A_s is the sampled OFDM values, A_i, A_{i-1} are the i-th and (i-1)-th quantization levels, L is the number of quantization levels and the value of L is 2^b with b being the quantization bits. g is the rectangular function defined as

$$g(x, x_1, x_2) = \begin{cases} 1, & x_1 \le x < x_2 \\ 0, & otherwise \end{cases} \tag{2.11}$$

From Eqs.(2.10-2.11), it can be understood that quantization noise is introduced by the quantization process, as the continuous amplitude waveform of A_s is mapped onto one set of discrete values within the dynamic range of [–Λ, Λ]. Therefore, the quantization bit b is required to be sufficiently high for considerably reducing the quantization noise.

2.2.4 Channel Estimation and Equalization

Due to the time delay between different subcarriers in a dispersive channel, as mentioned in subsection 2.2.2, the transmitted OFDM signal suffers from frequency dependent loss effects, which result in a rapid decay of the frequency response within the signal bandwidth region. Fortunately, such an effect can be effectively compensated by channel estimation and equalization, which is described in this subsection.

After transmitting through a link, the received OFDM signal is given by

$$S_r(t) = S_t(t) \otimes h(t) + n(t) \tag{2.12}$$

where $S_t(t)$ is the signal emerging from the transmitter OFDM modem, $S_r(t)$ is the received OFDM signal, ⊗ denotes the convolution operation, $n(t)$ is noise associated with the transmission link, and $h(t)$ is the impulse response of the transmission link, which includes the dispersive effect induced by the channel. Equivalently, the time domain relationships between $S_t(t)$ and $S_r(t)$ in Eq. (2.12) can be transferred into the frequency domain by the Fourier transform, which is given by

$$S_r(f) = S_t(f)H(f) + N(f) \tag{2.13}$$

where $S_t(f)$ and $S_r(f)$ are the spectra of the OFDM signals in the transmitter and receiver front end, respectively; $H(f)$ and $N(f)$ are the frequency response and noise spectrum of the transmission link, respectively; it should be noted that the $H(f)$ can be easily estimated by $S_r(f)/S_t(f)$.

In practical OFDM systems, pilot-based channel estimation and equalization are used [3]. To perform channel estimation, a number of sets of pilot signals that are known are interspersed with the user data and are transmitted. After FFT in the receiver, the pilot signals are extracted from the received signals. Then the frequency response can be estimated by dividing the extracted pilot signals with the transmitted pilot signals, which is expressed as

$$H_k = Y_{k,p} / X_{k,p} \tag{2.14}$$

where H_k is the link frequency response of the k-th subcarrier; $X_{k,p}$ and $Y_{k,p}$ are the transmitted and received pilot signals of the k-th subcarrier before IFFT in the transmitter and after FFT in the receiver, respectively.

Following channel estimation, channel equalization can be undertaken. For the k-th subcarrier in the n-th OFDM symbol, the transmitted complex data $X_{k,n}$ can be recovered by multiplying the received data $Y_{k,n}$ after FFT with the inverse of the estimated frequency response H_k^{-1}, as given below

$$X'_{k,n} = Y_{k,n} H_k^{-1} = X_{k,n} + N_k H_k^{-1} \tag{2.15}$$

where $X'_{k,n}$ is the recovered complex data and $Y_{k,n} = X_{k,n} H_k + N_k$ with N_k being the channel noise for the k-th subcarrier.

It can be seen that, using a simple approach, the channel noise effect cannot be eliminated, this distorts the signal significantly when the received OFDM signal has a low power. To efficiently solve the problem, averaging the estimated link frequency response can be taken over a relatively long time duration, for say ≥ 32 OFDM symbols [9].

2.3 OOFDM

OOFDM is a technique in which an electrical OFDM signal emerging from a transmitter OFDM modem is up-converted into an optical carrier frequency (~100THz) using an Electrical-to-Optical (E/O) converter; after transmitting through an optical fibre link, the optical signal is converted into an electrical signal using an Optical-to-Electrical (O/E) converter and the resulting electrical OFDM signal is processed in a receiver OFDM modem using an inverse process to that of the transmitter. In addition to the OFDM modem similar to that shown in Fig.2.3, a number of other key optical components including E/O converters, optical fibres and O/E converters are also involved in typical OOFDM transmission systems.

OOFDM has a number of inherent and unique advantages including [10], for example, great potential for providing cost-effective technical solutions through fully exploiting the rapid advances in modern DSP technology and considerable reduction in optical network complexity owing to its excellent resistance to dispersion impairments as well as adaptive and efficient utilization of channel spectral characteristics. Therefore, OOFDM has attracted extensive R&D interest in the recent years.

2.3.1 Coherent OOFDM and IMDD OOFDM

In this section, discussions are made of two types of widely investigated OOFDM techniques: coherent OOFDM [11] and IMDD OOFDM [10, 12]. In coherent OOFDM, E/O (O/E) conversion is realized by coherent modulation (detection) using I/Q modulators (I/Q detectors); whilst in IMDD OOFDM, E/O (O/E) conversion is performed by intensity modulation (direct detection) using intensity modulators (photodetectors). Apart from coherent OOFDM and IMDD OOFDM, coherent modulation and direct detection has also been reported [5], which offers higher (lower) transmission capacity, increased (decreased) system complexity and cost when compared to IMDD OOFDM (coherent OOFDM) [5, 13]. The corresponding transceiver architecture can be easily understood, based on the descriptions detailed below.

2.3.1.1 Coherent OOFDM

Coherent OOFDM was first proposed by [14], which, in theory, can offer unlimited dispersion tolerance and high spectral efficiency, but requires high complexity in

transceiver design. Therefore, coherent OOFDM is also a promising solution for long-haul transmission systems. Recently, 1 Tb/s single-channel coherent OOFDM transmission over 600 km SMF links has been achieved using orthogonal band multiplexing [15]. In addition, 13.5 Tb/s no-guard-interval coherent OOFDM signal has been successfully demonstrated experimentally over 6248 km using the WDM technique [16]

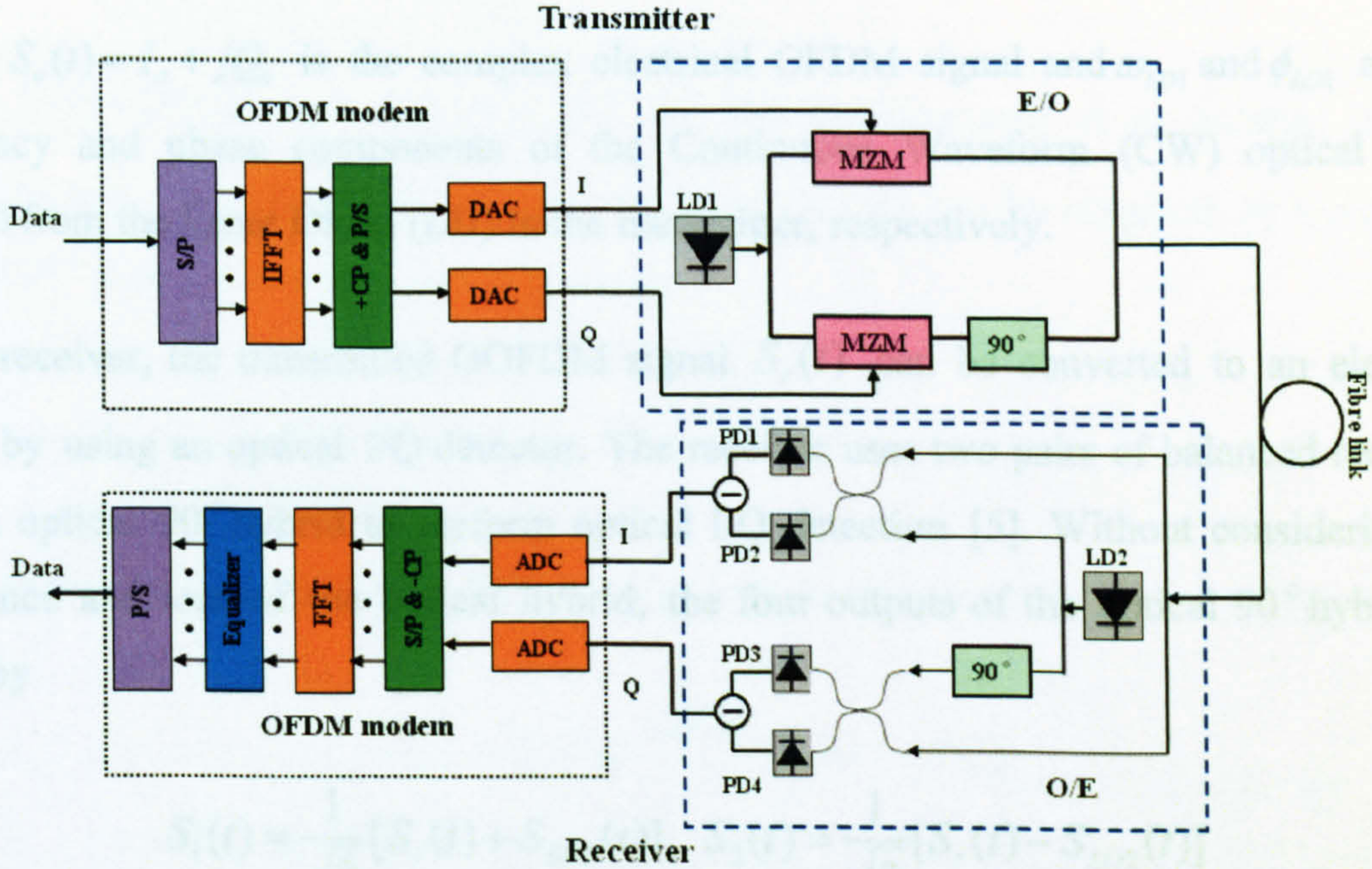

Fig.2.9 System diagram of coherent OOFDM. LD: laser diode; PD: photodetector; E/O: electrical-to-optical conversion; O/E: optical-to-electrical conversion, I: in-phase components of the OFDM signal; Q: quadrature components of the OFDM signal.

In a typical coherent OOFDM transmission system shown in Fig.2.9, an electrical OFDM signal emerging from the transmitter OFDM modem has complex values, whose in-phase and quadrature components are denote as I_a and Q_a. To perform E/O conversion, an optical I/Q modulator is utilized, which consists of two Mach-Zehnder Modulators (MZMs) to up-convert the I_a and Q_a from the electrical domain to the optical domain. Each MZM is respectively driven by I_a or Q_a and the resulting OOFDM signal can be expressed as

$$S_{opt}(t) = I_{opt} + jQ_{opt} \tag{2.16}$$

where I_{opt} and Q_{opt} are in-phase and quadrature components of the OOFDM signal.

It is worth mentioning that I_a and Q_a can be linearly converted into I_{opt} and Q_{opt} if MZMs are biased at a current corresponding to the half-wave switching current of the MZMs [11]. The resulting OOFDM signal $S_{opt}(t)$ thus can be expressed as

$$S_{opt}(t) = S_a(t)e^{j\omega_{LD1}t+\phi_{LD1}} \tag{2.17}$$

where $S_a(t) = I_a + jQ_a$ is the complex electrical OFDM signal and ω_{LD1} and ϕ_{LD1} are the frequency and phase components of the Continuous Waveform (CW) optical wave emitted from the Laser Diode (LD) in the transmitter, respectively.

In the receiver, the transmitted OOFDM signal $S_r(t)$ can be converted to an electrical signal by using an optical I/Q detector. The receiver uses two pairs of balanced receivers and an optical 90° hybrid to perform optical I/Q detection [5]. Without considering the imbalance and loss of the optical hybrid, the four outputs of the optical 90° hybrid are given by

$$\begin{aligned} S_1(t) &= \frac{1}{\sqrt{2}}[S_r(t)+S_{LO2}(t)],\ S_2(t) = \frac{1}{\sqrt{2}}[S_r(t)-S_{LO2}(t)] \\ S_3(t) &= \frac{1}{\sqrt{2}}[S_r(t)-jS_{LO2}(t)],\ S_4(t) = \frac{1}{\sqrt{2}}[S_r(t)+jS_{LO2}(t)] \end{aligned} \tag{2.18}$$

where $S_{LO2}(t)$ is the CW optical wave emitted from LD2 with ω_{LD2} and ϕ_{LD2} being its frequency and phase components. For the purpose of recovering I_a in the transmitter, a pair of photodetectors is required to perform square-law photon detection of $S_1(t)$ and $S_2(t)$, respectively. The resulting photocurrents $I_1(t)$ and $I_2(t)$ are written as

$$I_1(t) = |S_1(t)|^2 = \frac{1}{2}\{|S_r(t)|^2 + |S_{LO2}(t)|^2 + 2\mathrm{Re}[S_r(t)S_{LO2}^*(t)]\} \tag{2.19}$$

$$I_2(t) = |S_2(t)|^2 = \frac{1}{2}\{|S_r(t)|^2 + |S_{LO2}(t)|^2 - 2\mathrm{Re}[S_r(t)S_{LO2}^*(t)]\} \tag{2.20}$$

with * denoting the complex conjugate operation.

The in-phase component of the OFDM symbol can be obtained using

$$I_{a\_r} = I_1(t) - I_2(t) = 2\,\mathrm{Re}[S_r(t)S^*_{LO2}(t)] \tag{2.21}$$

Similarly, the quadrature component of the OFDM symbol can be recovered using a similar process, which can be expressed by

$$Q_{a\_r} = I_3(t) - I_4(t) = 2\,\mathrm{Im}[S_r(t)S^*_{LO2}(t)] \tag{2.22}$$

where $I_3(t) = |S_3(t)|^2$ and $I_4(t) = |S_4(t)|^2$ are the photocurrents from another pair of photodetectors. Therefore, the complex electrical OFDM can be obtained by combining I_{a_r} and 90° phase shifted Q_{a_r} and is given by

$$S_{a\_r} = I_{a\_r} + jQ_{a\_r} = 2S_r(t)S^*_{LO2}(t) \tag{2.23}$$

Based on Eq.(2.12, 2.17) and Eq.(2.23), S_{a_r} can be expressed as

$$S_{a\_r} = S_a(t)e^{j\Delta\omega t+\Delta\phi} \otimes h(t) + n(t) \tag{2.24}$$

with $\Delta\omega = \omega_{LD1} - \omega_{LD2}$ and $\Delta\phi = \phi_{LD1} - \phi_{LD2}$ being the frequency and phase difference between the LD1 and LD2 in the transmitter and receiver, respectively. Compared with $S_a(t)$ in the transmitter, S_{a_r} is linearly scaled and thus fibre dispersion effects can be fully compensated theoretically with frequency domain equalization after FFT as well as cyclic prefix. The frequency offset $\Delta\omega$ shown in Eq. (2.24) should be estimated and compensated through synchronization [11], which can be realized by frequency acquisition and frequency tracking processes described in [5].

2.3.1.2 IMDD OOFDM

Another major type of OOFDM is IMDD OOFDM which was proposed in 2005 [16]. In recent years, extensive investigations of IMDD OOFDM have been undertaken both theoretically and experimentally [10,17]. In particular, the highest ever transmission performance of 11.25 Gb/s OOFDM signals over 25km SMFs has been experimentally demonstrated in DML-based end-to-end real-time IMDD OOFDM transmission systems

[10] and more recently, in similar systems, end-to-end real-time symbol synchronization of OOFDM signals encoded using signal modulation format up to 128QAM has also been achieved experimentally [7].

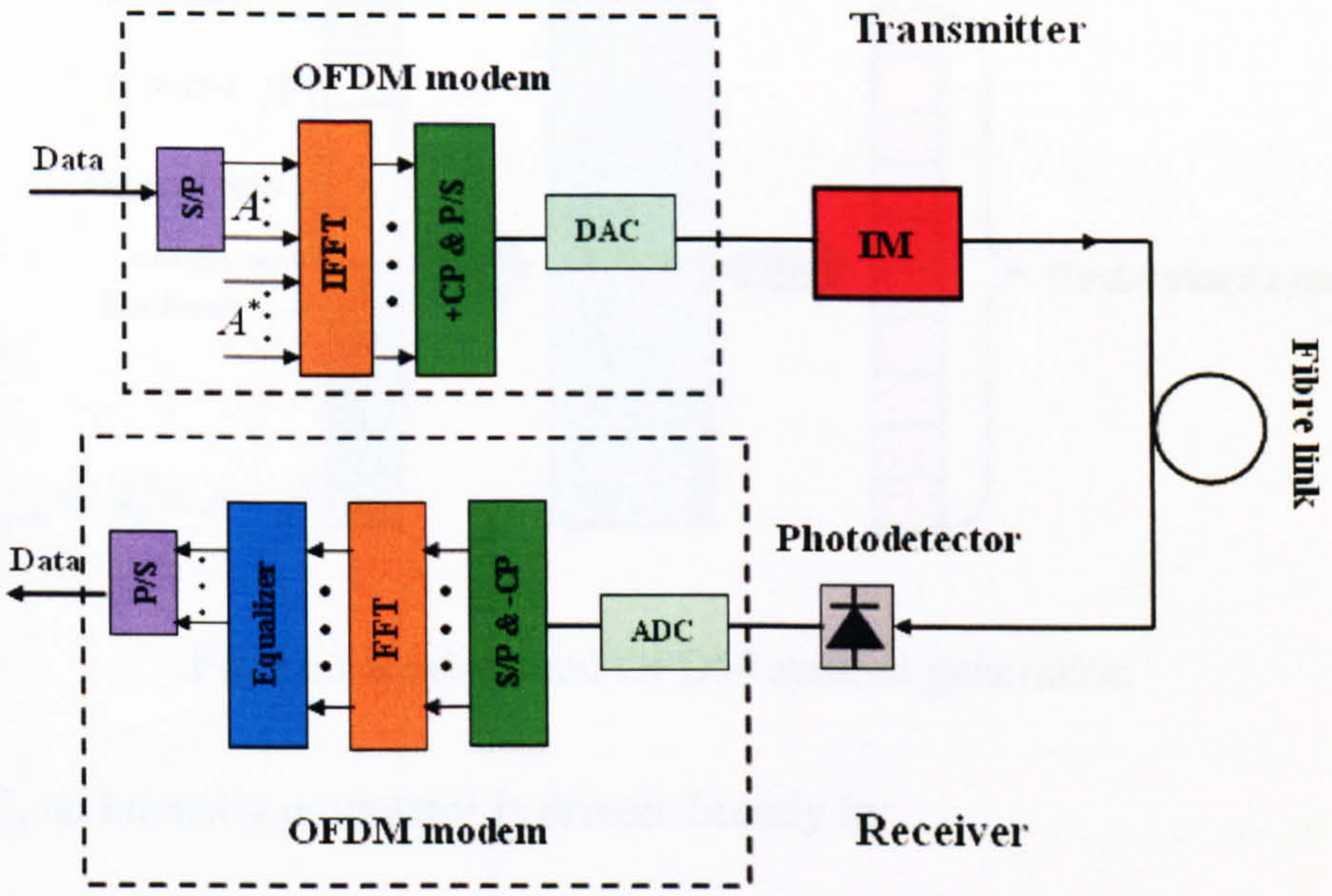

Fig. 2.10 System diagram of the IMDD OOFDM. A : encoded original data; A^* : conjugate counterpart of A ; IM: intensity modulator.

The configuration of a typical IMDD OOFDM transmission system is shown in Fig. 2.10. In comparison with coherent OOFDM, the major differences are the utilization of low complexity and cost-effective intensity modulators and square-law photodetectors to perform E/O conversion in the transmitter and O/E conversion in the receiver, instead of the I/Q modulator in the transmitter and the I/Q detector in the receiver, as mentioned in subsection 2.3.1. In this section, this IMDD OOFDM system is outlined. Detailed descriptions of IMDD OOFDM systems will be given in Chapter 4, including the key optical components such as optical fibres, photodetectors and intensity modulators, and several challenging issues in such OOFDM systems.

In the IMDD OOFDM transmitter, for the purpose of directly driving an intensity modulator, real-valued OFDM signals are necessary, which can be obtained by arranging the encoded original data (together with a zero-valued first subcarrier) and their conjugate counterparts to satisfy Hermitian symmetry at the input of the IFFT [16], as shown in Fig.2.11. In this figure, N_{sub} is the total number of the subcarriers at the input of IFFT; n is

the index of the subcarrier carrying original data and n =1,2…N_{sub}/2-1; a and b represent the in-phase and quadrature components of A_n, which is the original complex data at the input of IFFT.

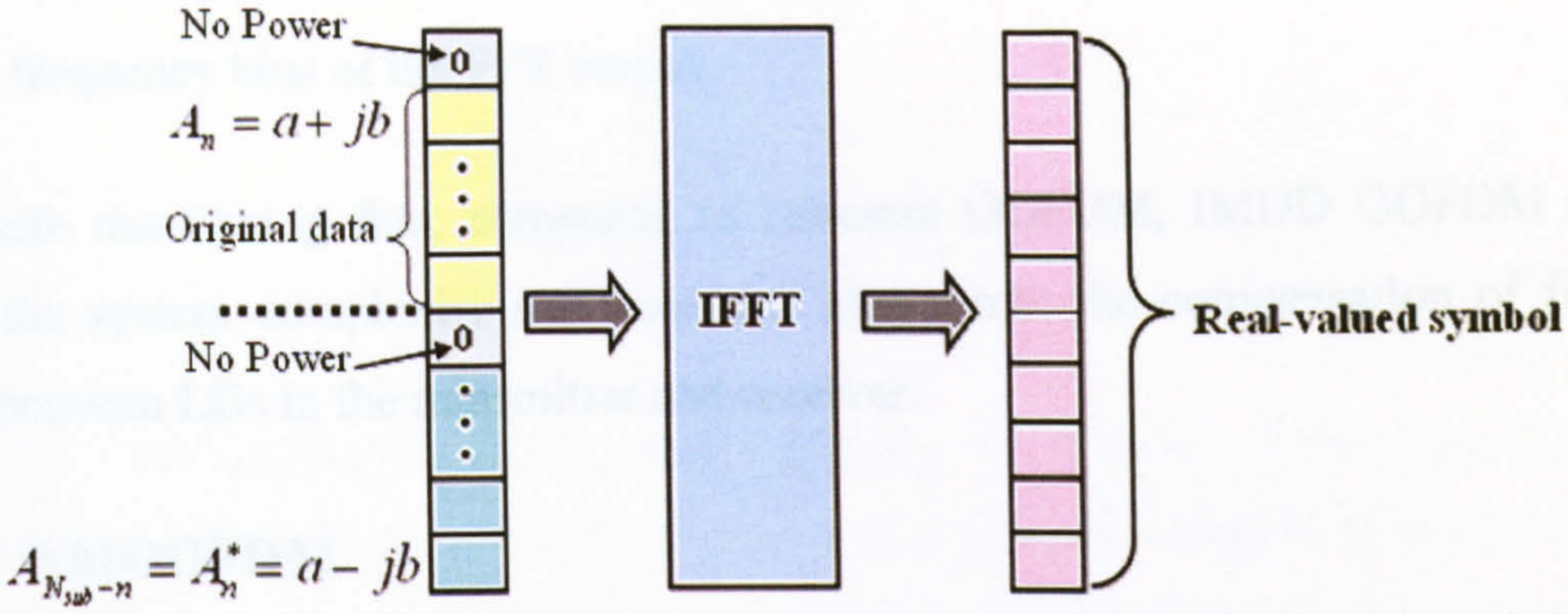

Fig.2.11 Real-valued OFDM symbol generation

After a DAC, an intensity modulator is driven directly by

$$S_e = S_a + I_{DC} \tag{2.25}$$

where S_a is the real-valued electrical OFDM signal emerging from the DAC and I_{DC} is the DC bias current to ensure that S_e is always positive. An optimum driving current is required to ensure that the current locates at a preferred linear amplification region shown in Fig.4.2 of Chapter 4.

If use is made of an ideal intensity modulator, the waveform of the generated OOFDM signal is given by

$$S_o = \sqrt{S_e} \tag{2.26}$$

For a practical intensity modulator such as a DML, direct modulation of a laser driving current introduces a nonlinear frequency chirp to the optical field, thus decreases the dispersion tolerance of the OOFDM technique [18]. Discussion of the DML frequency chirp and its compensation will be given in Chapter 4.

In the receiver, the transmitted OOFDM signal is detected by a square-law photodetector. Such nonlinear detection introduces intermixing impairments and considerably lowers the

transmission performance. The discussions of the direct detection-induced intermixing effect will be given in Chapter 4. After photon detection, the electrical OFDM signal is processed by a receiver OFDM modem, which is the inverse of that of the transmitter. Finally, the received data can be recovered by decoding the complex numbers at the positive frequency bins of the FFT output.

It is worth mentioning that, compared to coherent OOFDM, IMDD OOFDM not only lowers the system complexity and cost, but also omits the compensation of frequency offsets between LDs in the transmitter and receiver.

2.3.1.3 AMOOFDM

In IMDD AMOOFDM using BL [16], the modulation format taken on each individual subcarrier can be varied according to the frequency response of a given transmission link, i.e. a high (low) modulation format is used on a subcarrier experiencing a high (low) Signal-to-Noise Ratio (SNR), as shown in Fig.2.12. Such an adaptive signal modulation capability provides a unique feature for utilizing effectively the frequency response characteristics within the entire transmitted signal spectral region.

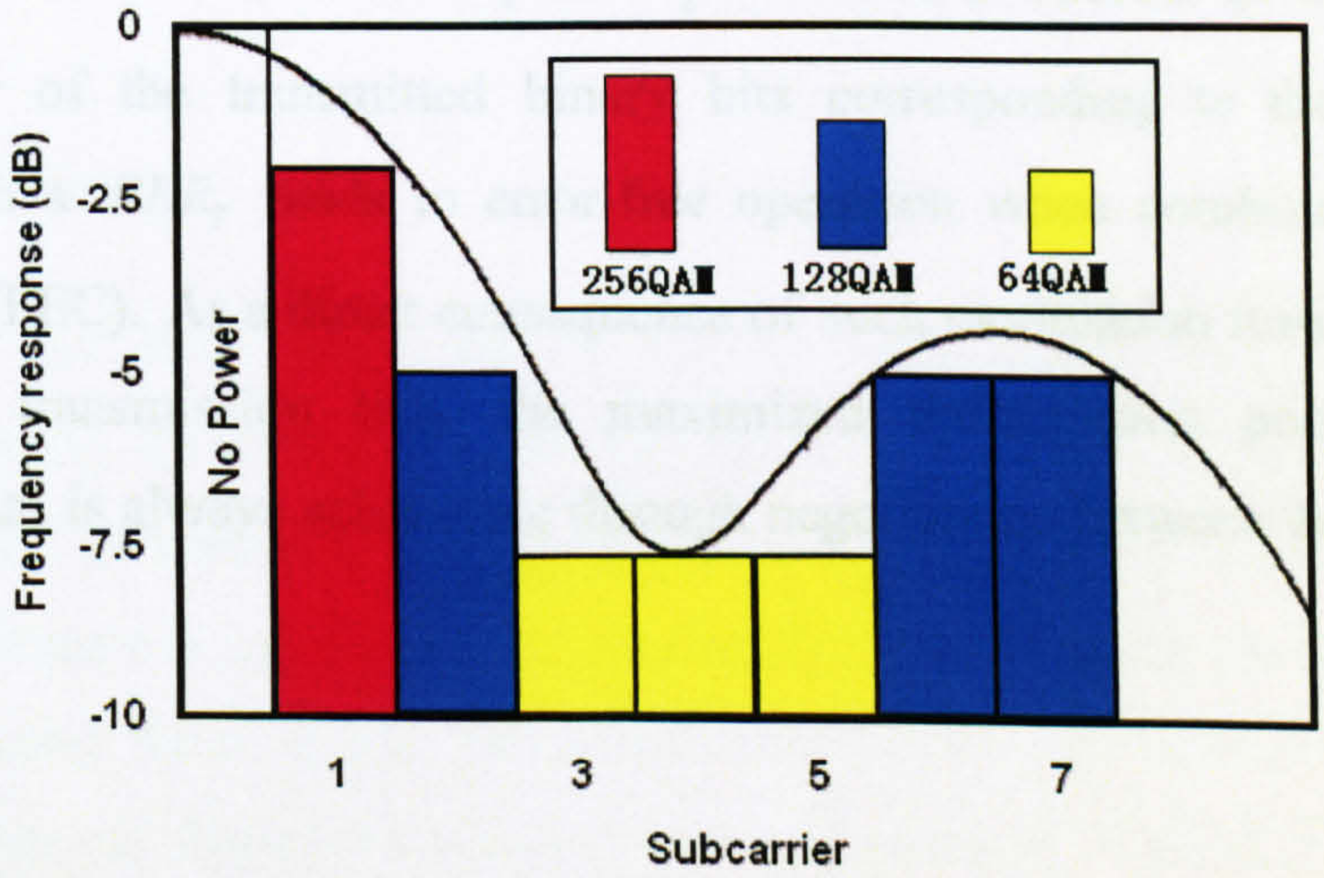

Fig. 2.12 Operating principles of AMOOFDM.

Apart from BL, there are other adaptive loading schemes including Power Loading (PL) and Bit-and-Power Loading (BPL) [19]. Statistical investigations [19] have shown that the BPL (PL) algorithm always offers the best (worst) transmission performance. Moreover, results presented in [10] indicate that the achievable transmission capacity difference between BPL and BL is very small for IMDD SMF links of up to 100km. For example, the

difference is less than about 3.5% at 25km. Also considering the fact that BPL significantly increases the transceiver complexity, only the BL algorithm is utilized in this thesis.

In AMOOFDM, the maximum achievable signal line rate R_s can be expressed as:

$$R_s = \frac{\sum_{k=1}^{N_{sub}/2-1} M_k}{\left(N_{sub} + N_{cp}\right) T_s} \tag{2.27}$$

where M_k is the number of binary bits carried by the k-th subcarrier, N_{sub} is the total number of subcarriers, N_{cp} is the number of sampling periods occupied by the cyclic prefix. M_k, N_{sub} and N_{cp} are taken to be the values for a single AMOOFDM symbol. T_s is the ADC sampling period. R_s is considered to be valid only when the total channel BER (represented by BER_T) defined below,

$$BER_T = \sum_{k=1}^{N_{sub}/2-1} En_k \Big/ \sum_{k=1}^{N_{sub}/2-1} n_k \tag{2.28}$$

remains at 1.0×10^{-3} or better, where En_k and n_k are the total number of the error bits and the total number of the transmitted binary bits corresponding to the k-th subcarrier respectively. Such a BER_T leads to error-free operation when combined with Forward Error Correction (FEC). As a direct consequence of such modulation format manipulation, for an arbitrary transmission link, the maximized transmission performance of an AMOOFDM signal is always achievable through negotiations between the transmitter and receiver.

2.3.1.4 IMDD OOFDM Applications

Based on the discussions of both coherent OOFDM and IMDD OOFDM in subsection 2.3.1.1-2.3.1.3, the major differences between coherent OOFDM systems and IMDD OOFDM systems are summarized in Table 2.1.

Table 2.1

	Coherent OOFDM	IMDD OOFDM
E/O converter	I/Q modulator	Intensity modulator
O/E converter	I/Q detector	Square-law photodetector
OFDM signal	In-phase and quadrature components	Real value
Dispersion tolerance	Unlimited (theoretically)	Limited by DMLs and square-law photon detection*
System complexity and cost	Complex and expensive	Simple and low-cost

* Discussed in Chapter 4 and [20].

Table 2.1 indicates that, compared with coherent OOFDM which is applicable for long-haul transmission, IMDD OOFDM is a very promising solution in cost-sensitive application scenarios including, for example, Local Area Networks (LANs), access networks, and Metropolitan Area Networks (MANs). In the next chapter, the background of access networks especially PONs will be reviewed.

2.4 Conclusion

In this chapter, the basic concepts of OFDM have been discussed briefly. The orthogonality among all subcarriers in OFDM is the major difference compared to conventional FDM. A typical OFDM system has been described, with a number of key transceiver components being discussed including IFFT/FFT, cyclic prefix, DAC/ADC and equalization. Among them, cyclic prefix and equalization are two critical elements for combating the channel dispersive effects. Two categories of OOFDM including coherent OOFDM and IMDD OOFDM are presented and compared. In IMDD OOFDM, a promising BL scheme called AMOOFDM is also described, which can maximize the OOFDM system performance for an arbitrary transmission link. Coherent OOFDM is promising for long-haul transmission systems, while IMDD OOFDM is more competitive in cost sensitive application scenarios such as access networks.

References

[1] R. W. Chang, "Synthesis of band limited orthogonal signals for multichannel data transmission," Bell Syst. Tech. Journal., vol. 45, pp. 1775-1796, Dec. 1966.

[2] H. Liu and G. Q. Li, *OFDM-Based Broadband Wireless Networks: Design and Optimization*, Wiley, 2005.

[3] J. Heiskala and J. Terry, *OFDM Wireless LANs: A Theoretical and Practical Guide*, Sams, 2002.

[4] S. B. Weinstein and P. M. Ebert, "Data transmission by frequency division multiplexing using the discrete Fourier transform," IEEE Trans. Comm. Technol., vol. 19, no. 5, pp. 628-634, Oct. 1971.

[5] W. Shieh and I. Djordjevic, *Orthogonal Frequency Division Multiplexing for Optical Communications*, Academic Press, Inc., 2010.

[6] C. Liu and F. Li, "Spectrum modelling of OFDM signals for WLAN," Electron. Lett., vol. 40, no. 22, pp. 1431–1432, Oct. 2004.

[7] X. Q. Jin, R. P. Giddings, E. Hugues-Salas and J. M. Tang, "Real-time experimental demonstration of optical OFDM symbol synchronization in directly modulated DFB laser-based 25km SMF IMDD systems," Opt. Express., vol. 18, no. 20, pp. 21100-21110, Sep. 2010.

[8] J. M. Tang, P. M. Lane and K. A. Shore, "High-speed transmission of adaptively modulated optical OFDM signals over multimode fibres using directly modulated DFBs," J. Lightw. Technol., vol. 24, no. 1, pp. 429–441, Jan. 2006.

[9] X. Q .Jin, R. P. Giddings and J. M .Tang, "Real-time transmission of 3Gb/s 16-QAM encoded optical OFDM signals over 75km SMFs with negative power penalties," Opt. Express., vol. 17, no. 17, pp. 14574-14585, Aug. 2009.

[10] R. P. Giddings, X. Q. Jin, E. Hugues-Salas, E. Giacoumidis, J. L. Wei, and J. M. Tang, "Experimental demonstration of a record high 11.25Gb/s real-time optical OFDM transceiver supporting 25km SMF end-to-end transmission in simple IMDD systems," Opt. Express., vol.18, no. 6, pp. 5541-5555, Mar. 2010.

[11] W. Shieh, H.Bao and Y. Yang, "Coherent optical OFDM: theory and design," Opt. Express., vol. 6, no.2, pp. 841-859, Jan. 2008.

[12] J. M. Tang and K. A. Shore, "30Gb/s signal transmission over 40-km directly modulated DFB-laser-based single-mode-fiber links without optical amplification and dispersion compensation," J. Lightw. Technol., vol. 24, no. 6, pp. 2318-2327, June. 2006.

[13] W. R. Peng, H. Takahashi, I. Morita, and H. Tanaka, "Transmission of a 213.7-Gb/s single-polarization direct-detection Optical OFDM superchannel over 720-km standard single mode fiber with EDFA-only Amplification," presented at European Conference and Exhibition on Optical Communication (ECOC), (Torino, Italy, 2010), Post-Deadline (PD) Paper PD 2.5.

[14] W. Shieh and C. Athaudage, "Coherent optical orthogonal frequency division multiplexing," Electron. Lett., vol. 42, no. 10, pp. 587-589, May. 2006.

[15] Y. R. Ma, Q. Yang, Y. Tang, S. Chen, and W. Shieh, "1-Tb/s Single-channel coherent optical OFDM transmission with orthogonal-band multiplexing and subwavelength bandwidth access," J. Lightw. Technol., vol. 28, no. 4, pp. 308-315, Feb. 2010.

[16] H. Masuda, E. Yamazaki, A. Sano, T. Yoshimatsu, T. Kobayashi, E. Yoshida, Y. Miyamoto, S. Matsuoka, Y. Takatori, M. Mizoguchi, K. Okada, K. Hagimoto, T. Yamada, and S. Kamei, "13.5-Tb/s (135×111-Gb/s/ch) no-guard-interval coherent OFDM transmission over 6248 km using SNR maximized second-order DRA in the extended-band," OFC/NFOEC, (OSA, 2009), Paper PDPB5.

[17] J. L. Wei, C. Sánchez, R. P. Giddings, E. Hugues-Salas, and J. M. Tang, "Significant improvements in optical power budgets of real-time optical OFDM PON systems," Opt. Express., vol. 18, no. 20, pp. 20732-20745, Sep. 2010.

[18] J. M. Tang and K. A. Shore, "30-Gb/s signal transmission over 40-km directly modulated DFB-laser-based single-mode-fiber links without optical amplification and dispersion compensation," J. Lightw. Technol., vol. 24, no. 6, pp. 2318-2327, June. 2006.

[19] E. Giacoumidis, X. Q. Jin, A. Tsokanos and J. M. Tang, "Statistical performance comparisons of optical OFDM adaptive loading algorithms in multimode fiber-based transmission systems," IEEE Photonics Journal., vol. 2, no. 6, pp. 1051-1059, Dec. 2010.

[20] X. Q. Jin, J. M. Tang, P. S. Spencer and K. A. Shore, "Optimization of adaptively modulated optical OFDM modems for multimode fiber-based local area networks," J. Opt. Netw., vol. 7, no. 3, pp. 198-214, Feb. 2008.

3 PONs

Contents

As mentioned in Chapter 2, IMDD OOFDM is considered to be a strong candidate for practical implementation in NG-PONs. Since detailed discussions of the general background of PONs are essential for gaining an in-depth understanding of the key aspects related to practical applications of the OOFDM technique in NG-PONs, in this chapter, access networks especially PONs are described in detail.

3.1 General Background of Access Networks

In this section, a general telecommunication network architecture is first introduced, followed by discussions of different access networks including Digital Subscriber Lines (DSLs) and PONs. In particular, effort is given to describing PON systems ranging from first generation PONs to NG-PONs.

3.1.1 General Telecommunication Network Architecture

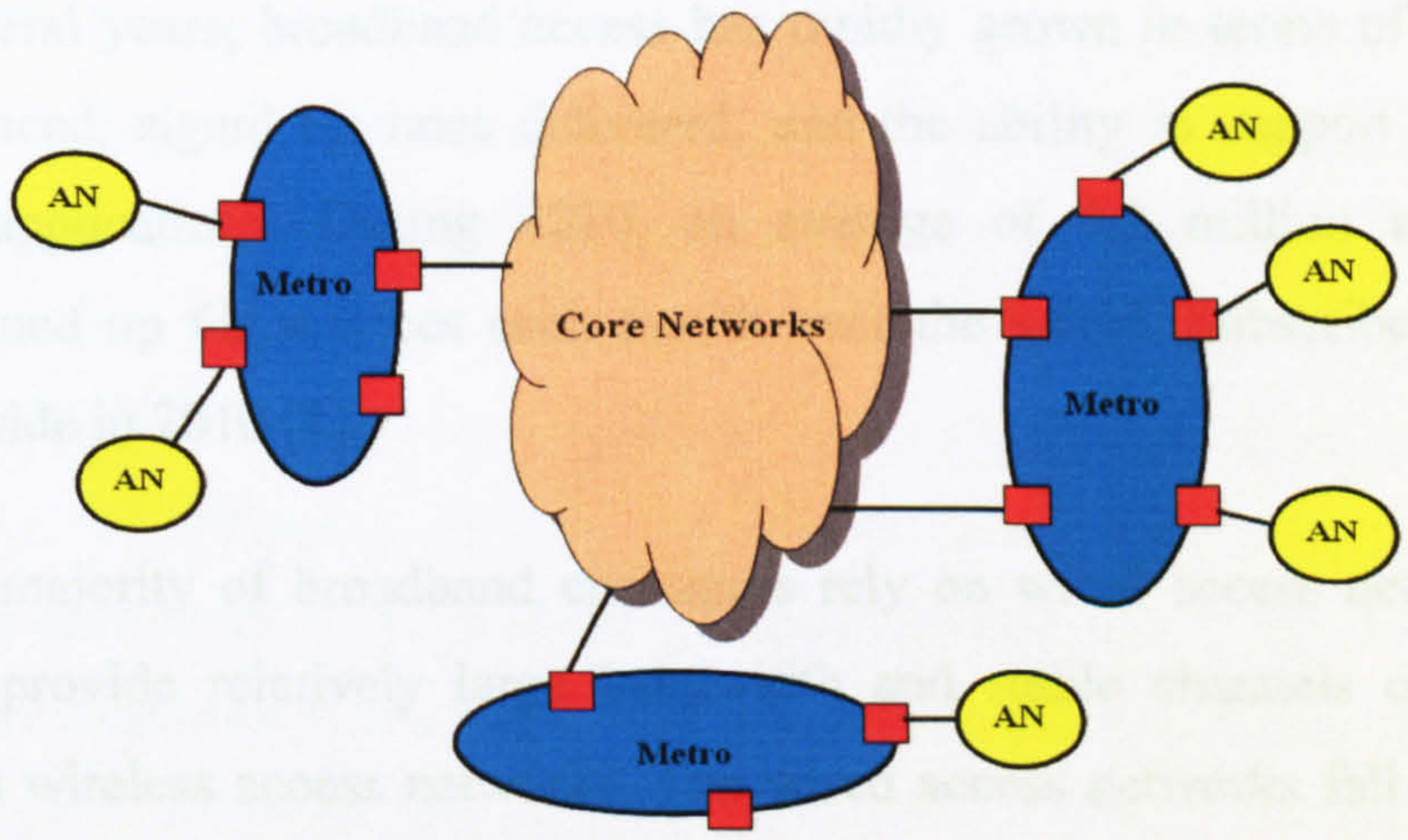

Fig. 3.1 The general structure of telecommunication networks. Metro: metro/regional sub-networks; AN: access networks.

The general telecommunication network architecture is shown in Fig.3.1, which consists of three sub-networks namely core networks, metro/regional networks and access networks. These sub-networks are classified depending on their geographical coverage and are connected with each other by robust physical links.

The core networks are the central parts of the telecommunication networks, and interconnect big cities or major communication hubs and have mesh topologies. A typical

core network can commonly support bandwidth in a Tb/s scale over transmission distances of at least several hundred kilometres [1].

The metro/regional networks are those deployed within smaller geographical areas such as a city and support signal line rates of 10Gb/s over transmission distances of up to 320km [2]. These networks interconnect core networks and access networks, and pass traffic from the core networks to the access networks or backwards.

Located at the edge of the telecommunication networks are the access networks, which deal with the individual end-users such as corporate business units, university departments, medical centres, or private residential users. Compared with the enormous bandwidth provided by the core networks, the existing access networks only support signal line rates of <60Mb/s per user over a transmission distance of up to 20km [3].

3.1.2 Techniques in Access Networks

In the past several years, broadband access has rapidly grown in terms of the number of customers serviced, signal bit rates delivered, and the ability to support a larger set of services and applications. During 2010, an average of 9.2 million new broadband subscribers signed up for services each month over the world. Subscribers reached 763 million worldwide in 2010 [4].

Currently, the majority of broadband customers rely on wired access networks, as such networks can provide relatively large bandwidth and stable channels over time when compared with wireless access networks. The wired access networks fall into two major categories including copper cable-based access networks and optical fibre-based access networks. At present, the most popular wired access networks are copper cable-based access networks using DSL. In 2009, DSL accounted for two-thirds of all broadband deployments [5]. However, optical access networks especially PONs show more competitiveness than DSL, as PONs can offer significantly increased bandwidth over extended transmission distances. Therefore, optical access networks have been considered to be a promising strategy for satisfying the ever increasing end-users' demands. The population of broadband customers relying on optical access networks has undergone a rapid increase in recent years [4-6]. In the following two subsections, both DSL and optical access networks are described with emphasis being given to PONs.

3.1.2.1 DSL

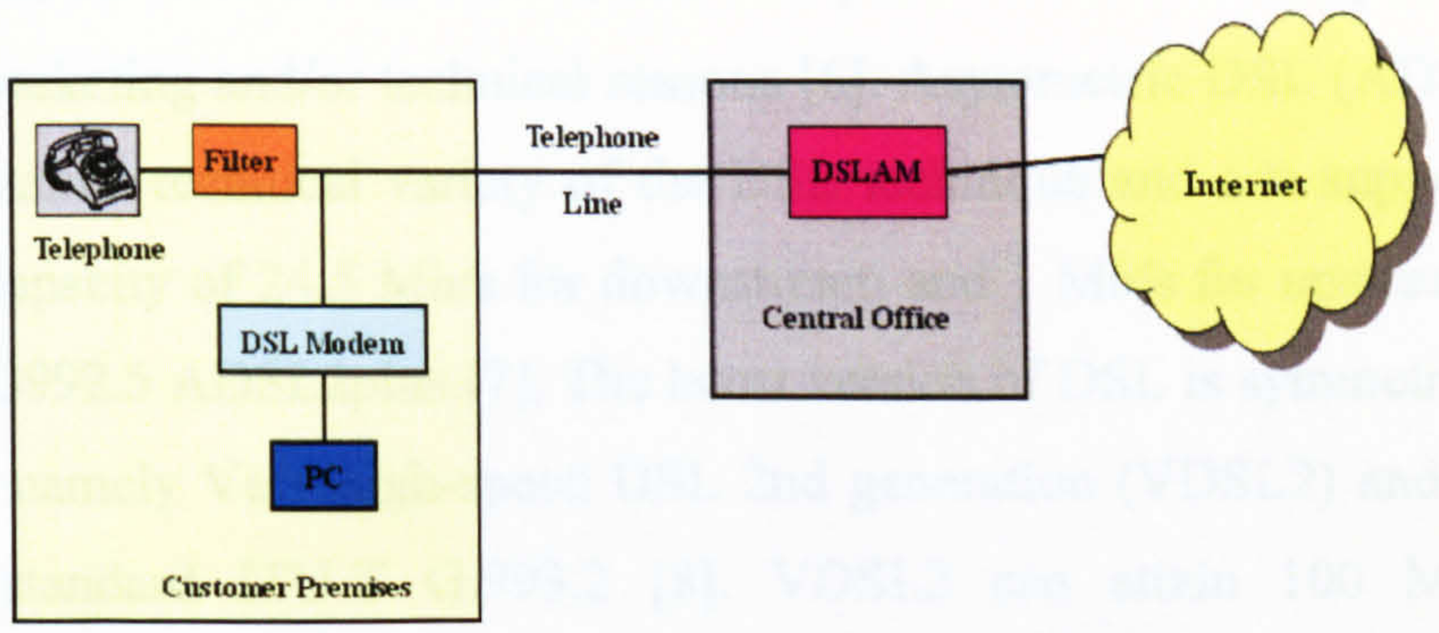

Fig. 3.2 A typical structure of a DSL system. PC: personal computer.

DSL was developed in the 1980s by the telephone industry and is a family of techniques for transmitting digital data over copper wires of local telephone networks. The typical structure of a DSL system is illustrated in Fig.3.2, where a DSL modem is employed at the user end for connecting the customer devices to the Central Office (CO) and a DSL Access Multiplexer (DSLAM) located in the CO is utilized for sending (receiving) the voice signal and digital data to (from) the Internet. In DSL, data service is delivered simultaneously with the voice signal from a regular telephone on the same telephone line. This is achieved using FDM, in which the digital data and voice signals are transmitted in different frequency bands and these frequency bands are subsequently separated by filtering. As shown in Fig.3.3, the frequency band of 0-4 kHz is used for the voice signal, and the frequency band of about 25 kHz-1 MHz is utilized for digital data traffic with 25 kHz-130 kHz for upstream transmission and 140 kHz-1 MHz for downstream transmission.

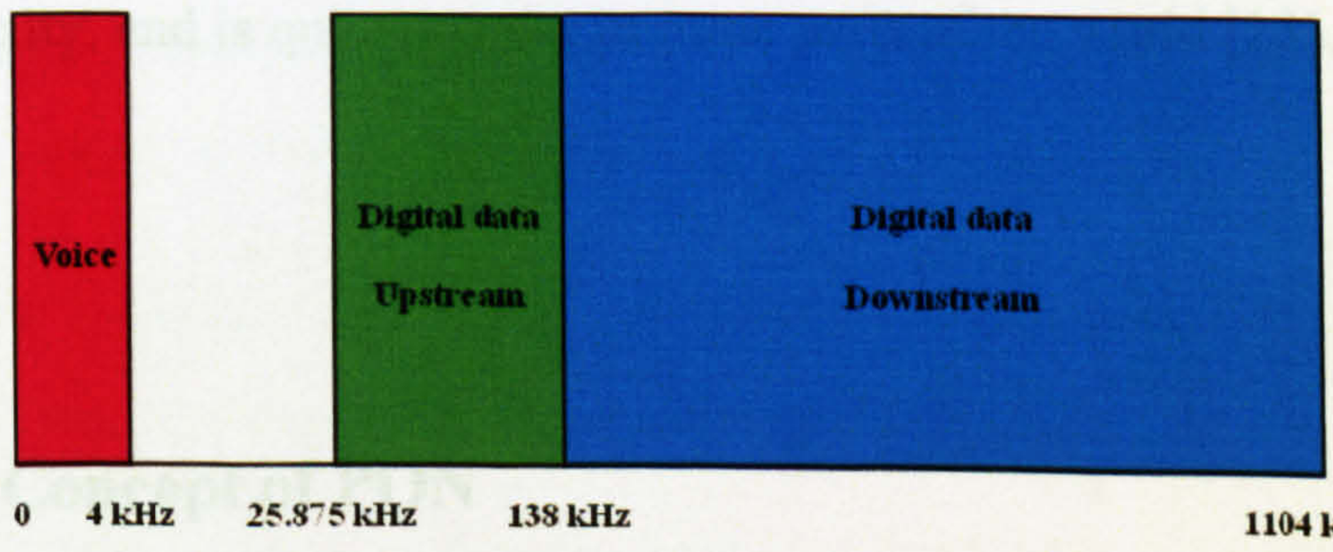

Fig.3.3 Frequency bands of typical DSL systems.

Most DSL is asymmetric in signal line rate, with a higher rate downstream toward a customer and a lower rate upstream backwards. The achievable signal line rates are

determined by many factors: the specific type of DSL employed, the length of the copper wire over which services are delivered, and the specific limitations imposed by a service provider for marketing and/or technical reasons [6]. Asymmetric DSL (ADSL) is the most commonly installed technical variety of the DSL technique and can support a maximum transmission capacity of 24.5 Mb/s for downstream and 1 Mb/s for upstream over 5.5 km as defined in G992.5 ADSL2plus [7]. The latest version of DSL is symmetric in signal line rate, which is namely Very-high-speed DSL 2nd generation (VDSL2) and defined by the international standard ITU-T G.993.2 [8]. VDSL2 can attain 100 Mb/s symmetric transmission speed over about 500m and reduced rates over longer distances [6].

3.1.2.2 Optical Access Networks

It is worth pointing out that DSL is reaching its bandwidth limit and causes the so-called last-mile bottleneck [9]. Fortunately, optical access networks [10] can easily meet and exceed the transmission capacity versus reach target support by DSL, on a per-customer basis, while still offering the capability to evolve in the future to far higher speeds without requiring fundamental changes to network infrastructures [6]. As a promising solution for realizing optical access networks, FTTH has surpassed thirty million users globally in 2009 and is continuing to grow at a rapid rate [11]. This is mainly due to its positive influence on economy, society and environment as well as being a key sustainable utility driver [11,12].

For practical implementation of FTTH, PONs which are based on the point-to-multipoint topology, have been considered as the most competitive technology [6]. It should be noted that the point-to-point topology also has a part to play in terms of bandwidth per user and network complexity, and is quite popular in some parts of the world [13].

3.2 PONs

3.2.1 Basic Concept of PON

PONs are the optical networks which physically employ a point-to-multipoint topology to maximize the coverage, and no active power-consuming elements are deployed in the signal path from the source to the destination [3,10].

A representative PON system is shown in Fig.3.4, which consists of a CO node referred to as an Optical Line Termination (OLT), a number of user nodes referred to as Optical Network Units (ONUs), and the fibres and splitter/combiner between them. The section between OLT and ONUs is referred to as the Optical Distribution Network (ODN) [3]. It can be seen that a single fibre carries all traffic from OLT to an ODN which feeds the individual short branching fibres to ONUs.

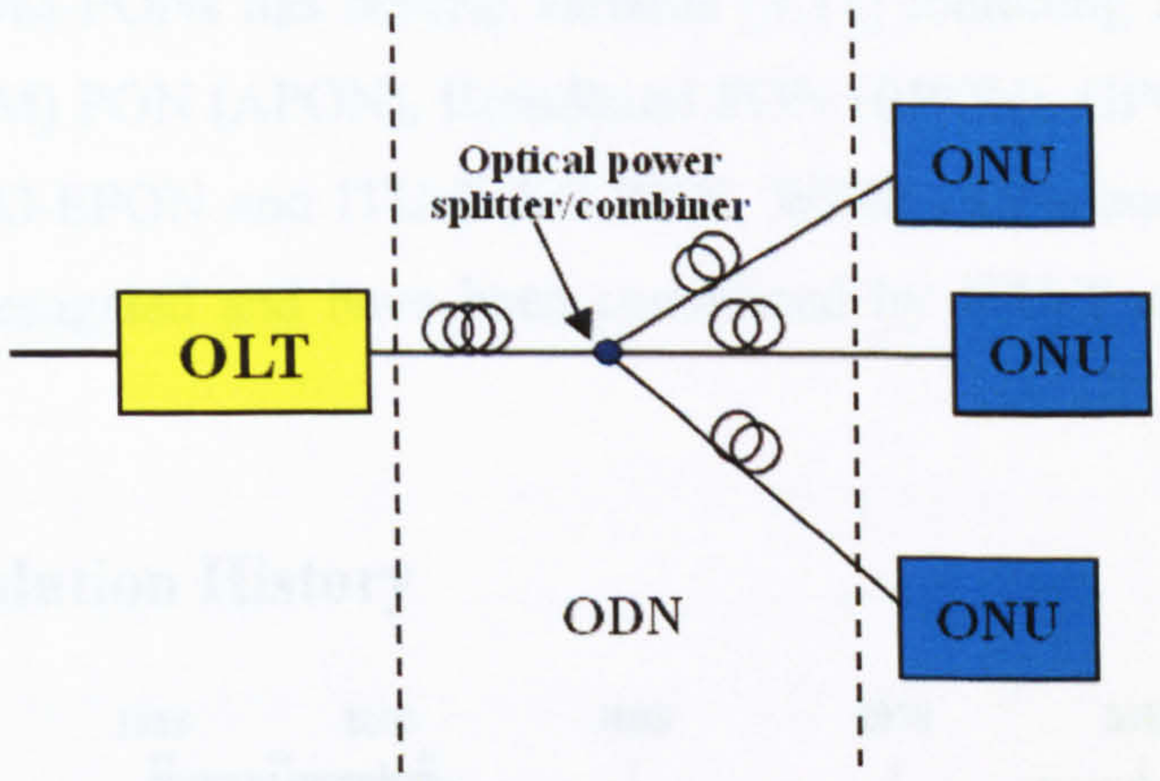

Fig.3.4 Typical PON structure.

The PON has a number of salient advantages including:

(1) The elimination of active optoelectronic and electronic devices located in a cabinet in the harsh outside environment, leading to low maintenance cost and better system performance stability [6].

(2) Low power consumption (almost 50% reduction in lifetime emission) due to the exclusion of active power-consuming elements, which is highly beneficial for the ever-increasing global energy consumption [11].

(3) Cost-effective (comparable to DSL) by sharing OLT devices, fibre installation and maintenance cost amongst a number of end-users [11].

For designing and developing a PON system, several crucial parameters have to be considered including signal line rate, transmission distance/reach, wavelengths for downstream and upstream, split ratio and optical power budget. The optical carriers at the wavelengths defined in a specific PON standard are used for carrying downstream and upstream traffic separately [11]. The split ratio is closely related with the number of

subscribers supported by a single OLT. In addition, the signal line rate, reach and split ratio are also limited by the optical power budget.

Due to its point-to-multipoint architecture, multiplexing techniques are required to provide the multiple-access capability in PONs [3]. According to different types of multiplexing techniques, a number of PON architectures have been investigated, including TDM-PONs, WDM-PONs and OOFDM-PONs. Existing PONs are overwhelmingly based on the TDM technology. The TDM-PONs has several variants [3,11] including ITU-T Asynchronous Transfer Mode (ATM) PON (APON), Broadband PON (BPON), GPON and IEEE EPON, as well as IEEE 10G-EPON and ITU-T XG-PON. WDM-PONs and OOFDM-PONs are currently being investigated and have been considered by ITU-T as long-term solutions after XG-PON [14].

3.2.2 PON Evolution History

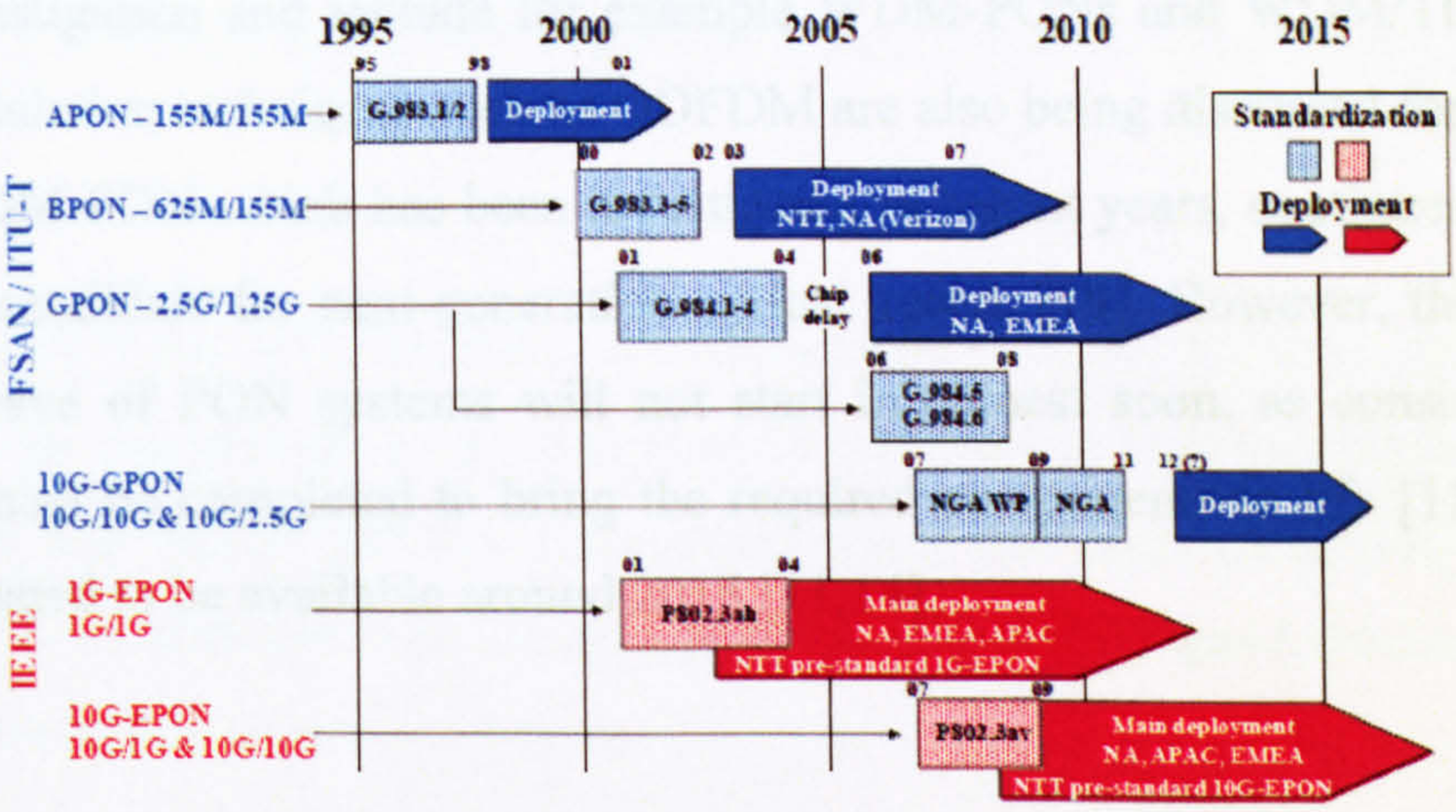

Fig.3.5 Evolution of PON technologies. (from [15])

The evolution of PON technologies is shown in Fig.3.5, together with reference to actual deployments in major global areas. It can be seen in Fig.3.5 that APONs were the first PON standard proposed by ITU G983.1/2 in the middle of 1990s, followed by BPONs which were proposed by G983.3-5 around 2000. APON/BPON only support signal line rates of up to several hundred Mb/s in both downstream and upstream, and thus were deployed on a very small scale.

Present PONs are based on the IEEE 802.3ah EPON and ITU-T G.984 GPON standards, which were proposed around 2001. EPONs are deployed in many Asian countries. In Japan,

the number of EPON users overtook the number of DSL users in March 2008 and has exceeded fifteen million [11]. In the USA and Europe, some companies plan to introduce GPON, but few major carriers have done so yet and carriers are waiting for a market trigger to push them to deploy fibre more widely [11].

The next wave of PONs that will be deployed are those based on 10Gb/s transmission technology. These systems are referred to as NG-PON1 by ITU-T or called 10Gb/s NG-PONs in the open literature [11]. In the IEEE P802.3 family, the new architecture is called 10G-EPON, which was successfully standardized by the IEEE 802.3av task force in September 2009 [11,16]. In the ITU-T SG15 family, XG-PON is currently being standardized by question 2/15 of ITU [11,17,18].

The NG-PON which is beyond 10Gb/s NG-PONs is referred to as NG-PON2 by ITU-T [14]. To enable NG-PON2, new PON systems based on advanced WDM technologies are under investigation and include for example WDM-PONs and WDM/TDM-PONs. Also, novel modulation techniques such as OOFDM are also being discussed for NG-PON2 [14], and OOFDM-PON which has been investigated in recent years, continues to emerge as an attractive candidate for next-generation optical access [19]. However, the standardization for this wave of PON systems will not start in earnest soon, as considerable technical research must be completed to bring the required components to life [11]. The standards are anticipated to be available around 2015 [11,14].

3.3 Different PON Technologies

In this Section, different PON technologies are reviewed in detail. The physical layer, also commonly referred to as the Physical Media Dependent (PMD) layer [20], of the PON systems is the major concern in this section, as the dissertation work presented in Chapter 5-10 are closely related to the PMD layer. Other layers such as Media Access Control (MAC) layer are also of great importance, which are however beyond the scope of the thesis.

3.3.1 TDM-PONs

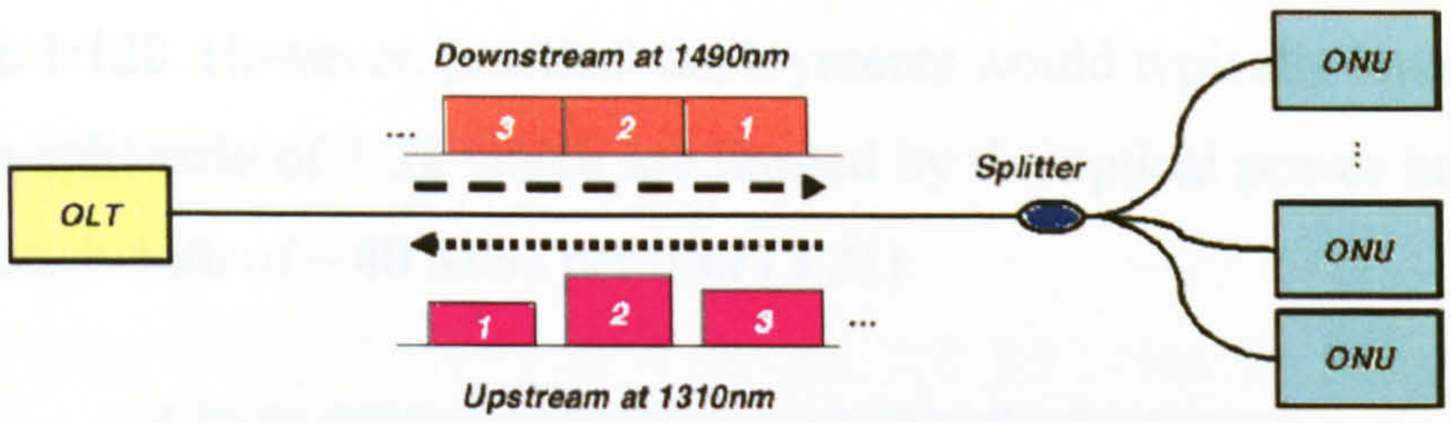

Fig.3.6 A typical structure of a TDM-PON system (from [3])

In Fig.3.6, a typical TDM-PON system is illustrated. Separate wavelength bands with central wavelengths at 1490 nm and 1310 nm are used to carry downstream and upstream traffic, respectively. The downstream traffic is continuously broadcast to all ONUs, and each ONU selects the packets destined to it and discards the packets addressed to other ONUs. In upstream, each ONU transmits data during the time slots that are allocated by the OLT [3]. Different types of TDM-PONs are described in subsection 3.3.2-3.3.4.

3.3.2 APON/BPON

In both APONs and BPONs, their downstream and upstream frames are based on ATM cells. APONs can provide signal line rates of 155Mb/s in both downstream and upstream over 20km, and typical BPONs can support signal line rates of 622Mb/s in downstream and 155Mb/s in upstream over 20km. BPONs are the higher speed versions of APONs and thus only BPONs are reviewed below.

In BPON standards, several power budgets are described and the most common power budget is 28dB which can support a split ratio of up to 1:32. As a result, typical BPONs can only provide a bandwidth of ~ 20Mb/s per user [3]. Also specified in the standards, BPONs use 1260-1360nm for upstream and 1480-1500 nm for downstream, with 1550-1560 nm used for video overlay services.

3.3.3 Present PONs

GPON

ITU-T G.984 GPON is an evolution of the BPON standard [20], which can not only inherit many features of BPON standard such as wavelength plan and power budget, but also support higher signal line rates of 2.488 Gb/s for downstream and 1.244 Gb/s for

upstream [21], as shown in Fig.3.7. Moreover, GPONs support transmission reach of at least 20 km, which can be extended to 60 km. In addition, the split ratio supported by GPONs is up to 1:128. However, practical deployments would typically have a lower reach of 20 km and a split ratio of 1:32 which are limited by the optical power budget, and thus can provide a bandwidth of ~ 40 Mb/s per user [3,21].

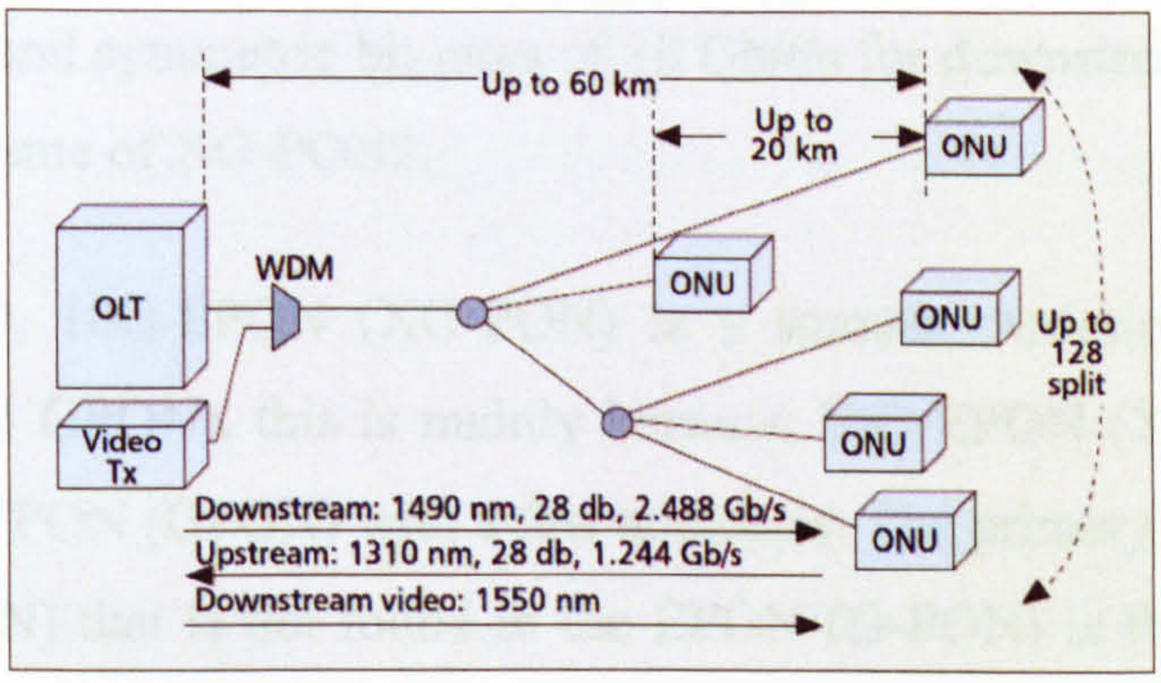

Fig.3.7 Typical structure of GPON system (from [19])

EPON

An EPON is a PON combined with Ethernet protocol and provides bidirectional 1 Gb/s over a transmission distance of up to 20 km by using the entire O-band (1260-1360 nm) for upstream and 1480-1500nm for downstream and reserving 1550 nm for future extensions or additional services such as analog video broadcast [10].

In the IEEE 802.3ah standard EPON, the power budget is conservatively specified as 24 dB with a minimum 1:16 split ratio. In practice, the transceiver technology has matured sufficiently so that components providing 29 dB power budget have become commercially available, resulting in most EPON-based networks being deployed with a split ratio of 1:32, with some being as high as 1:64 [3,10]. The average bandwidth provided to each end-user can be as high as 60 Mb/s.

3.3.4 10Gb/s NG-PON

Although EPON and GPON enable a significant bandwidth boost as compared to copper cable-based access networks, their capacity will be exhausted as soon as bandwidth-hungry applications such as IPTV and peer-to-peer multimedia service become available. To meet the anticipated future demand, the IEEE and ITU-T are actively developing NG-PONs, which target a transmission capacity of 10 Gb/s or beyond.

The first step of NG-PON are the 10Gb/s NG-PONs including 10G-EPON and XG-PON, as mentioned in subsection 3.2.2. IEEE 802.3av defines two types of bit rates for 10G-EPON, including asymmetry bit rates of 10 Gbit/s for downstream and 1 Gbit/s for upstream under the name of PRX, and symmetric bit rates of 10 Gbit/s for downstream and 10 Gbit/s for upstream under the name of PR. Equivalently, ITU-T also defines asymmetric bit rates of 10 Gbit/s for downstream and 2.5 Gbit/s for upstream under the name of XG-PON1, and symmetric bit rates of 10 Gbit/s for downstream and 10 Gbit/s for upstream under the name of XG-PON2.

According to Ref.20, 10G-EPON (XG-PON) is a smooth evolution of IEEE 802.3ah EPON (ITU-T G.984 GPON), this is mainly because 10G-EPON (XG-PON) inherits all the requirements of EPON (GPON) with a few additions. The primary new requirement for 10G-EPON (XG-PON) that is not found in the EPON (G-PON) is that 10G-EPON (XG-PON) must coexist with the EPON (G-PON) in the same ODN [22]. For achieving such a requirement, the wavelength plan is of great importance, which is shown in Fig.3.8 and summarized as below:

Downstream: The L-band (1575-1580 nm) is utilized for both 10G-EPON and XG-PON.

Upstream: the O-minus band (1260-1280 nm) is utilized for XG-PON1 and IEEE 802.3av-PR. The entire O-band (1260-1360 nm) is utilized for IEEE 802.3av-PRX, which is the same as EPON. It is worth mentioning that the upstream wavelength plan for XG-PON2 has not been defined yet but it is expected that XG-PON2 will adopt a similar wavelength plan to XG-PON1.

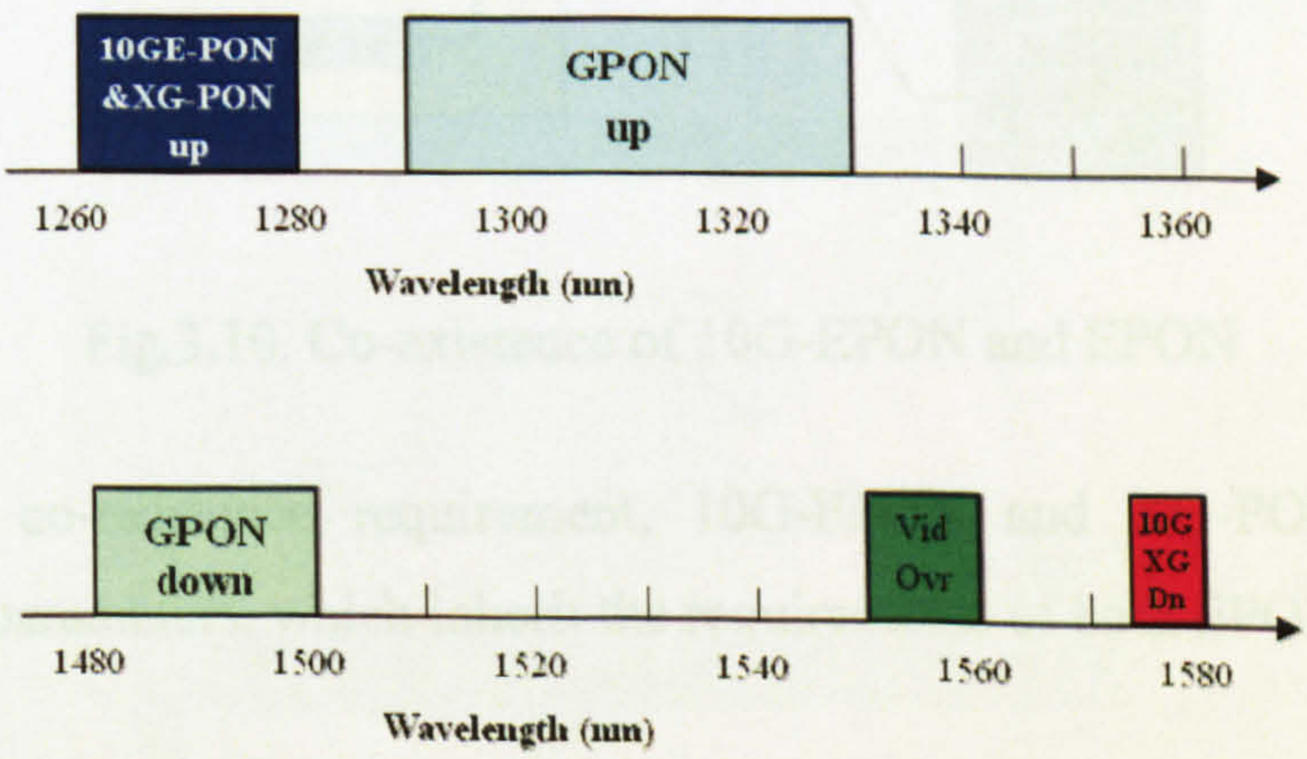

Fig.3.8 The wavelength plan for 10G-class PON system

Based on the above-mentioned wavelength plan, the co-existence of the existing GPONs and XG-PON is achieved by the WDM technique, where the downstream/upstream traffic of the GPONs and XG-PON can be multiplexed and separated easily, as shown in Fig.3.9. For EPON and 10G-EPON, the WDM technique is also used in downstream to separate their traffic. However, in the upstream, the wavelength bands overlap and cannot be separated by the WDM technique. Fortunately, this problem can be accommodated by using a dual rate TDM scheme, in which a dual rate burst mode OLT receiver shown in Fig.3.10 automatically switches between 1Gb/s and 10Gb/s based on the scheduled ONU transmission burst [16].

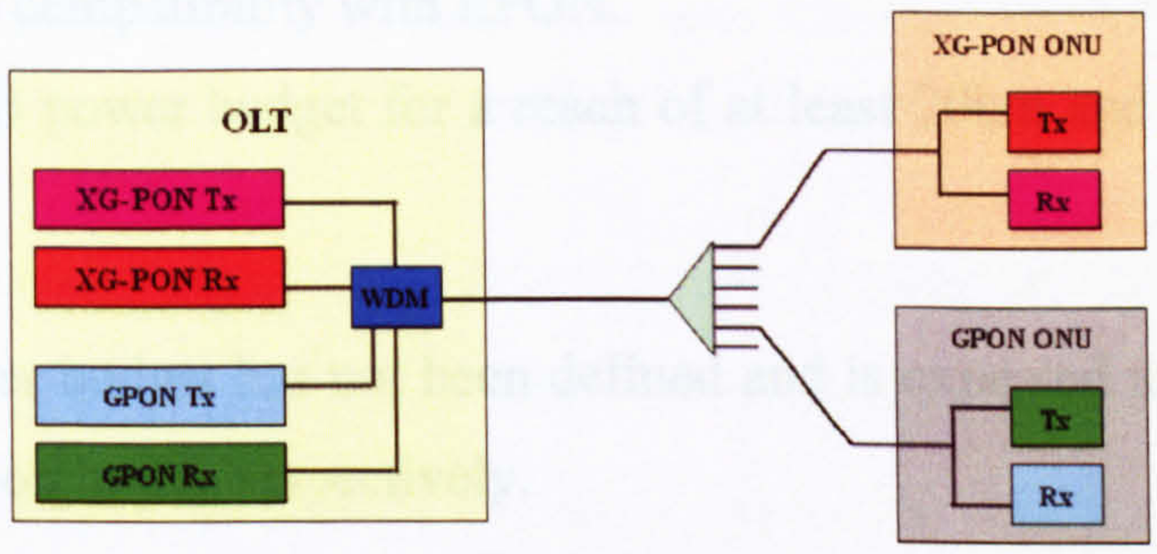

Fig. 3.9 Co-existence of XG-PON and GPON

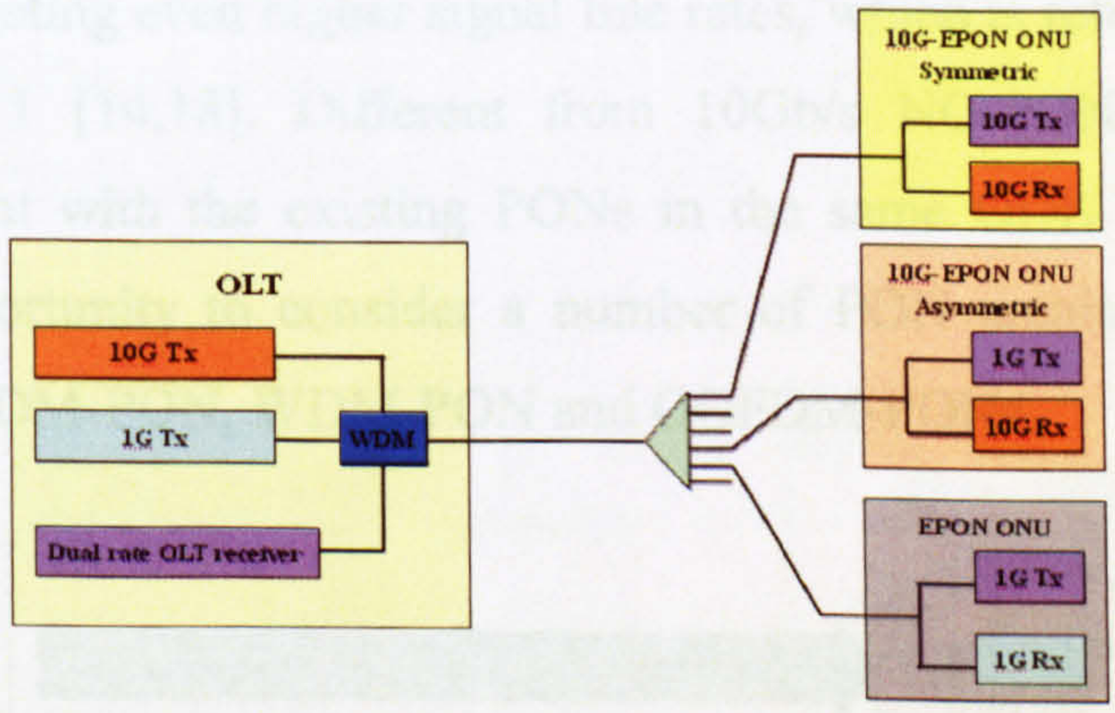

Fig.3.10. Co-existence of 10G-EPON and EPON

Apart from the co-existence requirement, 10G-EPON and XG-PON also have the following major parameters, which inherit the requirements of both EPON and GPON:

10G-EPON

- IEEE 802.3av-PR(X)10: 5-20 dB power budget for a reach of 10 km and split ratio of

at least 1:16.

- IEEE 802.3av-PR(X)20: 10-24 dB power budget for a reach of 20 km and split ratio of at least 1:16.
- IEEE 802.3av-PR(X)30: 15-29 dB power budget for a reach of 20 km and split ratio of at least 1:32; also PR30 assures compatibility with G-PON class B+ infrastructure (13-28 dB).

XG-PON1

ITU-T has identified two power budgets that were considered as "nominal" PON budgets:

- Nominal 1: 29dB power budget for a reach of at least 20km and split ratio of at least 1:64; also assure compatibility with EPON.
- Nominal 2: 31dB power budget for a reach of at least 20km and split ratio of at least 1:64.

XG-PON2: the power budget has not been defined and is expected to be 33 and 35dB for the Nominal 1 and Nominal 2, respectively.

3.3.5 Beyond 10Gb/s NG-PON

In parallel with developing XG-PON, ITU-T also offers a long-term plan beyond the 10Gb/s NG-PON targeting even higher signal line rates, which is referred to as NG-PON2, as shown in Fig.3.11 [14,18]. Different from 10Gb/s NG-PON, NG-PON2 are not necessarily co-existent with the existing PONs in the same ODN [22]. Therefore, NG-PON2 offers an opportunity to consider a number of PON architectures with potential excellence, such as TDM-PON, WDM-PON and OOFDM-PONs.

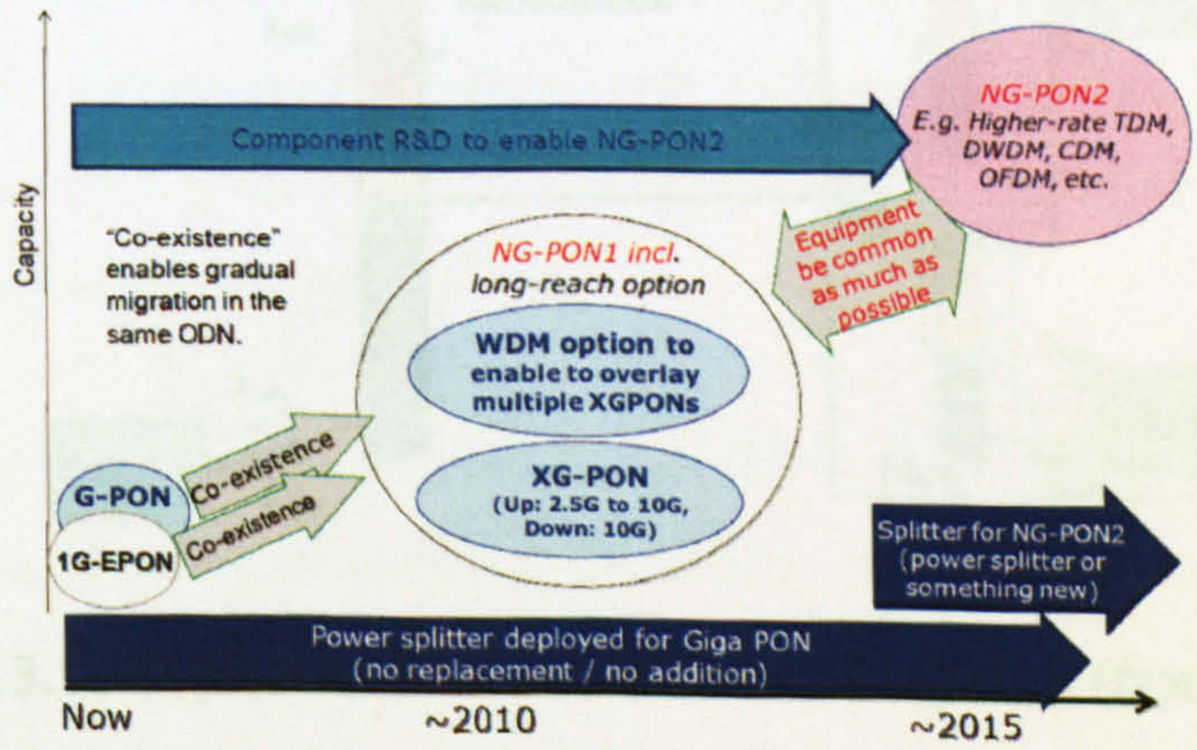

Fig.3.11 Definition of scope of NG-PON (from [14])

Most agree that TDM-PONs cannot cope with the requirements of future access network evolution with respect to aggregated bandwidth [23]. Compared with TDM-PONs, the major advantages of WDM-PONs are that ONUs are assigned individual wavelengths, which enables each ONU to operate on the individual signal line rate rather than the aggregate rate and thus provides higher bandwidth to each ONU. In the next subsection, WDM-PONs and hybrid WDM/TDM-PONs are described.

3.3.5.1 WDM-PON and WDM/TDM-PON

WDM-PON

WDM-PON is generally recognized as a PON in which each ONU uses a different wavelength, i.e. an independent wavelength, in each direction for communication with the OLT. The typical architecture of WDM-PON system is shown in Fig. 3.12.

In the WDM-PON system, ONU k (k = 1 to n) emits an upstream signal with a wavelength λ_{uk} and receives a downstream signal with a wavelength λ_{dk}. To achieve wavelength multiplexing of upstream signals from λ_{u1} to λ_{un} as well as wavelength demultiplexing of downstream signals from λ_{d1} to λ_{dn}, a wavelength splitter/router is used as an optical branching device instead of the power splitter used in TDM-PON systems [24]. In an OLT, there are n interface cards (denoted as IF 1 to n, as shown in Fig.3.12) and point-to-point communication is facilitated between IF k and ONU k logically. Therefore, the WDM-PON system is recognized as a "virtual point-to-point" system [11, 24].

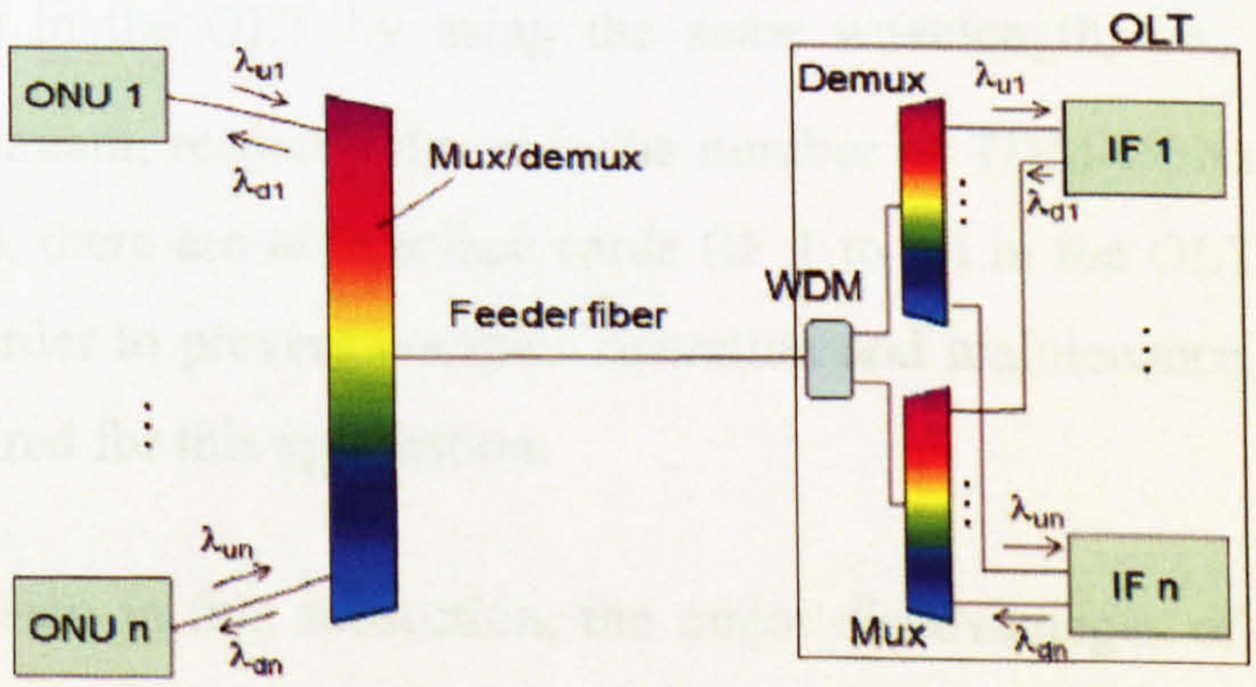

Fig.3.12 Typical structure of WDM-PON system (from [24])

The simplest way of realizing WDM-PONs is to employ a coloured laser in each ONU,

which is however significantly increase the system cost. Therefore, for the recent years extensive investigations have been undertaken on the practical realization of "colourless" ONUs, i.e wavelength-independent ONUs [11,24].

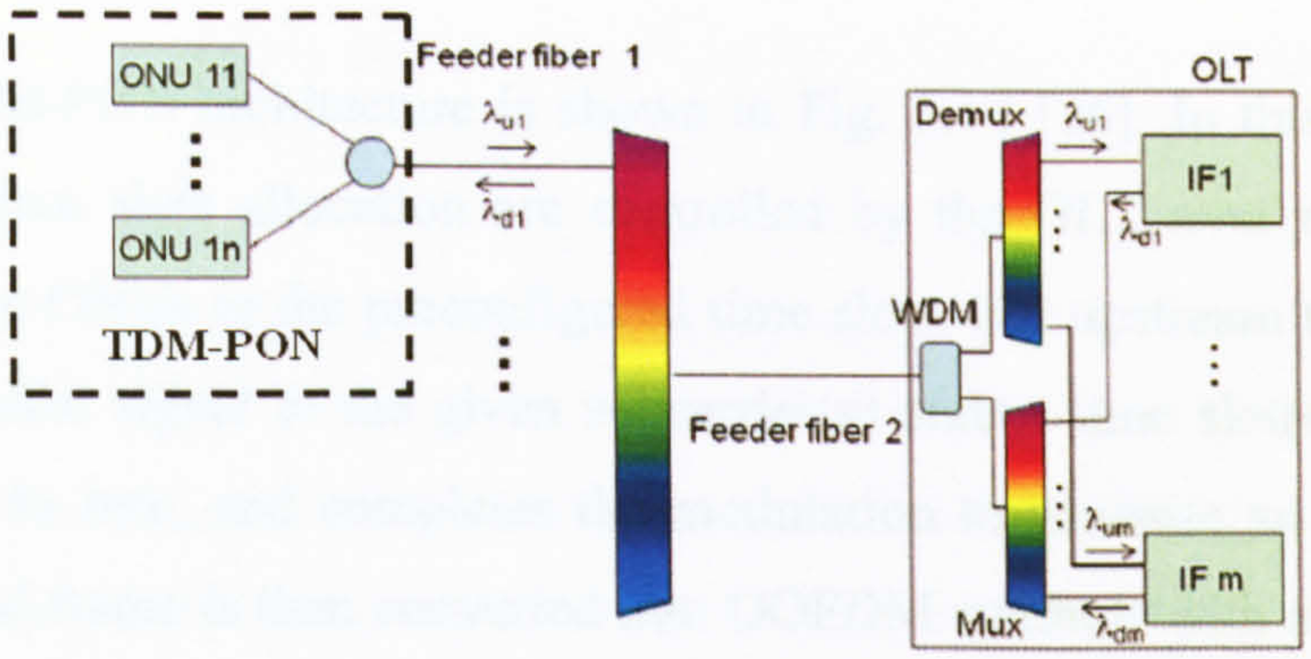

Fig.3.13 Typical structure of WDM/TDM-PON system (from [24])

WDM/TDM-PON

In addition, WDM-PONs can also be combined with additional TDM techniques, in particular those already used by the EPON and GPON standards. This leads to hybrid WDM/TDM-PONs and improves scalability by allowing splitting ratios of up to 1:1000 [23]. The WDM/TDM-PON is generally recognized as a PON in which more than one wavelength is used in each direction for communications between an OLT and a number of ONUs and each wavelength is shared among several ONUs by using the TDM technique. A typical WDM/TDM-PON is shown in Fig. 3.13, in which each TDM-PON uses different wavelength from the others. It can be seen that ONU_{j1} to ONU_{jn} (j=1 to m) access the same interface card (IF j) in the OLT by using the same wavelength, i.e., λ_{uj} and λ_{dj} for upstream and downstream, respectively. m is the number of TDM-PONs stacked/overlaid by WDM. Therefore, there are m interface cards (IF 1 to m) in the OLT side. It is worth mentioning that in order to prevent complex operation and maintenance, colourless ONU technologies are desired for this application.

Based on the discussion in this subsection, the major disadvantages of WDM-PONs are their high system cost and complexity. In addition, WDM-PON lacks the flexibility to dynamically allocate broadband services amongst various end-users. Consequently, a high-speed, cost-effective and highly-flexible PON system such as OOFDM-PONs is of great interest.

3.3.5.2 OOFDM-PON

The OOFDM-PONs can be thought of as a hybrid technique, which can combine pure OFDM [25-28] with TDM, such that the OFDM subcarriers can be dynamically assigned to different services in different time slots (TDM time slots) [25].

A typical OOFDM-PON architecture is shown in Fig. 3.14 [26]. In this architecture, the subcarriers and time slots allocation are controlled by the OLT over non-reserved sub-carriers sent to the ONUs in the preconfigured time slots. For upstream traffic, each ONU maps the data and/or signal to the given subcarrier(s) and/or time slot(s) and sets all the other subcarriers to zero, and completes the modulation to generate an electrical OFDM frame. The OFDM frame is then converted into OOFDM symbols with a low cost DML at different wavelengths following the schedule pre-decided by the OLT and transmitted over fibre. The OOFDM symbols from multiple ONUs are combined at the optical coupler, forming a single OOFDM frame. After transmitted through the ODN, the single OOFDM frame is detected by a single photodetector at the OLT receiver [25,26]. For downstream traffic, the OOFDM frame and other analog signals in OLT are mixed by the electrical coupler to drive the intensity modulator. When the mixed signal reach the ONUs, each ONU picks out its own data or signal from the proper subcarrier(s) and time slot(s).

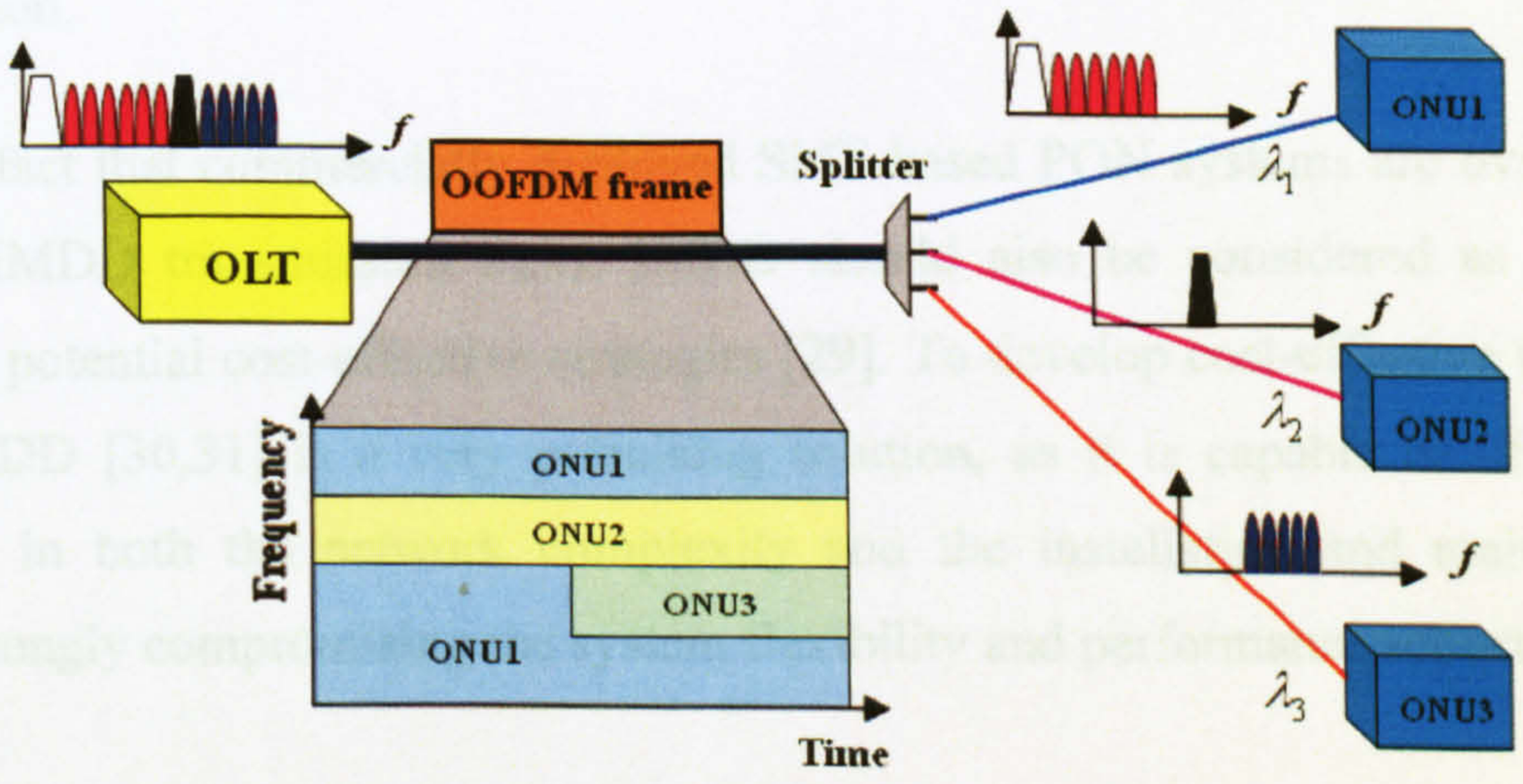

Fig.3.14 The typical structure of OOFDM-PON system (from [26])

Advantages of OOFDM NG-PONs

OOFDM can be regarded as either a modulation technique, or a multiple access technology. As a modulation technique, OOFDM has a number of unique and inherent advantages, including, for example, great potential for providing cost-effective technical solutions

through fully exploiting the rapid advances in modern DSP technology, and considerable reduction in optical network complexity owing to its excellent resistance to dispersion impairments, relatively high transmission speed, large spectral efficiency as well as adaptive and efficient utilization of channel spectral characteristics, as mentioned in Chapter 1 and 2. As a multiple access technology, OOFDM is capable of offering, in both the frequency and time domains, hybrid dynamic allocation of broadband services among various end-users, which not only improves the system flexibility but also can be compatible with existing PON systems in the same ODN.

Apart from the above-mentioned advantages, when use is made of OOFDM in WDM-PONs, OOFDM not only lowers system complexity and cost, but also offers dynamic bandwidth allocation. In addition, OOFDM can provide WDM-PONs with the following advantages:

(1) Spectral efficiency: currently, PONs already have crowded spectra on access fibres; therefore, OOFDM is very promising due to its high spectral efficiency properties.
(2) Bandwidth saving: in WDM-PONs, the bandwidth assigned to an ONU will be wasted if this ONU does not require the services on a specific time slot. However, such a drawback can be overcome by OOFDM, which can offer dynamic bandwidth allocation.

Given the fact that commercially deployed SMF-based PON systems are overwhelmingly based on IMDD transmission links, IMDD should also be considered as an important feature for potential cost-effective strategies [29]. To develop cost-effective OOFDM NG-PONs, IMDD [30,31] is a very promising solution, as it is capable of offering further reductions in both the network complexity and the installation and maintenance cost without strongly compromising the system flexibility and performance robustness.

3.4 Conclusion

In this chapter, a brief introduction to telecommunication networks has first been made, which consists of core networks, metro/regional networks and access networks. Then, two types of access networks including DSL and PONs have been described with effort being given to PONs. The PON evolution history is presented and different PON systems are

described and discussed.

Existing PON systems and 10Gb/s NG-PON are commonly based on the TDM technique, which, however, cannot cope with the requirements of future access network evolution with respect to aggregated bandwidth. Fortunately, these drawbacks can be overcome by WDM-PONs, in which ONUs are assigned individual wavelengths and therefore operate at the individual signal line rate rather than the aggregate rate. The major disadvantages of WDM-PONs are high system cost and complexity, and their lack of the flexibility to dynamically allocate the broadband service among various end-users. Consequently, a high-speed, cost-effective and highly-flexible PON system such as OOFDM-PONs is of great interest. Also, when use is made of OOFDM in WDM-PONs, OOFDM can offer high spectral efficiency and bandwidth saving properties. Furthermore, IMDD is preferable in OOFDM NG-PON, as it is capable of offering further reductions in both the network complexity and the installation and maintenance cost without considerably compromising the system flexibility and performance robustness. Therefore, IMDD OOFDM is a very promising solution for enabling high-speed and cost-effective NG-PON.

References

[1] E. Sasaoka, "Optical fibers for future high capacity networks," presented at OptoElectronics and Communications Conference (OECC), (Sapporo, Japan, 2010), Paper 8C4-4.

[2] H. S. Chung, Y. G. Jang, Y. C. Chung, "Directly modulated 10-Gb/s signal transmission over 320 km of negative dispersion fiber for regional metro network," IEEE Photon. Technol. Lett., vol. 15, no. 9, pp. 1306-1308, Sep. 2003.

[3] Leonid G. Kazovsky, Wei-Tao Shaw, D. Gutierrez, N. Cheng, and Shing-Wa Wong, "Next-generation optical access networks," J. Lightw. Technol., vol. 25, no. 11, pp. 3428-3442, Nov. 2007.

[4] Global broadband subscribers reached 763 million in 2010, available at http://www.circleid.com/posts/global_broadband_subscribers_reached_763_million_2010/.

[5] Next generation broadband access white paper, available at http://www.broadband-forum.org .

[6] P. W. Shumate, "Fiber-to-the-home: 1977-2007," J. Lightw. Technol., vol. 26, no. 9, pp. 1093-1103, May. 2008.

[7] ITU-T Recommendation G.992.5 series, "Asymmetric digital subscriber line (ADSL) transceivers – extended bandwidth ADSL2 (ADSL2plus)," 2009.

[8] ITU-T Recommendation G.993.2, "Very high speed digital subscriber line transceivers 2 (VDSL2)," 2006.

[9] P. E. Green, Jr., "Fiber to the home: The next big broadband thing," IEEE Comm. Mag., vol. 42, no. 9, pp. 100–106, Sep. 2004.

[10] IEEE Standard 802.3ah, "Carrier sense multiple access with collision detection (CSMA/CD) access method and physical layer specifications amendment: media access

control parameters, physical layers, and management parameters for subscriber access networks," 2004.

[11] F. J. Effenberger, J-I Kani and Y. Maeda, "Standardization trends and prospective views on the next generation of broadband optical access systems," IEEE J. Select. Area. Comm., vol. 28, no. 6, pp. 773-780, Aug.2010.

[12] FTTH council, Sep 22, 2008, http://www.ftthcouncil.org/en/newsroom/2008/09/22/study-shows-fiber-to-the-home-is-a-green-technology .

[13] D. Nowak and J. Murphy, "FTTH: The overview of existing technologies," in Proc. SPIE Opto-Ireland 2005: Optoelectronics, Photonic Devices, and Optical Networks, (Dublin, Ireland, 2005), vol. 5825, pp. 500-509.

[14] Ericsson White papers: BroadbandFull service broadband with GPON. http://www.ericsson.com/res/docs/whitepapers/Ericsson_GPON_RevA.pdf.

[15] M. Hajduczenia and H. J. A. da Silva, "Next Generation PON Systems – Current Status," presented at the International Conference on Transparent Optical Networks (ICTON), (Munich, Germany, 2009), Paper Tu.B5.2.

[16] IEEE Standard 802.3av, "Carrier sense multiple access with collision detection (CSMA/CD) access method and physical layer specifications amendment: physical layer specifications and management prameters for 10Gb/s passive optical networks," 2009.

[17] ITU-T Recommendation G.987 series, "10Gigabit-capable passive optical networks (XG-PON)," approved by ITU-T and available from November 2010.

[18] J. Kani, F. Bourgart, A. Cui, A. Rafel, M. Campbell, R. Davey, and S. Rodrigues, "Next-generation PON—part I: technology roadmap and general requirements," IEEE Comm. Mag., vol. 47, no. 11, Nov. 2009.

[19] N. Cvijetic, D. Qian and T. Wang, "Recent advances in ultra high-speed OFDMA-PON," presented at OECC (Sapporo, Japan, 2010), Paper 8A4-1 (Invited).

[20] M. Abrams, P. C. Becker, Y. Fujimoto, V. O'Byrne, and D. Piehler, "FTTP deployments in the United States and Japan—equipment choices and service provider imperatives," J. Lightw. Technol., vol. 23, no. 1, pp. 236-246, Jan. 2005.

[21] F. Effenberger, D. Cleary, O. Haran, R. D. Li, M. Oron and T. Pfeiffer, "An Introduction to PON Technologies," IEEE Comm. Mag., vol. 45, no. 3, pp. S17-S25, Mar. 2007.

[22] F. J. Effenberger, "the XG-PON system: cost effective 10Gb/s access," OFC/NFOEC (OSA, 2010), XG-PON Tutorial Paper.

[23] K. Grobe and J.-P. Elbers, "PON in Adolescence: From TDMA to WDM-PON," IEEE Comm. Mag., vol. 46, no. 1, pp. 26-34, Jan. 2008.

[24] J-I Kani, "Enabling Technologies for Future Scalable and Flexible WDM-PON and WDM/TDM-PON Systems," IEEE J. Select. Top. Quantum. Electron., vol. 16, no. 5, pp. 1290-1297, Sep. 2010.

[25] L. Xu, D. Y. Qian, J. Q. Hu, W. Wei, T. Wang, "OFDMA-based Passive Optical Networks (PON)," IEEE/LEOS Summer Topical Meetings (2008), Paper TuE3.1,

[26] D. Y. Qian, J. Q. Hu, P. N. Ji and T. Wang, "10-Gb/s OFDMA-PON for delivery of heterogeneous services", OFC/NFOEC (OSA 2008), Paper OWH4.

[27] N. Cvijetic, D. Y Qian, J. Q Hu, and T. Wang, "Orthogonal frequency division multiple access PON (OFDMA-PON) for colorless upstream transmission beyond 10 Gb/s," IEEE J. Select. Area. Comm., vol. 28, no. 6, pp. 781-790, Aug. 2010.

[28] M. Cvijetic, "Technologies and practical aspects of next generation optical networking," OFC/NFOEC, (OSA, 2009), Paper Tu.B5.1.

[29] J. M. Tang and K. A. Shore, "30Gb/s signal transmission over 40-km directly modulated DFB-laser-based single-mode-fiber links without optical amplification and dispersion compensation," J. Lightw. Technol., vol. 24, no. 6, pp. 2318-2327, June. 2006.

[30] J. L. Wei, E. Hugues-Salas, R.P. Giddings, X.Q. Jin, X. Zheng, S. Mansoor and J.M. Tang, "Wavelength reused bidirectional transmission of adaptively modulated optical OFDM signals in WDM-PONs incorporating SOA and RSOA intensity modulators," Opt. Express., vol. 18, no. 18, pp. 9791-9808, May. 2010.

[31] R. P. Giddings, E. Hugues-Salas, X. Q. Jin, J. L. Wei, and J. M. Tang, "Experimental demonstration of real-Time optical OFDM Transmission at 7.5 Gb/s Over 25-km SSMF

Using a 1-GHz RSOA," IEEE Photon. Technol. Lett., vol. 22, no. 11, pp. 745-747, June. 2010.

4 IMDD OOFDM System

Contents

In this chapter, IMDD OOFDM systems are described in detail. As mentioned in Chapter 2, a representative IMDD OOFDM system consists of an electrical OFDM modem and an IMDD fibre link. The OFDM modem has already been described in Chapter 2. However, the IMDD link which consists of an intensity modulator, an optical fibre and a photodetector [1] has not been discussed in detail yet. Therefore, in this chapter, effort is given to describing these key optical components. In Sections 4.1-4.2, optical fibres and photodetectors are discussed, since they are common to all IMDD links [1]. In Section 4.3, intensity modulators are described with attention being given to DMLs. The descriptions of these optical components not only illustrate their roles in IMDD OOFDM transmission systems, but also provide an in-depth understanding of their impacts on the system performance. Finally, further to the reviews in Chapters 1-3, five challenging issues associated with IMDD OOFDM systems are identified. Successfully solving these challenging issues is greatly beneficial for practical system implementation, as it can provide opportunities of considerably improving the transmission performance of the IMDD OOFDM systems and simultaneously reducing the system complexity and cost.

4.1 Optical Fibre Transmission

The role of optical fibres is to transport the optical signal from transmitter to receiver. Generally speaking, an optical fibre consists of a cylindrical core of silica glass surrounded by a cladding whose refractive index is lower than that of the core. The optical fibre can be commonly classified into two categories: MMFs and SMFs. SMFs have small core diameters and light can propagate in a single mode, whilst MMFs have large core diameters and light can propagate in multiple modes [2]. In MMFs, different modes propagate simultaneously and modal dispersion results in mode delay. This dispersive effect limits the link bandwidth and system performance. As mentioned in [2], the bandwidth×length products of MMFs are limited to several hundred Mb/s·km. Therefore, MMFs are mostly installed in LANs.

In long haul transmission, MANs and access networks, SMFs are the preferred optical transmission medium as modal dispersion can be completely eliminated in SMFs. This is because the energy of the injected pulse is transported in a single mode referred to as the fundamental mode [2]. However, when transmitted through SMFs, the optical signal still

suffers from dispersive effects due to chromatic dispersion.

4.1.1 Chromatic Dispersion

Chromatic dispersion is caused by the frequency dependence of the refractive index of optical fibre. As a result, different spectral components of an optical signal travel at slightly different group velocities and the resulting time delay ΔT for a SMF of length L is given by

$$\Delta T = DL\Delta\lambda \tag{4.1}$$

where D is the dispersion parameter and expressed in units of ps/(km·nm). $\Delta\lambda$ is the variation range of wavelengths emitted by the optical source. In practice, chromatic dispersion is characterized by D, which is defined as

$$D = -\frac{2\pi c}{\lambda^2}\beta_2 \tag{4.2}$$

where β_2 is the Group-Velocity Dispersion (GVD) parameter, c is the velocity of light in vacuum and λ is the central wavelength. D is wavelength dependent and for SSMFs, D is zero near 1310nm and around 17 ps/(km·nm) at 1550nm, as shown in Fig.4.1.

The chromatic dispersion-induced time delay brings about ISI in the received signal and thus imposes limitations for maximum achievable performance of optical communication systems. In a Non-Return to Zero (NRZ)/ Return to Zero (RZ) system for example, the achievable system capacity and reach are constrained by [2]

$$B^2 L \leq \frac{c}{4\lambda^2 D} \tag{4.3}$$

with B being the signal line rate. As an example, for an NRZ system operating at 1550nm, when the signal line rate increases from 1Gb/s to 10Gb/s, the achievable transmission distance is reduced from 1836km to 18km.

In OOFDM systems, the chromatic dispersion-induced ISI and frequency dependent loss effects can be overcome by using cyclic prefix and channel equalization, as mentioned in Chapter 2.

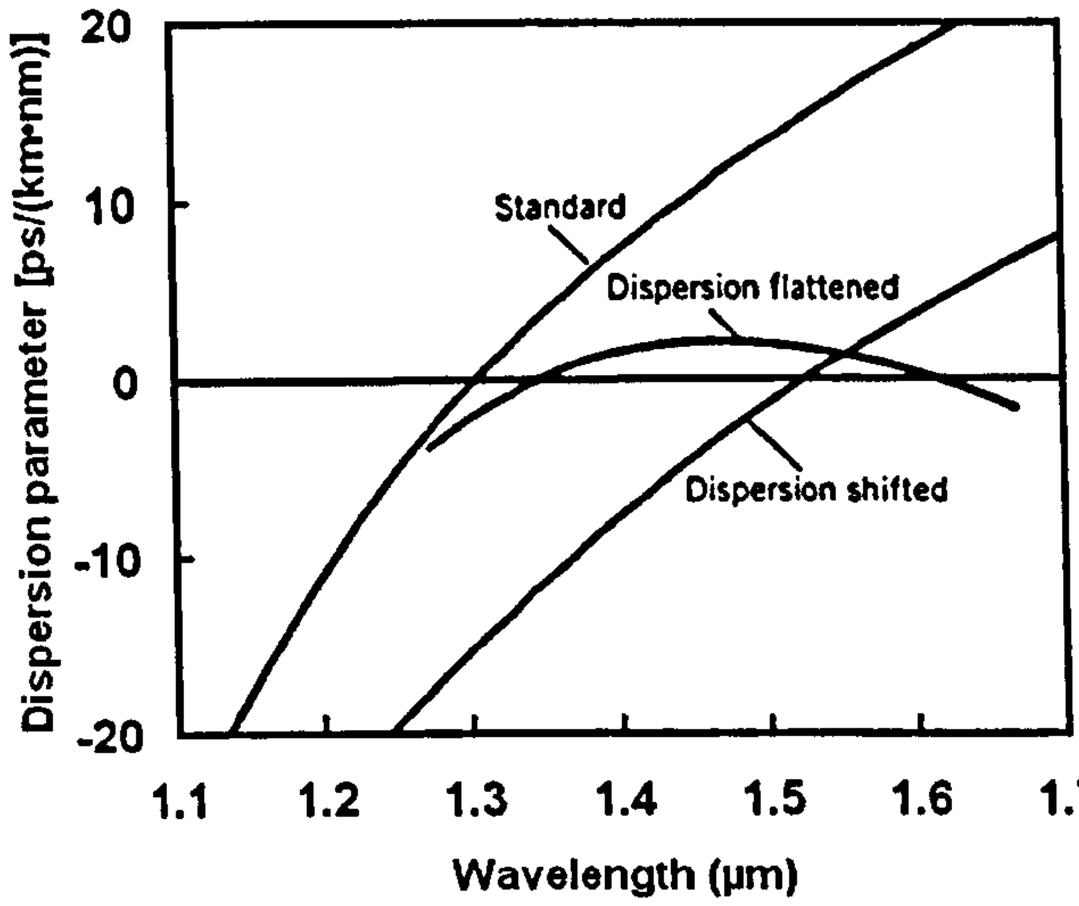

Fig.4.1 Typical wavelength dependence of the dispersion parameter D for standard, dispersion flattened, and dispersion shifted SMFs. (from [2])

4.1.2 Fibre Loss

When transmitted through SMFs, the signal power is attenuated due to fibre loss. The fibre loss can be described by [2]

$$P_{out} = P_{in} 10^{\frac{-\alpha L}{10}} \tag{4.4}$$

where α is the attenuation coefficient and expressed in units of dB/km, P_{in} is the power launched at the input end of a fibre with length L and P_{out} is the power at the output end of the fibre. Several factors contribute to the overall losses, and material absorption and Rayleigh scattering are dominant. Detailed descriptions of these factors can be found in [2,3].

4.1.3 Fibre Nonlinearity

The response of optical fibres to light becomes nonlinear for intense electromagnetic fields, this is known as fibre nonlinearity. Fibre nonlinearity effects affect the power and phase of optical signals when traveling through the SMF.

There are two major categories of optical fibre nonlinearity effects. The first type of nonlinearity effects exhibit energy transfer from the optical field to the medium via a stimulated inelastic scattering processes including Stimulated Brillouin Scattering (SBS)

and Stimulated Raman Scattering (SRS). SBS and SRS result in loss of power and frequency down-shifts to the optical signal and become important once the incident power exceeds their thresholds of typically ~7dBm for SBS and ~27dBm for SRS [2]. However, for the application scenarios of interest in this dissertation, SBS and SRS effects are negligible as optical launch powers used are well below these thresholds. The second type of fibre nonlinearity effects arise due to the dependence of refractive index on intensity of the propagating signal. The most important nonlinear effects in such a category are Self-Phase Modulation (SPM), Cross-Phase Modulation (XPM) and Four-Wave Mixing (FWM).

SPM and XPM

SPM refers to the self-induced phase shift experienced by an optical field during its propagation in optical fibres [3]. Due to the optical intensity dependence of refractive index, the nonlinear phase shift is given by

$$\phi_{NL} = n_2 k_0 L |E|^2 \tag{4.5}$$

where n_2 is the Kerr coefficient, $k_0 = 2\pi/\lambda$ with λ being the central wavelength, L is the fibre length and $|E|^2$ is the optical intensity inside the fibre. The time-dependent phase changes ϕ_{NL} lead to frequency chirp which convert phase shifts to power fluctuations though chromatic dispersion, and finally affect the system performance.

In WDM systems, XPM and FWM can have strong deleterious effects. XPM refers to the nonlinear phase shift of an optical field induced by not only the intensity of that optical field but also the intensity of the fields at other wavelengths [2,3]. When two optical fields E_1 and E_2 at frequencies ω_1 and ω_2 propagate simultaneously inside a fiber, the nonlinear phase shift for the field at ω_1 is given by

$$\phi_{NL} = n_2 k_0 L(|E_1|^2 + |E_2|^2) \tag{4.6}$$

It can be found from Eq.(4.5) and (4.6) that, for optical fields with identical power (E_1=E_2), the contribution of XPM to the nonlinear phase shift is twice that of SPM. Similar to SPM, XPM also introduce power fluctuations as signal propagates along the fibre due to the effect of chromatic dispersion.

FWM

When multiple optical signals at different wavelengths propagate in the fibre, the intensity dependence of refractive index not only induces SPM and XPM on each signal, but also causes these signals to interfere and generate refractive index gratings which interact with the signals and produce new frequencies. This nonlinear process is referred to as FWM. If three optical fields with frequencies ω_1, ω_2, ω_3 co-propagate simultaneously inside the fibre, a fourth field is generated, whose frequency ω_4 is related to other frequencies by a relation $\omega_4 = \omega_1 \pm \omega_2 \pm \omega_3$.

In practice, frequency combinations of the form $\omega_4 = \omega_1 + \omega_2 - \omega_3$ are often troublesome for multichannel communication systems since they can become nearly phase-matched when channel wavelengths lying close to the zero-dispersion wavelength [2]. As the energy of the optical field will flow into the fourth field, FWM results in the power loss for the channel. More seriously, the large combinations of new frequencies generated by FWM lead to either coherent in-band crosstalk or incoherent out-of-band crosstalk, and finally degrade the system performance because of a loss in the channel power.

As single-channel transmission links are utilized in the dissertation, FWM and XPM-induced crosstalk between different frequency channels and/or an imbalance of channel powers are not included, and the following effects are considered including chromatic dispersion, fibre loss and SPM.

4.2 Photodetector

In the receiver, the transmitted optical signal is detected by a photodetector, which converts the optical signal power into an electrical current. The generated photocurrent is proportional to the incident optical power and is given by [2],

$$I_p = RP_{in} = RS_o S_o^* \tag{4.7}$$

where I_p is the photocurrent, P_{in} is the incident optical power, S_o is the received optical signal and R is the responsivity of the photodetector (in units of A/W). In the open literature [4,5], such photon detection is often called direct detection, due to its square-law

operation to the optical field.

In Eq.(4.7) noise free operation is assumed. In practice, the photocurrent is also affected by two types of noises namely shot noise and thermal noise. These noises cause fluctuations in the photocurrent even when the incident optical power is constant. As PIN photodetectors are widely used in cost-sensitive network scenarios such as PONs, the noise associated with PINs are analyzed below.

Shot noise arises from the statistical nature of the generation of photo-electrons when an optical signal is incident on a photodetector. The noise variance (in units of mA^2) is proportional to the photocurrent, which is given by [2]

$$\sigma_s^2 = 2qI_p\Delta f \tag{4.8}$$

where q is the electron charge and Δf is the receiver bandwidth.

Thermal noise is however due to another mechanism detailed as follows: at a finite temperature, electrons move randomly in any conductor; random thermal motion of electrons manifests as a fluctuating current and adds such fluctuation to the photocurrent. The noise variance (in units of mA^2) is given by [2]

$$\sigma_T^2 = 4k_BT\Delta f / R_L \tag{4.9}$$

where R_L is the load resistor.

The total current noise can be obtained by adding the contributions from both shot noise and thermal noise,

$$I = I_p + I_s + I_t \tag{4.10}$$

where I_s and I_t are the current fluctuation induced by shot noise and thermal noise, respectively, which are independent random processes with approximately Gaussian statistics [2]. As a result, the noise lowers the received SNR and thus worsens the BERs in the receiver. To enable the receiver to operate at a BER of 10^{-9}, the received power should be higher than a minimum power which is referred to as the receiver sensitivity. Any

powers below the receiver sensitivity will give rise to a significant degradation of BER performance, which is mainly due to the thermal noise.

4.3 Intensity Modulator and DML

Having described the fibre links and the photodetectors, in this section intensity modulators are discussed in detail.

4.3.1 Basic Concept

The role of the intensity modulator is to convert an electrical OFDM signal into an optical signal, whose intensity consistently varies with the electrical signal, as shown Fig. 4.2.

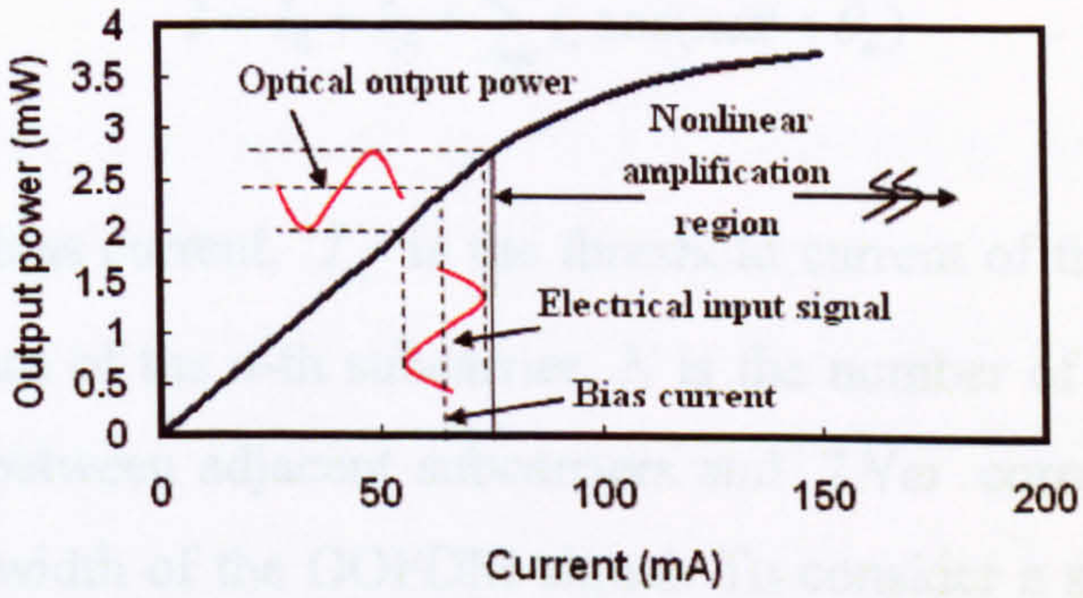

Fig.4.2. Optical output power versus electrical current for intensity modulation.

Generally speaking, intensity modulators can be classified into two main categories including DMLs and external intensity modulators [1,2]. In a DML, the optical output power is modulated by an electrical driving current applied directly to the laser device, whereas in an external intensity modulator, the laser is biased at a constant current to provide the CW output, and an optical modulator placed next to the laser converts the CW light into modulated optical power. Compared to external intensity modulators, DMLs such as DFB lasers can provide many advantages namely, low cost, compactness, low power consumption, relatively small driving voltage and high output power [6]. Therefore, in recent years, there has been a growing interest in utilizing DMLs in cost-sensitive optical access networks such as OOFDM-PONs [6].

4.3.2 Theoretical DML Model and DML Frequency Chirp

It is well known that driving current-induced carrier density modulation in DMLs results in frequency chirp due to residual PM which accompanies the desired intensity modulation. As the characteristics of the laser frequency chirp effect affects the performance of the system [6], detailed investigations of frequency chirp are necessary.

For a better understanding of frequency chirp, in the beginning of this subsection, a simple description based on small signal analysis is firstly given to investigate such an effect [7]. Since the subcarrier number of OFDM signals is large, the duration of an OFDM block is long, for simplicity, each subcarrier can be approximated as a single-frequency carrier. Hence, the modulation current of a DML can be assumed as,

$$I = I_0 + I_{th} + \sum_{n=1}^{N} i_n \cos(n\omega t + \theta_n) \tag{4.11}$$

where $I_0 + I_{th}$ is the bias current, I_{th} is the threshold current of the DML, i_n and θ_n are the amplitude and phase of the n-th subcarrier, N is the number of subcarriers, ω is the frequency difference between adjacent subcarriers and $2N\omega$ corresponds to the Double Sideband (DSB) bandwidth of the OOFDM signal. To consider a simplified DML model without considering nonlinear distortions, the output optical power is represented by $P = \eta(I - I_{th})$, where η is the laser slope efficiency, and I_0 is set to ensure $I_0 + \sum_{n=1}^{N} i_n \cos(n\omega t + \theta_n) > 0$, i.e. no clipping. An additional PM is introduced simultaneously [7]:

$$\frac{d\phi}{dt} = \frac{\alpha}{2P}\frac{dP}{dt} \Rightarrow \Delta\phi = \frac{\alpha}{2}\log P \tag{4.12}$$

where α is the linewidth enhancement factor and $\Delta\phi$ is the variation of optical phase. In Eq. (4.12), the adiabatic frequency chirp is omitted, as the transient frequency chirp dominates the DML chirp characteristics in OOFDM transmission systems, as will be discussed in subsection 4.3.2.2. Therefore, the optical field is given by

$$E = \sqrt{P}e^{-j(\Delta\phi+\varphi)} \tag{4.13}$$

with φ being its constant phase component. Based on the small signal approximation of $i_n << I_0$, the analysis in [7] shows that after square-law direction detection, the recovered OFDM signal is represented by $2\sqrt{1+\alpha^2}\sum_{n=1}^{N} x_n \cos(n^2\theta_D - \theta_\alpha)\cos(n\omega t + \theta_n)$, where $x_n = i_n/(2I_0)$, $\theta_\alpha = \tan^{-1}\alpha$ and $\theta_D = \beta_2 L\omega^2/2$ with β_2 being the GVD parameter and L being the transmission distance.

$(1+\alpha^2)\cos^2(n^2\theta_D - \theta_\alpha)$ governs the frequency response of the transmission link. Without the frequency chirp, it changes to $\cos^2(n^2\theta_D)$, which is the conventional formula of the frequency response of a SMF-based IMDD transmission link [8]. However, for IMDD SMFs with positive chromatic dispersion, the positive frequency chirp ($\alpha > 0$) intensifies the frequency dependent loss, resulting in the frequency response narrowing effect [7].

For gaining an in-depth understanding of the DML frequency chirp, a theoretical DFB model reported in [5] can be used. This DFB model takes into account linear and nonlinear carrier recombination and nonlinear gain effects. The feasibility of the DFB model has been verified by good agreement with experimental measurements [9].

In the DFB model, the output power and phase of the modulated optical signal are governed by

$$\frac{dN}{dt} = \frac{I_d}{edwl} - \frac{N}{\tau_C} - BN^2 - CN^3 - G\frac{(N-N_t)}{1+\varepsilon\phi}\phi \tag{4.14}$$

$$\frac{d\phi}{dt} = \frac{\Gamma G(N-N_t)}{1+\varepsilon\phi}\phi + \zeta BN^2 - \frac{\phi}{\tau_P} \tag{4.15}$$

$$P = \chi w_v w_h h\nu \frac{\phi c}{2n_g} \tag{4.16}$$

$$\frac{d\Phi}{dt} = -\frac{\Gamma\eta(N-N_t)}{n_p} \tag{4.17}$$

$$\omega = \omega_0\left(1 - \frac{\Gamma\eta(N-N_t)}{n_p}\right) \tag{4.18}$$

where N is the carrier density, ϕ is the photon density, P and Φ are the power and phase

of the modulated optical signal at the optical frequency of ω with respect to a central frequency ω_0. I_d is the total electrical current injected into the active region of the laser with length l, width w, and thickness d, e is the electronic charge. τ_c is the linear carrier recombination lifetime. B is the bimolecular carrier recombination coefficient. C is the Auger carrier recombination coefficient. G is the linear optical gain coefficient. N_t is the transparency carrier density. ε is the nonlinear gain coefficient. Γ is the mode confinement factor. ζ describes the fraction of spontaneous emission that is emitted into the fundamental mode of the laser. τ_p is the photon lifetime. χ is the coupling efficiency from the laser chip to the SMF, w_v and w_h are the vertical and horizontal widths of the guided mode power distributions, h is Planck's constant, c is the velocity of light in vacuum, hv is the photon energy, n_g is the group refractive index, n_p is the phase refractive index and η is the rate of refractive-index change with carrier density. In deriving Eqs. (4.16) and (4.17), it is assumed that all photons reaching the exit facet of the DML are emitted and that the optical frequency can track the resonant frequency of the DFB cavity.

Based on Eq. (4.17) and (4.18), the DML frequency chirp Δv can be expressed as

$$\Delta v = -\frac{\omega_0 \Gamma \eta (N - N_t)}{n_p} \tag{4.19}$$

As η is negative [4,5], the DML frequency chirp is, therefore, positive and varies with driving and bias currents, and optical characteristics of the DFB laser.

It is well known that the DML frequency chirp has two major elements namely the transient frequency chirp and the adiabatic frequency chirp. Their relationships can be expressed as [6,10]

$$\Delta v = \frac{\alpha}{4\pi}\left(\frac{1}{P}\frac{dP}{dt} + \kappa P\right) \tag{4.20}$$

where α is the linewidth enhancement factor and κ is the adiabatic frequency chirp coefficient. The first term in Eq.(4.20) denotes the transient frequency chirp and the second term denotes the adiabatic frequency chirp.

Based on Eq. (4.20), the transient chirp and adiabatic chirp can be represented in Fig. 4.3, by assuming that the DML output power has a waveform with Guassian distribution, as shown in Fig.4.3 (a). It can be seen that transient chirp is proportional to the time-variation of an optical signal waveform and adiabatic chirp depends on the instantaneous optical signal waveform.

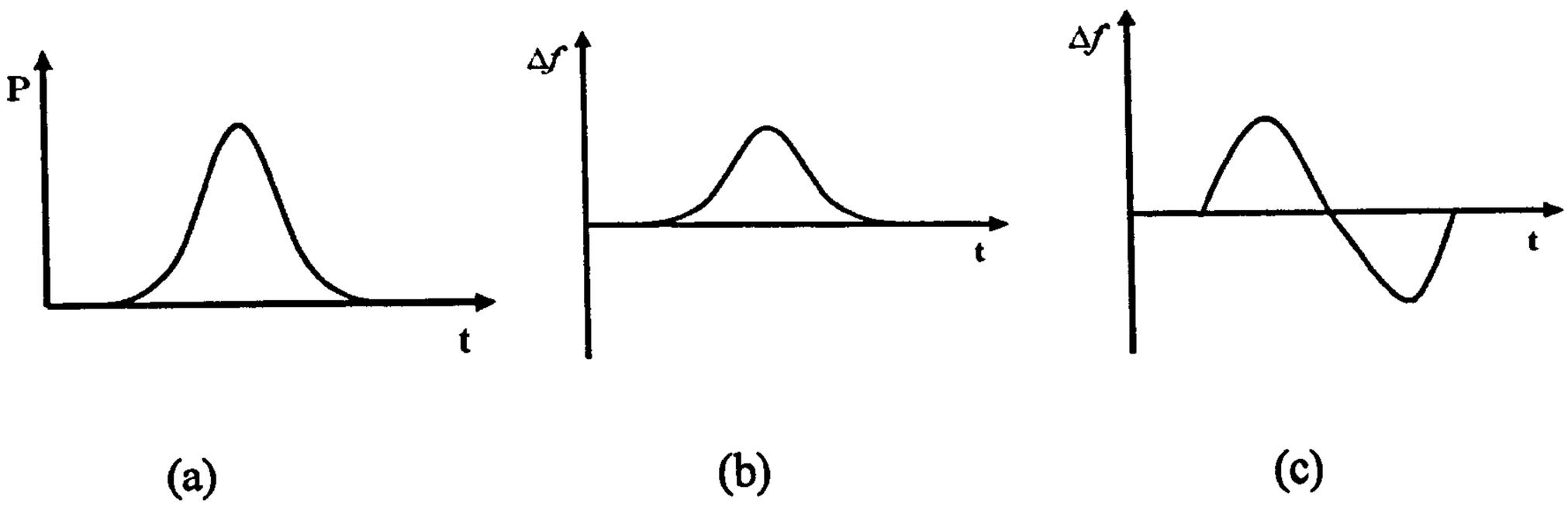

(a) (b) (c)

Fig.4.3 Representative waveforms of different chirp components. (a) DML output power; (b) adiabatic chirp; (c) transient chirp. P: optical output power; Δf : the frequency variation of the DML output signal.

To explicitly identify the origin of the frequency chirp associated with the theoretical DML model adopted here, Eq. (4.15) is rewritten as

$$\frac{1}{\phi}\frac{d\phi}{dt}=\frac{\Gamma G(N-N_t)}{1+\varepsilon\phi}+\frac{\zeta BN^2}{\phi}-\frac{1}{\tau_p} \tag{4.21}$$

Given the fact that an electrical OFDM signal has a noise-like waveform and a very small extinction ratio (typically <1dB) [11], for a DFB subject to optimum operating conditions, in Eq.(4.21) we have $1+\varepsilon\phi\approx 1$, and a negligible second term which takes into account the contributions from spontaneous emission. Moreover, the last term accounting for cavity loss does not considerably alter the dynamic frequency properties of the DML within the 3-dB modulation bandwidth region. Taking into account the above analysis and Eq. (4.16), Eq.(4.21) can be simplified and has the form shown below

$$\frac{1}{P}\frac{dP}{dt}=\frac{1}{\phi}\frac{d\phi}{dt}=\Gamma G(N-N_t) \tag{4.22}$$

From comparisons between Eqs.(4.19), (4.20) and (4.22), it can be noted that the transient

frequency chirp plays a dominant role in determining the DML chirp characteristics in OOFDM transmission systems over linear loss-dominant transmission distance region [4]. It is also worth mentioning that in dispersion-limited transmission systems, the frequency chirp significantly limits the maximum achievable OOFDM transmission performance, as will be discussed in Section 4.4.

4.4 Challenges Associated with IMDD OOFDM Systems

Having discussed OFDM and OOFDM in Chapter 2, reviewed the advantages of utilizing OOFDM and IMDD in NG-PON in Chapter 3, as well as analyzed IMDD links in Chapter 4, in this section, the challenges associated with IMDD OOFDM transmission systems are discussed.

Insufficient Utilization of Frequency Responses beyond Baseband

In a single-channel IMDD transmission system, the AMOOFDM technique simply utilizes the frequency response of a transmission link in the vicinity of the zero frequency (optical carrier frequency). A representative MMF link frequency response and the transmitted OOFDM spectrum are shown in Fig.4.4.

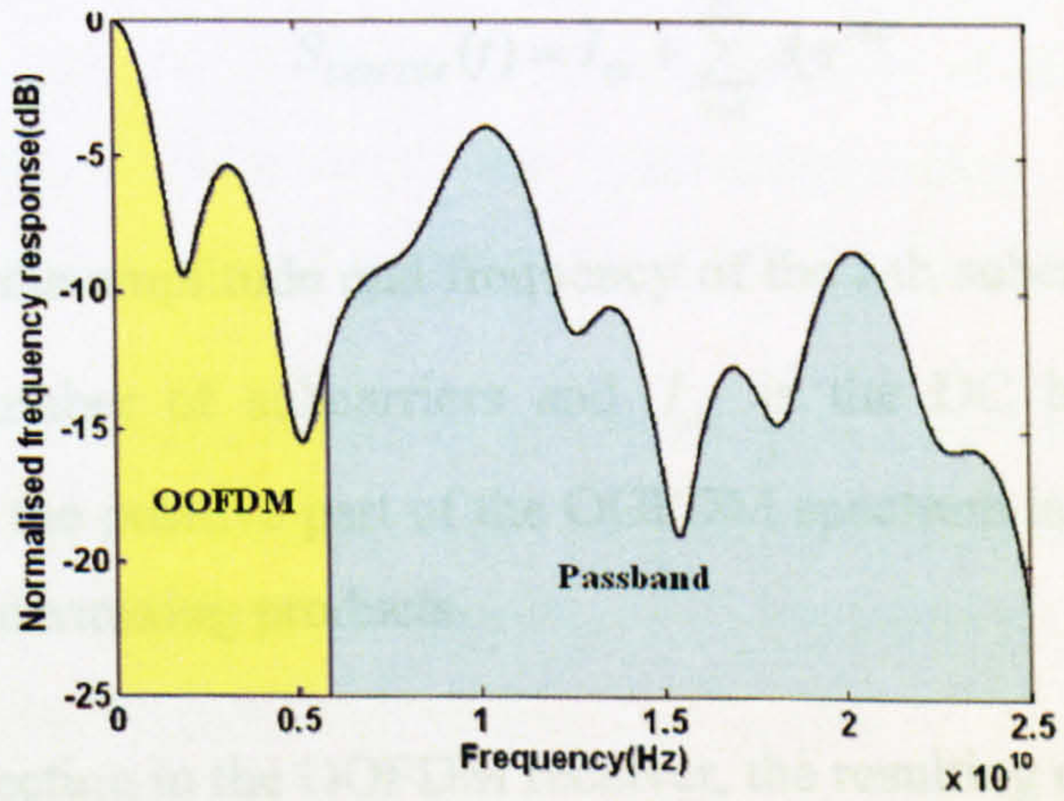

Fig.4.4. The frequency response of a MMF link, with the representative OOFDM signal spectrum being inserted.

It can be seen that a wide passband portion of the MMF link is still unused. This disadvantage significantly limits the maximum achievable transmission capacity [12]. It is shown [5] that, in the DML-based IMDD MMF links, the capacity×length products of the

AMOOFDM is limited below 9 Gb/s·km. As the AMOOFDM technique is capable of offering a large loss margin [4,5], sufficient utilization of the major portion of the link frequency response will obviously offer a significant potential for further increasing the transmission capacity of the IMDD OOFDM system. In the thesis, this challenge will be addressed by using AMOOFDM-SCM [13], which consists of two AMOOFDM modems in parallel with one operating at the baseband and the other being modulated onto a tunable intermediate RF carrier. Detailed investigations are undertaken in MMF-based IMDD links

AMOOFDM-SCM in SMF-Based IMDD Systems

Apart from MMF links, AMOOFDM-SCM is also applicable in single-channel, SMF-based IMDD links, as SMFs have much wider and flatter 3-dB bandwidth than MMFs and are widely deployed in networks of various architectures such as PONs. Therefore, the effective realization of the AMOOFDM-SCM technique in SMF links is also an interesting and challenging topic. However, the intermixing effect induced by direct detection is a crucial factor limiting the maximum achievable AMOOFDM-SCM performance in such links [14]. The intermixing effect can be understood by considering the following analysis. For the purpose of simplifying the analysis, the optical carrier frequency is set to zero and the transmitted optical signal only contains one OFDM band, which can be represented by

$$S_{OOFDM}(t) = I_{dc} + \sum_{i=1}^{N} A_i e^{j\omega_i t} \tag{4.23}$$

where A_i and ω_i are the amplitude and frequency of the i-th subcarrier within one OFDM symbol, N is the number of subcarriers and I_{dc} is the DC bias current. It is worth mentioning that only the positive part of the OOFDM spectrum is considered here in order to clearly show the intermixing products.

Due to the direct detection in the OOFDM receiver, the resulting electrical OFDM signal is given by

$$\begin{aligned} S_e(t) &= S_{OOFDM}(t) S^*_{OOFDM}(t) \\ &= (I_{dc} + \sum_{i=1}^{N} A_i e^{j\omega_i t})(I_{dc} + \sum_{i=1}^{N} A_i e^{-j\omega_i t}) \\ &= I_{dc}^2 + \sum_{i=1}^{N} A_i^2 + I_{dc} \sum_{i=1}^{N} A_i e^{j\omega_i t} + I_{dc} \sum_{i=1}^{N} A_i e^{-j\omega_i t} + \sum_{n=1}^{N-1} \sum_{i=1}^{N-n} A_i A_{i+n} e^{jn\Delta\omega t} + \sum_{n=1}^{N-1} \sum_{i=1}^{N-n} A_i A_{i+n} e^{-jn\Delta\omega t} \end{aligned} \tag{4.24}$$

where Δf is the frequency difference between adjacent subcarriers.

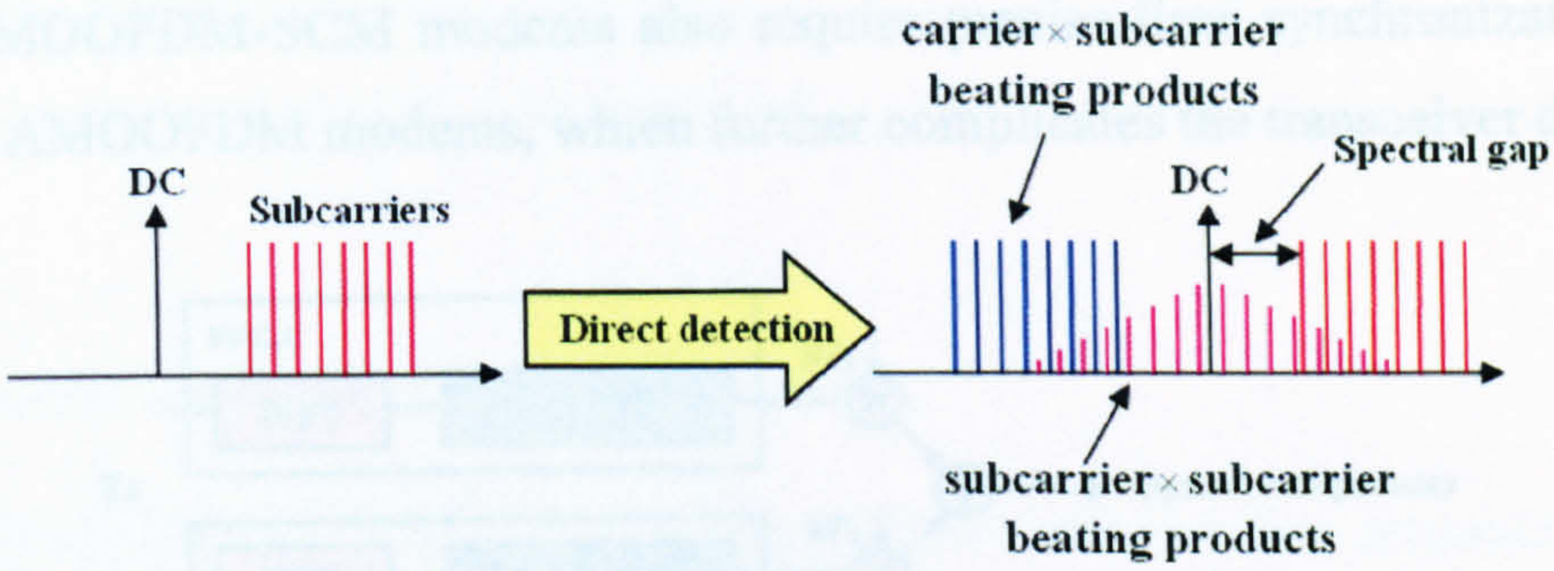

Fig.4.5 Intermixing effects due to direct detection in the OOFDM receiver.

On the right hand side of Eq. (4.24), the sum of first two terms denotes the DC component, the third term represents the wanted OFDM signal, the fourth term is the carrier × subcarrier beatings products and the remaining terms are the unwanted subcarrier × subcarrier beatings products.

As shown in Fig.4.5, if the spectral gap is smaller than the bandwidth of the electrical OFDM signal, the unwanted subcarrier × subcarrier beatings products are generated in the useful signal spectrum region, which considerably distort the OFDM signal spectrum and simultaneously lower the signal transmission performance. In Chapter 6, it is shown that the intermixing effects can reduce the transmission capacity of the OOFDM signal by a factor of approximately 2. Moreover, the intermixing effect increases with higher frequency chirp and chromatic dispersion effects, as mentioned in [7].

To maximize the transmission performance by reducing the intermixing impairments, three AMOOFDM-SCM designs of different complexity are proposed, by applying SSB and/or spectral gapping to AMOOFDM-SCM. Detailed discussions of the modem configurations and their transmission performance will be given in Chapter 6.

Cost-Effective and Simplified Transceiver Designs

In Chapter 6, each of the AMOOFDM-SCM modems [13, 14] requires two IFFT/FFT operations in transmitter/receiver, as shown in Fig.4.6. As the IFFT and FFT are the most computationally intensive functions in the OFDM transceiver, in practice, highly complex, computationally intense and high-speed DSP are required for realizing the IFFTs/FFTs.

This considerably increases the system complexity and cost. Furthermore, for practical implementations, apart from the synchronization in each AMOOFDM modem, the proposed AMOOFDM-SCM modems also require precise time synchronization between two parallel AMOOFDM modems, which further complicates the transceiver designs.

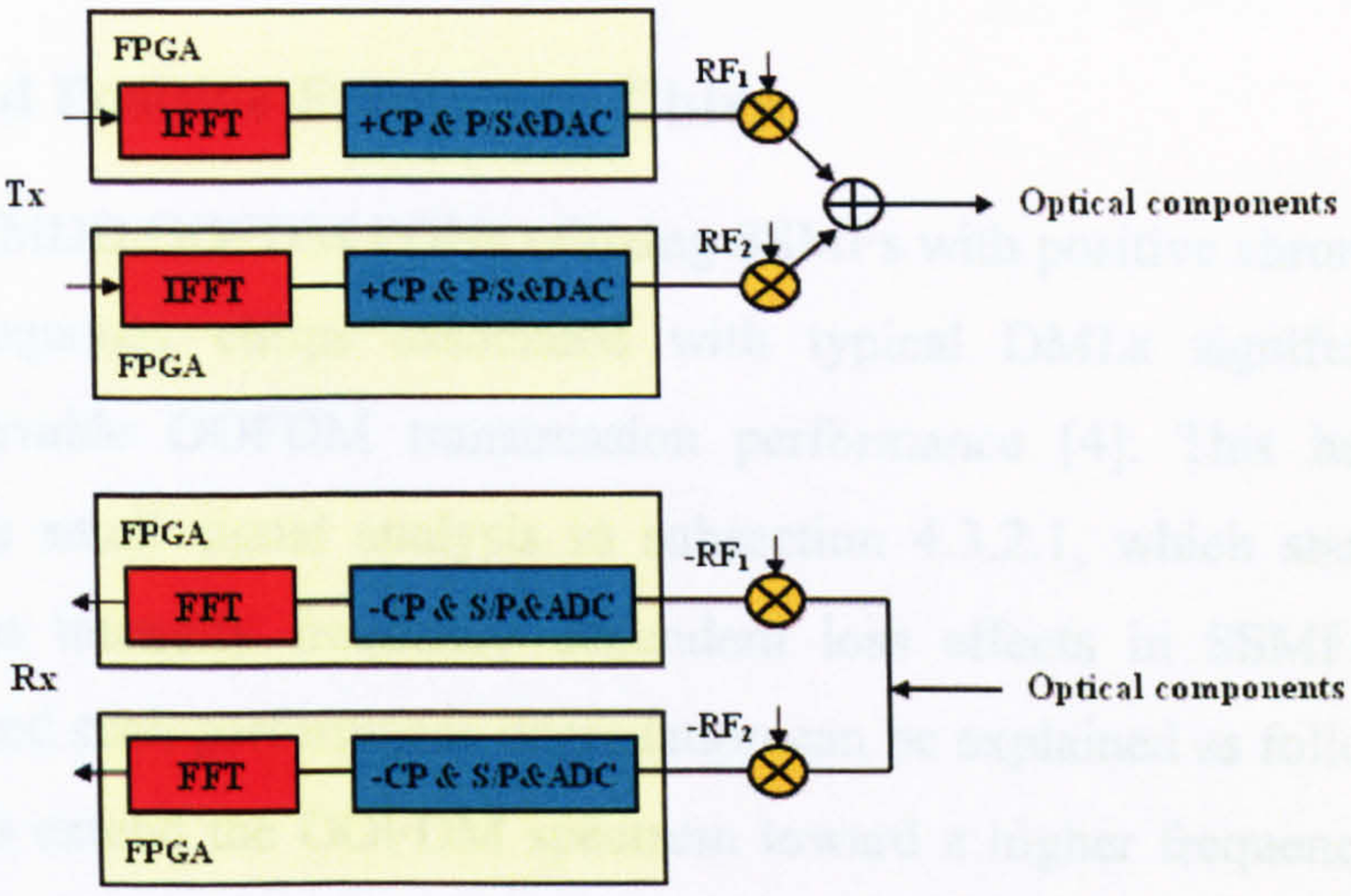

Fig.4.6. AMOOFDM-SCM modem designs.

In order to further reduce the system complexity and cost, in Chapter 7, three simplified AMOOFDM-SCM modems are proposed, each of which only requires a single IFFT/FFT operation only in the transmitter/receiver. Detailed discussions of these simplified modem designs will be given in that chapter.

Relaxed Requirements on Key Transceiver Components

For further reduction of the transceiver cost, one solution is to relax the minimum requirements on key transceiver components such as DACs and ADCs without compromising the transmission performance. It is well known that the OFDM signal waveform has high amplitude fluctuations that produce large PAPRs [15]. This is due to the fact that the OFDM symbol can be considered as the sum of a number of modulated subcarriers. The samples of an OFDM signal have approximately Gaussian distributions with large amplitude range and high PAPRs. The high PAPRs causes OFDM to be sensitive to nonlinear distortion caused by key transceiver components such as DAC/ADC, as the occasional peaks having amplitudes of higher than the average value may exceed the dynamic range of the DAC/ADC. Therefore, the OOFDM transceiver requires the DAC/ADC to have wide dynamic range which is expensive and complex. Clipping is a

common approach to solve such a challenging issue, which, however, introduces nonlinear distortion as well, as discussed in Chapter 2. To address the high PAPRs problem, in Chapter 8, the AMOOFDM-PM technique is proposed, in which an electrical OFDM signal is utilised to modulate the phase of a RF carrier prior to performing optical intensity modulation.

DML-Induced Positive Frequency Chirp

In DML-based IMDD OOFDM PONs utilizing SSMFs with positive chromatic dispersion, the positive frequency chirps associated with typical DMLs significantly limit the maximum achievable OOFDM transmission performance [4]. This has already been indicated by the small signal analysis in subsection 4.3.2.1, which states that positive frequency chirps intensify frequency dependent loss effects in SSMFs. The physical mechanism behind such performance degradation can be explained as follows: the positive frequency chirps extend the OOFDM spectrum toward a higher frequency region, which introduce extra frequency components into the OOFDM signal; due to chromatic dispersion, the ISI and frequency dependent loss become much more severe than in the non-chirp cases.

It is shown that [4], in comparison with the non-chirp case, the DML frequency chirp causes a reduction in transmission capacity of up to 25% for transmission distances of < 80km. To address such a challenging issue, two chirp compensation techniques are discussed in Chapter 9 and 10 respectively, including the utilization of negative dispersion fibre such as MetroCor fibre in replace of SSMFs, and a chirp compensation technique performing phase estimation and modulation by utilizing an electrical analogue circuit and an optical phase modulator.

4.5 Conclusion

In this chapter, the IMDD OOFDM systems have been described in detail, with effort being given to the key optical components. Several limiting effects associated with optical fibres have been discussed including modal dispersion, chromatic dispersion, fibre loss and fibre nonlinearity. Photon detection has also been discussed. Furthermore, intensity modulators have been analysed with special attention given to the DML model and the

frequency chirp model. Finally, the five challenging issues associated with IMDD OOFDM have been listed, which will form research topics of the following Chapters.

References

[1] C. Cox III, E. Ackerman, R. Helkey and G. E. Betts, "Techniques and performance of intensity-modulation direct-detection analog optical links," IEEE Trans. Microwave Theory Tech., vol. 45, no. 8, pp. 1375-1383, Aug. 1997.

[2] G. P. Agrawal, *Fibre-Optic Communication Systems*, Wiley, 1997.

[3] G. P. Agrawal, *Nonlinear Fibre Optics*, Academic, 1995.

[4] J. M. Tang and K. A. Shore, "30Gb/s signal transmission over 40-km directly modulated DFB-laser-based single-mode-fiber links without optical amplification and dispersion compensation," J. Lightw. Technol., vol. 24, no. 6, pp. 2318-2327, June. 2006.

[5] J. M. Tang, P. M. Lane and K. A. Shore, "High-speed transmission of adaptively modulated optical OFDM signals over multimode fibres using directly modulated DFBs," J. Lightw. Technol., vol. 24, no. 1, pp. 429–441, Jan. 2006.

[6] J. J. Yu, Z. S. Jia, M. F. Huang, M. Haris, P. N. Ji, T. Wang and G. K. Chang, "Applications of 40-Gb/s chirp managed laser in access and metro networks," J. Lightw. Technol., vol. 27, no. 3, pp. 253-265, Feb. 2009.

[7] Chia-Chien Wei, "Small signal analysis of OOFDM signals transmission with directly modulated laser and direct detection," Opt. Letters., vol. 36, no. 2, pp.151-153, Jan. 2011.

[8] U. Gliese, S. Ngrskov, and T. N. Nielsen, "Chromatic dispersion in fiber-optic microwave and millimeter-wave links," IEEE Trans. Microwave Theory Tech., vol. 44, no.10, pp. 1716-1724, Oct. 1996.

[9] N. E. Jolley, H. Kee, R. Rickard, J. M. Tang, and K. Cordina, "Generation and propagation of a 1550 nm 10 Gb/s optical orthogonal frequency division multiplexed signal over 1000 m of multimode fibre using a directly modulated DFB," OFC/NFOEC, (OSA 2005), Paper OFP3.

[10] P. Krehlik, "Characterization of semiconductor laser frequency chirp based on signal distortion in dispersive optical fiber," Opto-Electronics Review., vol. 14, no. 2, pp. 123-128, 2006.

[11] J. L. Wei, A. Hamié, R. P. Giddings, and J. M. Tang, "Semiconductor optical amplifier-enabled intensity modulation of adaptively modulated optical OFDM signals in SMF-based IMDD systems," J. Lightw. Technol., vol. 27, no.16, pp.3678-3688, Aug. 2009

[12] A. S. Tanenbaum, *Computer Networks*, Prentice Hall, 2003.

[13] X. Zheng, J. M. Tang and P. S. Spencer, "Transmission performance of adaptively modulated optical OFDM modems using subcarrier modulation over worst-case multimode fibre links," IEEE Comm. Lett., vol.12, no.10, pp. 788-790, Oct. 2008.

[14] X. Zheng, J. L. Wei and J. M. Tang, "Transmission performance of adaptively modulated optical OFDM modems using subcarrier modulation over SMF IMDD links for access and metropolitan area networks" Opt. Express., vol.16, no.25, pp. 20427-20440, Dec. 2008.

[15] S. C. Thompson, A. U. Ahemd, J. G. Proakis, J. R. Zeidler, M. J. Geile, "Constant envelope OFDM," IEEE Transactions on Comm., vol. 56, no. 8, pp. 1300-1312, Aug. 2008.

5 AMOOFDM-SCM over Worst-Case MMF Links

Contents

5.1 Introduction

In order to explore effective solutions to make full use of the link frequency response, investigations are first made in MMF links, as MMFs have relatively narrow and highly variable frequency responses, which are ideal for verifying the validity and effectiveness of the proposed technique. It is well known that the highly-variable modal dispersion present in the graded index MMFs limits the transmission performance of existing techniques to about 1.25 Gb/s over 550 m [1]. To satisfy the explosive growth in end-users' traffic, great effort has been expended on finding cost-effective solutions for upgrading 1 Gb/s MMF links to > 10 Gb/s with the installed fibre infrastructure being preserved. A wide range of strategies are being investigated, including spatially resolved receiver [2], restricted offset launch [3], multilevel coding [4] and electrical dispersion compensation [5]. All these schemes use only the relatively narrow baseband regions of MMF link frequency response. This may cause significant difficulties for any future upgrading of such links to higher signal bit rates of say 100 Gb/s.

AMOOFDM has demonstrated great potential for providing a high-speed, cost-effective solution with excellent flexibility and robustness for practical implementation in short-reach systems [6,7]. AMOOFDM is capable of utilizing the much wider region of a MMF link frequency response, the major portion of which is, however, still unused. This challenge can be solved by SCM [8], in which a baseband signal is modulated onto a RF carrier driving a DML. Unfortunately, the highest SCM signal transmission performance reported so far is just 10 Gb/s over 300 m MMFs [8]. By nature, AMOOFDM can be regarded as a special form of SCM, with the significant difference being the necessity for orthogonality between the various subcarriers.

In this chapter, a novel AMOOFDM-SCM is, for the first time, proposed, which consists of two AMOOFDM modems in parallel with one operating at the baseband and the other being modulated onto a tunable intermediate RF carrier (similar to frequency diversity in wireless systems [9]). This technique enables AMOOFDM-SCM to have the unique capability of fully exploiting the entire frequency response of an arbitrary MMF link. As a direct result, when compared against AMOOFDM, AMOOFDM-SCM not only enhances the capacity versus reach performance by a factor of about 2, but also considerably improves the flexibility and robustness of the MMF link performance.

5.2 AMOOFDM-SCM Modem

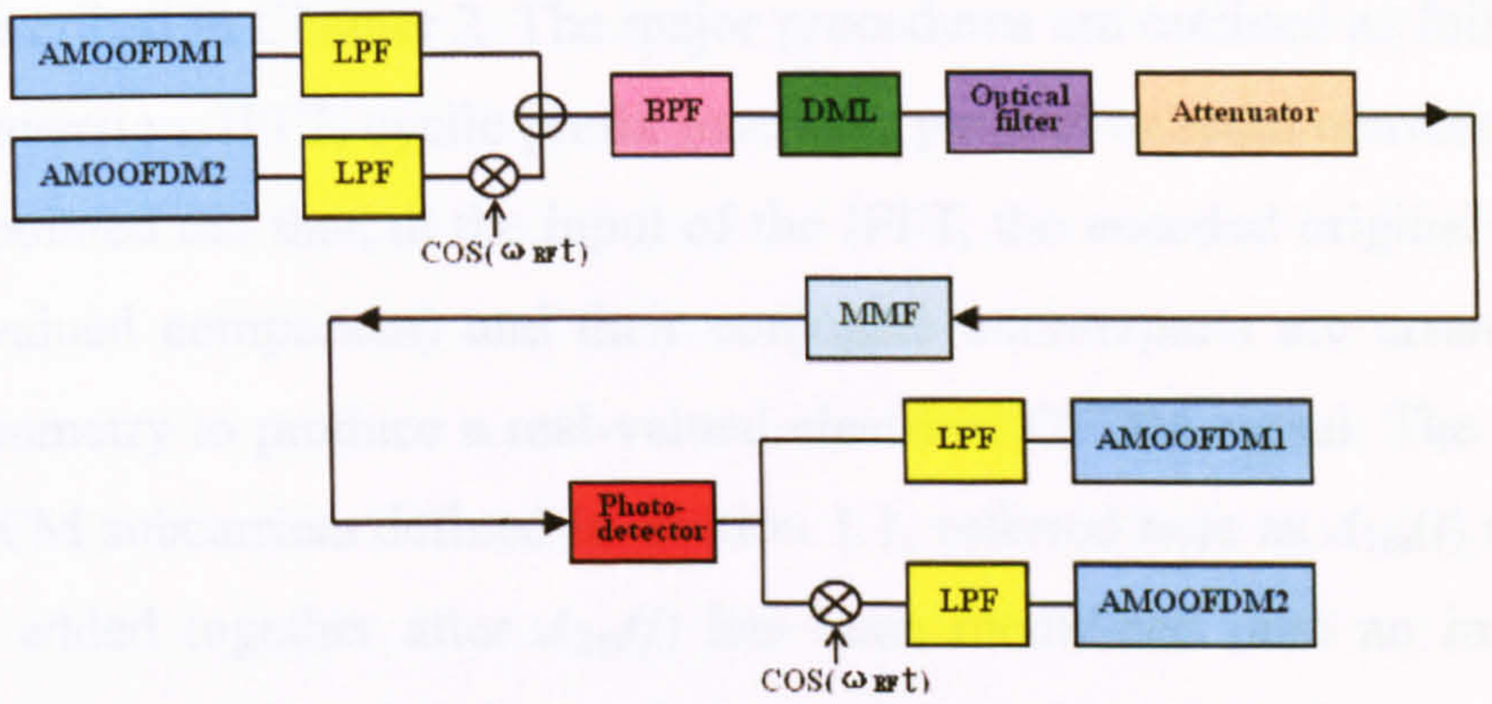

(a)

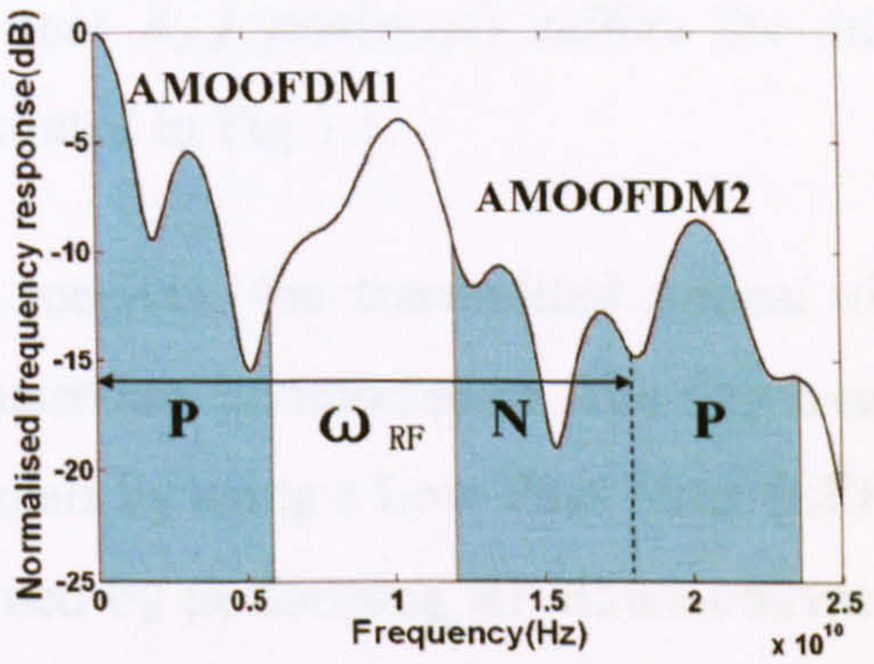

(b)

Fig. 5.1 AMOOFDM-SCM system. (a) Schematic illustration of the proposed AMOOFDM-SCM modem and the transmission link structure; (b) The 300 m MMF frequency rsponse and the signal spectrum are also shown in the inserted figure. BPF: band-pass filter; LPF: low-pass filter; P (N): positive (negative) part of the signal spectrum corresponding to the positive (negative) frequency bins used in the encoder.

A schematic diagram of the proposed AMOOFDM-SCM modem is given in Fig. 5.1 (a), together with the single-channel, optical amplifier-free MMF link based on IMDD. The frequency response of a 300 m MMF considered here is also shown in Fig.5.1 (b) with a representative AMOOFDM-SCM signal spectrum being inserted.

In the AMOOFDM-SCM transmitter, the encoded complex data is split into two streams, each of which is processed independently by an AMOOFDM modem according to the procedures described in Chapter 2. The major procedures are outlined as followings: serial to parallel conversion, IFFT, cyclic prefix insertion, parallel to serial conversion and DAC. It should be pointed out that, at the input of the IFFT, the encoded original data (together with a zero-valued component) and their conjugate counterparts are arranged to satisfy Hermitian symmetry to produce a real-valued electrical OFDM signal. The two generated continuous SCM subcarriers defined in Section 1.1, referred here as $A_{1in}(t)$ and $A_{2in}(t)$, are subsequently added together after $A_{2in}(t)$ has been modulated onto an intermediate RF carrier at ω_{RF}. The resulting signal waveform, $A_{1in}(t)+A_{2in}(t)\cos(\omega_{RF}t)$, is employed to drive a DML. The output optical signal is coupled into the MMF link under different launch conditions. According to the characteristics of the MMF link and transmission distance, ω_{RF} is adjusted to ensure that $A_{2in}(t)\cos(\omega_{RF}t)$ suffers the minimum loss and does not overlap with $A_{1in}(t)$, as illustrated in Fig.5.1.

In the AMOOFDM-SCM receiver, the transmitted optical signal is converted into an electrical signal using a square-law photodetector. The first baseband signal $A_{1out}(t)$ can be separated from all other signals by using a Low-Pass Filter (LPF), and the second baseband signal $A_{2out}(t)$ can be obtained by performing RF down-conversion followed by a LPF. In practice, the inserted cyclic prefix can be utilized to generate a synchronization signal through a correlation operation between the AMOOFDM signal and a delayed copy of the signal. The synchronization signal has a peak occurring in each of the time durations of cyclic prefix. To recover the received data, $A_{1out}(t)$ and $A_{2out}(t)$ are processed independently by two parallel AMOOFDM receivers, which are the inverse of the transmitters as described in Chapter 2.

5.3 Simulation Parameters

In numerical simulations, for each AMOOFDM modem, 64 subcarriers are considered, in which 31 having identical powers carry real data, one has no power, and the remaining 32 are the complex conjugate of the above-mentioned subcarriers. The modulation formats used on each subcarrier vary from DBPSK, DQPSK, and 16 to 256QAM, depending on the frequency response of a given transmission link. To improve the transmission performance,

Gray coding is adopted in mapping binary data into QAM. The cyclic prefix parameter defined in [6] is taken to be 25%. In order to reduce the PAPRs, signal clipping is applied separately for each SCM subcarrier, and the clipping level defined in [6] is fixed at 13 dB which is an optimum value identified in [7]. A measured worst-case MMF link at 1300 nm [7] for central launch and having the frequency response shown in Fig.5.1 is adopted, whose 3-dB bandwidth is assumed to be proportional to the inverse of transmission distance, L. It is sufficiently accurate to assume that the modal noise effect is negligible [6,7]. It should also be noted that, due to the nature of AMOOFDM [6,7] and SCM [8], AMOOFDM-SCM is applicable for any fibre types, launch conditions and operating wavelengths.

Here an ideal intensity modulator producing a 0 dBm optical power coupled into MMFs is employed. Such an assumption is practically achievable as a DML can have a modulation bandwidth as large as about 29 GHz [10], which is larger than the signal bandwidth of current interest. This leads to negligible impact of laser nonlinearities on the transmission performance of the technique [6]. All other parameters that are not explicitly mentioned above can be found in [7], where the procedures of calculating noises associated with the photodetector are also described.

5.4 Transmission Performance of AMOOFM-SCM in Worst-Case IMDD MMF Links

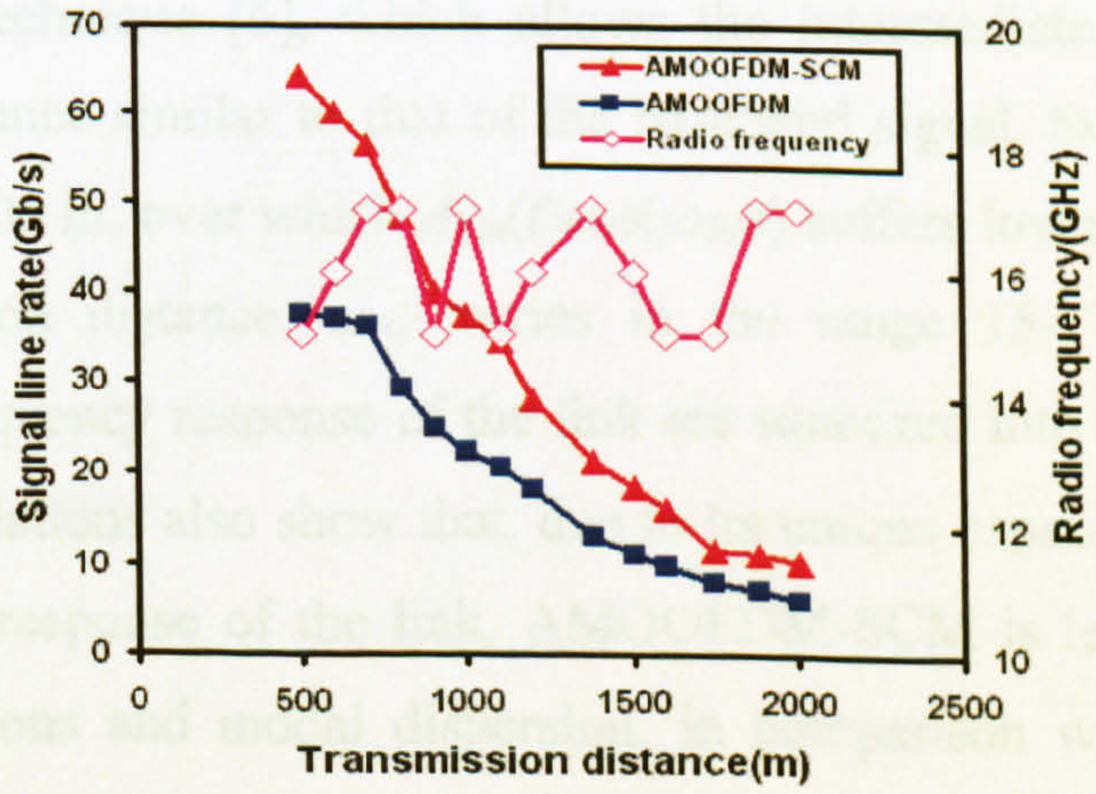

Fig.5.2 Signal transmission capacity and RF as a function of transmission distance.

The transmission performance of the AMOOFDM-SCM modem and the corresponding ω_{RF} used, are shown in Fig.5.2, where the signal line rate R_s is defined as

$$R_s = \sum_{m=1}^{2} \frac{\sum_{k=1}^{31} M_{mk}}{(N_{sub} + N_{CP})T_s} \tag{5.1}$$

here m is the number of the AMOOFDM modems used in parallel; M_{mk} is the number of binary bits carried by the k-th subcarrier of the m-th AMOOFDM modem; N_{sub} is the number of subcarriers within one symbol; T_s is the sampling period of DACs/ADCs and N_{cp} is the number of sampling periods occupied by the cyclic prefix within one symbol. In simulations, R_s corresponding to a total channel BER defined in Section 2.3.1.3 of 1.0×10^{-3} is considered, as such a BER provides error free operation after combining with FEC. In obtaining Fig.5.2, practically available DAC/ADC parameters of T_s= 80 ps and bits of quantization, b, of 7 are adopted. For comparison, the transmission performance of the AMOOFDM modems using the same parameters is also plotted, which agrees very well with that reported in [7]. This supports the validity of the AMOOFDM-SCM model developed here.

It can be seen from Fig.5.2 that 64 Gb/s over 500 m and 37 Gb/s over 1000 m AMOOFDM-SCM signal transmission is feasible in the single channel, optical amplifier-free, worst-case IMDD MMF link with a 3-dB bandwidth as small as 292.5 MHz·km. In comparison with the AMOOFDM technique, the almost doubled transmission capacity versus reach performance of AMOOFDM-SCM is due to the existence of an about 15 dB loss margin of the technique [6], which allows the intermediate RF signal to have a transmission performance similar to that of the baseband signal. Such an improvement is significant for L < 1000 m, over which $A_{2in}(t)\cos(\omega_{RF}t)$ suffers low transmission loss. With increasing transmission distance, ω_{RF} varies in the range 15-17 GHz because more peaks/nulls of the frequency response of the link are squeezed into the AMOOFDM-SCM spectral region. Simulations also show that, due to its unique capability of fully exploiting the entire frequency response of the link, AMOOFDM-SCM is less susceptible to fibre types, launch conditions and modal dispersion, in comparison with AMOOFDM. This indicates that AMOOFDM-SCM can also improve the flexibility and robustness of the MMF link performance.

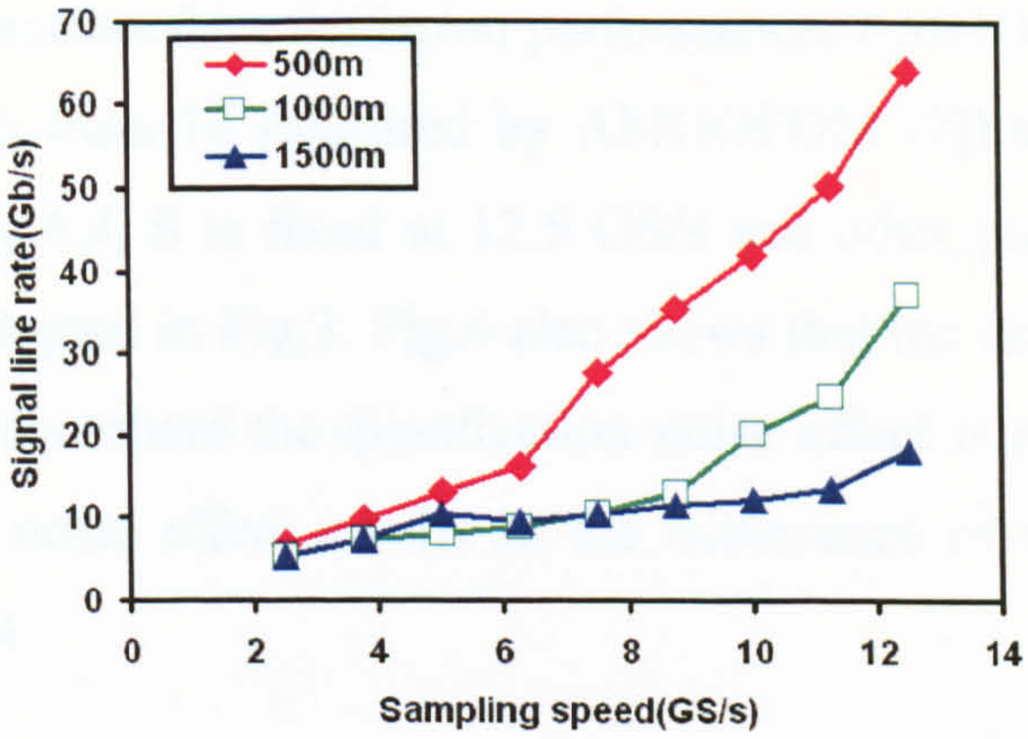

Fig. 5.3 Impact of DAC/ADC sampling speed on the AMOOFDM-SCM transmission performance.

In addition, when compared with AMOOFDM, AMOOFDM-SCM is capable of significantly lowering the minimum requirements on key component parameters for achieving a required transmission performance, as demonstrated in Figs.5.3 and 5.4. The impact of DAC/ADC sampling speed, S=1/T_s, on the transmission performance of AMOOFDM-SCM is plotted in Fig.5.3, where b and ω_{RF} are the same as those used in Fig.5.2. It can be found from Fig.5.3 that, for L < 1000 m, R_s is enhanced considerably with increasing S, resulting from the increased signal bandwidth. Whilst for L > 1000 m, over which the associated Differential Mode Delays (DMDs) are larger than the cyclic prefix used, the DMD effect is a dominant factor limiting the maximum achievable transmission performance. In particular, to achieve a required transmission performance of say 40 Gb/s over 500 m, AMOOFDM-SCM relaxes considerably the minimum required S from 12.5 GS/s (required by AMOOFDM [7]) to 9 GS/s.

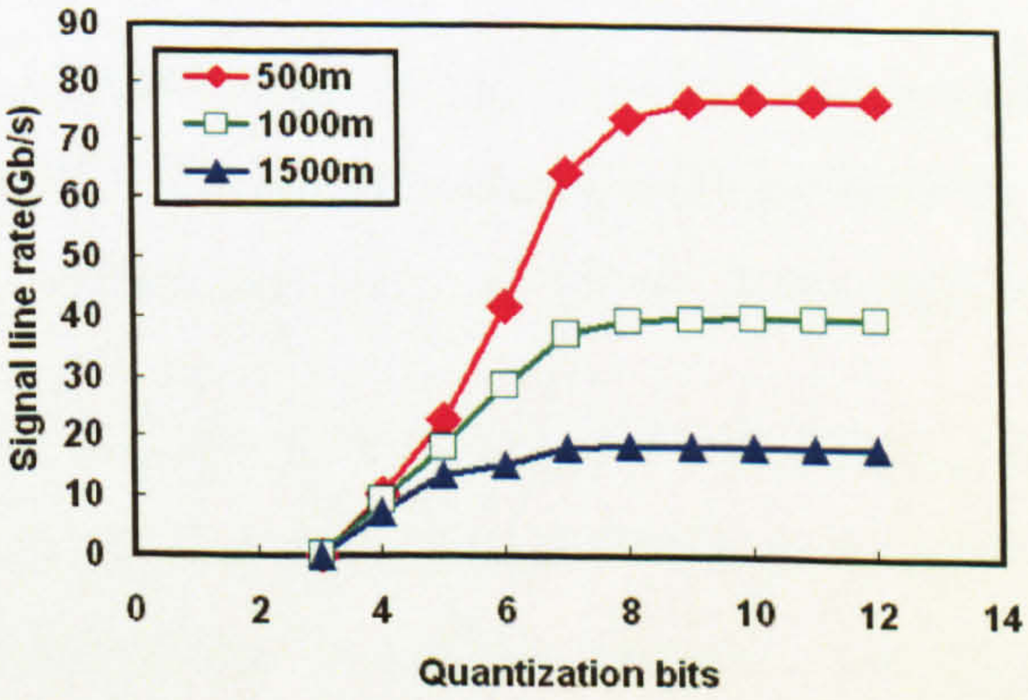

Fig. 5.4 Impact of bit quantization on the AMOOFDM-SCM transmission performance.

To achieve the above-mentioned transmission performance, AMOOFDM-SCM also lowers the minimum required b from 10 (required by AMOOFDM [7]) to about 6, as shown in Fig.5.4. In obtaining Fig.5.4, S is fixed at 12.5 GS/s and other parameters including ω_{RF} are the same as those adopted in Fig.3. Fig.4 also shows that the use of AMOOFDM-SCM is more effective for links where the quantization noise effect is not dominant [6,7]. The negligible quantization noise effect results in the occurrence of the flat signal line rate regions shown in Fig.5.4.

5.5 Conclusion

A novel AMOOFDM-SCM modem has been proposed, which, in comparison with the AMOOFDM modem not only improves significantly the capacity versus reach performance, but also considerably relaxes the minimum requirements on key components involved. It should be noted that AMOOFDM-SCM is also promising for SMF-based systems because of the existence of much wider and flatter frequency responses. In the next chapter, detailed investigations of transmission performance of AMOOFDM-SCM will be undertaken in SMF-based IMDD links.

References

[1] The Gigabit Ethernet Standard, IEEE Standard 802.3z, 1998.

[2] K. M. Patel and S. E. Ralph, "Enhanced multimode fibre link performance using a spatially resolved receiver," IEEE Photon. Technol. Lett., vol. 14, no. 3, pp. 393-395, Mar. 2002.

[3] M. Webster, L. Raddatz, I. H. White, and D. G. Cunningham, "A statistical analysis of conditioned launch for Gigabit Ethernet links using multimode fiber," J. Lightwave Technol., vol. 17, pp. 1532-1541, Sep.1999.

[4] M.Webster, A. B.Massara, I. H. White, and R. V. Penty, "10Gb/s transmission over 300m of standard multimode fibre using multilevel coding and 2-channel WDM," in Proc. Conf. Laser Electro-Optics (CLEO), San Francisco, CA, 2000, pp.94-95.

[5] Y. Sun, P. Hallemeier, H. Ereifei, O. V. Sinkin, B. S. Marks and C. R. Menyuk, "Statistics of electrical dispersion compensator penalties of 10-Gb/s multimode fibre links with offset connectors," IEEE Photon. Technol. Lett., vol. 19, no. 9, pp. 689-691, May 2007.

[6] J. M. Tang, P. M. Lane, and K. A. Shore, "High-speed transmission of adaptively modulated optical OFDM signals over multimode fibres using directly modulated DFBs," J. Lightw. Technol., vol. 24, no. 1, pp. 429-441, Jan. 2006.

[7] J. M. Tang and K. A. Shore, "Maximizing the transmission performance of adaptively modulated optical OFDM signals in multimode-fiber links by optimizing analog-to-digital converters," J. Lightw. Technol., vol. 25, no. 3, pp. 787-798, Mar. 2007.

[8] A. M. E.-A. Diab, J. D. Ingham, R. V. Penty, and I. H. White, "10-Gb/s transmission on single-wavelength multichannel SCM-based FDDI-grade MMF links at lengths over 300m; a statistical investigation," J. Lightw. Technol., vol. 25, no. 10, pp. 2976-2983, Oct. 2007.

[9] A. Ramachandram and J. Sarangapani, "Use of frequency diversity in signal strength based WLAN location determination systems," in 32nd IEEE Conf. Local Computer Networks (LCN), Oct 2007, pp.117-124.

[10] K. Nakahara, T. Tsuchiya, T. Kitatani, K. Shinoda, T. Taniguchi, T. Kikawa, M. Aoki, and M. Mukaikubo, "40-Gb/s direct modulation with high extinction ratio operation of 1.3- m InGaAlAs multiquantum well ridge waveguide distributed feedback lasers," IEEE Photon. Technol. Lett., vol. 19, no. 19, pp. 1436-1438, Oct. 2007.

6 AMOOFDM-SCM Using of SSB Modulation over SMF IMDD Links

Contents

6.1 Introduction

To fully utilize the frequency response beyond baseband, in the previous chapter, a novel AMOOFDM-SCM technique was proposed, which consists of two parallel AMOOFDM modems with one operating at the baseband and the other being modulated onto a RF carrier. As shown in Chapter 5, AMOOFDM-SCM offers major opportunities of not only manipulating the signal modulation format taken on each individual AMOOFDM subcarrier involved in a SCM subcarrier, but also positing each individual SCM subcarrier at an optimum link frequency response region. The transmission performance of the proposed AMOOFDM-SCM technique has been explored in amplifier-free, worst-case MMF IMDD links. As the existence of much wider and flatter frequency response associated with SMF IMDD links, compared to those corresponding to MMF links, it is greatly advantageous if detailed explorations of the maximum achievable transmission performance of the previously proposed AMOOFDM-SCM technique can be made in SMF-based IMDD transmission links without incorporating optical amplification and fibre chromatic dispersion compensation. The thrust of this chapter is, therefore, to address, for the first time, such a challenging issue for practical implementation in OOFDM-PONs. In addition, the intermixing effect induced by beatings between AMOOFDM subcarriers of various SCM subcarriers within the same AMOOFDM-SCM signal spectrum is identified to be a crucial physical factor limiting the maximum achievable transmission performance of the technique. The physical origin of such an effect is the generation of unwanted subcarrier × subcarrier beating products in the useful signal spectral region, upon square-law direct detection in the receiver, as described in Chapter 4.

To maximise the link performance by mitigating the intermixing effect, in this chapter, three AMOOFDM-SCM modem designs are proposed for different application scenarios that may be encountered in OOFDM-PONs. Here these designs are referred to as AMOOFDM-SCM scheme I, AMOOFDM-SCM scheme II and AMOOFDM-SCM scheme III. The configuration of AMOOFDM-SCM scheme I is identical to that presented in Chapter 5 [1], in which two real-valued DSB SCM subcarriers are involved with the first SCM subcarrier operating at the baseband and the other being modulated onto an intermediate RF carrier. Whilst the configuration of AMOOFDM-SCM scheme II is similar to AMOOFDM-SCM scheme I, except that, in AMOOFDM-SCM scheme II, a spectral

gap in the electrical domain is introduced between the optical carrier and the first SCM subcarrier. The only configuration difference between AMOOFDM-SCM scheme III and AMOOFDM-SCM scheme II is that the two SCM subcarriers in AMOOFDM-SCM scheme III are real-valued SSB electrical signals generated by using the phase-shift method [2]. It is worth emphasizing that optical SSB operation is retained in all the aforementioned three AMOOFDM-SCM modem designs.

It will be shown that, in comparison with the AMOOFDM technique, AMOOFDM-SCM modems of all the proposed designs can improve the capacity versus reach performance by a factor of at least 1.5 for transmission distances up to 60km. In addition, of the proposed three modem designs, AMOOFDM-SCM scheme III (AMOOFDM-SCM scheme I) always offers the highest (lowest) signal transmission performance for transmission distances up to 80km (60km). However, having the simplest modem structure and the highest bandwidth efficiency, AMOOFDM-SCM scheme I may be preferred in practice for short transmission distances of say <20km. In addition, for transmission distances in a range of 20km-40km, use may be made of AMOOFDM-SCM scheme II, since in comparison with AMOOFDM-SCM scheme III, it offers a very similar signal transmission performance of 67Gb/s over 40km, but has a modem structure of much less complexity. For transmission distances in a range from 40km to 80km, AMOOFDM-SCM scheme III may be the best choice and it is able to offer 48Gb/s over 80km signal transmission.

It should be noted that, in [3], a different SSB modulation technique has been reported, which, however, requires a complex coherent transmitter and is not inherently compatible with direct detection. To implement that technique in direct detection systems, a square-root operation has to be applied to the received electrical signals to compensate for the square operation in the photodetector [3].

6.2 Theoretical Models for AMOOFDM-SCM Modems and Transmission Links

Schematic transceiver diagrams of AMOOFDM-SCM scheme I, II and III are given in Fig. 6.1(a), Fig. 6.1(b) and Fig. 6.1(c), respectively. The operating principles for AMOOFDM-SCM scheme III are described in subsection 6.2.1, whilst the operating principles for AMOOFDM-SCM scheme I and II are not presented here, as all the relevant information can be derived easily by taking into account Fig. 6.1 and subsection 6.2.1. A single-channel,

SMF-based IMDD transmission link operating at 1550nm is considered throughout this chapter. In Fig. 6.1(c), a representative frequency response of the link is also shown, in which an AMOOFDM-SCM signal spectrum is inserted. It should be noted that the transmission link is free from both optical amplifiers and chromatic dispersion compensators.

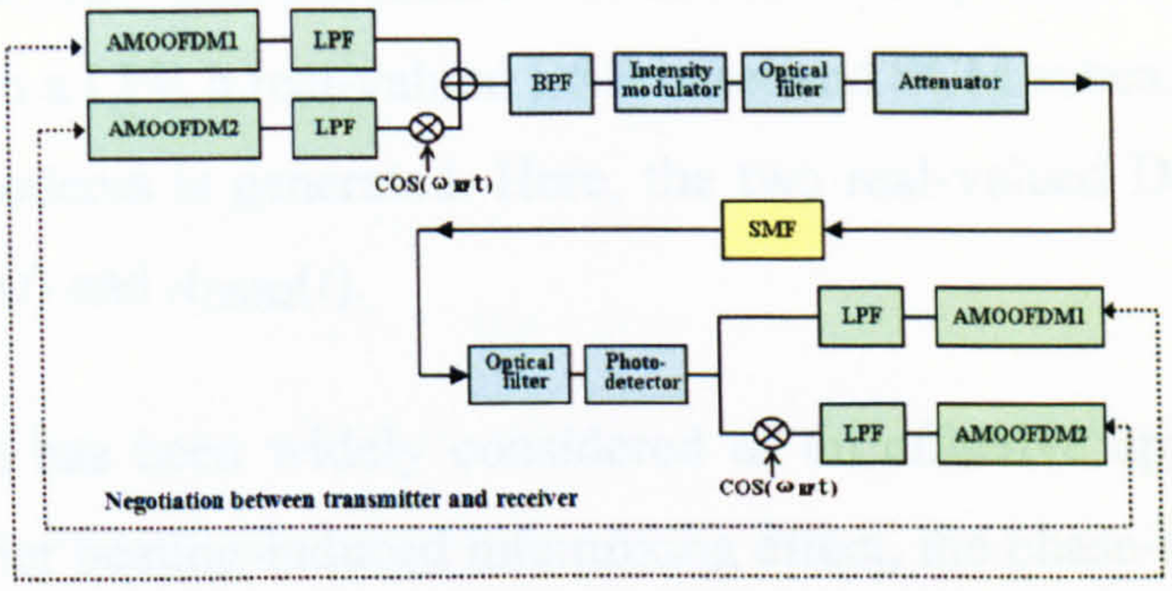

(a) AMOOFDM-SCM scheme I

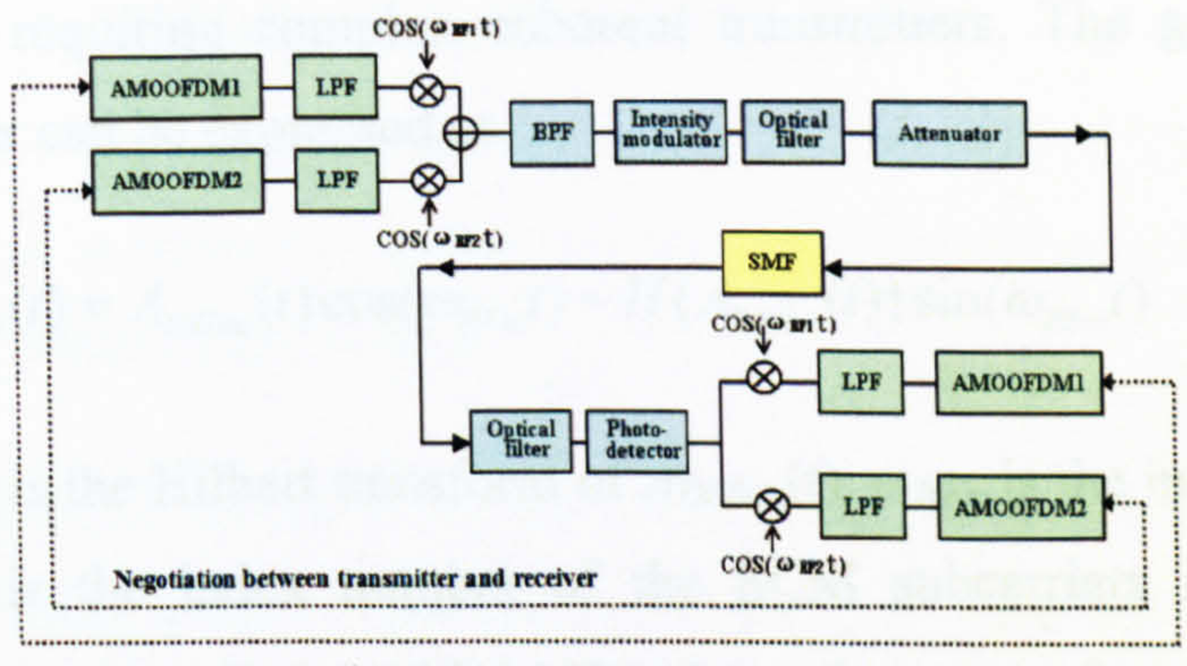

(b) AMOOFDM-SCM scheme II

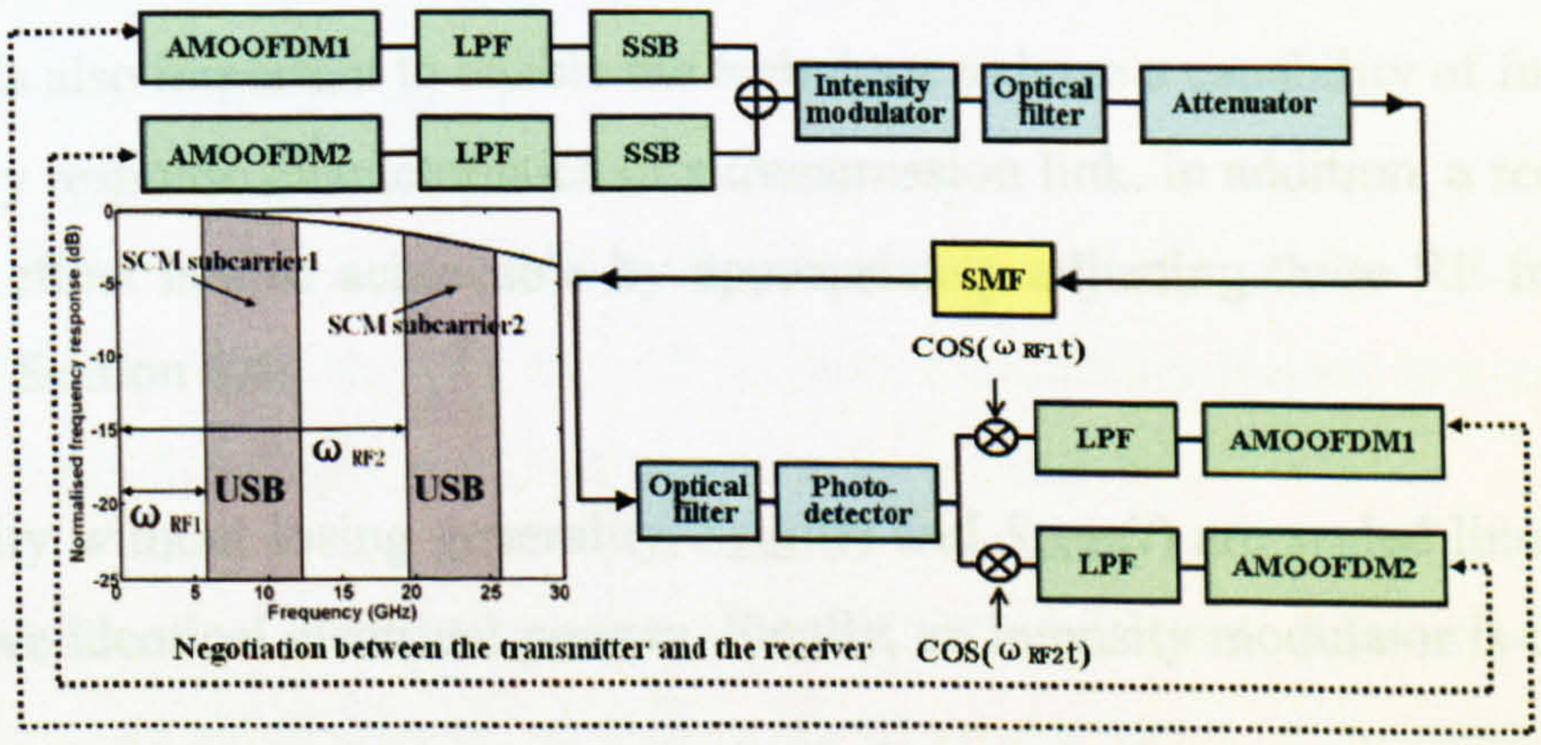

(c) AMOOFDM-SCM scheme III

Fig. 6.1 Schematic illustrations of the modem designs for AMOOFDM-SCM scheme I, II and III, together with the transmission link structure considered. A representative link frequency response and an AMOOFDM-SCM scheme III signal spectrum are also shown in Fig. 6.1(c). LPF: low-pass filter; USB: upper sideband spectrum of the SCM subcarrier.

6.2.1 AMOOFDM-SCM Scheme III Model

In the AMOOFDM-SCM scheme III transmitter, an input binary data sequence is split into two streams, each of which is encoded independently to serial complex data by using different modulation formats. The complex data is processed separately by each AMOOFDM modem following procedures similar to those presented in Chapter 2 and 5. After passing through a LPF, a real-valued DSB baseband SCM subcarrier from each of the two AMOOFDM modems is generated. Here, the two real-valued DSB SCM subcarriers are denoted as $A_{DSB1}(t)$ and $A_{\mathrm{DSB2}}(t)$.

As SSB modulation has been widely considered as an effective approach to reduce the subcarrier × subcarrier beating-induced intermixing effect, the phase-shift method based on the Hilbert transform [2] is applied to $A_{\mathrm{DSB1}}(t)$ and $A_{\mathrm{DSB2}}(t)$ to perform the SSB signal generation without requiring complex coherent transmitters. The generated real-valued SSB SCM subcarrier can be expressed as

$$S_{SSBm}(t) = A_{DSBm}(t)\cos(\omega_{RFm}t) - H\{A_{DSBm}(t)\}\sin(\omega_{RFm}t) \quad m=1,2 \tag{6.1}$$

where $H\{A_{\mathrm{DSBm}}(t)\}$ is the Hilbert transform of $A_{\mathrm{DSBm}}(t)$. ω_{RFm} is the intermediate RF carrier frequency, and m is the index number of the SCM subcarriers involved in a single AMOOFDM-SCM modem. It should be pointed out that, apart from the necessity for the generation of the real-valued SSB SCM subcarriers, the use of the intermediate RF frequencies is also important to enable the technique to have a capability of fully exploiting the frequency response characteristics of a transmission link. In addition, a reduction in the intermixing effect is also achievable by appropriately adjusting these RF frequencies, as discussed in Section 6.4.

For simplicity without losing generality, $S_{\mathrm{SSB1}}(t)$ and $S_{\mathrm{SSB2}}(t)$ are scaled linearly to ensure that they have identical electrical powers. Finally, an intensity modulator is driven directly by

$$S_e(t) = S_{SSB1}(t) + S_{SSB2}(t) + I_{dc} \tag{6.2}$$

with I_{dc} being the added DC component to ensure that $S_e(t)$ is always positive. If use is made of an ideal intensity modulator, as described in subsection 2.3.1.2, the output optical signal has a waveform given by

$$S_o(t) = \sqrt{S_e(t)} \tag{6.3}$$

It is worth addressing that, a Quantum Dot Semiconductor Optical Amplifier (QD-SOA) [4] with a typical carrier lifetime of approximately 10 ps, is able to achieve a modulation bandwidth as large as about 100 GHz. This value is much larger than the bandwidth of the AMOOFDM-SCM signals of interest of this chapter. This suggests that a QD-SOA may be used to perform the desired intensity modulation. In such an operation, $S_e(t)$ is used to drive directly the QD-SOA with a CW optical wave being injected. The power of the CW optical wave mimics the optical gain variation induced by the electrical waveform of $S_e(t)$. Investigations of the transmission performance of the AMOOFDM-SCM technique employing QD-SOAs as intensity modulators are currently being undertaken, and results will be reported elsewhere in due course.

In the AMOOFDM-SCM receiver, the transmitted optical signal is converted into an electrical signal by using a square-law photodetector. Two baseband SCM signals can be obtained by independently performing RF down-conversion followed by a LPF. Finally, the data can be recovered by each of the two AMOOFDM modems in a process of inverse of the transmitters described above.

In the initial stage of establishing a SMF link, negotiations between the transmitter and the receiver take place to identify the highest possible modulation format that should be used on each AMOOFDM subcarrier of individual SCM subcarriers.

It should be pointed out that, orthogonal band multiplexing reported for coherent OOFDM systems [5] can not be employed to reduce the aforementioned intermixing effect for the IMDD cases considered here, as IMDD systems do not preserve the phase information of transmitted signals, thus the achievement of perfect orthogonality between different SCM subcarriers is impossible, even if the following relationship is satisfied:

$$\Delta f_{SCM} = n\Delta f_{AMOOFDM} \tag{6.4}$$

where Δf_{SCM} and $\Delta f_{AMOOFDM}$ are the frequency spacing between the adjacent SCM and AMOOFDM subcarriers, respectively, and n is an integer.

6.2.2 Models of Other Components Involved in the Transmission Link

The widely adopted split-step Fourier method is used to model the propagation of the optical signal down an SMF [6]. It is well known that for a sufficiently small fibre step length, this treatment yields an accurate approximation to the real effects. In the SMF model, the effects of loss, chromatic dispersion and the optical power dependence of the refractive index are included. The effect of fibre nonlinearity-induced phase noise to intensity noise conversion is also considered upon photon detection in the receiver. This SMF model has been successfully used in [7].

As mentioned in subsection 6.2.1, a square-law photodetector is utilized in the receiver to detect the optical signals emerging from the transmission links. Shot noise and thermal noise are considered, which are simulated following the procedures similar to that presented in [8], noise generated by beating among signal spontaneous noises are not considered due to the absence of optical amplification in the transmission link.

It should be noted that, all the filters used in simulations are assumed to have ideal rectangular shapes in the frequency domain. Optical carrier suppression is not considered in generating optical SSB signals because of the use of the ideal optical filters. An optical attenuator is inserted between the optical filter and the input facet of the SMF link to adjust the optical power launched into the transmission link.

6.3 Simulation Parameters

Having described the AMOOFDM-SCM scheme III modem and the transmission link, in this section, detailed discussions are made of parameters adopted in numerical simulations. All the parameters listed below are used as default ones unless addressed explicitly in the corresponding text when necessary.

In numerical simulations, for each AMOOFDM modem generating a SCM subcarrier, 64 AMOOFDM subcarriers are considered, in which 31 having identical powers carry real data, one has no power, and the remaining 32 are the complex conjugation of the above-mentioned AMOOFDM subcarriers. The modulation formats used on each AMOOFDM subcarrier vary from DBPSK, DQPSK, and 16 to 256 QAM, depending on the frequency response of a given transmission link. The clipping level is fixed at 13 dB. The DAC/ADC used here operates at 7 bits quantization and 12.5 GS/s sampling speed. According to the aforementioned parameters, the SCM subcarrier has a bandwidth of 6.25 GHz. All other parameters which are not mentioned here can be found in Chapter 5.

An ideal intensity modulator is employed in the transmitter, and a fixed optical power of 6.3dBm is launched into the transmission link. In the receiver, a PIN with a sensitivity of -19 dBm (corresponding to 10 Gb/s with a BER of 1.0×10^{-9}) and a quantum efficiency of 0.8 is used.

For simulating SMF-based link operating at 1550 nm, the following SMF parameters are adopted: an effective area of 80 μm^2, a dispersion parameter of 17.0 ps/(km·nm), a dispersion slope of 0.07 ps/(km·nm^2), a loss of 0.20 dB/km and the Kerr coefficient is taken to be 2.35×10^{-20} m^2/W.

6.4 Simulation Results

In obtaining the signal transmission performance presented in this section, the signal line rate, R_s, is computed using the definition given below:

$$R_s = \sum_{m=1}^{2} \frac{\sum_{k=1}^{31} M_{mk}}{(N_{sub} + N_{CP})T_s} \tag{6.5}$$

where m is the index of SCM subcarriers involved in a single AMOOFDM-SCM modem of any types. M_{mk} is the number of binary bits carried by the k-th AMOOFDM subcarrier in the m-th SCM subcarrier. N_{sub} is the total number of AMOOFDM subcarriers. N_{cp} is the number of sampling periods occupied by the cyclic prefix. M_{mk}, N_{sub} and N_{cp} are taken to be the values for a single AMOOFDM symbol. T_s is the ADC sampling period, which is fixed at 80 ps, according to the simulation parameters listed in Section 6.3.

$M_{mk}/[(N_{sub}+N_{CP})T_s]$ is the data rate conveyed by the *k*-th AMOOFDM subcarrier in the *m*-th SCM subcarrier. A R_S is considered to be valid only when the total channel BER defined in Section 2.3.1.3 [7,9] remains at 1.0×10^{-3} or better, as such a BER leads to error-free operation when combined with FEC.

6.4.1 Transmission Performance of AMOOFDM-SCM Scheme I and the Intermixing Effect

As already described in Sections 6.1 and 6.2, AMOOFDM-SCM scheme I consists of two real-valued DSB SCM subcarriers with the first SCM subcarrier operating at the baseband and the other being modulated onto an intermediate RF carrier. For such a modem, the signal transmission capacity and the corresponding optimum RF carrier frequency are plotted in Fig. 6.2 as a function of transmission distance. In simulating Fig. 6.2, both the RF carrier frequency and the signal modulation format taken on each AMOOFDM subcarrier are adjusted until a maximum signal transmission capacity is obtained for a specific transmission distance. To demonstrate the effectiveness of the AMOOFDM-SCM technique, the transmission performance of an AMOOFDM modem is also given in Fig. 6.2.

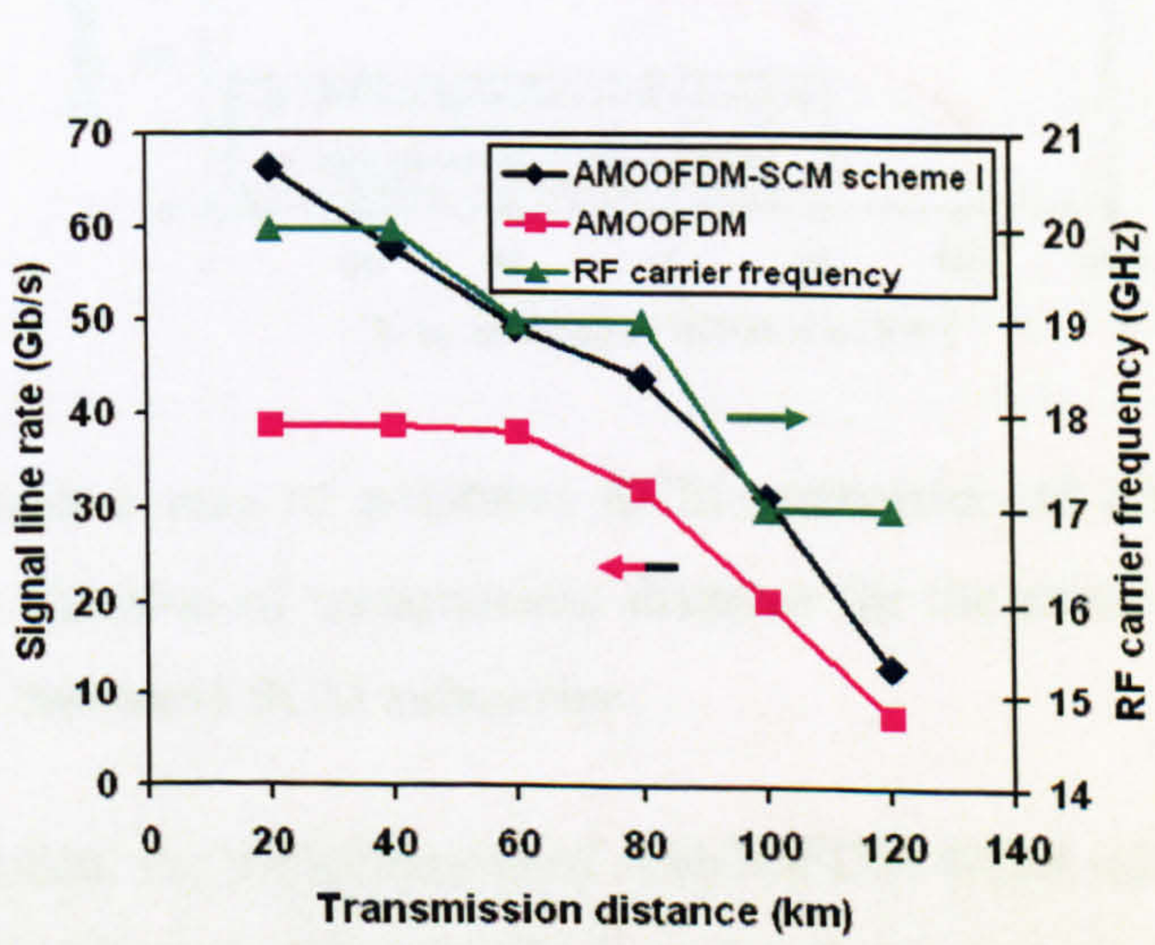

Fig. 6.2 Signal transmission capacity and RF carrier frequency as a function of transmission distance for AMOOFDM-SCM scheme I.

It can be seen from Fig. 6.2 that, in comparison with the AMOOFDM modem, AMOOFDM-SCM scheme I improves considerably the signal transmission performance, especially for short transmission distances; >66.5Gb/s AMOOFDM-SCM signal transmission over 20km is feasible, which almost doubles the transmission performance

achieved by the AMOOFDM modem. On the other hand, the frequency response narrowing effect induced by a long SMF causes an increase in transmission loss for AMOOFDM subcarriers contained in the passband SCM subcarrier, such a loss increase can be compensated partially when the RF carrier frequency is decreased appropriately to ensure that the passband SCM subcarrier spectrum locates at a relatively low transmission loss region of the link frequency response. However, as discussed below, the reduced RF carrier frequency also strengthens the intermixing effect occurring between the two SCM subcarriers. As a direct result of the co-existence of the above-mentioned two effects, the optimum RF carrier frequency reduces with increasing transmission distance and a stair-like optimum RF frequency developing curve occurs, as observed in Fig. 6.2. All the above-mentioned characteristics agree very well with those reported in [1], confirming the validity of the AMOOFDM-SCM model developed here.

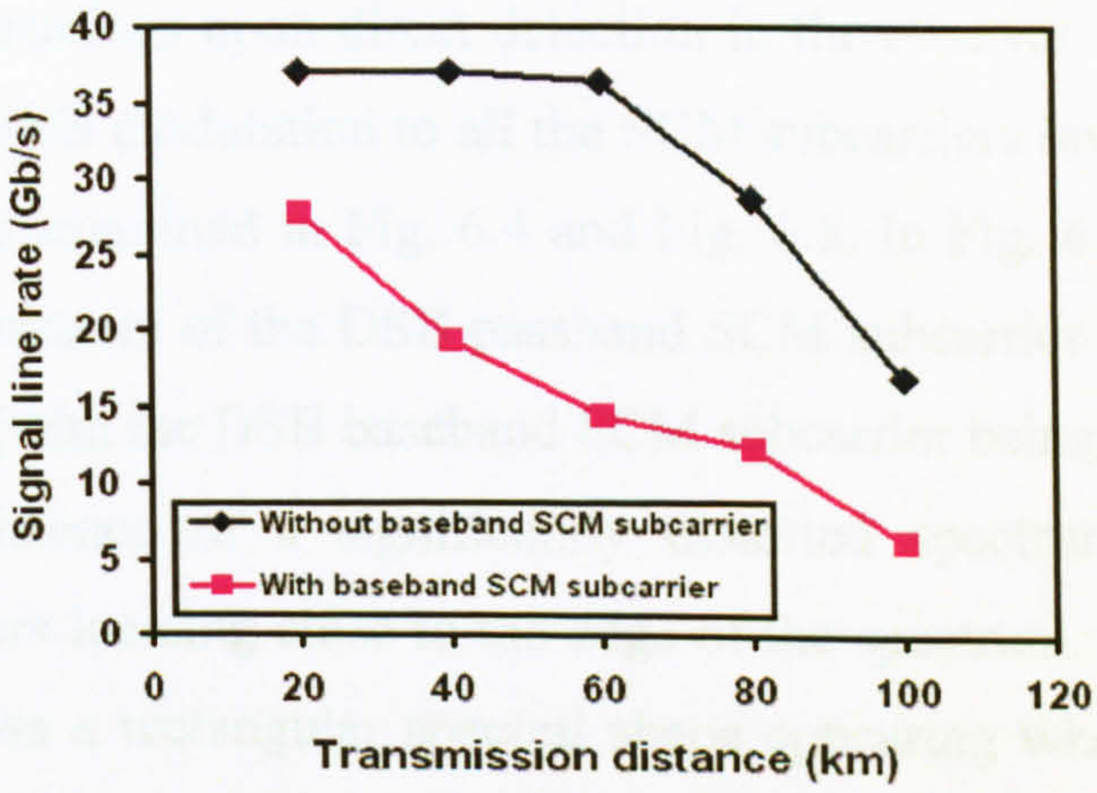

Fig.6.3 Signal line rate of passband SCM subcarrier of AMOOFDM-SCM scheme I as a function of transmission distance for the cases of including and excluding the baseband SCM subcarrier.

Fig. 6.2 also shows that, the effectiveness of AMOOFDM-SCM scheme I declines quickly with increasing transmission distance. Such a developing trend is underpinned by the frequency response narrowing effect, and the intermixing encountering between different AMOOFDM subcarriers of various SCM subcarriers. To obtain an in-depth understanding of the significance of the impact of the intermixing effect on the signal transmission performance of the technique, Fig. 6.3 is presented, where the signal line rate of the passband SCM subcarrier is plotted as a function of transmission distance for the cases of excluding and including the baseband SCM subcarrier. It should be noted that, to perform a

fair comparison between Fig. 6.3 and Fig. 6.2, the optimum RF carrier frequencies obtained in Fig. 6.2 are also adopted in calculating Fig. 6.3. The exclusion of the baseband SCM subcarrier in AMOOFDM-SCM scheme I can remove completely the intermixing effect experienced by the passband SCM subcarrier. By considering Fig. 6.2 and comparing the two lineshapes shown in Fig. 6.3, it is deduced that the intermixing effect can lower the signal transmission capacity of the passband SCM subcarrier by a factor of approximately 2. In addition, the intermixing effect is less pronounced for short transmission distances, as expected from discussions in [1].

Having demonstrated the crucial role of the intermixing effect in determining the maximum achievable transmission performance of the AMOOFDM-SCM technique, special attention is given to identify practical solutions to minimize the impact of such an effect. Considering the fact that the physical origin of the intermixing effect is subcarrier×subcarrier beatings upon direct detection in the receiver, an effective approach is, therefore, to apply SSB modulation to all the SCM subcarriers involved. The feasibility of such an approach is examined in Fig. 6.4 and Fig. 6.5. In Fig. 6.4, a frequency down-converted electrical spectrum of the DSB passband SCM subcarrier received after passing through a 60km SMF (with the DSB baseband SCM subcarrier being present) is illustrated, which shows the existence of a significantly distorted spectrum, especially for the AMOOFDM subcarriers locating close to the edge of the spectrum. In sharp contrast with Fig. 6.4, Fig. 6.5 shows a rectangular spectral shape appearing when SSB modulation is applied to both SCM subcarriers. As a direct result of that, AMOOFDM-SCM scheme III is proposed and discussed in subsection 6.4.3 and subsection 6.4.4.

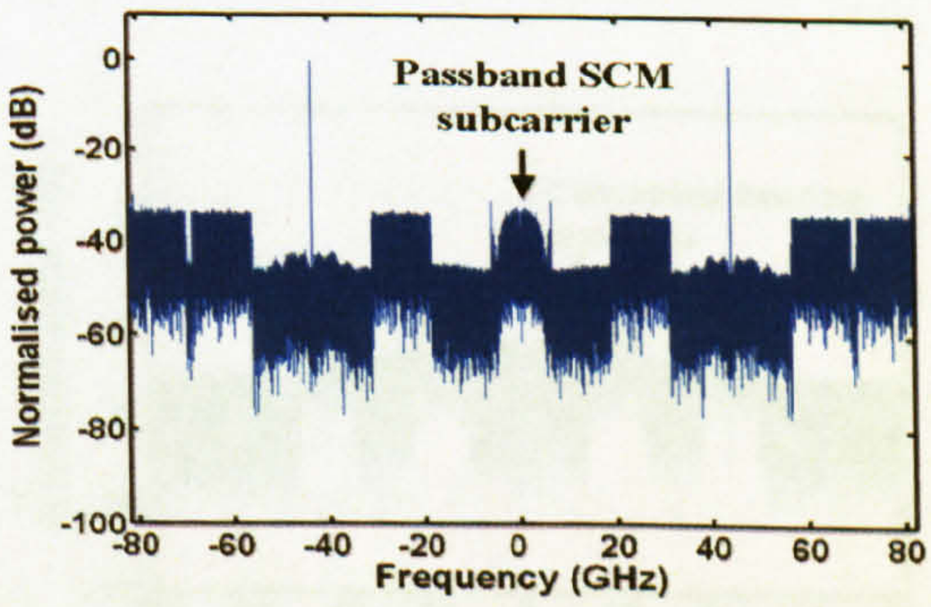

Fig. 6.4 Frequency down-converted spectrum of the DSB passband SCM subcarrier after passing through 60km SMF. The RF carrier frequency is 19GHz.

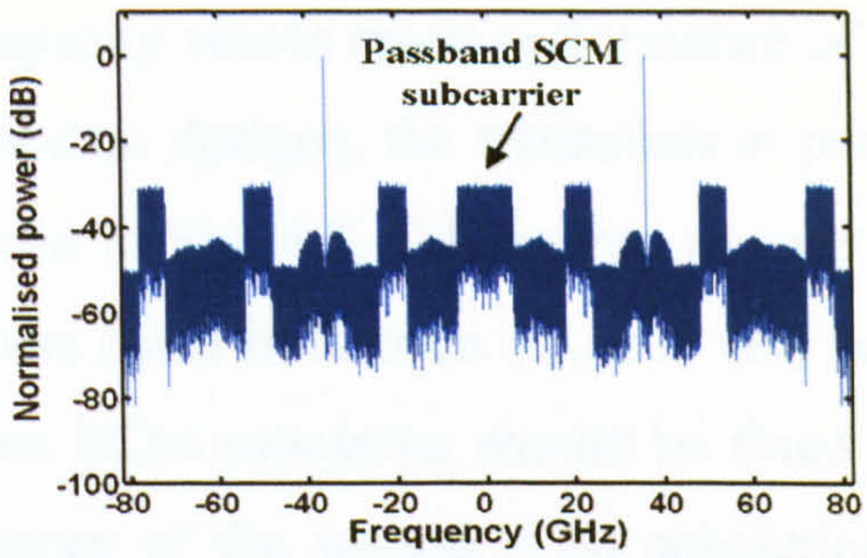

Fig. 6.5 Frequency down-converted spectrum of the SSB passband SCM subcarrier after passing through 60km SMF. The RF carrier frequency is 19GHz.

6.4.2 Transmission Performance of AMOOFDM-SCM Scheme II

Based on the analysis in subsection 6.4.1, it is envisaged that, upon direction detection in the receiver, beating between different AMOOFDM subcarriers of the same SCM subcarrier also causes the unwanted spectral distortion region in the vicinity of the optical carrier. This statement is confirmed in Fig. 6.6, where a spectral distortion region having a bandwidth equal to the SCM subcarrier bandwidth is observed around the zero frequency point. To enable the separation of such an unwanted spectral region from the useful SCM subcarrier spectrum, here AMOOFDM-SCM scheme II is proposed, in which a spectral gap having a bandwidth of the SCM subcarrier bandwidth is introduced between the optical carrier and the spectral band of the first SCM subcarrier. In addition, similar to AMOOFDM-SCM scheme I, the two SCM subcarriers are DSB signals in AMOOFDM-SCM scheme II. It is interesting to note that use has also been made of the spectral gap approach in experimental investigations of long-haul OOFDM transmission [10].

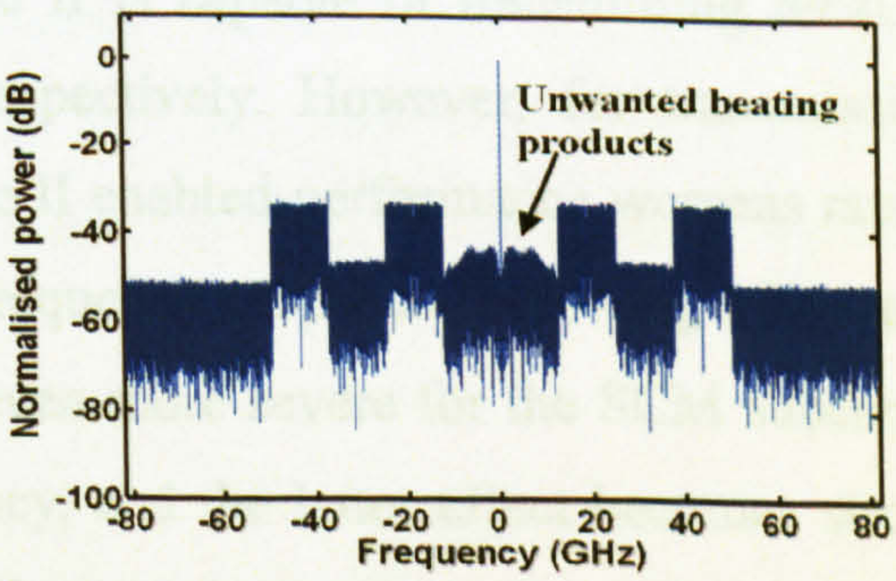

Fig.6.6 Received signal spectrum of AMOOFDM-SCM scheme II after transmitting 40 km. The two SCM subcarriers operate at RF carrier frequencies of 18.75GHz and 43.75GHz.

Fig. 6.7 shows the signal capacity versus reach performance of AMOOFDM-SCM scheme II. To compare different modem designs, the transmission performance of AMOOFDM-SCM scheme I is also plotted in Fig. 6.7. Taking into account the discussions in Fig. 6.6 and the simulation parameters listed in Section 6.3, it is very easy to work out that the RF carrier frequency of the first SCM subcarrier should be fixed at 18.75GHz. On the other hand, the RF carrier frequency of the second SCM subcarrier is taken to be 43.75GHz, which is an optimized value corresponding to a transmission distance of 40km. The validity of the adoption of such a constant RF carrier frequency for the second SCM subcarrier is discussed in subsection 6.4.3.

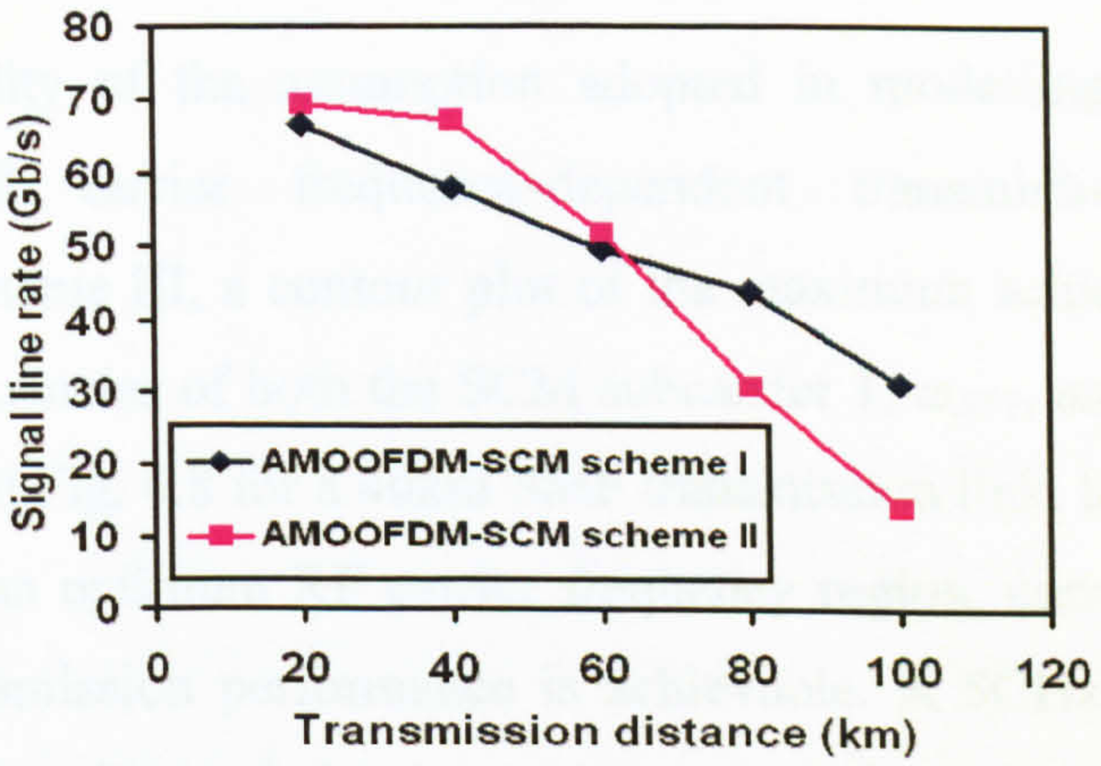

Fig. 6.7 Transmission capacity versus reach performance of AMOOFDM-SCM scheme II. The two SCM subcarriers are taken to be 18.75GHz and 43.75GHz.

It is shown in Fig. 6.7 that, in comparison with AMOOFDM-SCM scheme I, a notable enhancement in signal transmission performance is observed for AMOOFDM-SCM scheme II when transmission distances are shorter than about 60km. As an example, AMOOFDM-SCM scheme II is capable of transmitting 69.4Gb/s and 67.2Gb/s signals over 20km and 40km, respectively. However, for transmission distances >60km, the AMOOFDM-SCM scheme II enabled-performance worsens rapidly. This arises due to the co-existence of the link frequency response narrowing effect and the intermixing effect. The first effect becomes even more severe for the SCM subcarrier located far away from the optical carrier frequency, and the latter effect becomes strong when the transmission distance increases due to fibre chromatic dispersion and nonlinearity.

6.4.3 RF Carrier Frequency Dependent Transmission Performance of AMOOFDM-SCM Scheme III

Having demonstrated the importance of SSB modulation and spectral gapping in enhancing the transmission performance of AMOOFDM-SCM modems of two different designs, in subsection 6.4.3 and subsection 6.4.4, an integration of these two individual approaches into a single AMOOFDM-SCM modem is undertaken, which brings about a new modem design called as AMOOFDM-SCM scheme III. In such a scheme, SSB modulation is applied to all the involved SCM subcarriers with a spectral gap of desired width being inserted between the optical carrier and the first SCM subcarrier.

To examine the validity of the assumption adopted in modelling Fig. 6.7 and, more importantly, the RF carrier frequency-dependent transmission performance of AMOOFDM-SCM scheme III, a contour plot of the maximum achievable signal line rate versus RF carrier frequencies of both the SCM subcarrier 1, ω_{RF1}, and the SCM subcarrier 2, ω_{RF2}, is presented in Fig. 6.8 for a 40km SMF transmission link. It can be seen from Fig. 6.8 that, there exists an optimum RF carrier frequency region, corresponding to which a maximum signal transmission performance is achievable. A 5GHz (3GHz) alteration of ω_{RF2} (ω_{RF1}) gives rise to <3% variation in signal transmission capacity of the technique. In addition, simulations also show that, the optimum ω_{RF1} is independent of transmission distance, as expected from the discussions in subsection 6.4.2, and that an extension of the transmission distance from 40km to 80km just reduces the optimum ω_{RF2} value by approximately 2GHz. All the above-mentioned characteristics indicate that the transmission performance of AMOOFDM-SCM scheme III is very robust to transmission distance and RF carrier frequency. Therefore, for practical cases including the conditions used in Fig. 6.7, it is sufficiently accurate to fix both RF carrier frequencies at their values optimized for a specific link operating condition. Such robustness may not only speed up considerably the modem design processes, but also reduce significantly the modem cost.

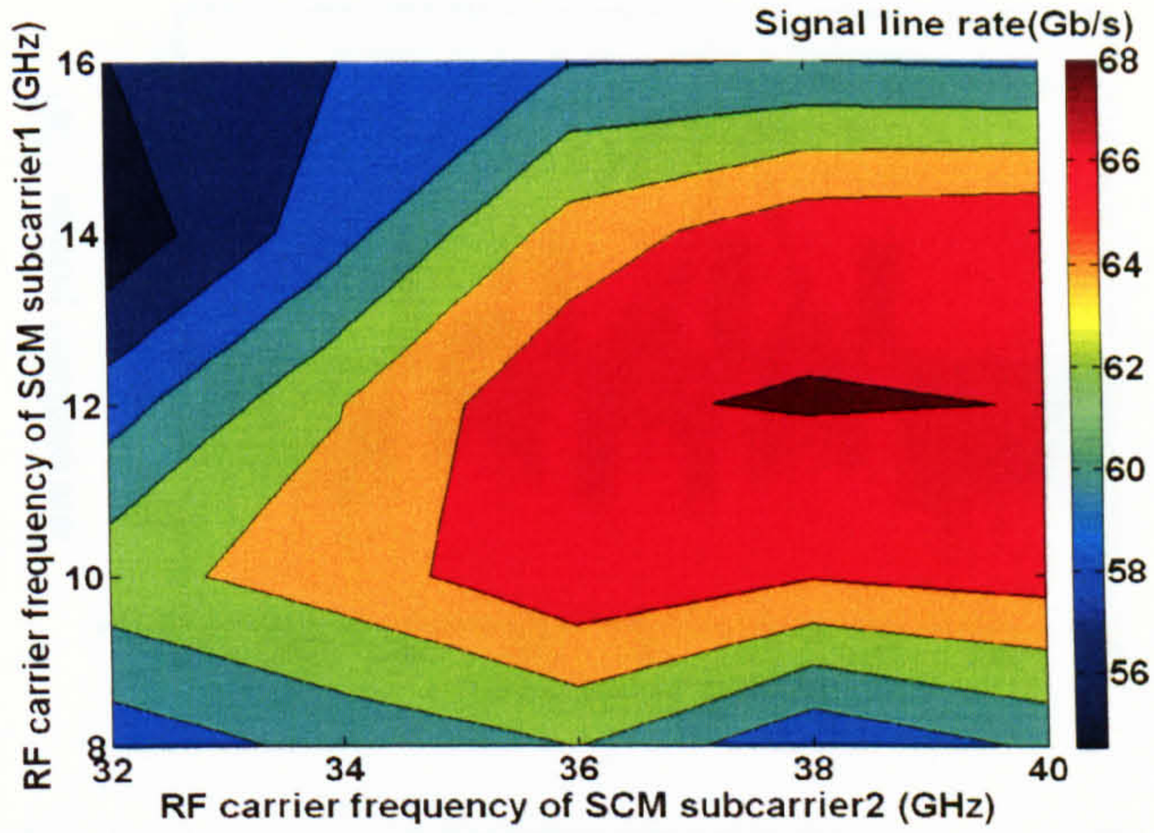

Fig. 6.8 Contour plot of signal transmission capacity as a function of RF carrier frequencies of the first and second SCM subcarriers for AMOOFDM-SCM scheme III. Numerical simulations are undertaken for a 40 km transmission link.

It should also be noted, in particular, that the optimum ω_{RF1} value of approximately 12GHz, as shown in Fig. 6.8, is almost twice of the SSB SCM subcarrier bandwidth, and almost equal to the DSB SCM subcarrier bandwidth discussed in subsection 6.4.2. The physical reason behind such a behavior is that the phase-shift method using the Hilbert transform creates a SSB output by phasing its corresponding DSB sidebands in a way that the DSB sidebands cancel out on one side of the RF carrier frequency and add on the other side [2]. Clearly, such a cancellation operation can not be maintained perfectly if the spectral gap identical to the SSB SCM subcarrier bandwidth is introduced, as one sideband of the DSB signal overlaps with the newly generated spectral distortion region, as illustrated in Fig. 6.6 and Fig. 6.9.

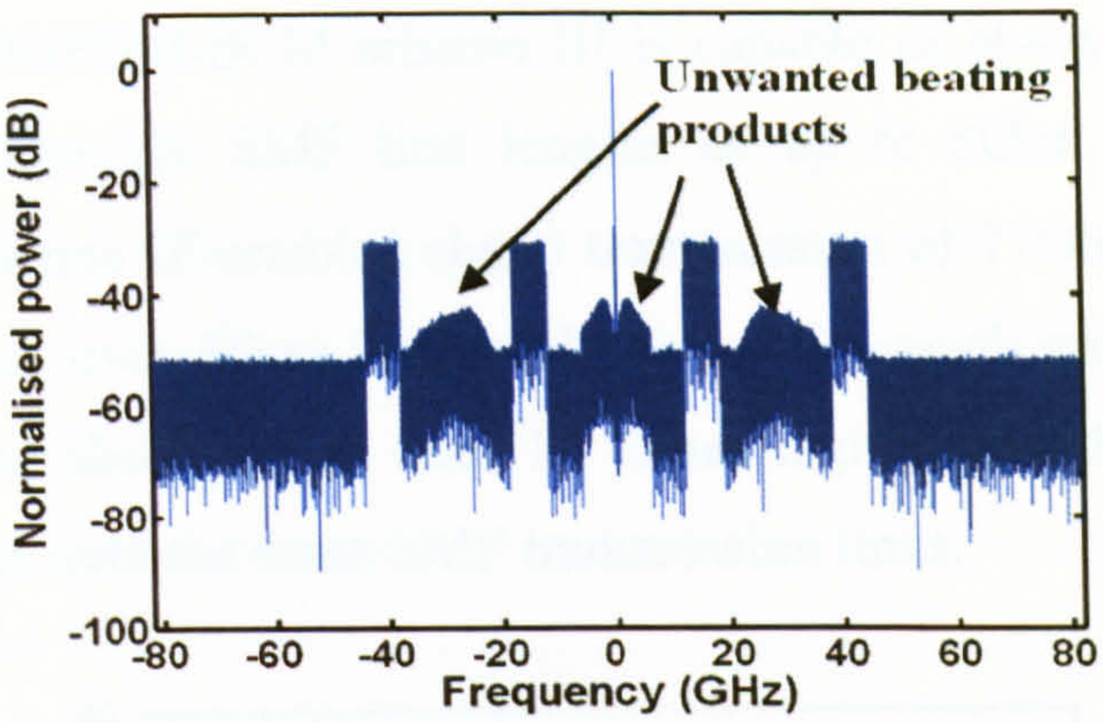

Fig. 6.9 Received spectrum of AMOOFDM-SCM scheme III after a 40km transmission distance.

It is also very interesting to see from Fig. 6.8 that, for a given ω_{RF2}, a similar transmission performance is obtainable in two ω_{RF1} regimes. This can be explained by considering Fig. 6.9, where two residual spectral distortion regions are still present in the SSB signal spectrum after direct detection. The first spectral distortion region close to the zero frequency point occurs because of beatings of various AMOOFDM subcarriers within the same SCM subcarrier. Whilst the second spectral distortion region present between the two SCM subcarriers occurs due to the co-existence of both the above-mentioned physical mechanism and beatings between various AMOOFDM subcarriers of different SCM subcarriers within the same modem. Shifting ω_{RF1} towards the low (high) frequency side results in the first SCM subcarrier experiencing increased distortions induced by the first (second) spectral distortion region, and simultaneously experiencing decreased distortions induced by the second (first) spectral distortion region. The co-existence of all these effects gives rise to the occurrence of the two ω_{RF1} regions, over which the same transmission performances can be observed.

6.4.4 Transmission Performance of AMOOFDM-SCM Scheme III and Modem Design Criteria

The transmission performance of AMOOFDM-SCM scheme III is presented in Fig. 6.10 for the operating conditions of adopting two optimum RF carrier frequencies of ω_{RF1} =12GHz and ω_{RF2} = 37.5GHz, as identified in Fig. 6.8. To undertake performance comparisons between different modem designs, the signal capacity versus reach performances are also plotted for AMOOFDM-SCM scheme I, AMOOFDM-SCM scheme II and AMOOFDM. It can be found from Fig. 6.10 that, of the proposed three types of

modem designs, AMOOFDM-SCM scheme III is capable of always offering the highest transmission performance for SMF link lengths of up to 80km. As an example, the AMOOFDM-SCM scheme III-enabled signal transmission of 71Gb/s over 20km, 63Gb/s over 60km and 48Gb/s over 80km is feasible. It is also worth emphasizing that all the performances specified above are at least 1.5 times higher than those supported by the AMOOFDM technique over the same SMF transmission links.

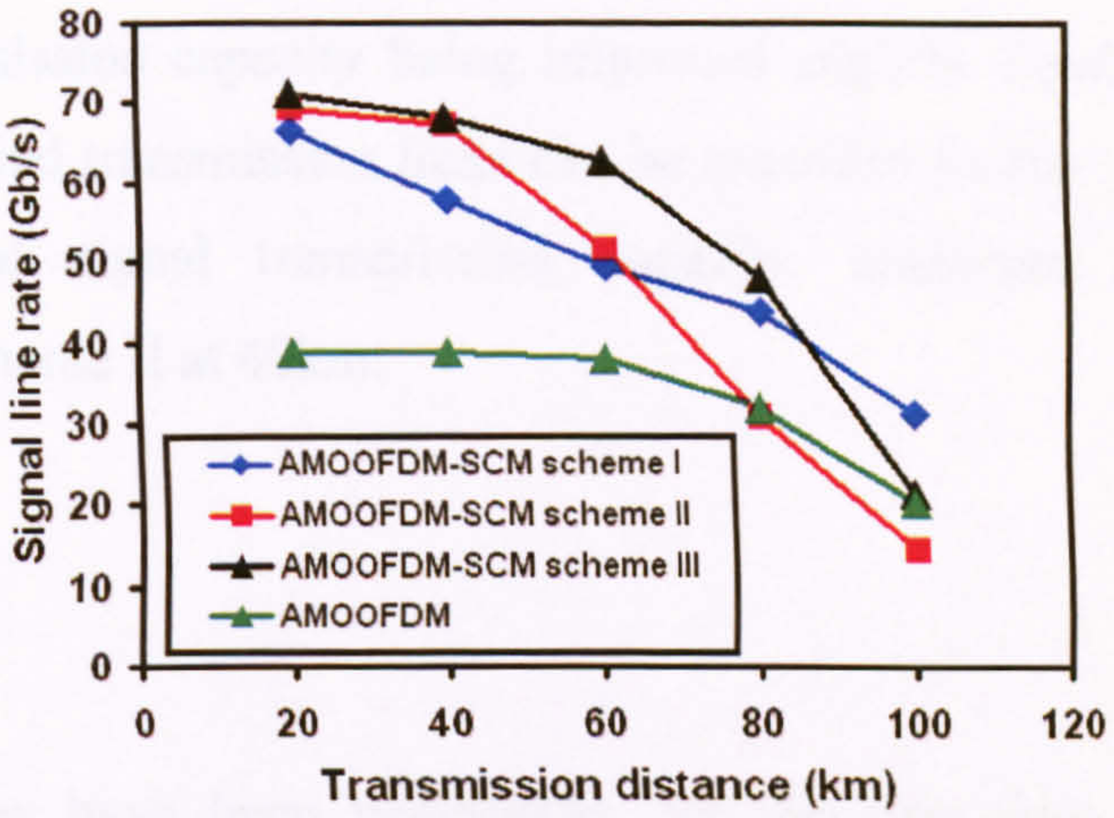

Fig.6.10 Signal transmission capacity versus reach performance of AMOOFDM-SCM scheme III. For comparison, the transmission performances for AMOOFDM-SCM scheme I, AMOOFDM-SCM scheme II and AMOOFDM are also illustrated.

As also seen in Fig. 6.10, for SMF link lengths in a range from 20km to 40km, the transmission performances of AMOOFDM-SCM scheme II and AMOOFDM-SCM scheme III are very similar, both of which are, however, higher than those offered by AMOOFDM-SCM scheme I. This indicates that the impact of the reduction in the intermixing effect due to applying SSB modulation to SCM subcarriers is negligible on the signal transmission performance of AMOOFDM-SCM scheme III. On the other hand, such an intermixing reduction is crucial for transmission distances of >60km, because over such a distance region, AMOOFDM-SCM scheme III can improve considerably the signal transmission performance compared to the AMOOFDM-SCM scheme II. Finally, for transmission distances beyond 90km, the link frequency response becomes very narrow and is not able to provide the AMOOFDM-SCM scheme III with a sufficiently broad bandwidth, thus resulting in the most rapid performance degradation with increasing transmission distance among all the modem types proposed in this chapter.

Use may be made of each of the three modem designs to satisfy requirements of different application scenarios that may be encountered in NG-PONs. Firstly, given the fact that AMOOFDM-SCM scheme I has the simplest modem structure and the highest bandwidth efficiency, it may be preferred for practical implementation in very short transmission links of, say 20km, to enable 66.5Gb/s signal transmission. Secondly, AMOOFDM-SCM scheme II consists of a structure less complex than AMOOFDM-SCM scheme III, it may be employed to extend the above-mentioned transmission links to approximately 40km, with the signal transmission capacity being improved slightly. Finally, the AMOOFDM-SCM scheme II- enabled transmission links can be extended further to about 60km with a 10% enhancement of signal transmission capacity, compared to that offered by AMOOFDM-SCM scheme II at 40km.

6.5 Conclusion

Detailed investigations have been undertaken, for the first time, of the transmission performance of a recently proposed novel AMOOFDM-SCM modem in single-channel, SMF-based IMDD transmission links without optical amplification and chromatic dispersion compensation for practical applications in NG-PONs. It has been shown that the intermixing effect induced by beating between subcarriers of various types is a crucial factor limiting the maximum achievable AMOOFDM-SCM performance. To mitigate such an effect, SSB modulation and spectral gapping are applied to AMOOFDM-SCM. As a direct result, three AMOOFDM-SCM modem designs of varying electrical complexity have been proposed, which include, for example, AMOOFDM-SCM scheme I, AMOOFDM-SCM scheme II and AMOOFDM-SCM scheme III.

Numerical simulations have shown that, in comparison with AMOOFDM modems, all the proposed three modem designs can improve significantly the signal transmission capacity versus reach performance by a factor of at least 1.5 for transmission distances of up to 60km. AMOOFDM-SCM scheme I has the least modem complexity and the highest bandwidth efficiency, it may be preferred for use in very short transmission links of up to 20km to enable 66.5Gb/s signal transmission. With an approximately 1Gb/s increase to such a signal capacity, AMOOFDM-SCM scheme II having a structure less complex than AMOOFDM-SCM scheme III, may be employed to extend the transmission link to 40km.

Once again, the AMOOFDM-SCM scheme II-supported transmission links may be upgraded even further to 63Gb/s over 60km, when use is made of AMOOFDM-SCM scheme III.

References

[1] X. Zheng, J. M. Tang and P. S. Spencer, "Transmission performance of adaptively modulated optical OFDM modems using subcarrier modulation over worst-case multimode fibre links," IEEE Comm. Lett., vol. 12, no. 10, pp. 788-790, Aug. 2008.

[2] A. B. Carlson, P. B. Crilly and J. C. Rutledge, *Communication Systems: An Introduction to Signals and Noise in Electrical Communication*, McGraw-Hill Higher Education, 2002.

[3] M. Schuster, S. Randel, C.A. Bunge, S. C. J.Lee, F. Breyer, B. Spinnler and K. Petermann, "Spectrally efficient compatible single-sideband modulation for OFDM transmission with direct detection," IEEE Photon.Technol.Lett. vol. 20, no. 9, pp. 670-672, May. 2008.

[4] R. Brenot, F. Lelarge, O. Legouezigou, F. Pommereau, F. Poingt, L. Legouezogou, E. Derouin, O. Drisse, B. Rousseau, F. Martin and G. H. Duan, "Quantum dot semiconductor optical amplifier with a -3dB bandwidth of up to 120 nm in semi-cooled operation," OFC/NFOEC, (OSA, 2008), Paper OTuC1.

[5] T. Kobayashi, A. Sano, E. Yamada, Y. Miyamoto, H. Takara and A. Takada, "Electro-optically multiplexed 110 Gbit/s optical OFDM signal transmission over 80 km SMF without dispersion compensation," Electron. Lett., vol. 44, no. 3, pp. 225-226, Jan. 2008.

[6] G. P. Agrawal, *Nonlinear Fibre Optics*, Academic, 1995.

[7] J. M. Tang and K. A. Shore, "30Gb/s signal transmission over 40-km directly modulated DFB-laser-based single-mode-fiber links without optical amplification and dispersion compensation," J. Lightw. Technol., vol. 24, no. 6, pp. 2318-2327, June. 2006.

[8] G. P. Agrawal, *Fibre-Optic Communication Systems*, Wiley, 1997.

[9] J. M. Tang, P. M. Lane and K. A. Shore, "High-speed transmission of adaptively modulated optical OFDM signals over multimode fibres using directly modulated DFBs," J. Lightw. Technol., vol. 24, no. 1, pp. 429–441, Jan. 2006.

[10] B. J. C. Schmidt, A. J. Lowery and J. Armstrong, "Experimental demonstrations of electronic dispersion compensation for long-haul transmission using direct-detection optical OFDM," J. Lightwave Technol., vol. 26, no. 1, pp. 196-203, Jan. 2008.

7 Simplified AMOOFDM-SCM with Added Input/Output Reconfigurability

Contents

7.1 Introduction

In each of the AMOOFDM-SCM schemes described in Chapter 6, two IFFT/FFT operations are required to produce two real-valued SCM subcarriers, which complicate the system design as mentioned in Chapter 4. To reduce the system complexity and cost, in this chapter, three significantly simplified AMOOFDM-SCM modem configurations, referred to as Reconfigurable Scheme (RS) I, II and III, are proposed, for the first time, each of which requires a single IFFT/FFT operation. The general structures of the three proposed RS modems are similar to those corresponding to the AMOOFDM-SCM schemes described in Chapter 6 [1]. The differences between these two sets of modems are the signal processing approaches used in distributing the encoded incoming data prior to the IFFT operation in the transmitter and those adopted in recovering the received data after the FFT operation in the receiver, as discussed in Section 7.2. The RS modem configurations support transmission performances identical to those presented in Chapter 6 without compromising system flexibility and performance robustness to variations in transmission link characteristics. More importantly, the simplified RS modems also offer input/output reconfigurability. In the transmitter, the input data can be either from two independent data sources, or from a single data source, which is then split into two sets of data. For simplicity, these two sets of data are denoted as $\{A\}$ and $\{B\}$. As shown in Section 7.2, an appropriate arrangement of these two sets of data at the input of the IFFT operation enables that the in-phase (I) and quadrature (Q) components at the output of the IFFT operation convey information only from $\{A\}$ and $\{B\}$, respectively. Therefore, $\{A\}$ and $\{B\}$ can be recovered independently by two individual end-users in the receiver. Alternatively, these two sets of data can also be recovered simultaneously by a single end-user using a similar receiver. It is also worth addressing, in particular, that coherent OOFDM [2] is not capable of offering the abovementioned input/output reconfigurability, as the resulting I and Q components in the transmitter are not separable.

Apart from the features mentioned above, when use is made of the proposed RS modems in WDM-PONs, the RS modems also reveal the following salient advantages:

- Dynamic bandwidth allocation capability: in pure WDM-PONs, one optical carrier having a fixed bandwidth is assigned to one dedicated end-user. Without requiring any modifications to the fibre infrastructure and by using a single optical carrier, the use of

the RS modems allows two end-users to share dynamically a total bandwidth of twice of that corresponding to a single end-user.

- Doubled number of end-users: in comparison with the number of end-users supported by a pure WDM-PON having a specific number of optical wavelengths, the employment of the RS modems in such a network is able to double the number of end-users without compromising the bandwidth offered to each end-user.
- Broadcasting functionality: instead of transmitting end-user data, one of the data sets can be utilised to carry a broadcasting signal, which is distributed to the end-user along with its own traffic carried by the other data set.
- Network monitoring functionality: it can be seen from Section 7.2 that, $\{A\}$, $\{B\}$ and $\{A\}+\{B\}$ can be recovered simultaneously and independently. This suggests that use can be made of the RS modems to perform network functionalities such as network monitoring and resilience.
- Cost reduction: when compared with AMOOFDM-SCM schemes, the use of the RS modems in WDM-PONs brings significant cost savings, due to their aforementioned features including, for example, simplified modem configurations and doubled number of end-users served.

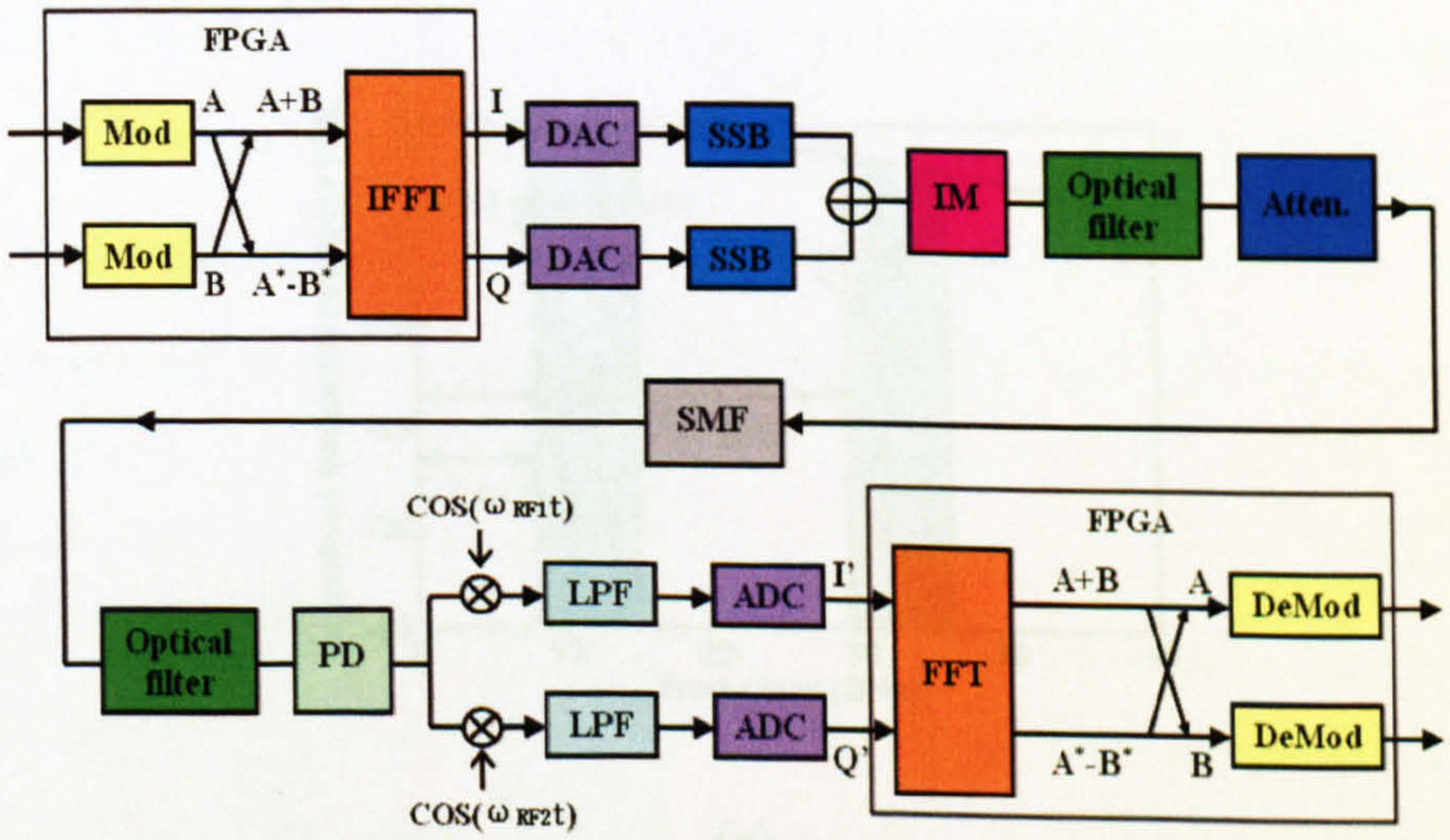

Fig.7.1 Schematic illustration of RS III modem configuration and corresponding transmission link structure. Mod: modulation; IM: intensity modulator; Atten: attenuator; PD: photodetector; DeMod: demodulation; FPGA: field programmable gate array.

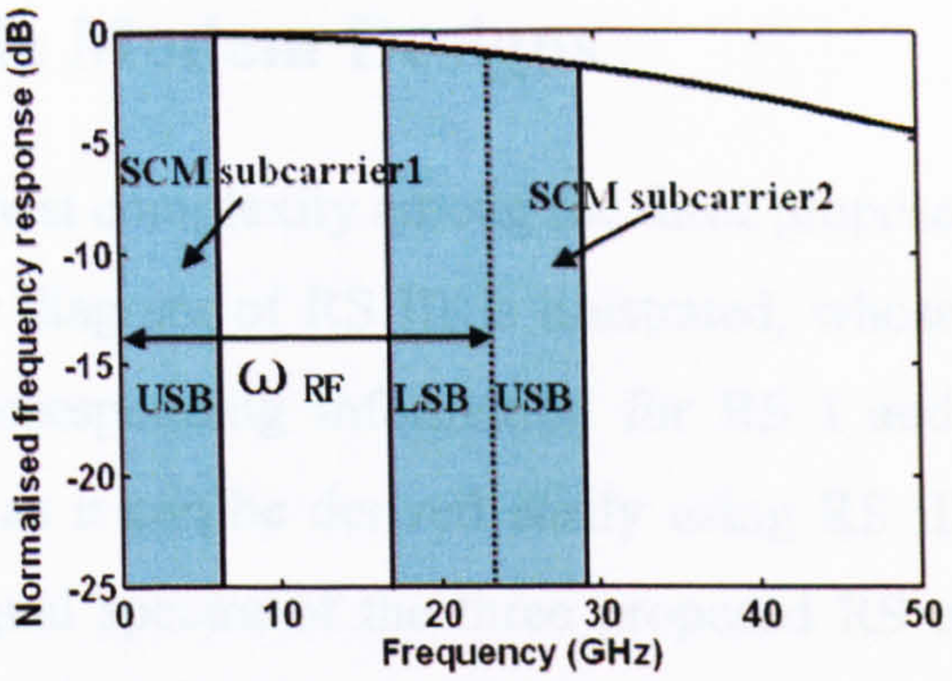

(a)

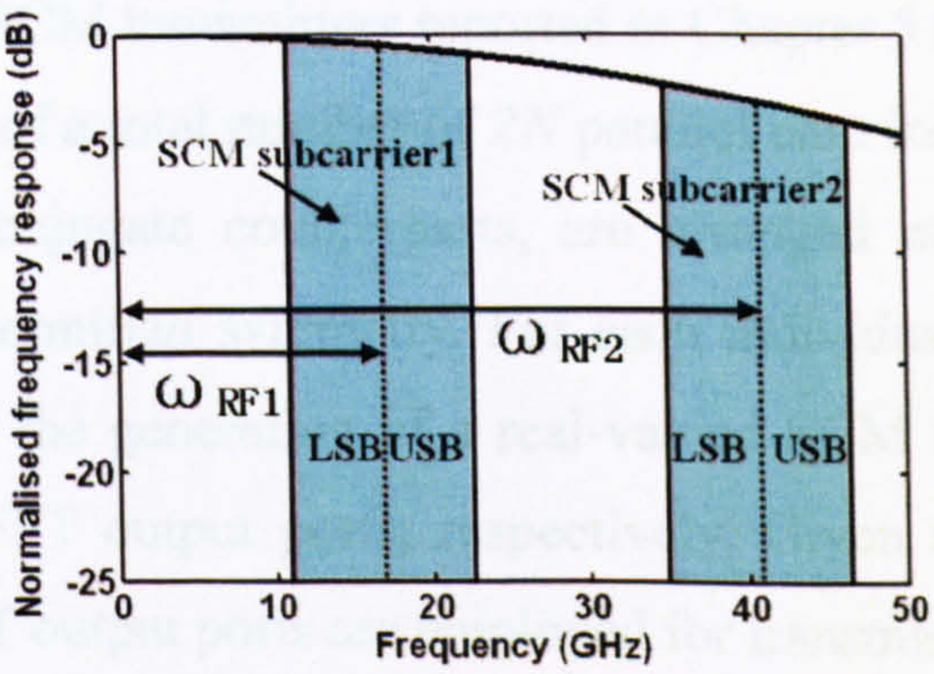

(b)

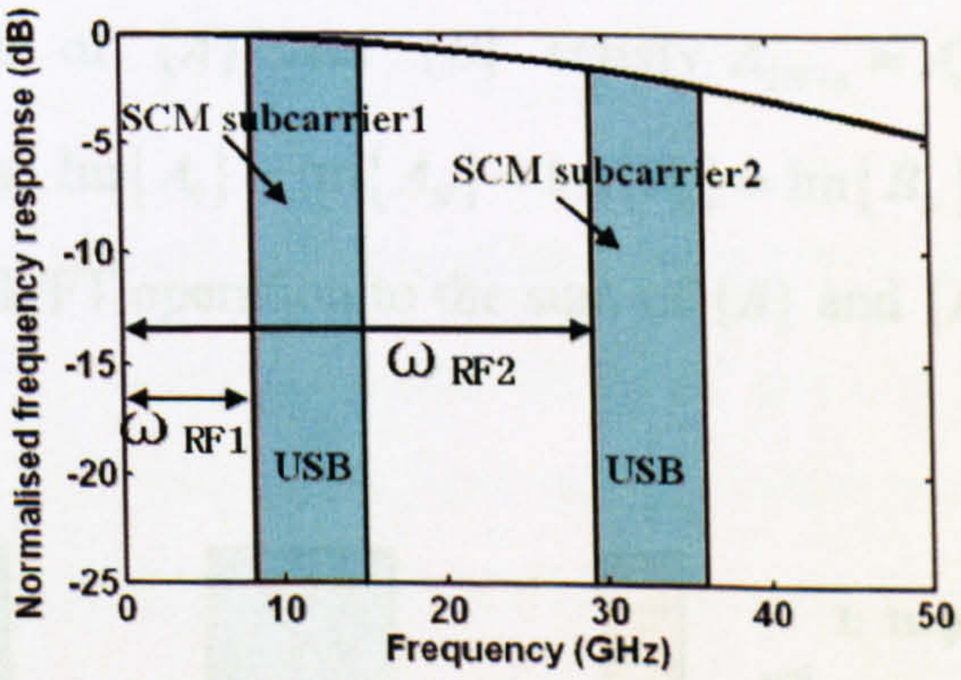

(c)

Fig.7.2 Signal spectra of the proposed RS modems. USB: upper sideband spectrum of the SCM subcarrier; LSB: lower sideband spectrum of the SCM subcarrier. (a) RS I; (b) RS II; (c) RS III.

7.2 Reconfigurable Modem Designs

Since RS III is of the highest complexity among the three proposed RS modems, in Fig.7.1, the schematic transceiver diagram of RS III is illustrated, whose operating principles are described below. The corresponding information for RS I and RS II is, however, not presented in detail here, as it can be derived easily using RS III and AMOOFDM-SCM scheme I and II. The signal spectra of the three proposed RS modems are illustrated in Fig.7.2. A single-channel IMDD SMF transmission link operating at 1550nm is considered, in which optical amplification and chromatic dispersion compensation are excluded.

In all of the AMOOFDM-SCM transmitters reported in Chapter 5 and 6 [1,3], AMOOFDM subcarriers, which consist of a total number of *2N* parallel data including both the encoded original data and their conjugate counterparts, are arranged at the input of the IFFT operation to satisfy the Hermitian symmetry. For each individual modem, such an input data arrangement leads to the generation of a real-valued SCM subcarrier and zero from the real and imaginary IFFT output ports, respectively. Given the complex property of IFFT, only half of the IFFT output ports are employed for transmission.

In the proposed RS I, II and III transmitters, AMOOFDM subcarriers are a sum of two individual sets of data, $\{A\}$ and $\{B\}$, each of which contains *2N* parallel encoded data. When the *n*-th elements of $\{A\}$ and $\{B\}$ satisfy $A_{2N-n} = A_n^*$ and $B_{2N-n} = -B_n^*$ for *n*=1,2…2*N*-1, as well as $\mathrm{Im}\{A_0\} = \mathrm{Im}\{A_N\} = \mathrm{Im}\{B_0\} = \mathrm{Im}\{B_N\} = 0$, as illustrated in Fig.7.3, after applying an IFFT operation to the sum of $\{A\}$ and $\{B\}$, a *k*-th output symbol can be written as

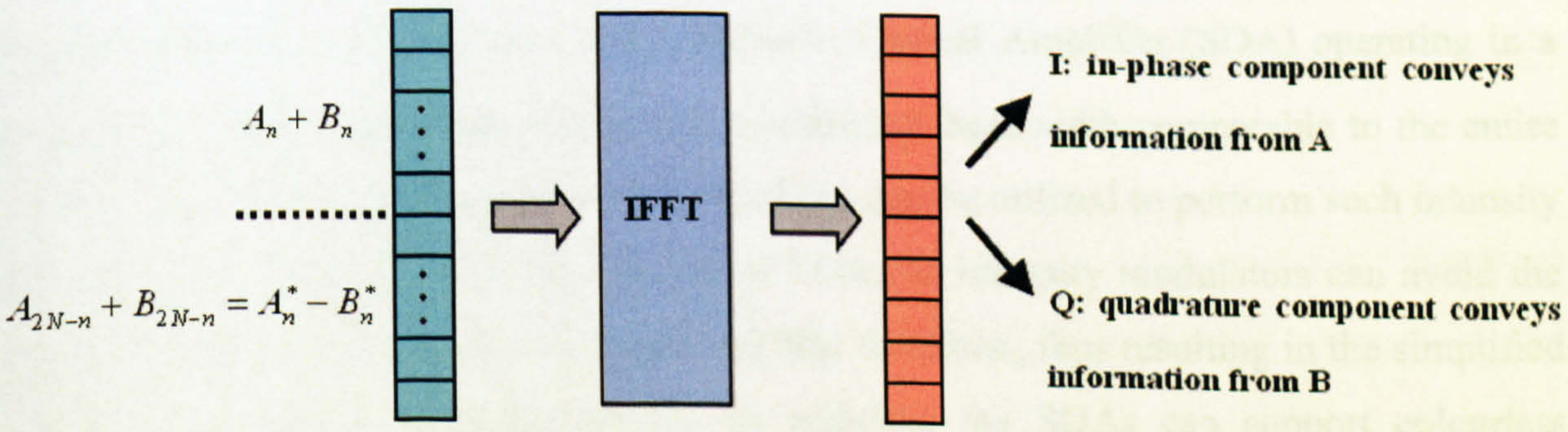

Fig. 7.3 Illustration of the generation of pure real-valued symbols and pure imaginary-valued symbols

$$S_k^{A+B}(t)=\sum_{n=0}^{2N-1}A_n e^{j2\pi n\Delta ft}+\sum_{n=0}^{2N-1}B_n e^{j2\pi n\Delta ft}=I_{k\_A}(t)+jQ_{k\_B}(t) \tag{7.1}$$

where Δf is the frequency spacing between adjacent AMOOFDM subcarriers. Eq.(7.1) indicates that the input data distribution adopted here enables full use of both the components $I_{k\_A}(t)$ and $Q_{k\_B}(t)$. More importantly, $I_{k\_A}(t)$ conveys information only from $\{A\}$ and $Q_{k\_B}(t)$ conveys information only from $\{B\}$. Such a feature enables the independent transmission of two sets of data with a single IFFT operation being involved. $I_{k\_A}(t)$ and $Q_{k\_B}(t)$ are then used to generate two SCM subcarriers, which are transformed into two real-valued DSB baseband analogue SCM subcarriers, $A_{DSB1}(t)$ and $A_{DSB2}(t)$, after applying a number of operations including cyclic prefix insertion, parallel-to-serial conversion and DAC.

To reduce the subcarrier×subcarrier beating-induced intermixing effect, in RS III, the phase-shift method based on the Hilbert transform [4] is applied to $A_{DSB1}(t)$ and $A_{DSB2}(t)$ to generate real-valued SSB SCM subcarriers, $S_{SSB1}(t)$ and $S_{SSB2}(t)$, which are expressed in Eq. (6.1).

An intensity modulator is driven directly by

$$S_e(t)=S_{SSB1}(t)+S_{SSB2}(t)+I_{dc} \tag{7.2}$$

where I_{dc} is the added DC component to ensure that $S_e(t)$ is always positive. $S_{SSB1}(t)$ and $S_{SSB2}(t)$ are linearly scaled to have identical electrical powers. For simplicity, an ideal intensity modulator is assumed, which produces optical output signals having waveforms governed by $S_o(t)=\sqrt{S_e(t)}$. As a Semiconductor Optical Amplifier (SOA) operating in a strongly saturated optical gain region has an effective bandwidth comparable to the entire AMOOFDM-SCM signal bandwidth [5], the SOA can be utilized to perform such intensity modulation. Compared to MZMs, the use of SOAs as intensity modulators can avoid the need for compensation of I/Q imbalance and bias deviation, thus resulting in the simplified modem design and cost reduction [6]. In addition, the SOAs can support colourless transmitters [7]. An ideal optical filter is also introduced to produce optical SSB signals for all transmission cases considered in this chapter.

At the output facet of the SMF link, the transmitted optical signal is converted into the electrical domain by using a square-law photodetector. After independently performing RF down-conversion using different RF frequencies, and undertaking, in the reverse procedure of that of the transmitter, a sequence of essential signal processing operations required prior to the FFT, two digital baseband SCM subcarriers are obtained. When both of these baseband SCM subcarriers are used as the inputs to the real and imaginary input ports of the FFT operation, both $\{A\}$ and $\{B\}$ can be recovered simultaneously by making use of the formulae

$$A_n = \frac{1}{2}\left\{\left[\mathrm{Re}\left(S_n^{'}\right)+\mathrm{Re}\left(S'_{2N-n}\right)\right]+j\left[\mathrm{Im}\left(S'_n\right)-\mathrm{Im}\left(S'_{2N-n}\right)\right]\right\} \tag{7.3}$$

$$B_n = \frac{1}{2}\left\{\left[\mathrm{Re}\left(S_n^{'}\right)-\mathrm{Re}\left(S_{2N-n}^{'}\right)\right]+j\left[\mathrm{Im}\left(S_n^{'}\right)+\mathrm{Im}\left(S_{2N-n}^{'}\right)\right]\right\} \tag{7.4}$$

where $S_n^{'}$ is the n-th AMOOFDM subcarrier at the FFT output. On the other hand, when use is made of a single baseband SCM subcarrier, only $\{A\}$ or $\{B\}$ can be recovered directly without requiring Eqs.(7.3) and (7.4). It should be noted, in particular, that the aforementioned data recovering processes are independent of each other and can take place simultaneously, if a dedicated FFT operation is provided for the selected SCM subcarrier(s). Clearly, the aforementioned input/output reconfigurability also holds for RS I and RS II.

7.3 Simulation Parameters and Transmission Performance

In simulating the transmission performances of RS I, RS II and RS III, 64 AMOOFDM subcarriers are considered, of which 31 having identical powers carry real data and one has no power. All other parameters that are not explicitly mentioned can be found in Chapter 6 and [8,9].

In addition, a comprehensive theoretical SMF model and a photodetector model are adopted, both of which were employed successfully in Chapter 6 and [8].

To demonstrate the maximum achievable signal transmission performances of the proposed RS modems, the signal line rate is defined in Eq. (6.5).

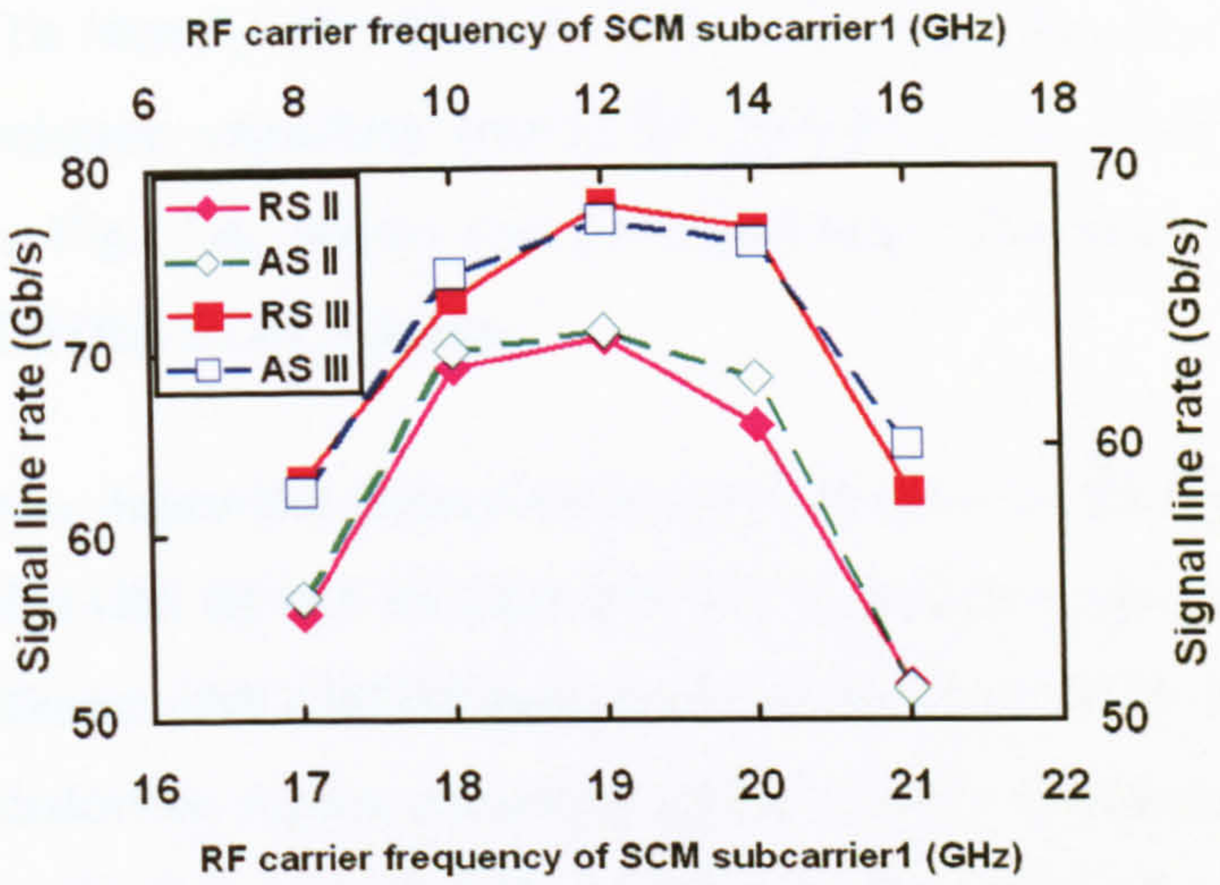

(a)

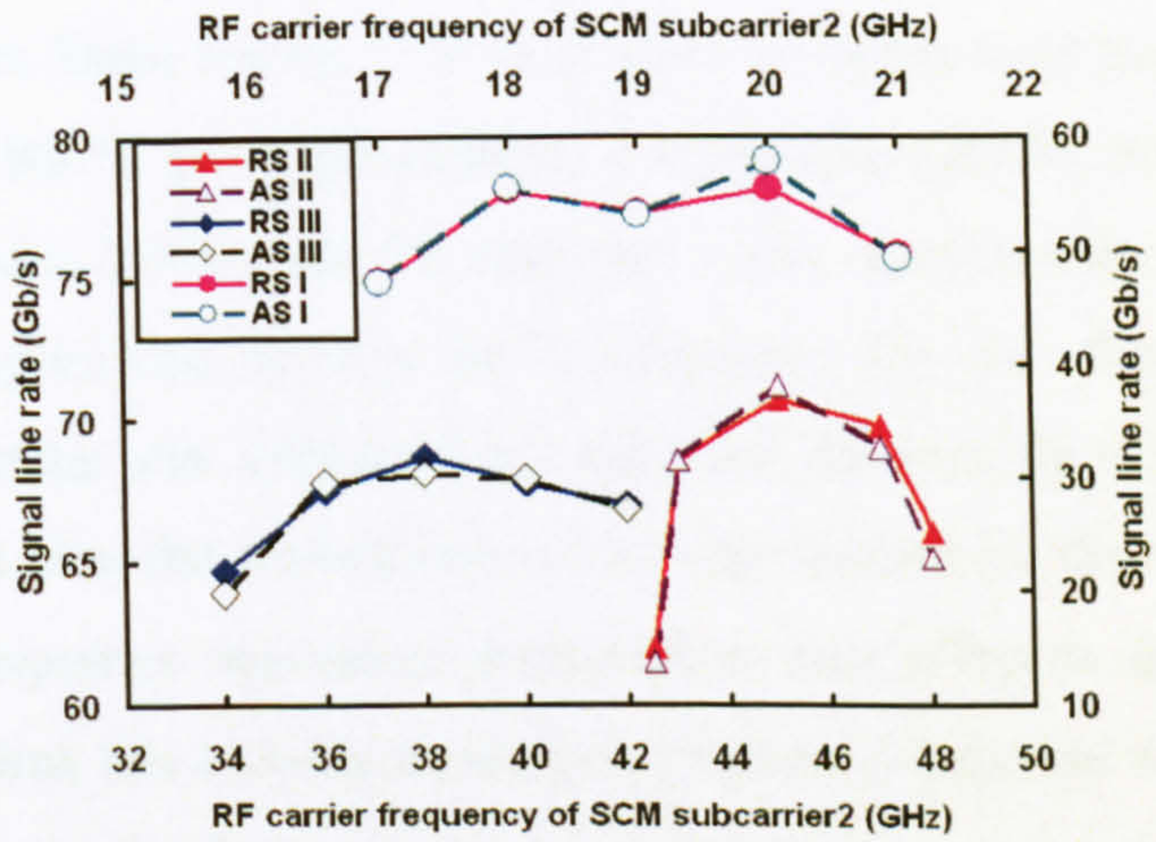

(b)

Fig.7.4 Optimum SCM subcarrier frequencies for different modem designs. (a) Transmission performance as a function of ω_{RF1} for RS (AS) scheme II and III. AS: conventional AMOOFDM-SCM scheme. (b) Transmission performance as a function of ω_{RF2} for RS (AS) scheme I, II and III. AS: conventional AMOOFDM-SCM scheme.

When use is made of RS modems, the maximum achievable transmission capacity for each optical channel depends on the intermediate RF frequency of the SCM subcarrier in each RS modem. For a given transmission link, an appropriate frequency adjustment is essential to position the SCM subcarrier in a desired link frequency response region, where the SCM subcarrier suffers a relatively low transmission loss and simultaneously the reduced

intermixing effect. To identify the optimum SCM subcarrier frequencies of the three RS modems, the transmission capacities versus RF frequency for 40km SMF transmission links are shown in Fig. 7.4, where the corresponding behaviours are also given for conventional AMOOFDM-SCM modems.

Fig. 7.4(a) shows ω_{RF1} dependent transmission performances of RS II and RS III for fixed ω_{RF2} values of 45GHz (RS II) and 38 GHz (RS III). Upon direct detection in the receiver, beating between different AMOOFDM subcarriers of the same SCM subcarrier produce an unwanted spectral distortion region occurring in the vicinity of the optical carrier. Such a spectral distortion region has a bandwidth of twice of the SCM subcarrier bandwidth [1]. The use of ω_{RF1} is to separate such an unwanted spectral region from the useful SCM subcarrier spectrum. Taking into account Fig.7.2, discussions in Section 7.2 and the simulation parameters listed above, it is very easy to understand that the optimum ω_{RF1} values for RS II and RS III are approximately 19GHz and 12GHz, respectively, as seen in Fig.7.4(a). A ω_{RF1} value lower than the optimum value increases the overlap between the spectral distortion region and the first SCM subcarrier. On the other hand, a ω_{RF1} value higher than the optimum one enhances not only the intermixing effect between the two SCM subcarriers but also the transmission loss experienced by the first SCM subcarrier. The origin of the frequency dependent transmission loss effect is due to the fact that an IMDD transmission link has a Gaussian-shaped frequency response with its peak occurring at the optical carrier, and the frequency response becomes narrower for a long transmission distance [8, 10].

Based on the identified optimum ω_{RF1} values for different RS modems, ω_{RF2} dependent transmission performances of RS I, II and III are shown in Fig.7.4(b), from which the optimum ω_{RF2} values of approximately 20GHz, 45GHz and 38GHz are identified for RS I, RS II and RS III, respectively. The beating between different SCM subcarriers causes the generation of unwanted products occurring at a spectral region between the two SCM subcarriers. A decrease in ω_{RF2} increases the intermixing effect. On the other hand, as explained above, a large ω_{RF2} value results in a high transmission loss. The co-existence of the SCM subcarrier beating-induced intermixing effect and the transmission loss effect contributes to the occurrence of optimum ω_{RF2} values for the RS modems. In comparison with RS II, the reduction in the optimum ω_{RF2} value for RS III is a direct result of the use of SSB modulation in RS III. Furthermore, it is also very interesting to note from Fig.7.4

that the optimum ω_{RF2} value for RS I is very similar to the optimum ω_{RF1} value for RS II. This confirms the physical origin of the optimum RF frequencies.

In addition, numerical simulations also show that, for RS I and RS II the optimum ω_{RF1} value is independent of the transmission distance, and that an extension of the transmission distance from 40km to 80km reduces the optimum ω_{RF2} by approximately 1GHz, 4GHz and 2GHz for RS I, RS II and RS III, respectively. Such behaviour can be explained easily by considering the physical mechanisms discussed above.

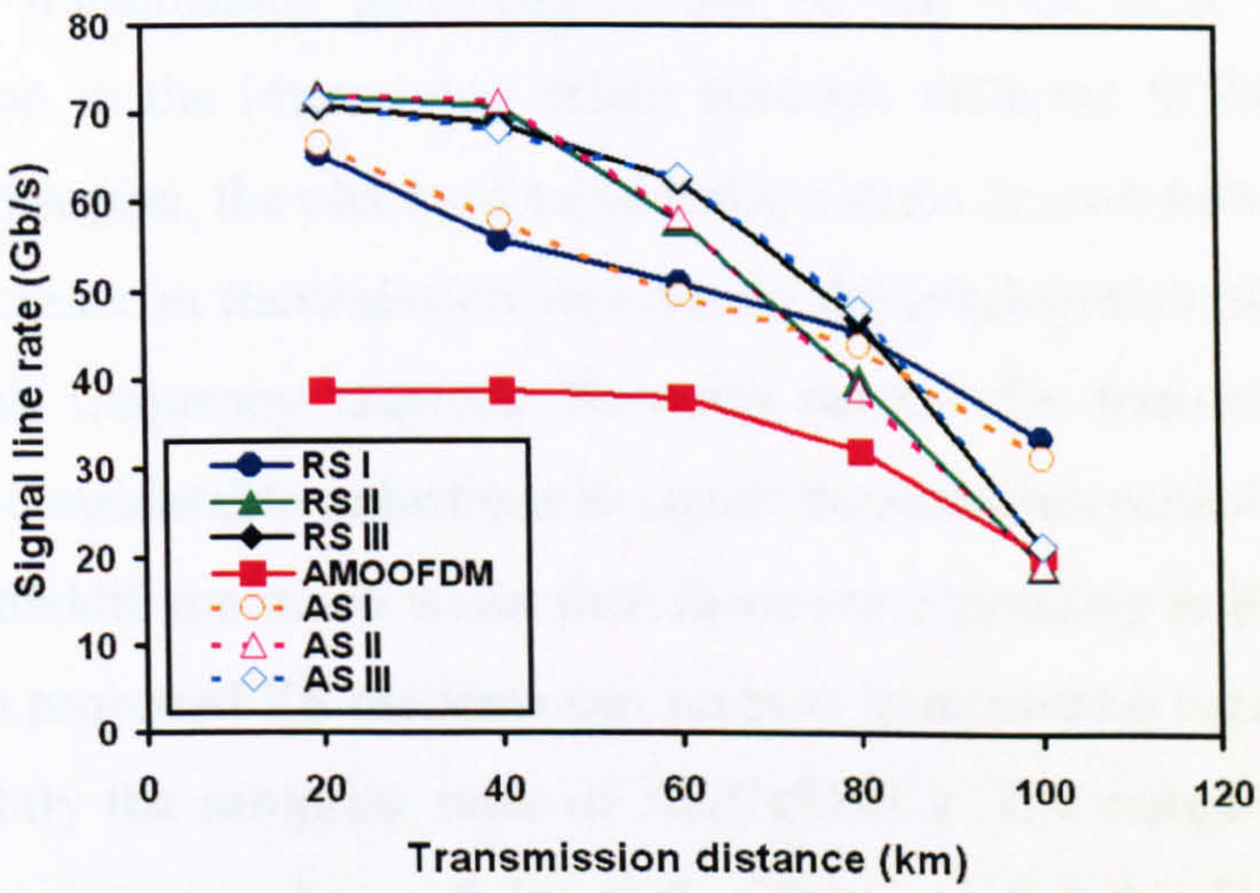

Fig.7.5 Signal transmission capacity versus reach performance of different modem designs. RS: reconfigurable modem; AS: AMOOFDM-SCM scheme.

Fig.7.5 shows the maximum achievable transmission performances of RS I, II and III, by taking into account the identified optimum RF frequencies. For performance comparisons and examination of the validity of the proposed modems, achievable transmission performances of AMOOFDM-SCM schemes I, II and III as well as AMOOFDM modems are also plotted in the same figure. It is shown that, over the entire transmission range of up to 100km, the transmission capacity versus reach performances achieved by the proposed RS modems are almost identical to those supported by the corresponding AMOOFDM-SCM schemes. It should be pointed out, in particular, that such transmission capacities are achieved using the simplified modem designs. This verifies the validity and effectiveness of the proposed RS modems. In comparison with the AMOOFDM modems, the RS modem designs can not only improve the signal transmission capacity versus reach performance by a factor of at least 1.5 for transmission distances of up to 60km, but also retain excellent performance robustness to variations of the transmission link characteristics.

For short transmission distances of, say <20km, almost no performance difference among the three RS modem designs is observed. This is because the intermixing effect is much less pronounced owing to short transmission distances [1, 3]. Whilst for SMF link lengths in the range from 20km to 40km, the signal transmission capacities achieved by RS II and RS III are very similar, which are, however, much higher than those supported by RS I, as shown in Fig.7.5. This is due to the use of spectral gaps in RS II and III, which distinguishes the first SCM subcarrier from the unwanted beating products occurring in the vicinity of the optical carrier. Over a transmission distance region of 40-80km, RS III offers the highest transmission performance due to the SSB SCM subcarrier-induced significant reduction in the intermixing effect between different SCM subcarriers. Over such a transmission region, the observed rapid performance degradation of RS II originates mainly from an increase in transmission loss due to the employment of a large ω_{RF2} in RS II. The IMDD link frequency response becomes narrow for transmission distances of >80km, leading to considerable reductions in signal transmission capacity for RS II and III, as their signal bandwidth are much wider than those corresponding to RS I. It is also worth addressing that the proposed RS modems can support transmission capacities of >100Gb/s by increasing slightly the sampling rates of ADCs/DACs. The sampling rates adopted in the RS modems can, however, be much lower than those predicted in [11].

7.4 Conclusion

Three novel RS modems have been proposed, each of which, has a number of major advantages including a significantly simplified modem configuration due to the involvement of a single IFFT/FFT operation, input/output reconfigurability, dynamic bandwidth allocation capability, cost reduction and system flexibility and performance robustness to variations in transmission link conditions. In addition, the proposed RS modems also offer broadcasting and performance monitoring functionalities. Investigations have shown that RS I, II and III modems are capable of supporting >60Gb/s signal transmission over 20km, 40km and 60km SMFs respectively in IMDD SMF transmission links without optical amplification and chromatic dispersion compensation.

References

[1] X. Zheng, J. L. Wei and J. M. Tang, "Transmission performance of adaptively modulated optical OFDM modems using subcarrier modulation over SMF IMDD links for access and metropolitan area networks" Opt. Express., vol. 16, no. 25, pp. 20427-20440, Dec. 2008.

[2] S. L. Jansen, I. Morita, T. C. W. Schenk, N. Takeda and H. Tanaka, "Coherent optical 25.8Gb/s OFDM transmission over 4160-km SSMF," J. Lightw. Technol., vol. 26, no.1, pp. 6-15, Jan. 2008.

[3] X. Zheng, J. M. Tang and P. S. Spencer, "Transmission performance of adaptively modulated optical OFDM modems using subcarrier modulation over worst-case multimode fibre links," IEEE Comm. Lett., vol.12, no.10, pp. 788-790, Oct. 2008.

[4] A. B. Carlson, P. B. Crilly and J. C. Rutledge, *Communication Systems: An Introduction to Signals and Noise in Electrical Communication*, McGraw-Hill Higher Education, 2002.

[5] J. L. Wei, A. Hamie, R. P. Giddings and J. M. Tang, "Semiconductor optical amplifier-enabled intensity modulation of adaptively modulated optical OFDM signals in SMF-based IMDD systems," J. Lightw. Technol., vol. 27, no.16, pp. 3678-3688, Aug. 2009.

[6] W. R. Peng, B. Zhang, X. X. Wu, K. M. Feng, A. E. Willner and S. Chi, "Compensation for I/Q imbalances and bias deviation of the Mach-Zehnder modulators in direct-detected optical OFDM systems," IEEE Photon. Technol. Lett., vol. 21, no. 2, pp. 103-105, Jan. 2009.

[7] J. L. Wei, X. L. Yang, R. P. Giddings and J. M. Tang, "Colourless adaptively modulated optical OFDM transmitters using SOA as intensity modulators," Opt. Express., vol. 17, no. 11, pp. 9012-9027, May. 2009.

[8] J. M. Tang and K. A. Shore, "30Gb/s signal transmission over 40-km directly modulated DFB-laser-based single-mode-fiber links without optical amplification and

dispersion compensation," J. Lightw. Technol., vol. 24, no. 6, pp. 2318-2327, June. 2006.

[9] J. M. Tang, P. M. Lane and K. A. Shore, "High-speed transmission of adaptively modulated optical OFDM signals over multimode fibres using directly modulated DFBs," J. Lightw. Technol., vol. 24, no. 1, pp. 429–441, Jan. 2006.

[10] E. Giacoumidis, J. L. Wei, X. Q. Jin and J. M. Tang, "Improved transmission performance of adaptively modulated optical OFDM signals over directly modulated DFB laser-based IMDD links using adaptive cyclic prefix," Opt. Express., vol. 16, no. 13, pp. 9480-9494, Jun. 2008.

[11] X. Q. Jin, J. M. Tang, P. S. Spencer and K. A. Shore, "Optimization of adaptively modulated optical OFDM modems for multimode fiber-based local area networks," J. Opt. Netw., vol. 7, no.3, pp. 198-214, March 2008.

8 PM-Enabled OOFDM Transmission Performance Improvement in IMDD SMF Systems Incorporating Parameter-Relaxed DACs/ADCs.

Contents

8.1 Introduction

For further reducing the transceiver cost with the desired transmission performance being maintained, opportunities can be explored to utilize low-cost DACs/ADCs, which normally have low quantization bits and sampling rates. As mentioned in Section 4.4, high PAPRs associated with OFDM signals increase the minimum requirements on quantization bits and sampling rates of the DACs/ADCs. Therefore, it is very important to investigate effective schemes to reduce the PAPRs of OFDM signals.

As presented in Chapters 5-7, to convert an electrical OFDM signal into the optical domain, a real-valued electrical OFDM signal emerging from the transmitter Field-Programmable Gate Array (FPGA) is utilised, whose phase is, however, unused. This raises a very interesting question, i.e., can such an OFDM signal be used to modulate only the phase of a RF carrier? A significant advantage associated with the PM approach is that the PAPRs of the OFDM signals can be reduced significantly [1]. In fact, theoretical investigations of PM-induced constant envelope OFDM waveforms have been reported in a coherent OFDM transceiver configuration for applications in wireless transmission systems [1]. However, PM has not been reported in IMDD AMOOFDM transmission systems. Furthermore, it is also greatly advantageous if the use of PM in IMDD AMOOFDM systems does not introduce extra complexity into the transceiver design.

In this chapter, AMOOFDM-PM is proposed and explored, for the first time, in IMDD SMF transmission systems. In AMOOFDM-PM, an electrical OFDM signal is used to directly modulate the phase of a RF carrier prior to performing optical intensity modulation. It should be mentioned that, from the physical point of view, the PM scheme plays a role in determining nonlinear quantization. The use of "PM" here is to ensure the consistency between the present work and previous publications [1].

When compared to AMOOFDM based on amplitude modulation [2-6], the proposed technique has important advantages including:

1) Significant reduced PAPRs, as discussed in Section 8.3 of the chapter.

2) Relaxed requirements on key transceiver components: it is well known that DACs/ADCs limit considerably the maximum achievable signal transmission capacity of

real-time OOFDM transceivers [7]. As a direct result of the PAPR reduction, for achieving a specific transmission performance, AMOOFDM-PM can considerably relax the minimum requirements on both the sampling rates and bits of quantization of the DACs/ADCs.

3) Cost-effective implementation: AMOOFDM-PM can be implemented directly in FPGAs without increasing the transceiver complexity.

4) Spectral efficiency: By appropriately choosing the modulation coefficient, AMOOFDM-PM does not broaden the signal bandwidth compared to that of AMOOFDM.

In addition, AMOOFDM-PM shows better tolerance to link loss, excellent system flexibility and performance robustness to variations in transmission link characteristics.

Our numerical simulations show that, when small DAC/ADC quantization bits and/or low DAC/ADC sampling rates are adopted, AMOOFDM-PM can double the transmission capacity, compared to AMOOFDM. In particular, such improvement is more pronounced for relatively long transmission distances. Therefore, AMOOFDM-PM has potential for providing a cost-effective technical solution for practical implementations in cost-sensitive access networks.

8.2 AMOOFDM-PM Transmission Systems

A single channel AMOOFDM-PM IMDD transmission system considered is illustrated in Fig.8.1, which is free from both chromatic dispersion compensation and in-line optical amplification. When compared with the AMOOFDM modem, the key transceiver configuration differences shown in Fig.8.1 are the application of PM in OFDM symbols immediately after the IFFT in the transmitter, and phase detection before the FFT in the receiver.

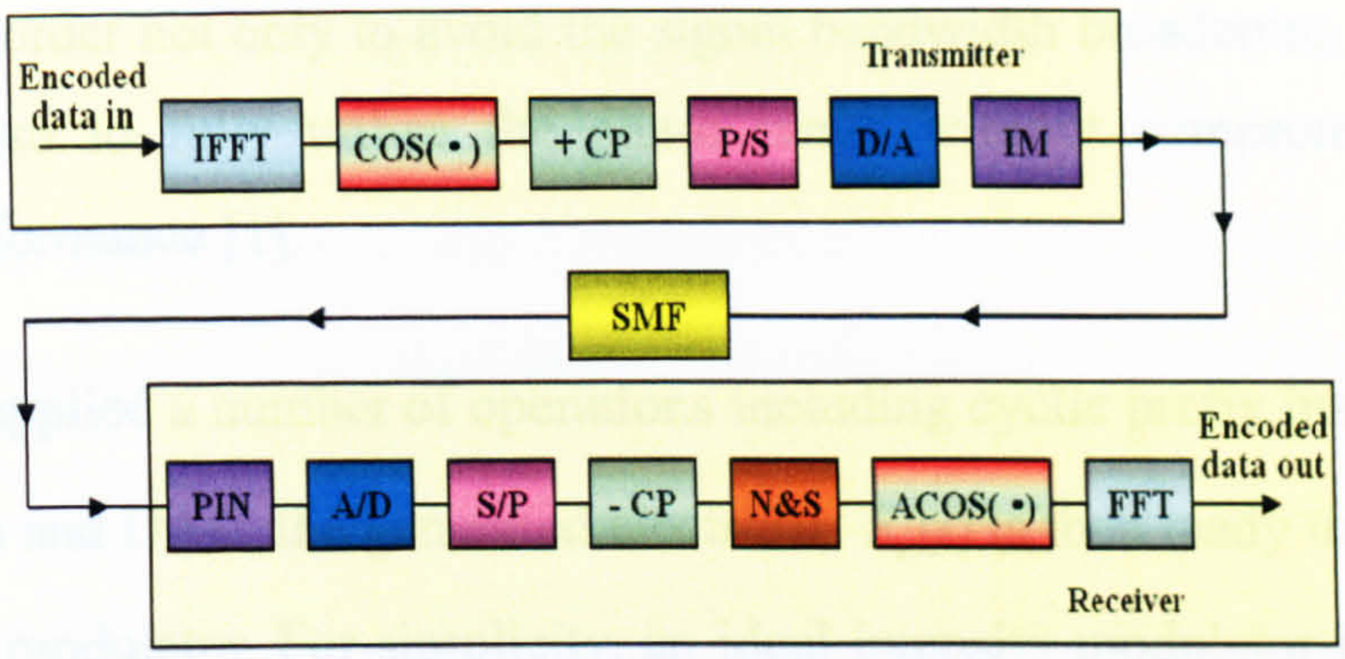

Fig. 8.1 Schematic illustration of AMOOFDM-PM IMDD transmission systems. COS: cosine function; +CP: cyclic prefix insertion; P/S: parallel to serial conversion; D/A: digital to analogue conversion; IM: intensity modulation; A/D: analogue to digital conversion; S/P: serial to parallel conversion; -CP: cyclic prefix removing; N&S: normalization and shift; ACOS: arccos function.

In the transmitter, by arranging the positive bin subcarriers containing encoded original data, a zero-valued subcarrier and their conjugate counterparts to satisfy Hermitian symmetry, a real-valued electrical OFDM symbol $A(t)$ emerging from the IFFT is produced, which is then up-shifted appropriately to ensure that the minimum peaks occurring in the entire OFDM signal are positive. The up-shifted symbol $A_p(t)$ is given by

$$A_p(t) = A(t) + I_1 \tag{8.1}$$

where I_1 is the added DC component. $A_p(t)$ is multiplied by a modulation coefficient C to confine all the sample values in a range of 0-π for phase detection in the receiver. Any phase variation beyond that boundary should be avoided. The phase modulated OFDM symbol $S_{PM}(t)$ can be expressed as

$$S_{PM}(t) = \cos[CA_p(t)] \tag{8.2}$$

Compared to the complex-valued OFDM symbol with constant envelope [1], the real-valued OFDM symbol $S_{PM}(t)$ varies from -1 to 1, giving rise to a reduced PAPR in comparison with AMOOFDM. Here it is also worth mentioning that the bandwidth of $S_{PM}(t)$ depends upon the modulation coefficient C, whose value should be chosen

appropriately, in order not only to avoid the signal bandwidth broadening effect associated with PM but also to fully utilise the phase range without compromising the signal transmission performance [1].

After $S_{PM}(t)$ is applied a number of operations including cyclic prefix insertion, parallel to serial conversion and DAC, the generated electrical $S_e(t)$ is then ready to directly drive an optical intensity modulator. For simplicity, an ideal intensity modulator is employed here, which produces an output optical signal having a waveform governed by

$$S_o(t) = \sqrt{S_e(t) + I_{dc}} \tag{8.3}$$

with I_{dc} being the added DC component to ensure that $S_e(t) + I_{dc}$ is always positive [6]. After appropriately adjusting the output optical power, the optical signal is coupled into SMF links.

In the receiver, the AMOOFDM-PM signal is detected using a square-law photodetector. After digitalisation, serial-to-parallel conversion and remove of cyclic prefix, the OFDM symbol $S_{PM\_r}(t)$ is normalized by

$$S_{PM\_n}(t) = S_{PM\_r}(t) \frac{2}{S_{PM\_r\_\max} - S_{PM\_r\_\min}} \tag{8.4}$$

where $S_{PM\_n}(t)$ is the normalized OFDM symbol, $S_{PM\_r\_\max}$ and $S_{PM\_r\_\min}$ are the maximum and minimum values occurring in $S_{PM\_r}(t)$, respectively. This operation is to restore the peak-to-peak value assigned in the transmitter. To ensure that $S_{PM\_n}(t)$ has its value varying in the range of -1 to 1, the following operation is also applied

$$S_{PM\_s}(t) = S_{PM\_n}(t) - S_{PM\_n\_\min} - 1 \tag{8.5}$$

where $S_{PM\_s}(t)$ is the shifted symbol, $S_{PM\_n\_\min}$ is the minimum value of $S_{PM\_n}(t)$ and the last term denotes the minimum value of $S_{PM}(t)$ defined in Eq.(8.2).

Phase information is recovered by

$$A_r(t) = \arccos[S_{PM\_n}(t)] \tag{8.6}$$

After multiplying $A_r(t)$ with $1/C$, and down-shifting the resulting product at an amount of I_1 (identical to that used in the corresponding transmitter), the OFDM symbol $A_{r\_s}(t)$ at the input of the FFT is given by

$$A_{r\_s}(t) = \frac{1}{C} A_r(t) - I_1 \tag{8.7}$$

After performing the FFT operation, the data can be finally recovered. Here it is worth addressing that, although the phase modulation (demodulation) can also be applied after the DAC in the transmitter (before ADC in the receiver), the phase modulation (demodulation) proposed here can be easily implemented in FPGAs without introducing significant complexity to the transceiver design.

The SMF model used successfully in Chapter 6 and 7 is adopted here. In modeling the PIN, both shot noise and thermal noise are considered, which are simulated following the procedure similar to that presented in [8]. The validity of the theoretical fibre and PIN models has been confirmed in [3, 4, 9].

8.3 Simulation Parameters

In this section, the parameters adopted in numerical simulations are discussed in detail. Throughout this chapter, all the parameters listed below are utilized as default ones unless addressed explicitly in the corresponding text when necessary.

In simulating AMOOFDM-PM modems, 64 subcarriers are considered, in which 31 convey user data, one has no power and the remaining 32 are the complex conjugate of the above-mentioned subcarriers. The modulation format taken on each subcarrier may vary from DBPSK, DQPSK, and 16 to 256 QAM, depending on the frequency response of a specific transmission link. The cyclic prefix parameter is fixed at 25%. The optimum clipping ratio of 10dB is used, which is approximately 3dB lower than that corresponding to AMOOFDM [10]. The optical powers launched into the SMF links are fixed at 6.3 dBm.

The modulation coefficient C defined in Eq.(8.2) is set at a value of 2.94, which corresponds to a modulation index of 0.36 (according to the definition in [1]). The purpose of employing such a value is to retain the signal bandwidth compared to that corresponding to AMOOFDM.

For simulating SMF links at 1550nm, use is made of parameters found in Chapter 6. Finally, a PIN with a quantum efficiency of 0.8 and a noise current density of 8 pA/$\sqrt{Hz}$ is used [4,9].

8.4 Simulation Results

The transmission performance of AMOOFDM-PM is investigated in this section, while the performance of AMOOFDM is also presented for comparison. The signal line rate corresponding to a total channel BER of $<1.0\times10^{-3}$ is considered to be valid as such a BER leads to error-free operation when combined with FEC.

For different transmission distances, the signal line rate as a function of DAC/ADC quantization bits is shown in Fig.8.2 (a), and the relative improvement in signal capacity in comparison with AMOOFDM is also plotted in Fig.8.2 (b), where the capacity improvement R_i is defined as:

$$R_i = \frac{S_{AMOOFDM-PM} - S_{AMOOFDM}}{S_{AMOOFDM}} \times 100\% \tag{8.8}$$

where $S_{AMOOFDM-PM}$ and $S_{AMOOFDM}$ are the signal line rates for AMOOFDM-PM and AMOOFDM, respectively. In obtaining Fig.8.2, the DAC/ADC sampling rate is fixed at 8 GS/s. It can be seen in Fig.8.2 that, for various transmission lengths of up to 80km and quantization bits of >6, almost constant AMOOFDM-PM capacities occur, implying that the quantization noise effect is negligible for such a quantization level region. It is very interesting to note that, compared to AMOOFDM, the AMOOFDM-PM transmission capacity significantly increases for quantization bits of <6. For example, the AMOOFDM-PM transmission capacity is doubled for quantization bits of <4, indicating that AMOOFDM-PM can lower the minimum requirements on quantization bits of DACs/ADCs. In particular, to achieve a required transmission performance of say 25 Gb/s

over 80km, AMOOFDM-PM can reduce the quantization bits of DACs/ADCs from 7 (required by AMOOFDM) to 6, as shown in Fig.8.2. In addition, Fig.8.2 also shows that AMOOFDM-PM has significant flexibility and excellent performance robustness to variations in transmission link characteristics. The above-discussed results confirm the effectiveness of the proposed AMOOFDM-PM technique.

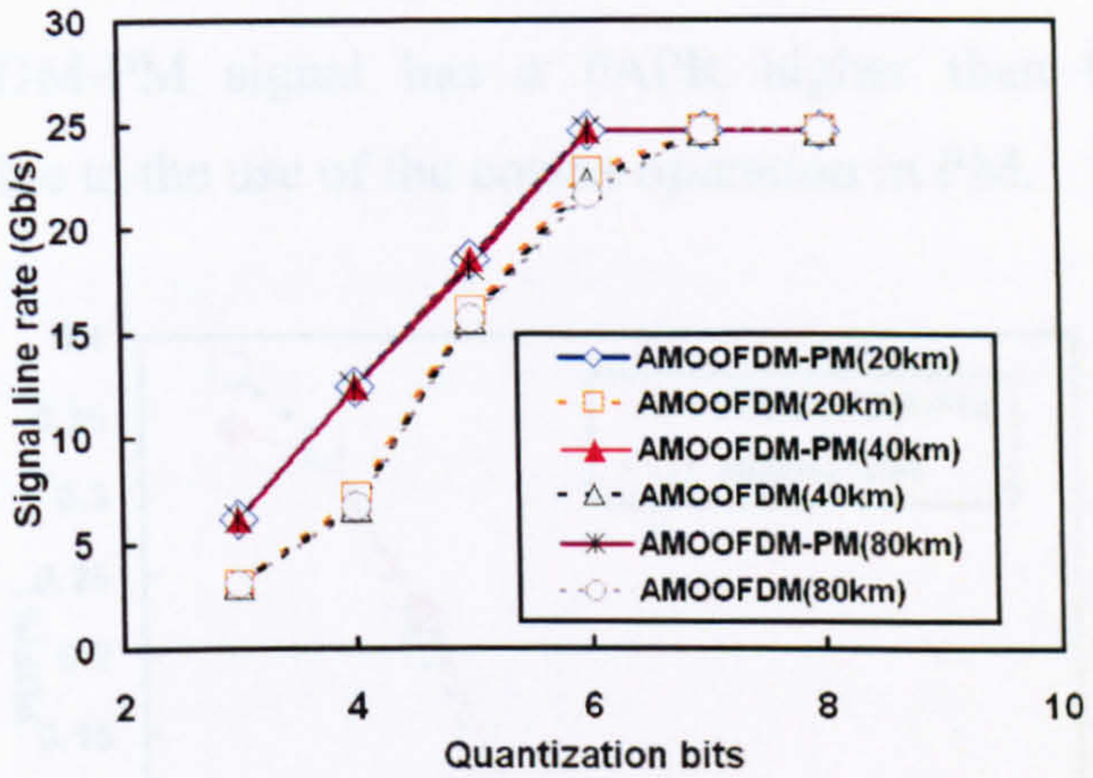

(a)

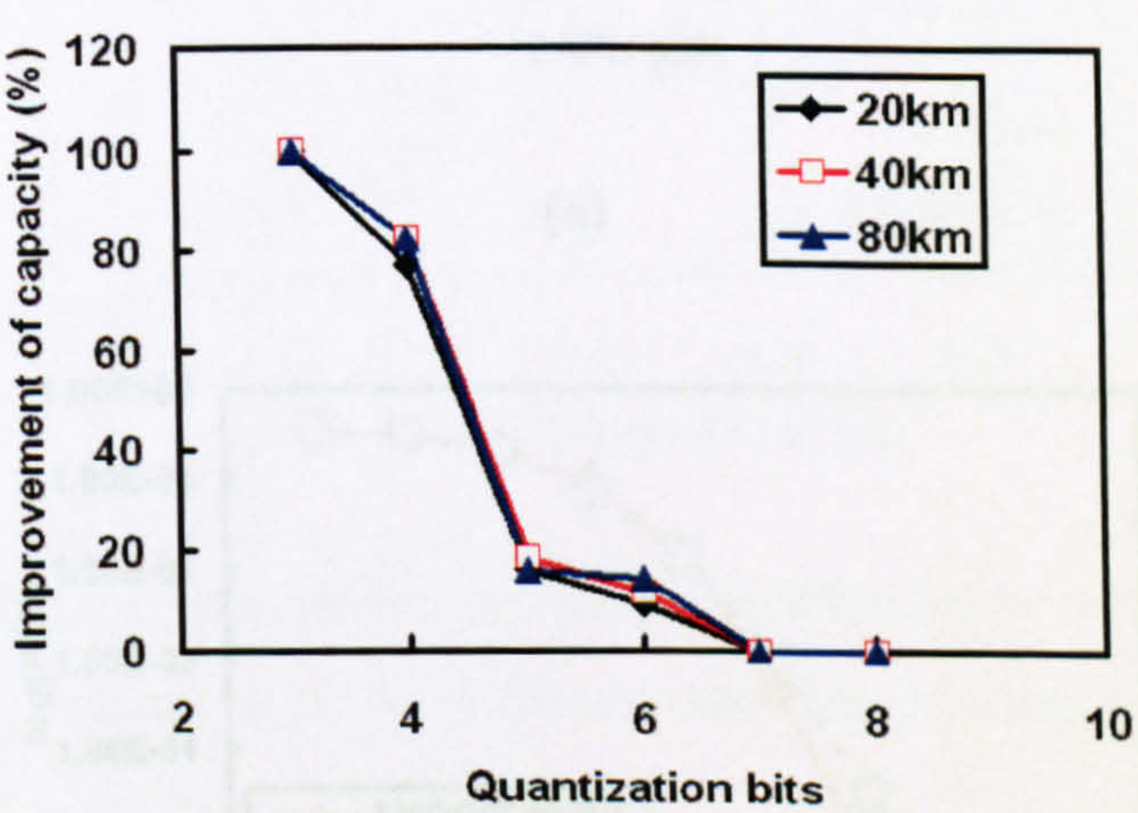

(b)

Fig. 8.2 Impact of AMOOFDM-PM on the choice of DACs/ADCs. (a) Transmission capacity versus DAC/ADC quantization bits for different transmission lengths. (b) Improvement in transmission capacity for different transmission lengths.

The significant signal capacity improvement presented in Fig.8.2 is due to the reduction in signal PAPR, thus leading to a decreased signal dynamic range and the reduced

quantization noise effect. Such a statement is verified in Fig.8.3, in calculating which use is made of AMOOFDM-PM/AMOOFDM signals emerging from their corresponding transmitters as well as 8GS/s and 7-bit quantization DACs/ADCs. It can be seen in Fig.8.3 that the use of AMOOFDM-PM considerably reduces the signal peak occurrence probability density defined in [11] for PAPR>3dB, as illustrated in Fig.8.3 (b) where a logarithmic y-axis is used. It can also be found in Fig.8.3 that, over the 1.5-2 dB PAPR region, the AMOOFDM-PM signal has a PAPR higher than that corresponding to AMOOFDM. This is due to the use of the cosine operation in PM.

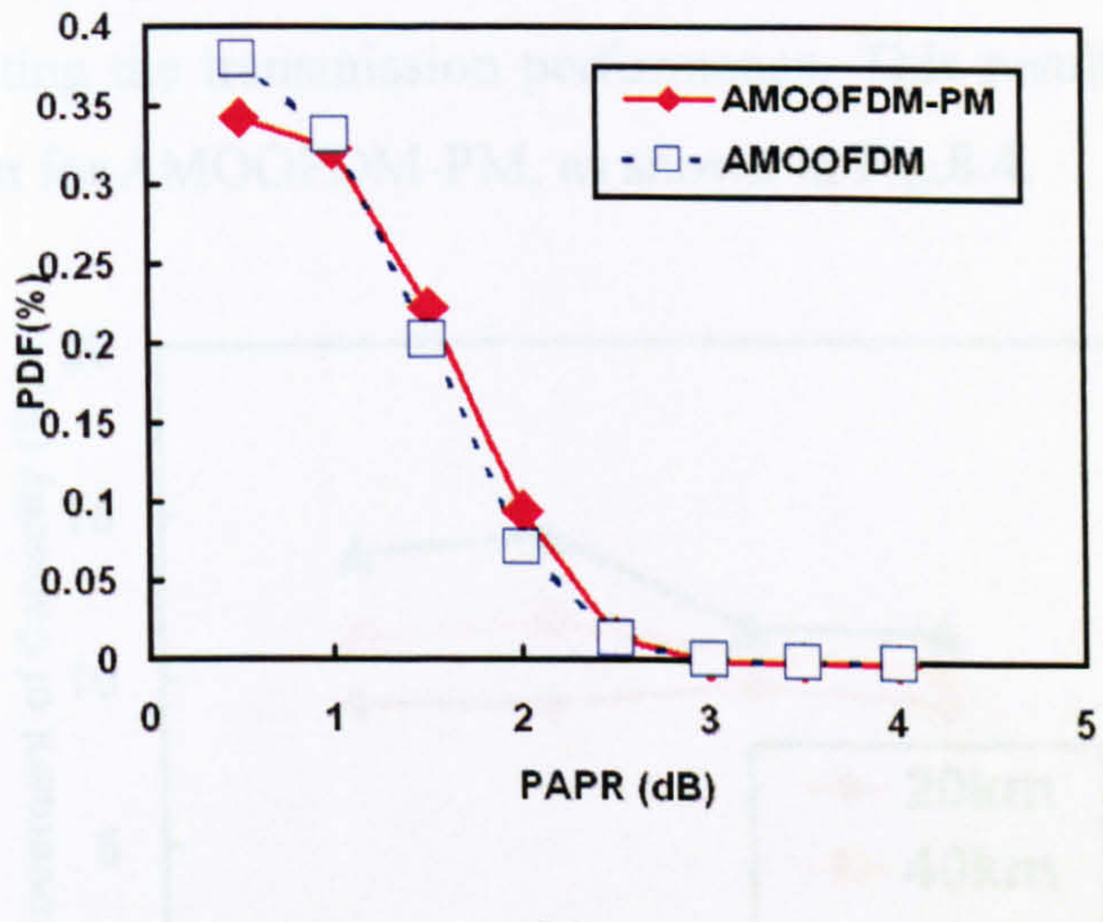

(a)

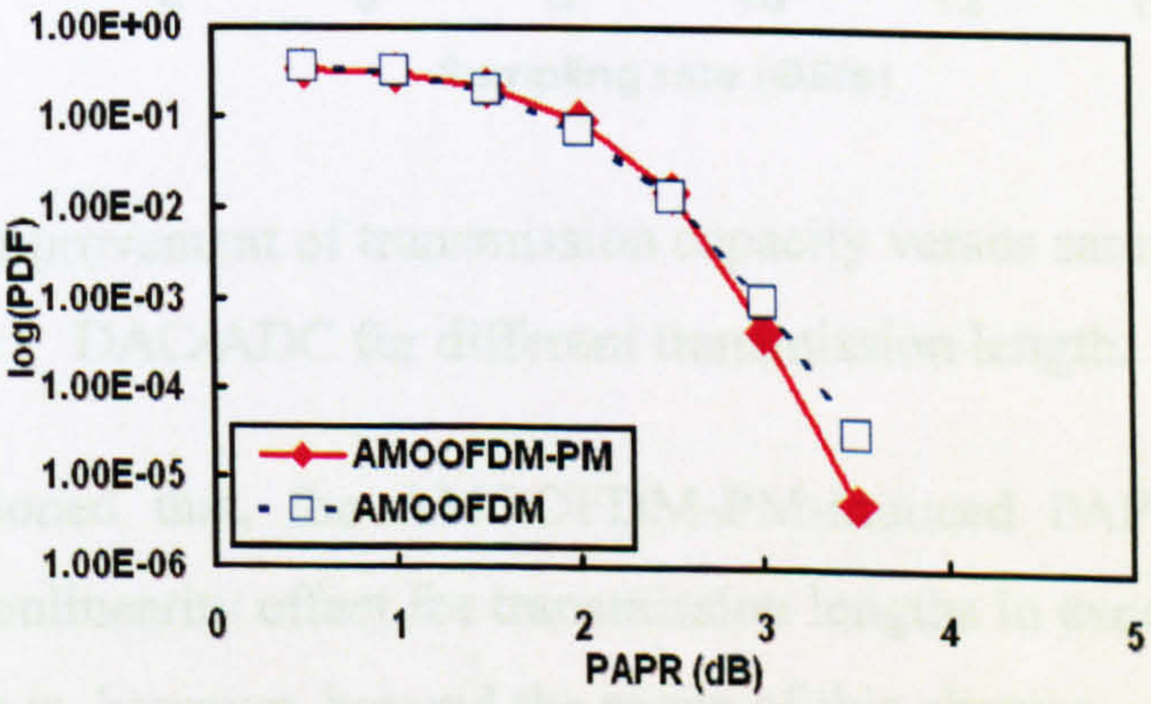

(b)

Fig. 8.3 Signal peak occurrence probability density as a function of PAPR. (a) Probability Density Function (PDF) versus PAPR; (b) logarithmic value of PDF versus PAPR.

In comparison with AMOOFDM, the obtained AMOOFDM-PM-induced transmission capacity improvement is plotted in Fig.8.4 as a function of DAC/ADC sampling rate for different transmission lengths. In obtaining Fig.8.4, 6-bit quantization is considered. It can be seen in Fig.8.4 that, for long transmission distances, the capacity improvement trend is more pronounced, especially when low ADC/DAC sampling rates are adopted. This phenomenon indicates that AMOOFDM-PM is capable of offering better tolerance to fibre loss, as for low DAC/ADC sampling rates, the adopted cyclic prefix is sufficient long to compensate for the chromatic dispersion effect. However, for high DAC/ADC sampling rates, the corresponding signal bandwidth is broad, thus chromatic dispersion becomes an important factor limiting the transmission performance. This results in a slightly reduced capacity improvement for AMOOFDM-PM, as shown in Fig.8.4.

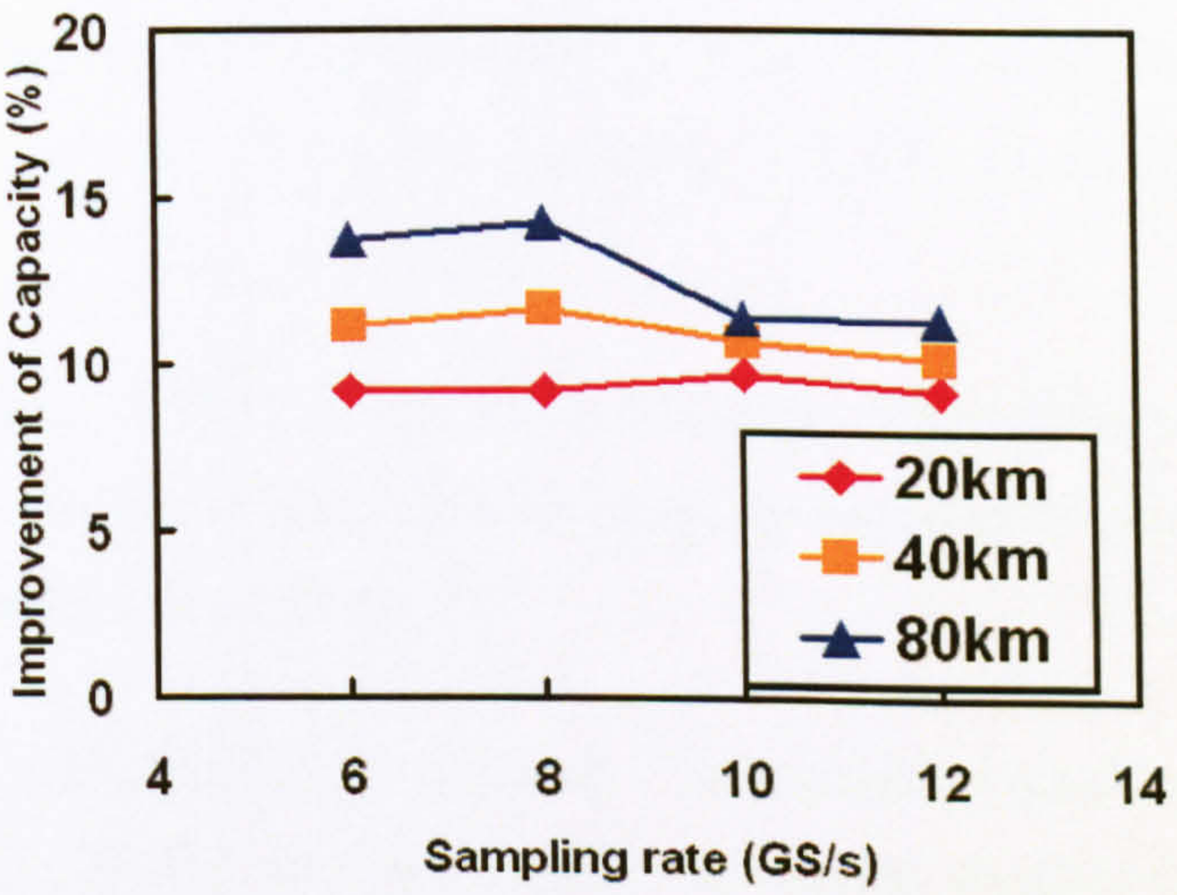

Fig. 8.4 Improvement of transmission capacity versus sampling rate of DAC/ADC for different transmission length.

It should be mentioned that, the AMOOFDM-PM-induced PAPR reduction can also decrease the fibre nonlinearity effect for transmission lengths in excess of several hundreds of kilometres, which is, however, beyond the scope of this chapter.

8.5 Conclusion

A novel AMOOFDM-PM technique has been proposed and theoretically explored, for the first time, in IMDD SMF systems for cost-sensitive access networks. In comparison with AMOOFDM, AMOOFDM-PM not only lowers the minimum requirements on the key

parameters associated with DACs/ADCs, but also simultaneously improves considerably the transmission performance. In addition, AMOOFDM-PM also shows better tolerance to fibre loss and excellent system flexibility and performance robustness to variations in transmission link characteristics.

References

[1] S. C. Thompson, A. U. Ahemd, J. G. Proakis, J. R. Zeidler, M. J. Geile, "Constant envelope OFDM," IEEE Trans. Comm., vol. 56, no. 8, pp. 1300-1312, Aug. 2008.

[2] T-N. Duong, N. Genay, M. Ouzzif, J. L. Masson, B. Charbonnier, P. Chanclou and J. C. Simon, "Adaptive loading algorithm implemented in AMOOFDM for NG-PON system integrating cost-effective and low bandwidth optical devices," IEEE Photon. Technol. Lett., vol. 21, no. 12, pp. 790-792, Jun. 2009.

[3] J. M. Tang and K. A. Shore, "30Gb/s signal transmission over 40-km directly modulated DFB-laser-based single-mode-fiber links without optical amplification and dispersion compensation," J. Lightw. Technol., vol. 24, no. 6, pp. 2318-2327, June. 2006.

[4] J. L. Wei, X. L. Yang, R. P. Giddings and J. M. Tang, "Colourless adaptively modulated optical OFDM transmitters using SOA as intensity modulator," Opt. Express., vol. 17, no. 11, pp. 9012-9027, May. 2009.

[5] X. Zheng, J. M. Tang and P. S. Spencer, "Transmission performance of adaptively modulated optical OFDM modems using subcarrier modulation over worst-case multimode fibre links," IEEE Comm. Lett., vol.12, no.10, pp. 788-790, Oct. 2008.

[6] X. Zheng, J. L. Wei and J. M. Tang, "Transmission performance of adaptively modulated optical OFDM modems using subcarrier modulation over SMF IMDD links for access and metropolitan area networks" Opt. Express. vol. 16, no. 25, pp. 20427-20440, Dec. 2008.

[7] X. Q. Jin, R. P. Giddings, E. Hugues-Salas and J. M. Tang, "Real-time demonstration of 128-QAM-encoded optical OFDM transmission with a 5.25bit/s/Hz spectral efficiency in simple IMDD systems utilizing directly modulated DFB lasers," Opt. Express. vol. 17, no. 22, pp. 20484-20493, Oct. 2009.

[8] G. P. Agrawal, *Fibre-Optic Communication Systems*, Wiley, 1997.

[9] J. L. Wei, A. Hamie, R. P. Giddings and J.M. Tang, "Semiconductor optical amplifier-enabled intensity modulation of adaptively modulated optical OFDM signals in SMF-based IMDD systems," J. Lightw. Technol., vol. 27, no. 16, pp. 3678-3688, Aug. 2009.

[10] J. M. Tang and K. Alan Shore, "Maximizing the transmission performance of adaptively modulated optical OFDM signals in multimode-fiber links by optimizing analog-to-digital converters" J. Lightw.Technol., vol. 25, no. 3, pp. 787–798 , Mar. 2007.

[11] E. Giacoumidis, J. L. Wei, X. L. Yang, A. Tsokanos, and J. M. Tang, "Adaptive-modulation-enabled WDM impairment reduction in multichannel optical OFDM transmission systems for next-generation PONs," IEEE Photon. Journal., vol. 2, no. 2, pp. 130-140, Apr. 2010.

9 Negative Power Penalties of OOFDM Signal Transmissions in DML-based IMDD Systems Incorporating Negative Dispersion Fibres

Contents

9.1 Introduction

As mentioned in Chapter 4, to develop cost-effective OOFDM NG-PONs, IMDD is a very promising solution, as it is capable of offering considerable reductions in both the network complexity and the installation and maintenance cost without considerably compromising the system flexibility and performance robustness. In addition, compared to other intensity modulators such as conventional external intensity modulators, the use of DMLs is also preferable due to their many advantages namely low cost, compactness, low power consumption, relatively small driving voltage and high output power.

However, in DML-based IMDD OOFDM PONs utilizing SSMFs with positive chromatic dispersion, the positive frequency chirp associated with typical DMLs significantly limits the maximum achievable OOFDM transmission performance, as discussed in Chapter 4. In traditional NRZ DML-based IMDD transmission systems, use can be made of negative dispersion SMFs such as MetroCor fibres to compensate for the DML-induced positive frequency chirps, and negative power penalties have been observed experimentally at specific BERs [1,2]. More importantly, such a dispersion compensation technique has also been confirmed to be very effective for OOFDM systems. It has been experimentally demonstrated [3,4] that net signal bit rates of 3Gb/s 16QAM-encoded, 4.5Gb/s 64QAM-encoded and 5.25Gb/s 128QAM-encoded real-time OOFDM signals modulated by DMLs can be transmitted over 75km, 25km and 25km MetroCor SMFs, respectively, with respective negative power penalties of -2dB, -0.5dB, -0.5dB.

Given the fact that OOFDM has strong resilience to chromatic dispersion, the occurrence of negative power penalties in DML-based IMDD OOFDM MetroCor SMF systems raises three very interesting open questions:

- What are the physical mechanisms underlying the observed negative power penalties?
- Does cyclic prefix contribute to such a phenomenon?
- What technical approaches may be adopted to control the effect?

The provision of answers to these three open questions is of great importance, as the answers enable us not only to gain an in-depth understanding of the IMDD OOFDM

technique, but also offer effective means for further maximizing the transmission performance of the systems of interest of the present work. Therefore, this chapter is dedicated to address, for the first time, such challenging issues.

In this chapter, detailed investigations are undertaken, for the first time, to explore the dynamic negative power penalty characteristics of OOFDM signal transmissions over DML-based IMDD MetroCor systems. Excellent agreement between numerical simulations and real-time experimental measurements [3,4] is observed. This leads to the identification of the physical origin underpinning the negative power penalties: 1) in the electrical domain, the imperfect preservation of the OOFDM signal phase due to subcarrier intermixing upon square-law direct detection in the receiver, and 2) the reduced subcarrier intermixing effect [5] due to a MetroCor fibre-induced reduction in DML modulated OOFDM signal phase. In addition, results also indicate that, for a given DML-based IMDD OOFDM MetroCor SMF system, the resulting negative power penalty is independent of both cyclic prefix and signal modulation format. Furthermore, it is also shown that the negative power penalty is controllable by applying adaptive modulation and/or variation in DML operating condition.

The chapter is organized as follows. In Section 9.2, the considered transmission link model is outlined with special attention being given to the DML frequency chirp effect. In Section 9.3, parameters adopted in numerical simulations are presented and discussed in detail. In Section 9.4, extensive comparisons between numerical simulations and experimental results are made, based on which the physical origin of negative power penalties is identified. In addition, detailed discussions are also made of the impacts of cyclic prefix, adaptive modulation, signal modulation format and DML operating conditions on the negative power penalty effect. Finally, this chapter is summarized in Section 9.5.

9.2 Transmission Link Model

9.2.1 Transmission Link Diagram

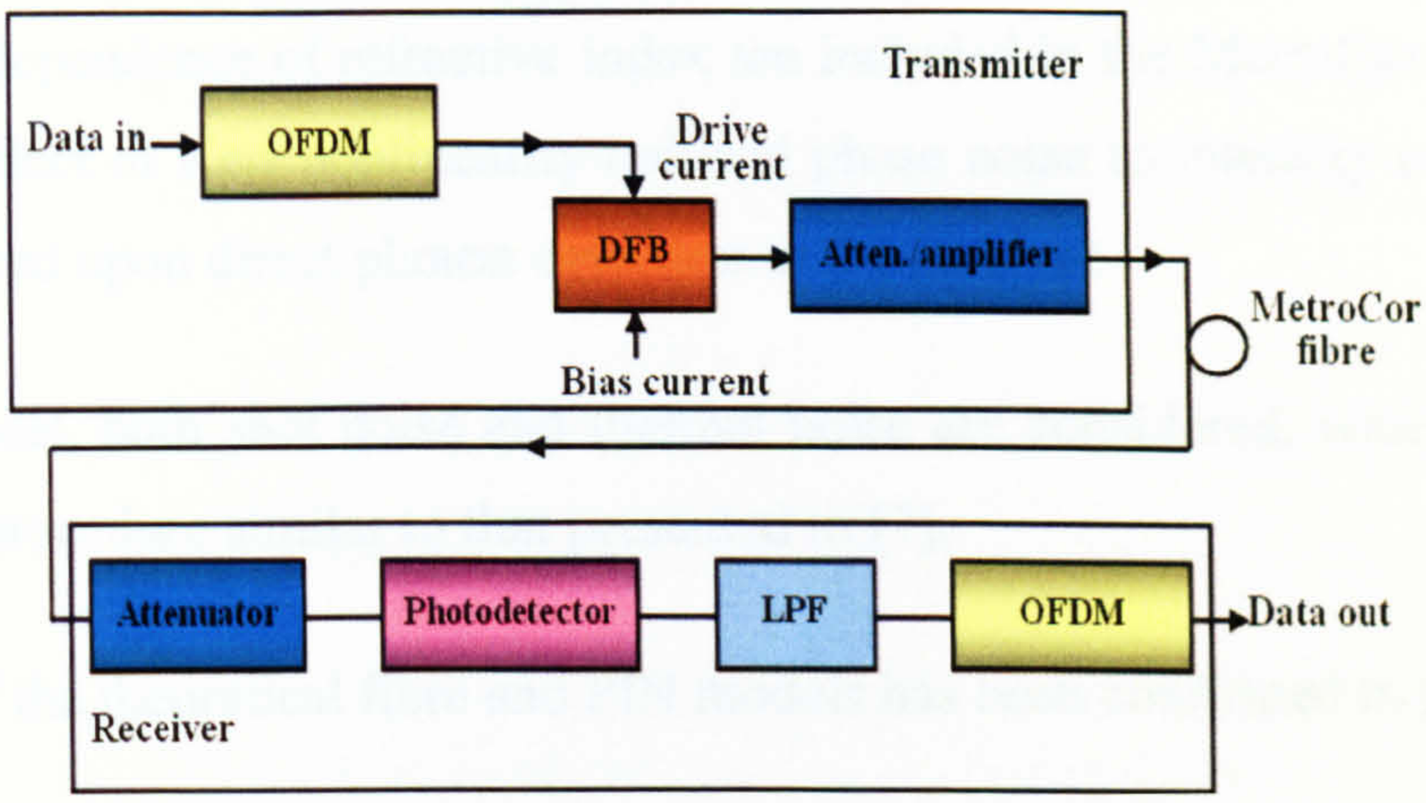

Fig.9.1 Schematic illustration of DML-based IMDD OOFDM transmission systems. Atten.: attenuator; LPF: low-pass filter.

Similar to those used in real-time experimental measurements [3,4], the OOFDM transmission link considered here is a single channel, DML-based IMDD MetroCor SMF system, as shown in Fig.9.1, which is free from both chromatic dispersion compensation and in-line optical amplification. The transmission link consists of an OOFDM transmitter, an OOFDM receiver and MetroCor fibres in between. In the transmitter, an input binary data sequence is encoded by different modulation formats, which may vary from DBPSK, DQPSK, and 16 to 128QAM. The encoded complex data is processed by a transmitter OFDM modem following the procedures described in Chapter 2. The generated electrical OFDM signal is first multiplexed with an optimum DC bias current, and then employed to directly drive the DML to generate an OOFDM signal at 1550 nm. The DML model is identical to that presented in Section 4.3.2. After appropriately adjusting the output optical power, the OOFDM signal is coupled into the MetroCor fibres.

In the receiver, the optical signal emerging from the optical attenuator is detected using a square-law photodetector. To recover the data, the low-pass-filtered electrical OFDM waveform is processed in a receiver OFDM modem by using an inverse process of that of the transmitter. Detailed descriptions of the processes outlined above have been reported in [3,4].

9.2.2 Models for Other Components

The propagation of OOFDM signals over MetroCor fibres is modelled using the widely adopted split-step Fourier method [6]. The effects of loss, chromatic dispersion and the optical power dependence of refractive index are included in the MetroCor fibre model. In addition, the effect of Kerr nonlinearity-induced phase noise to intensity noise conversion is also considered upon direct photon detection in the receiver.

In the PIN model, both shot noise and thermal noise are considered, which are simulated following the procedure similar to that presented in [7].

The validity of the theoretical fibre and PIN models has been confirmed in [5,8,9].

9.3 Simulation Parameters

In this section, the parameters adopted in numerical simulations are discussed in detail. Throughout this chapter, all the parameters listed below are utilised as default ones unless addressed explicitly in the corresponding text when necessary.

Table 9.1
Parameters for different modulation formats

Optimum simulation parameters			
Modulation format	16QAM	64QAM	128QAM
Bias current of DML	35mA	37mA	39mA
Peak-to-peak drive current of DML	12.7mA	12.7mA	12.7mA
Clipping ratio	13.8dB	13.5dB	11dB

In simulating OFDM modems, the parameter values identical to those utilised in the experiments [3, 4] are adopted, which include 32 subcarriers with 15 conveying user data in the positive frequency bins, a cyclic prefix parameter of 25% and an ADC/DAC with a 2 GS/s sampling rate and 8-bit quantization. According to the above-mentioned parameters, the electrical OFDM signal has a bandwidth of 1GHz. For different signal modulation formats, the optimum DML bias currents, peak-to-peak driving currents and signal clipping ratios identified in the real-time experiments [3, 4] are also considered, which are

summarized in Table 9.1. In addition, the experimentally measured DAC frequency response is also included, which has about 5dB roll-off within the signal bandwidth region.

In numerical simulations, the following system parameters adopted in the experiments [3, 4] are also taken, which are a 7dBm optical power launched into a SMF system, a noise equivalent power density of 27 pw/$\sqrt{Hz}$ and a responsivity of 0.91 A/W for the PIN.

Table 9.2
DFB Parameters

DFB	
Symbol	Value
l	300 μm
w	2 μm
d	0.033 μm
τ_c	10 ns
B	1×10^{-16} m^3/s
C	6.5×10^{-41} m^6/s
G	1.1×10^{-12} m^3/s
N_t	1.5×10^{24} m^{-3}
ε	7.4×10^{-23} m^{-3}
Γ	0.07
τ_p	3.6 ps
n_g	3.7
n_p	3.2203
w_v	0.47 μm
w_h	1.80 μm
η	-1.38×10^{-26} m^{-3}
ζ	1×10^{-5}
χ	37%

All the parameter values employed in the DFB laser model (described in Section 4.3.2) are listed in Table 9.2. These parameters are, in general, taken from the literature [10, 11]. However, some parameters including the linear optical gain coefficient G, the nonlinear gain coefficient ε and the transparency carrier density N_t were adjusted to obtain agreement between the simulation and the experimental measurements. It is also worth mentioning that by adopting the DML parameters in Table 9.2, the DML model gives rise to a DFB threshold current of about 27 mA. The 3-dB modulation bandwidth is approximately 10GHz. Such characteristics are very similar to those measured in the experiments [3, 4].

Finally, in simulating the MetroCor fibres, their typical parameter values at a wavelength of 1550nm are employed, which are a dispersion parameter of -7.6 ps/(km·nm), a dispersion slope of 0.1 ps/(km·nm^2), a linear loss of 0.2 dB/km, an effective area of 70 μm^2 and a Kerr coefficient of 2.35×10^{-20} m^2/W.

9.4 Results and Discussions

To rigorously verify the developed transmission link model, extensive comparisons between numerical simulations and experimental measurements are first made in various transmission systems. After that, detailed numerical results are presented to explore the physical origin of the observed negative power penalties and subsequently identify effective technical approaches that can be used to improve the DML-based IMDD OOFDM system performance.

Throughout this chapter, the power penalty is defined as, for achieving a BER of 1×10^{-3}, the received optical power difference between a full transmission link of a specific transmission distance and the corresponding optical back-to-back system configuration. It should be pointed out that, for fair comparisons between numerical simulations and experimental measurements, both the power penalty definition and its corresponding calculation procedure used in numerical simulations are identical to those reported in [3,4]. Here it is also worth mentioning that, in numerical simulations, the BER is obtained by directly counting errors occurring within 2000 OFDM symbols, which, prior to being transmitted over a SMF link, are oversampled to give a total number of sample points of 512488 per data sequence. Similar to those reported in [3,4], net OOFDM signal bit rates are used in describing the system transmission capacity. For all results presented in this section, 16QAM is considered across all the subcarriers within an OFDM symbol in both numerical simulations and experimental measurements, except that, in Fig.9.4 (Fig.9.7), different signal modulation formats (adaptive signal modulation) are employed.

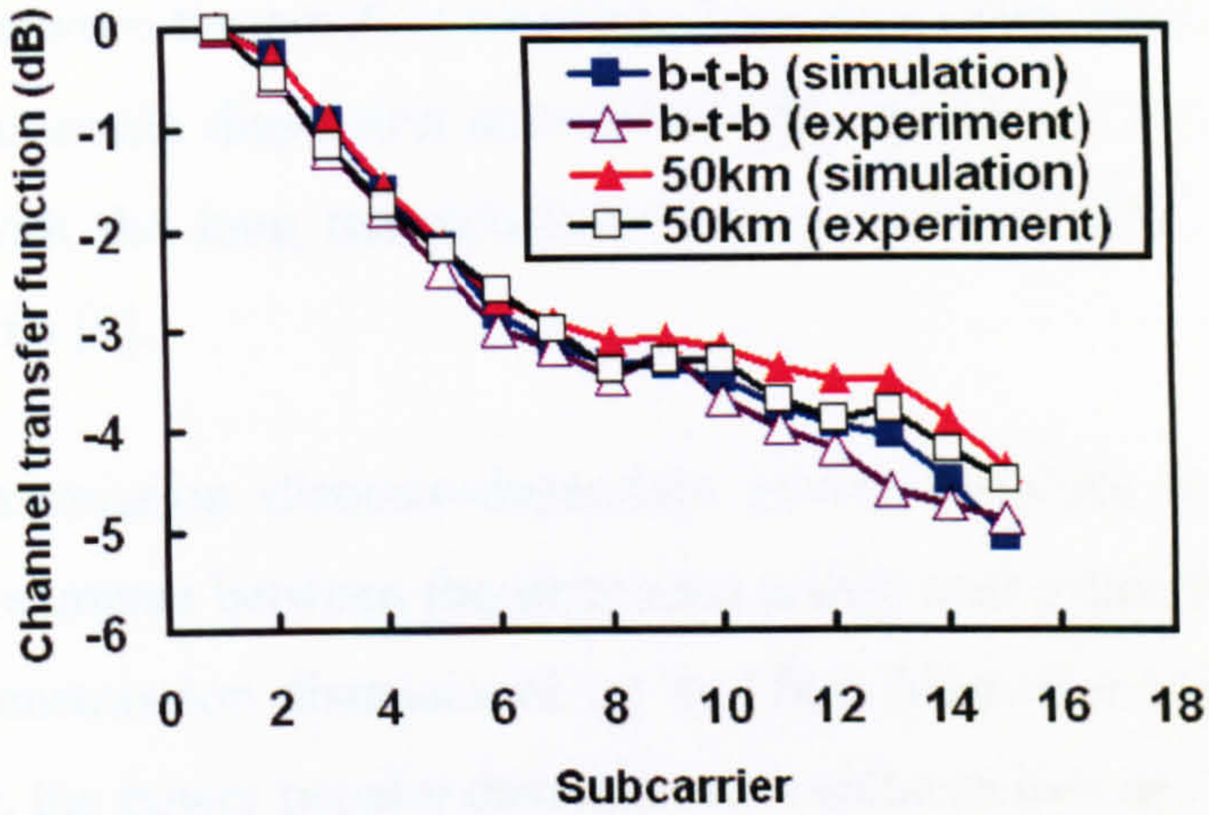

Fig.9.2 Comparisons of normalised channel transfer functions for different DML-based IMDD link configurations.

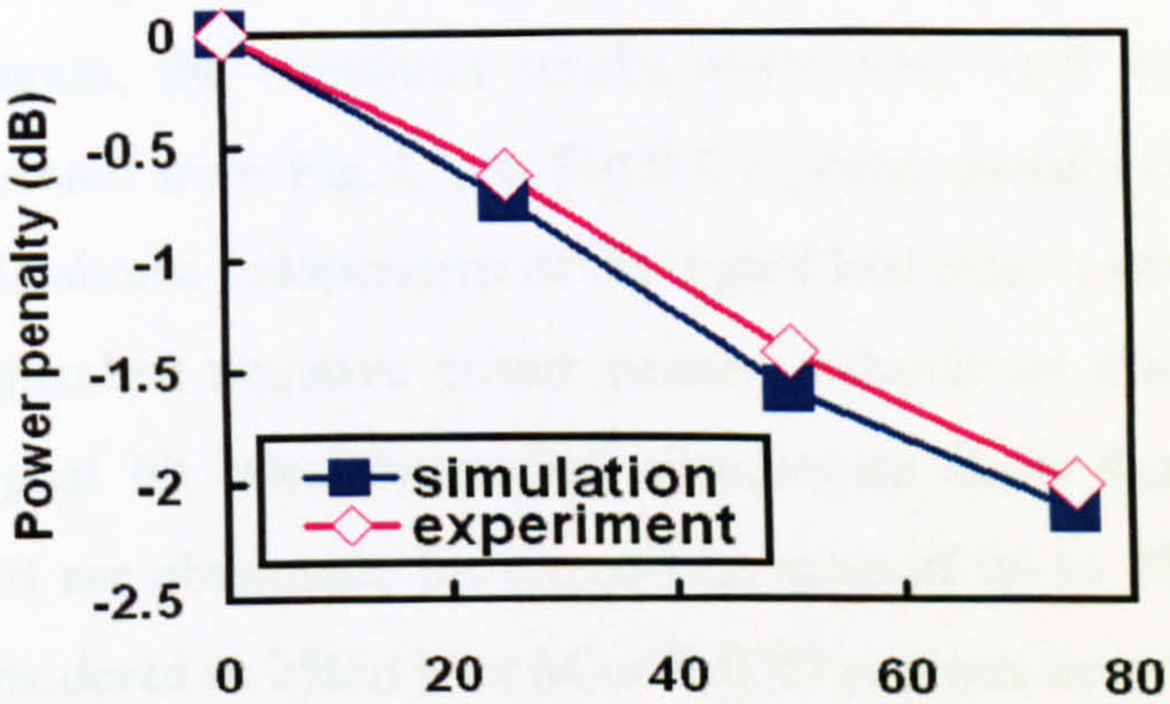

Fig.9.3 Comparisons of power penalty versus transmission distance for 16QAM-encoded OOFDM signals of net signal bit rates of 3Gb/s.

9.4.1 Comparisons between Numerical and Experimental Results

For optical back-to-back and DML-based 50km MetroCor IMDD links, comparison of their normalized Channel Transfer Functions (CTFs) measured from the input of the IFFT in the transmitter and the output of the FFT in the receiver are shown in Fig.9.2. It can be seen in Fig.9.2 that, for all the cases considered, the simulated CTFs are in good agreement with the experimental results. The rapid CTF decays of approximately 5dB within the signal spectral region are mainly attributed to the DAC due to its output filtering and inherent sin(x)/x response. In comparison with the optical back-to-back case, the slightly up-shifted 50km CTFs corresponding to high frequency subcarriers are a direct result of

the compensation between the positive transient frequency chirp associated with the DML and the negative chromatic dispersion associated with the MetroCor fibre. This behavior contrasts sharply with the long transmission distance-induced *CTF* narrowing effect in SSMF IMDD systems [9].

Comparison of transmission distance-dependent power penalties is plotted in Fig.9.3, where excellent agreements between the simulated results and experimental measurements are observed for transmission distances of up to 75km MetroCor SMFs. With increasing transmission length, the power penalty decreases to a value as low as -2 dB for 75 km.

The power penalty as a function of OOFDM signal line rate for 25km MetroCor fibres is shown in Fig. 9.4, where the signal line rates of 3 Gb/s, 4.5 Gb/s and 5.25 Gb/s are achieved by different signal modulation formats of 16QAM, 64QAM and 128QAM, respectively. Once again, the simulated results agree very well with the experimental observations. As expected from Fig.9.3, in Fig.9.4 a power penalty of approximately -0.6 dB is shown, which is almost independent of the signal line rate. It should be noted that the signal line rate-independent negative power penalty behaviours also occur for OOFDM signals of higher signal bit rates. Numerical simulations show that power penalties of approximately -0.6dB are obtainable for signal line rates of up to 30Gb/s when 12.5GS/s DACs/ADCs are considered in 25km MetroCor IMDD systems involving DMLs operating under conditions identical to those adopted in Fig.9.4.

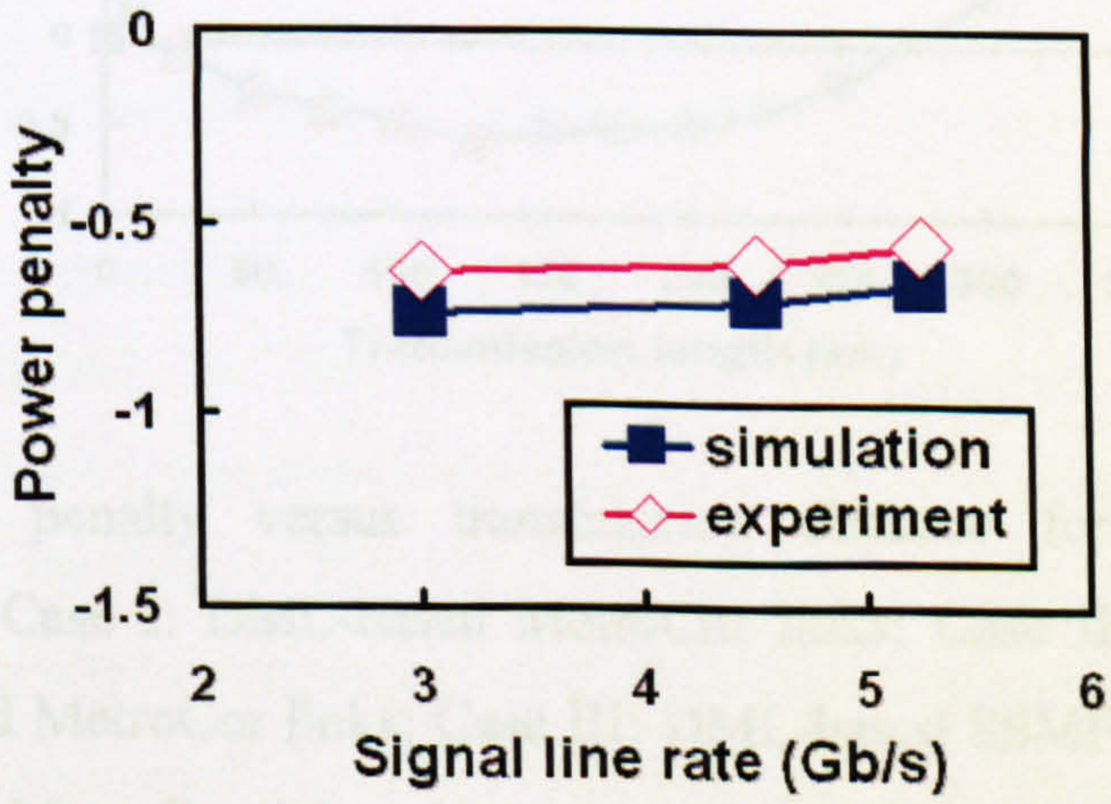

Fig.9.4 Power penalties versus signal line rate obtained for different net signal line rates for 25km MetroCor systems.

The above-mentioned excellent agreements between the numerical simulations and the experimental measurements for a wide diversity of different systems, strongly confirm the validity of the theoretical link model developed here. The link model can, therefore, serve as an excellent base for further exploring the physical origin and dynamic characteristics of negative power penalties observed in such systems.

9.4.2 Physical Origin of Negative Power Penalty

To explore the physical origin of the negative power penalties observed in DML-based IMDD OOFDM MetroCor systems, Fig.9.5 is plotted, where the transmission distance-dependent power penalties are given for various IMDD link configurations: Case I: DML-based MetroCor links; Case II: ideal intensity modulator-based MetroCor links; Case III: DML-based SSMF links, and Case IV: DML-based MetroCor links without considering fibre linear losses. In obtaining Fig.9.5, a 38mA bias current is employed for all the cases. For Case I and Case II, the maximum transmission distances of 125 km occur due to the fact that the received optical signal powers are too low to achieve total channel BERs of 1×10^{-3}.

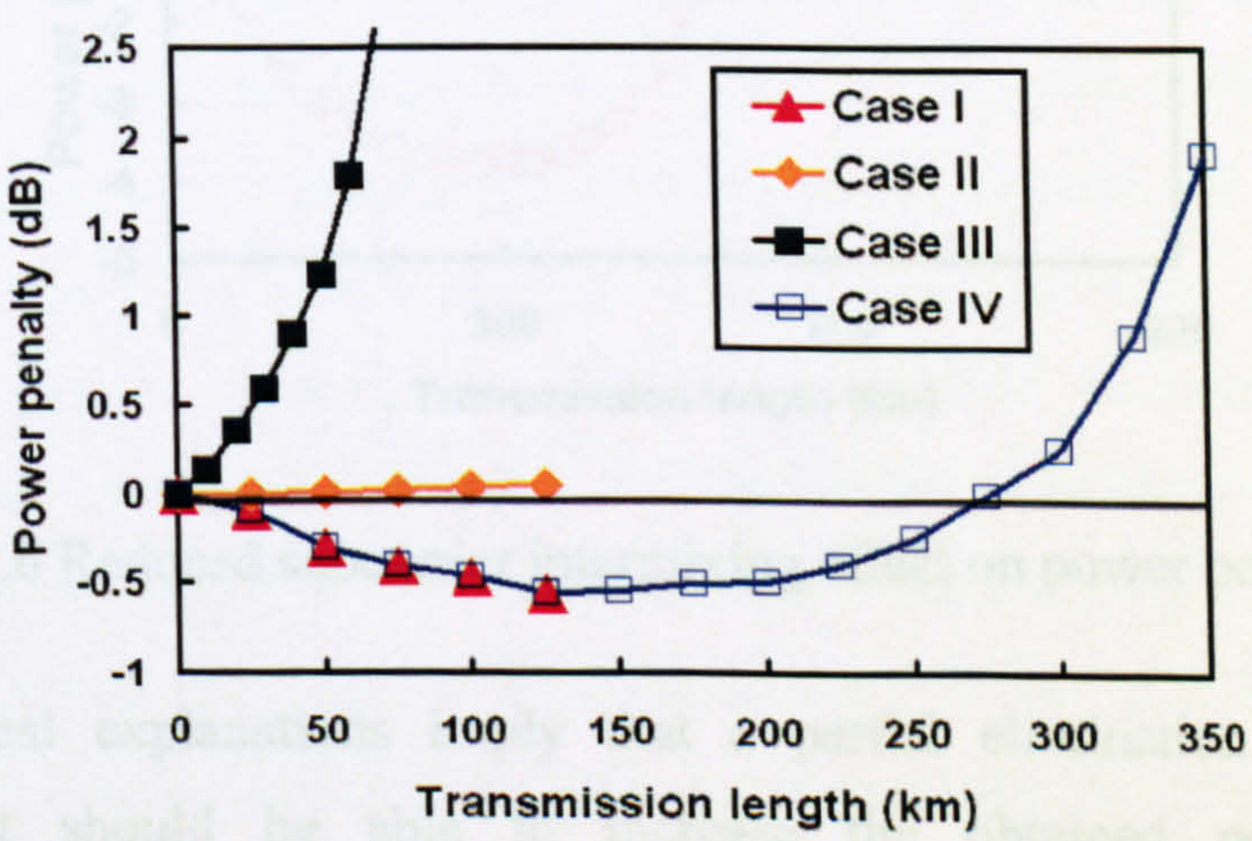

Fig.9.5 Power penalty versus transmission distance for different link configurations. Case I: DML-based MetroCor links; Case II: ideal intensity modulator-based MetroCor links; Case III: DML-based SSMF links, and Case IV: DML-based MetroCor links without considering fibre linear losses.

Comparison between the different cases considered in Fig.9.5 shows that only the co-existence of the DML and MetroCor fibres in Case I and Case IV leads to the occurrence of negative power penalties, whose values depend upon transmission distance. This implies

that the negative power penalty is a direct result of the negative dispersion fibre-enabled compensation of the DML positive transient frequency chirp. Based on Fig. 9.5, the physical mechanisms behind the negative power penalty can be explained as follows: the optical-domain OOFDM signal phase cannot be preserved perfectly in the electrical domain due to subcarrier intermixing upon square-law photon detection in the receiver. As the unwanted subcarrier intermixing effect decreases with decreasing optical phase at the input facet of the PIN, thus the MetroCor fibre-induced reduction in the DML-modulated OOFDM signal phase gives rise to the observed negative power penalty. Whilst for coherent OOFDM MetroCor transmission systems, the OOFDM signal phase can be preserved perfectly in the electrical domain, therefore no negative power penalties exist. This is verified by our numerical simulations, even when the optical phases identical to those corresponding to the IMDD cases are introduced into the coherent OOFDM signals.

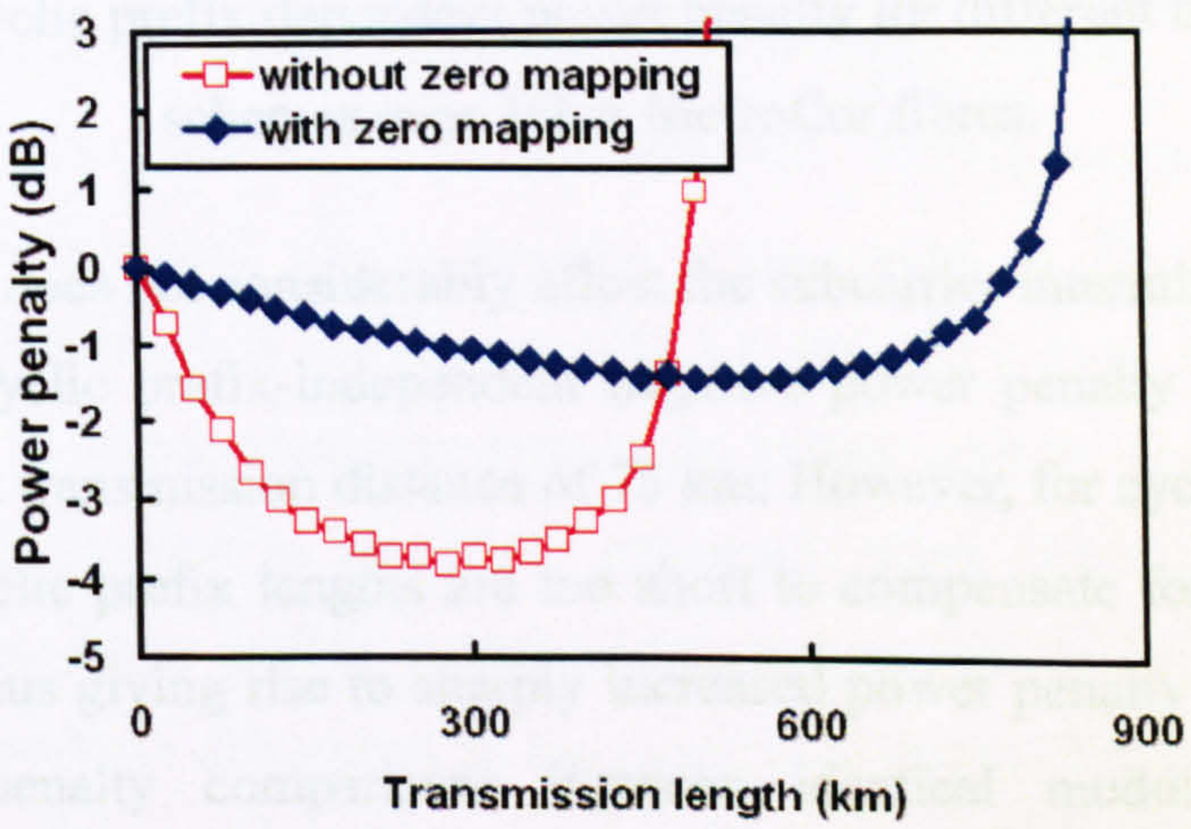

Fig.9.6 Reduced subcarrier intermixing effect on power penalty.

The above physical explanations imply that a partial elimination of the subcarrier intermixing effect should be able to increase the obtained power penalty and simultaneously extend the transmission distance, over which the minimum power penalty is observed. This is verified in Fig. 9.6, in obtaining which, to partly eliminate the subcarrier intermixing effect, zero-mapping of the first 8 subcarriers close to the optical carrier is performed, and other parameter values identical to those used in Fig. 9.3 are adopted without considering the fibre linear loss effect.

9.4.3 Impacts of Adaptive Modulation and Cyclic Prefix on Negative Power Penalty

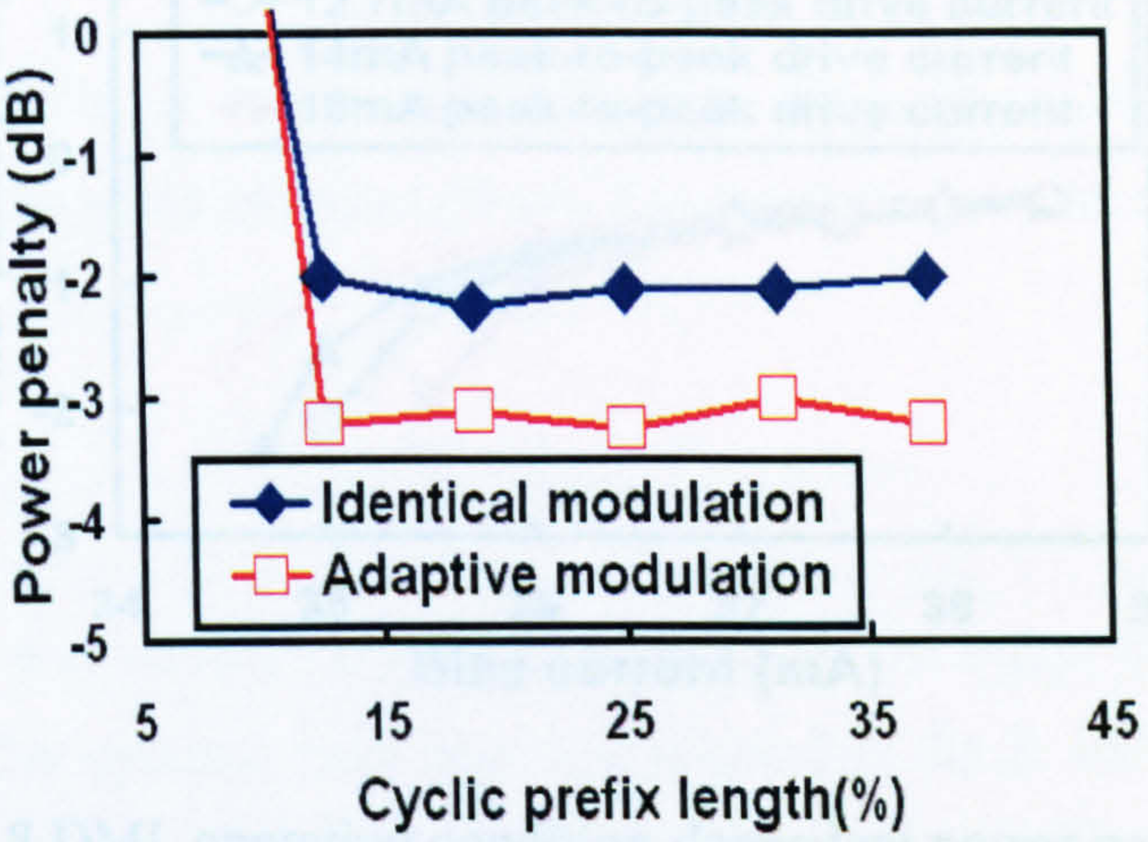

Fig.9.7 Cyclic prefix dependent power penalty for different modulation schemes over 75km MetroCor fibres.

As the cyclic prefix does not considerably affect the subcarrier intermixing effect occurring in the receiver, a cyclic prefix-independent negative power penalty is thus observed, as seen in Fig.9.7 for a transmission distance of 75 km. However, for cyclic prefix parameters of < 6.25%, the cyclic prefix lengths are too short to compensate for the fibre chromatic dispersion effect, thus giving rise to sharply increased power penalty shown in Fig.9.7. In addition, power penalty comparisons between identical modulation and adaptive modulation are also presented in Fig.9.7. For the adaptive modulation case, a DQPSK (32QAM) modulation format is taken on subcarriers experiencing a low (high) SNR to ensure that the resulting total channel BER remains at $< 1\times10^{-3}$ and the signal line rate is still fixed at 3 Gb/s (corresponding to a cyclic prefix parameter of 25%). It can also be seen in Fig.9.7 that, in comparison with identical modulation, the use of adaptive modulation can further reduce the power penalty by about 1dB. This is because adaptive modulation has better tolerance to the subcarrier intermixing effect owing to the assignment of different signal modulation formats on individual subcarriers experiencing different SNRs.

9.4.4 DML Operating Condition-Dependent Negative Power Penalty

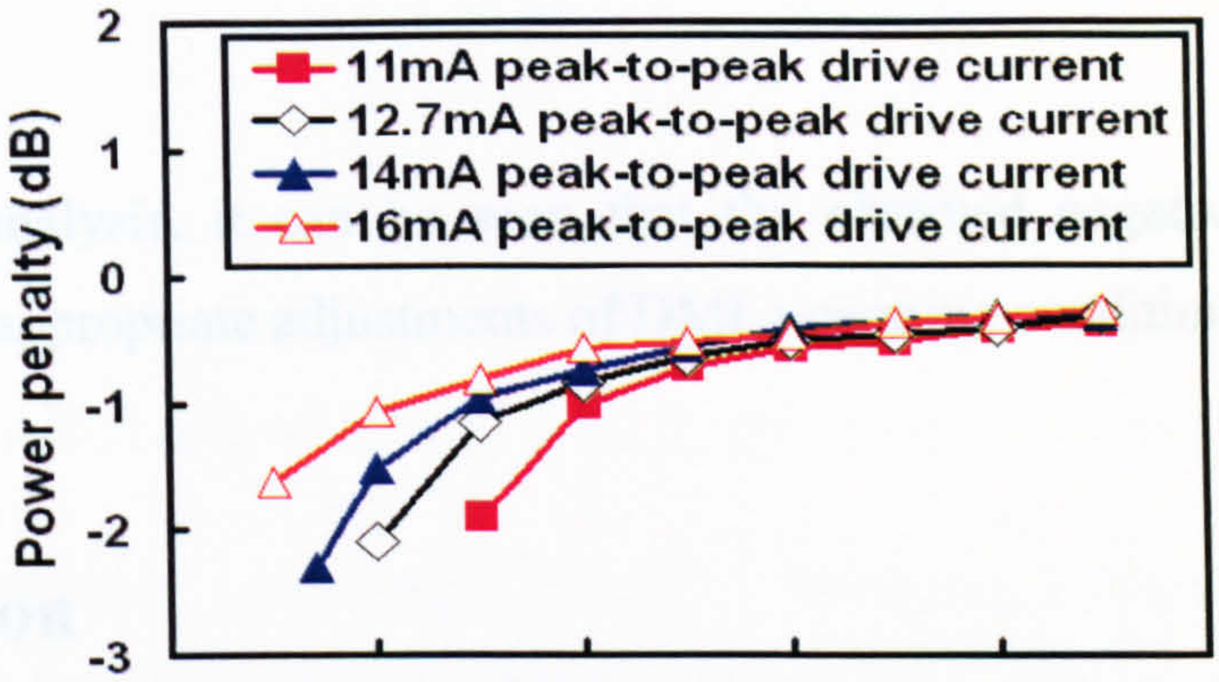

Fig.9.8 DML operating condition-dependent power penalty.

Since the DML frequency chirp characteristics strongly depend on DML operation conditions including bias currents and peak-to-peak driving currents [10], the DML operating condition-dependent power penalty is thus seen in Fig.9.8, where a 75km MetroCor fibre is considered. It is shown in Fig.9.8 that, for a fixed peak-to-peak driving current, a reduction in bias current can reduce the power penalty, resulting from the low bias current-induced increase in the DML frequency chirp effect. A reduction in bias current also produces a low optical output power and introduces strong unwanted signal clipping-induced waveform distortions to the modulated optical signals. These two effects significantly worsen the signal transmission performance and subsequently give rise to total channel BERs of $> 1\times10^{-3}$ even for optical back-to-back links. Thus, for a specific peak-to-peak driving current, a minimum bias current occurs, corresponding to which a minimum power penalty is observed.

On the other hand, over the low bias current region, the power penalty increases with increasing peak-to-peak driving current, as shown in Fig.9.8. This is due to the enhanced signal clipping effect associated with the large peak-to-peak driving currents employed, as under such conditions, the signal clipping effect plays an important role in determining the system transmission performance. In addition, a low peak-to-peak driving current also requires a relatively high bias current to maintain the optical output power at an acceptable level, thus resulting in a minimum power penalty occurring in a relatively high bias current region, as shown in Fig.9.8. It can also be seen in Fig.9.8 that, for bias currents of >37mA,

the power penalty differences among various peak-to-peak driving currents are negligible, this implies that, over such a bias current region, the DML frequency chirp is sufficiently small.

From the above analysis, it can be seen that the obtained negative power penalty is controllable when appropriate adjustments of DML operating conditions are applied.

9.5 Conclusion

Dynamic negative power penalty characteristics of OOFDM signal transmissions in DML-based IMDD MetroCor systems have been investigated in detail and excellent agreements between numerical simulations and experimental measurements have been obtained for a wide diversity of system conditions. Based on a rigorously verified comprehensive theoretical transmission link model, the physical origin of the observed negative power penalties has been identified, i.e., the reduction in subcarrier intermixing impairment in the receiver due to the compensation between the DML positive frequency chirp and the MetroCor negative chromatic dispersion. Results have also shown that the negative power penalty is independent of cyclic prefix and signal modulation format, and controllable when adaptive modulation and/or variations in DML operating conditions are applied.

References

[1] J. A. P. Morgado and A. V. T. Cartaxo, "Directly modulated laser parameters optimization for metropolitan area networks utilizing negative dispersion fibre," IEEE J. Select. Top. Quantum. Electron., vol. 9, no. 5, pp. 1315-1324, Sep/Oct. 2003.

[2] I. Tomkos, B. Hallock, I. Roudas, R. Hesse, A. Boskovic, J. Nakano and R. Vodhanel, "10-Gb/s transmission of 1.55-μm directly modulated signal over 100 km of negative dispersion fiber," IEEE Photon. Technol. Lett., vol.13, no.7, pp.735-737, Jul. 2001.

[3] X. Q .Jin, R. P. Giddings and J. M .Tang, "Real-time transmission of 3Gb/s 16-QAM encoded optical OFDM signals over 75km SMFs with negative power penalties," Opt. Express. vol. 17, no. 17, pp. 14574-14585, Aug. 2009.

[4] X. Q. Jin, R. P. Giddings, E. Hugues-Salas and J. M. Tang, "Real-time demonstration of 128-QAM-encoded optical OFDM transmission with a 5.25bit/s/Hz spectral efficiency in simple IMDD systems utilizing directly modulated DFB lasers," Opt. Express. vol. 17, no. 22, pp. 20484-20493, Oct. 2009.

[5] J. L. Wei, X. L. Yang, R. P. Giddings and J. M. Tang, "Colourless adaptively modulated optical OFDM transmitters using SOA as intensity modulator," Opt. Express., vol. 17, no. 11, pp. 9012-9027, May. 2009.

[6] G. P. Agrawal, *Nonlinear Fibre Optics*, Academic, 1995.

[7] G. P. Agrawal, *Fibre-Optic Communication Systems*, Wiley, 1997.

[8] J. M. Tang and K. A. Shore, "30Gb/s signal transmission over 40-km directly modulated DFB-laser-based single-mode-fiber links without optical amplification and dispersion compensation," J. Lightw. Technol., vol. 24, no. 6, pp. 2318-2327, June. 2006.

[9] J. L. Wei, A. Hamié, R. P. Giddings, and J. M. Tang, "Semiconductor optical amplifier-enabled intensity modulation of adaptively modulated optical OFDM signals in SMF-based IMDD systems," J. Lightw. Technol., vol. 27, no.16, pp.3678-3688, Aug. 2009.

[10] J. M. Tang, P. M. Lane and K. A. Shore, "High-speed transmission of adaptively modulated optical OFDM signals over multimode fibres using directly modulated DFBs," J. Lightw. Technol., vol. 24, no. 1, pp. 429–441, Jan. 2006.

[11] J. E. A. Whiteaway, G. H. B. Thompson, A. J. Collar, and C. J. Armistead, "The design and assessment of $\lambda/4$ phase-shifted DFB laser structures," IEEE J. Quantum Electron., vol. 25, no. 6, pp. 1261–1279, Jun. 1989.

10 Compensation of Directly Modulated DFB Laser Frequency Chirps for IMDD OOFDM PON Systems

Contents

10.1 Introduction

Apart from the employment of negative dispersion fibres discussed in chapter 9, in traditional NRZ/RZ transmission systems, several frequency chirp compensation techniques have also been proposed to reduce the DML frequency chirp effect [1-5]. In [1], SPM is utilized to compensate for the DML transient frequency chirps, as SPM induces negative frequency chirp at the pulse leading edges and positive frequency chirp at the pulse trailing edges, both of which have opposite signs with respect to the DML transient frequency chirp in the corresponding pulse edges. Unfortunately, the SPM technique can not compensate for the DML adiabatic frequency chirp. Spectral conversion based on FWM is capable of simultaneously alleviating the DML transient and adiabatic frequency chirp [2]. However, the technique has strong system-dependent performance and extremely low spectral conversion efficiency. The implementation of the technique may considerably increase the complexity of the PON systems due to the requirement of two independent conversion devices for both up-link and down-link transmission. In addition, use can also be made of SOAs [3], whose negative frequency chirp are, however, strongly dependent upon their operating conditions. This inevitably causes difficulties in practical system realization and control. Moreover, to achieve the desired DML frequency chirp compensation, special DML cavity designs have also been considered, which include extended DML cavities [4] as well as separate gain and phase sections [5].

In this chapter, for DML-based AMOOFDM IMDD PON systems, a simple and effective DML frequency chirp compensation technique is proposed, for the first time, which utilizes an electrical analogue circuit to produce an electrical signal, which is, throughout the chapter, referred to as a phase signal. The phase signal that mimics the original optical phase of the DML-modulated AMOOFDM signal emerging from the DML is used to drive an optical phase modulator, in which frequency chirp compensation of the DML-modulated AMOOFDM signal is performed in the optical domain. The proposed technique has the following major advantages:

- Effective compensation of two major DML frequency chirp components including transient frequency chirp and adiabatic frequency chirp;

- Significant improvements in both the transmission capacity and system robustness;
- Considerably enhanced performance tolerance to DML operating condition.

Numerical simulations show that, in comparison with previously reported DML-based AMOOFDM IMDD systems without DML frequency chirp compensation [6], the proposed technique can significantly increase the signal line rate by approximately 25% for transmission distances ranging from 30km to 80km. Here it is also worth pointing out that the electrical analogue circuit required can be easily integrated with other electrical components incorporated in the AMOOFDM transceivers, and the integration between the DMLs and optical phase modulators is also practically feasible. These facts suggest that the proposed frequency chirp compensation technique is more cost-effective than traditional MZM intensity modulators, and the simplicity of both AMOOFDM transceivers and PON architectures can still be retained.

The chapter is organized as follows: in Section 10.2, the DML-based AMOOFDM IMDD PON system is described with special attention being given to the operating principles of the proposed technique. In Section 10.3, the component/system parameters adopted in numerical simulations are presented. In Section 10.4, the physical origin underpinning the effectiveness of the proposed technique is explored in detail, and the optimum circuit design parameters are identified. Detailed explorations are also made of the sensitivity of the system performance to DML operating conditions. Finally, the chapter is summarized in Section 10.5.

10.2 Transmission Systems with DML Frequency Chirp Compensation

10.2.1 Transmission System

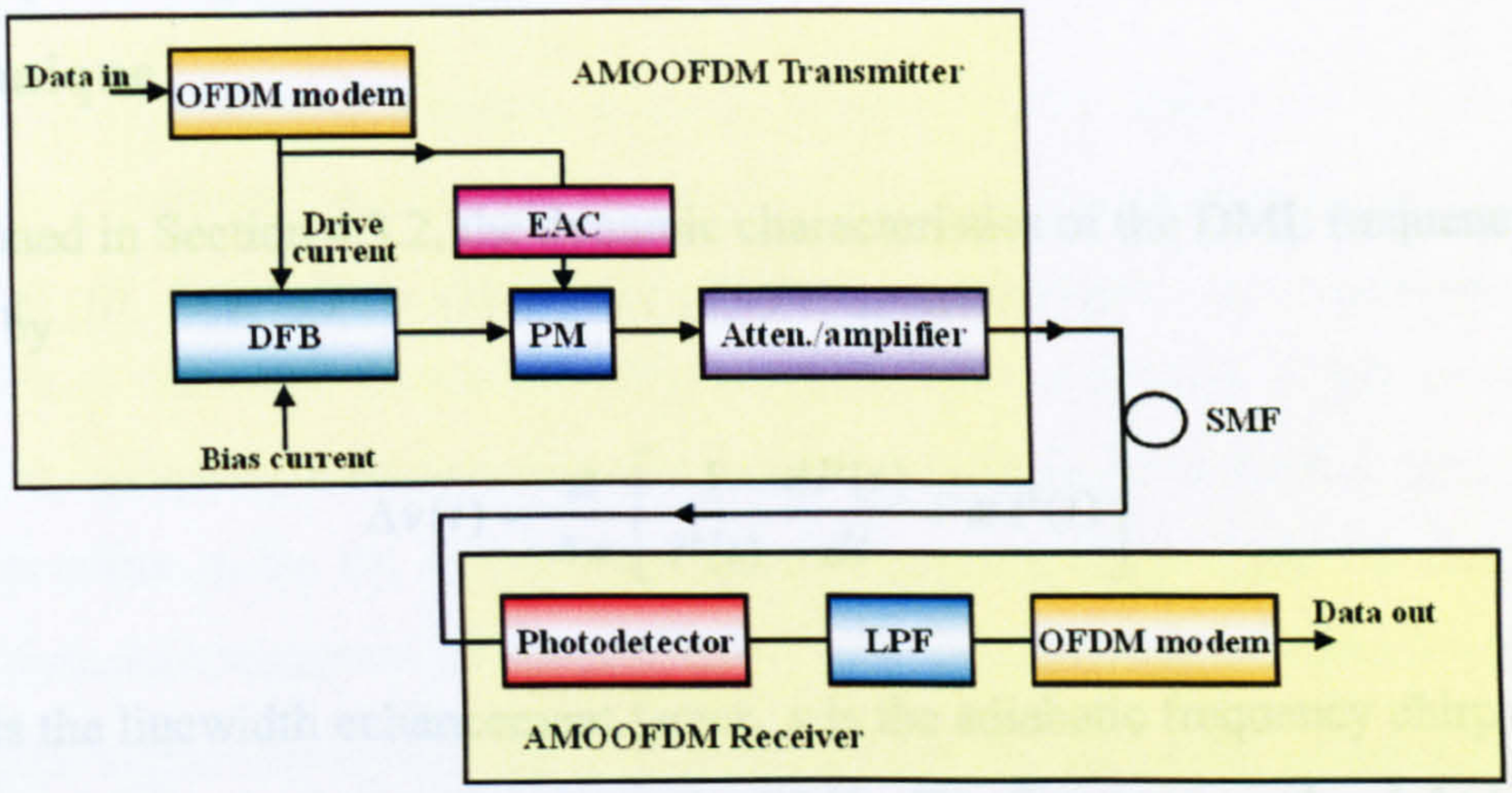

Fig.10.1 Schematic diagram of the DML-based AMOOFDM IMDD PON system using the proposed frequency chirp compensation technique. EAC: electrical analogue circuit; PM: phase modulator; Atten: attenuator; LPF: low-pass filter.

A single wavelength channel, DML-based AMOOFDM IMDD PON system using the proposed frequency chirp compensation technique is illustrated in Fig.10.1, which is free from both chromatic dispersion compensation and in-line optical amplification. The transmission system consists of an AMOOFDM transmitter, an AMOOFDM receiver and SSMFs in between. When compared with a chirp compensation-free, conventional AMOOFDM system [6], the differences exist only in the transmitter due to the inclusion of an electrical analogue circuit for producing a phase signal, and the employment of an optical phase modulator for performing DML frequency chirp compensation. As shown in Fig. 10.1, in the transmitter, an electrical analogue OFDM signal emerging from a DAC in the OFDM modem [6] is divided into two parts: the first part is combined with an optimum bias current and is then employed to directly modulate a DML; whilst the second part is input to the electrical analogue circuit, whose output is the phase signal. The AMOOFDM signal from the DML is injected into the phase modulator driven by the phase signal. After appropriately adjusting the optical launch power by an optical attenuator/amplifier, the

optical signal from the optical phase modulator is coupled into the SSMF system. In the AMOOFDM receiver, the transmitted optical signal is detected using a square-law photodetector. After passing through a low pass filter, the received electrical signal is processed, in a receiver OFDM modem, via an inverse procedure of the transmitter.

10.2.2 Operating Principle of the DML Frequency Chirp Compensation Technique

As mentioned in Section 4.3.2, the dynamic characteristics of the DML frequency chirp are governed by

$$\Delta v(t) = \frac{\alpha}{4\pi}\left[\frac{1}{P(t)}\frac{dP(t)}{dt} + \kappa P(t)\right] \tag{10.1}$$

where α is the linewidth enhancement factor, κ is the adiabatic frequency chirp coefficient, $P(t)$ is the output optical power from the DML. The first term on the right hand side of Eq.(10.1) denotes the DML transient frequency chirp and the second term denotes the DML adiabatic frequency chirp.

As $P(t)$ has a "noise-like" time-domain waveform with a typical signal extinction ratio as small as 0.2dB [7], the transient frequency chirp term in Eq.(10.1) can be simplified to the form $\frac{1}{P_0}\frac{dP(t)}{dt}$ with P_0 being the average output optical power. On the other hand, considering the waveform similarity between $P(t)$ and the electrical OFDM signal from the OFDM modem, $S_{OFDM}(t)$, $P(t)$ can be replaced by $S_{OFDM}(t)$ in Eq.(10.1). The validity of the assumptions made above is verified by the effectiveness of the proposed technique, as discussed in Section 10.4.1. Taking into account the aforementioned facts and applying some necessary manipulations to Eq.(10.1), the formula given below is obtained

$$\phi(t) = \frac{\alpha}{4\pi}\left[\int_{S_{OFDM\_0}}^{S_{OFDM}(t)} \frac{d(S_{OFDM}(t))}{P_{av}} + \kappa\int_{t_0}^{t} S_{OFDM}(t)dt\right] \tag{10.2}$$

where $\phi(t)$ is the phase signal representing the optical phase of the DML-modulated AMOOFDM signal, P_{av} is the average electrical OFDM signal power, S_{OFDM-0} is the

electrical signal waveform at the start time, t_0. Based on Eq. (10.2), the final relationships between the phase signal, $\phi(t)$, and the electrical OFDM signal from the OFDM modem, $S_{OFDM}(t)$, can be described as

$$\phi(t) = bS_{OFDM}(t) + a\int_{t_0}^{t} S_{OFDM}(t)dt + const \tag{10.3}$$

where the circuit design parameters, *a* and *b*, contain all the DML-related factors and the scaling factors generated in deriving Eq.(10.3). Clearly, for a specific transmission system, optimisation of these two design parameters is necessary for achieving the best performance of the DML frequency chirp compensation technique. Although an arbitrary value can be assigned to the last constant term in Eq.(10.3), in numerical simulations, the last term is taken to be 10, as this value gives rise to a phase signal in the vicinity of t_0 with a dynamic variation range similar to that of the original optical phase of the AMOOFDM signal modulated by the DML subject to optimum operating conditions. Eq.(10.3) describes the operating principle of the electrical analogue circuit and forms a fundamental base for practical design of such a circuit.

The generated phase signal is finally employed to drive the optical phase modulator to modulate the AMOOFDM signal from the DML. The output optical signal of the optical phase modulator, $S_{OOFDM\_com}(t)$, can be written as

$$S_{OOFDM\_com}(t) = S_{OOFDM}(t)e^{-j\phi(t)} \tag{10.4}$$

where $S_{OOFDM}(t)$ is the AMOOFDM signal directly emerging from the DML and $P(t) = S_{OOFDM}(t)S^{*}_{OOFDM}(t)$. It can be seen in Eq.(10.4) that, when $\phi(t)$ mimics the original optical phase of the DML-modulated AMOOFDM signal, the DML frequency chirp can be compensated effectively.

10.2.3 Other Component Modeling

The generation/recovery of the electrical OFDM signal in the transmitter/receiver OFDM modem is modeled following the procedure presented in Chapter 2. As an example, the major operations involved in the transmitter OFDM modem include data encoding using different signal modulation formats, IFFT, cyclic prefix insertion, OFDM symbol

serialization and digital-to-analog conversion. An identical subcarrier power is applied to all non-dropped subcarriers prior to the IFFT, and amplification/attenuation is employed to adjust the electrical OFDM signal from the DAC to an optimum power level.

To simulate the nonlinear properties of the DFB-based DML, the DFB laser theoretical model presented in Chapter 4 is adopted. The propagation of the AMOOFDM signals over SSMFs is modeled by using the method mentioned in Chapter 6-9. A square-law photodetector is employed in the receiver to detect the optical signals emerging from the transmission systems. Both shot noise and thermal noise are considered, which are simulated following the procedure similar to that presented in Chapter 9.

It should be noted, in particular, that the validity of all the theoretical models mentioned in Section 10.2.3 has been rigorously verified by comparing numerical results with end-to-end real-time experimental measurements at signal bit rates of up to 11.25Gb/s. Excellent agreement between experimental measurements and numerical results at both component and system levels have been observed over a wide diversity of component/system operating conditions [7,8].

10.3 Simulation Parameters

Throughout this chapter, all the parameters listed below are adopted as default unless addressed explicitly in the corresponding text.

In simulating the OFDM modems, 64 subcarriers are utilised, in which 31 carry real user data, one subcarrier has no power, and the remaining 32 are the complex conjugation of the abovementioned subcarriers. Depending upon the frequency response of a specific transmission system, the modulation format taken on each individual subcarrier may vary from DBPSK, DQPSK, and 16 to 256 QAM. The ADC operating at 12.5 GS/s has quantization bits of 7. The cyclic prefix and signal clipping ratio parameter are fixed at 25% and 13dB, respectively.

In simulating SSMFs at 1550nm, the following SSMF parameters are adopted, which are a dispersion parameter of 18.0 ps/(km·nm), a dispersion slope of 0.07 ps/(km·nm^2), a linear loss of 0.2 dB/km, an effective area of 80 μm^2 and a Kerr coefficient of 2.35×10^{-20} m^2/W

[6]. The optical launch power at the input facet of the SSMF systems is taken to be 6.3dBm.

A PIN photodetector with a quantum efficiency of 0.8 and a noise current density of 8 pA/$\sqrt{Hz}$ are considered [9]. These parameter values give rise to a receiver sensitivity of approximately -17dBm corresponding a 10Gb/s NRZ signal at a BER of 1.0×10^{-9}.

In simulating the DML operating at 1550nm, the parameters identical to those reported in [10] are adopted: a cavity length of 300 μm; a cavity width of 2 μm; a cavity thickness of 0.033μm; a photon lifetime of 3.6 ps; a nonlinear gain coefficient of 7.4×10^{-23} m^{-3}; a differential gain coefficient of 7.5×10^{-20} m^2; a rate of refractive-index change with carrier density of -1.38×10^{-26} m^{-3} ; a 38% coupling efficiency from the laser chip to the SSMF; a carrier lifetime of 10 ns; a bimolecular carrier recombination coefficient of 1×10^{-16} m^3/s; an Auger carrier recombination coefficient of 6.5×10^{-41} m^6/s; and a transparency carrier density of 1.5×10^{24} m^{-3}. Other parameters that are not mentioned explicitly here are taken from [6,10].

10.4 Simulation Results

In this section, the effectiveness of the proposed DML frequency chirp compensation technique is extensively explored with the physical mechanism underpinning such effectiveness being explained. Attention is also given to the identification of optimum electrical analogue circuit design parameters for various system configurations. In addition, the system transmission performance robustness to DML operating condition is also investigated in detail.

10.4.1 Effectiveness and Physical Mechanism

The effectiveness of the proposed DML frequency chirp compensation technique is explored in Fig.10.2, in obtaining which the major electrical analogue circuit design parameters, *a* and *b*, are chosen to be their optimum values identified in Section 10.4.2. A 30mA DML bias current and a 15mA peak-to-peak driving current are adopted. In simulating the case of removing the DML frequency chirp effect, the phase component of the DML-modulated AMOOFDM signal at the output facet of the DML is taken to be a constant value and the corresponding amplitude component is retained. To highlight the

effectiveness of the technique, the signal capacity versus reach performances for two other AMOOFDM IMDD system configurations are also plotted in Fig.10.2, which include conventional DML-based systems without considering the DML frequency chirp compensation technique, and ideal intensity modulator-based systems.

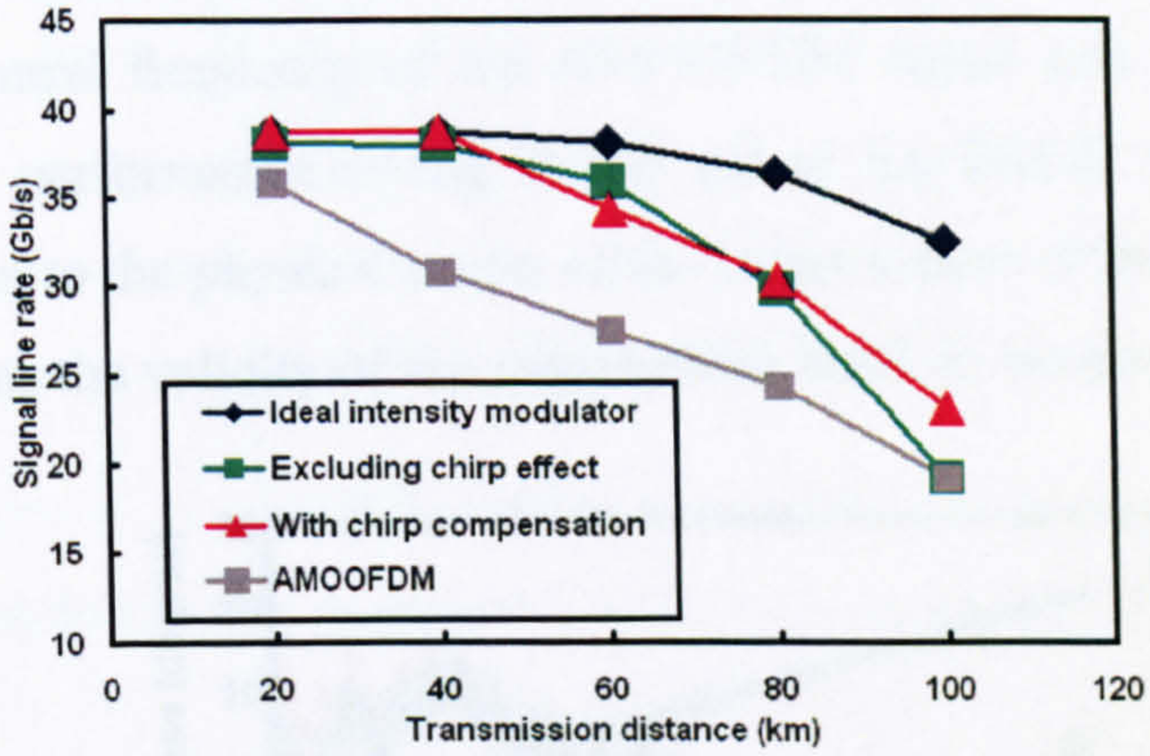

Fig.10.2 Signal line rate versus transmission distance for different transmission system configurations. DML are considered for all the systems except the case of using an ideal intensity modulator.

It can be seen in Fig.10.2 that the DML frequency chirp compensation technique allows the achievement of signal transmission capacities almost identical to those corresponding to the case of completely excluding the DML frequency chirp effect, and that, compared to the conventional DML-based systems, the DML frequency chirp compensation-enabled transmission capacity improvement is as large as 25% over a wide transmission distance region ranging from 30km to 80km. Below (beyond) such a distance region, the decreased signal capacity differences between the conventional systems and the systems incorporating the proposed technique are a direct result of the weakened chromatic dispersion effect (pronounced thermal noise effect) due to short (long) transmission distances. In addition, the long transmission distance-induced increase of the signal bit rate difference between the case of employing the ideal intensity modulator and the case of excluding the DML frequency chirp effect is because of the DML-caused reduction in signal extinction ratio of the IMDD AMOOFDM signals [7].

The observed excellent compensation of the DML frequency chirp effect can be explicitly explained by considering Fig.10.3, where, based on the parameters identical to those adopted in Fig.10.2, comparisons are made between the phase signal produced by the

electrical analogue circuit and the original optical phase of the DML-modulated AMOOFDM signal at the output facet of the DML. The phase difference between these two cases is also plotted in the same figure. Fig.10.3 shows that the phase signal is capable of closely tracking the original optical phase of the AMOOFDM signal, except that there exists a linear phase difference between them. Such a linear phase difference, however, just slightly shifts the central frequency of the AMOOFDM signal and does not degrade the system transmission performance owing to the use of the IMDD system configuration. Therefore, in addition to the physical origin of the effectiveness of the proposed technique, Fig.10.3 also confirms the validity of the assumptions made in Section 10.2.2.

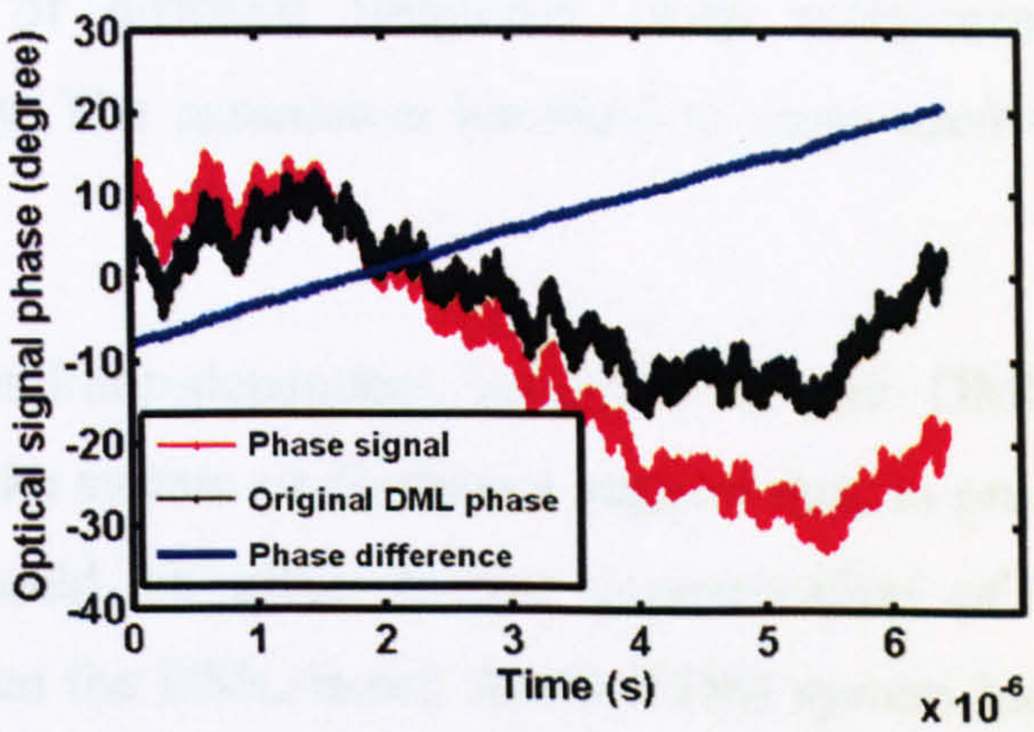

Fig.10.3 Comparison between the phase signal produced by the electrical analogue circuit and the original optical phase of the DML-modulated AMOOFDM signal at the output facet of the DML.

Fig.10.4 is plotted to explicitly distinguish between the impact of the DML transient frequency chirp and that of the DML adiabatic frequency chirp. In numerically simulating the case where only the DML adiabatic frequency chirp effect is alleviated, the electrical analogue circuit design parameter, b, in Eq.(10.3) is set to be zero to exclude the DML transient frequency chirp effect. It is shown in Fig.10.4 that, within the chromatic dispersion-dominant distance region (<80km) [6], the DML adiabatic frequency chirp effect is much more severe; whilst in the linear loss-dominant transmission distance region (>80km) [6], the DML transient frequency chirp is a major limiting factor. Such behaviours agree very well with end-to-end real-time OOFDM experimental results presented in Chapter 9, in which linear loss-dominant operating conditions are automatically selected by launching a minimum optical signal power to the photodetector to achieve the maximum achievable optical power budgets for different system configurations.

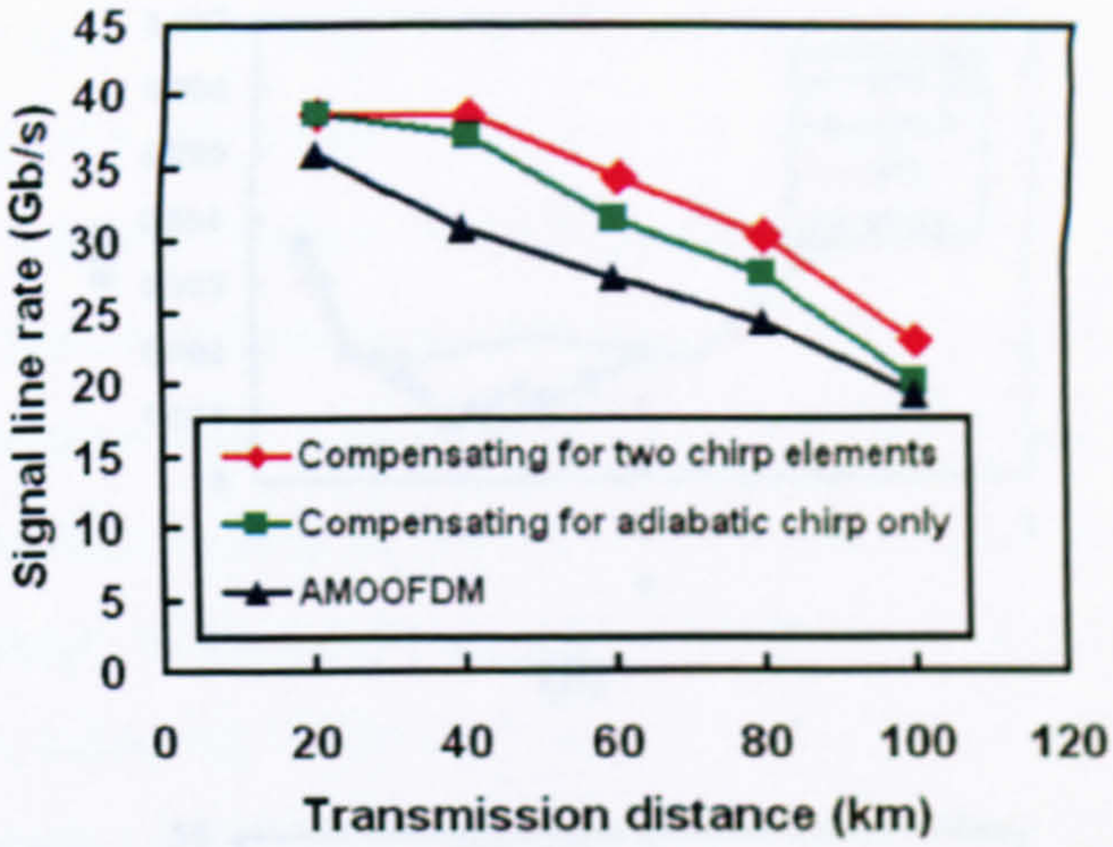

Fig. 10.4 Impacts of different frequency chirp components on system transmission capacity. The parameters identical to those used in Fig.10.2 are adopted.

The observed system condition-dependent influence of the DML transient/adiabatic frequency chirp effect on the system performance suggest that, in practical system design, special considerations should be given to the compensation of the DML adiabatic frequency chirp effect when the DML-based AMOOFDM system has a sufficiently large optical power budget. Whilst when the AMOOFDM system has a limited optical power budget, the compensation of the DML transient frequency chirp effect is more important.

10.4.2 Identification of Optimum Electrical Analogue Circuit Design Parameters

In order to optimize the design of the electrical analogue circuit for practical implementation, the identification of optimum values of circuit parameters, *a* and *b*, is vital. To achieve such an objective, the signal line rate as a function of parameter *a* for different values of the parameter *b* are shown in Fig.10.5, in obtaining which a bias current of 30mA and a peak-to-peak driving current of 15mA are employed. In the 20km SSMF systems, for several parameter combination sets, total channel BERs of $<1\times10^{-3}$ are obtainable even when use is made of the highest signal modulation format of 256-QAM on all the subcarriers, therefore, to smooth the corresponding curves, the total channel BERs instead of signal bit rates are shown in Fig.10.5 (a).

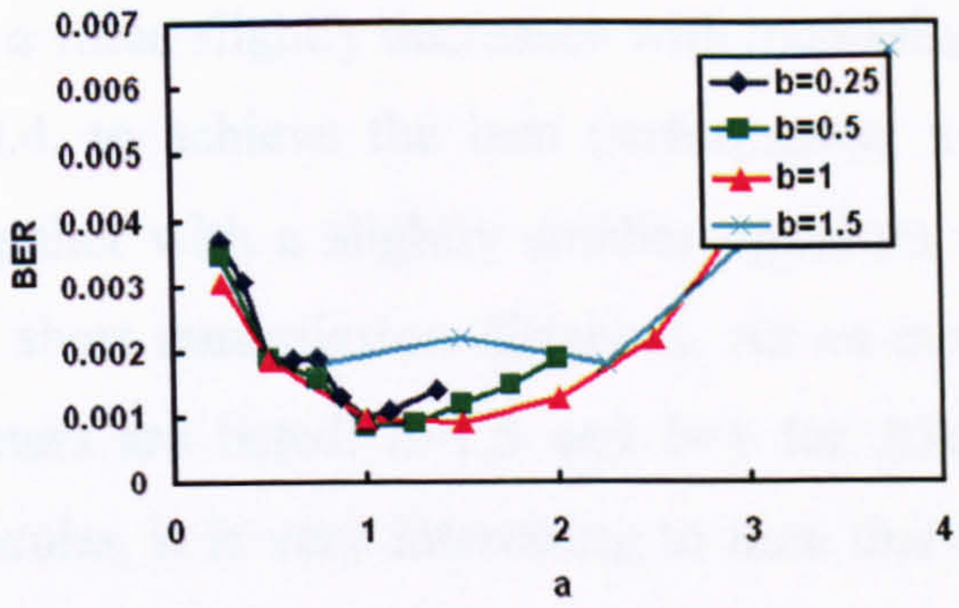

(a)

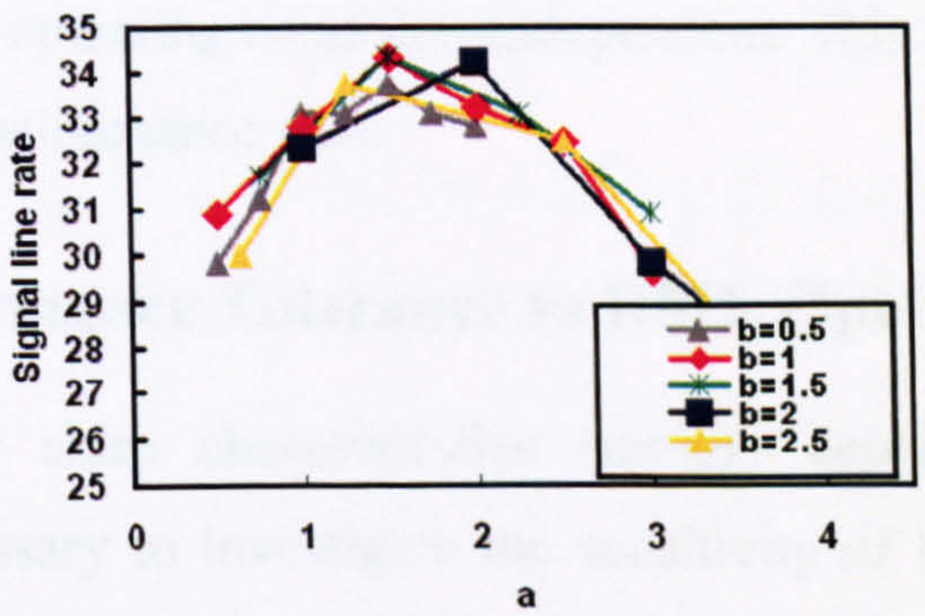

(b)

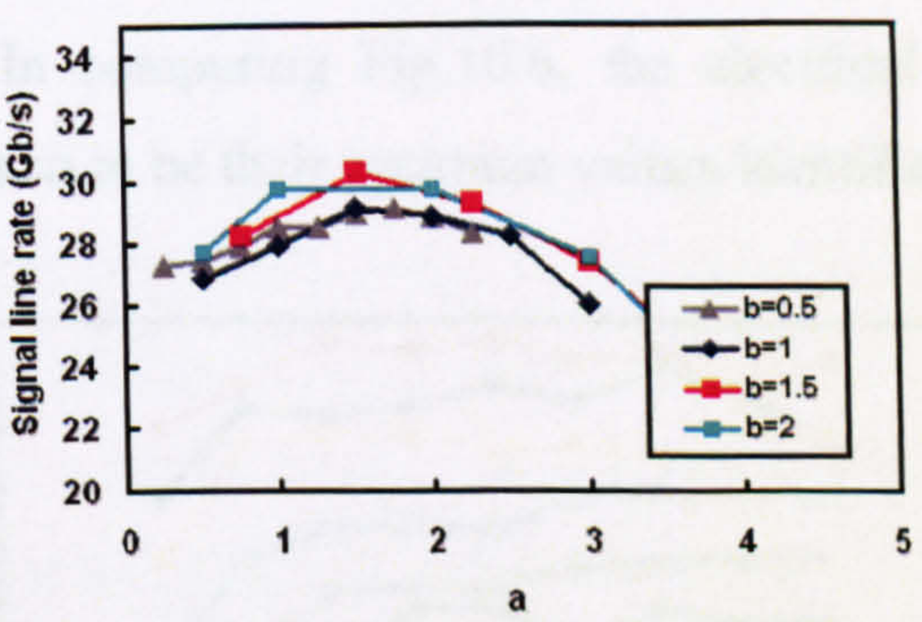

(c)

Fig.10.5 Identification of optimum electrical analogue circuit design parameters, *a* and *b*, for different transmission distances. (a) 20km; (b) 60km and (c) 80km.

It can be seen in Fig.10.5 that, for a given transmission distance and a specific value of parameter *b*, an optimum value of parameter *a* exists, which enables the best compensation of the DML frequency chirp effect, thus resulting in the highest (lowest) signal bit rate (total channel BER). Fig.10.5 also shows that, for all transmission distances of interest in

the chapter, the optimum *a* value slightly decreases with increasing parameter *b*. Moreover, as expected from Fig.10.4, to achieve the best performance, a slightly larger optimum value of parameter *a* together with a slightly smaller optimum value of parameter *b* are observed in Fig.10.5 for short transmission distances. As an example, the following two sets of optimum parameters are listed: a=1.5 and b=1 for 20km-60km, and a=1.5 and b=1.5 for 80km. In particular, it is very interesting to note that the maximum achievable transmission performance is almost independent of different choices of optimum circuit design parameter sets, implying that the proposed technique using an optimised electrical analogue circuit is system operating condition-independent. This would considerably lower both the installation and maintenance cost.

10.4.3 System Performance Tolerance to DML Operating Condition

As the DML frequency chirp characteristics strongly depend upon laser operating conditions [6], it is necessary to investigate the sensitivity of the DML frequency chirp compensation technique to variation in DML operating condition. Such numerical results are presented in Fig.10.6, which shows the DML operating condition-dependent performances for 60km SSMF systems including/excluding the DML frequency chirp compensation technique. In computing Fig.10.6, the electrical analogue circuit design parameters, *a* and *b*, are taken to be their optimum values identified in Fig.10.5.

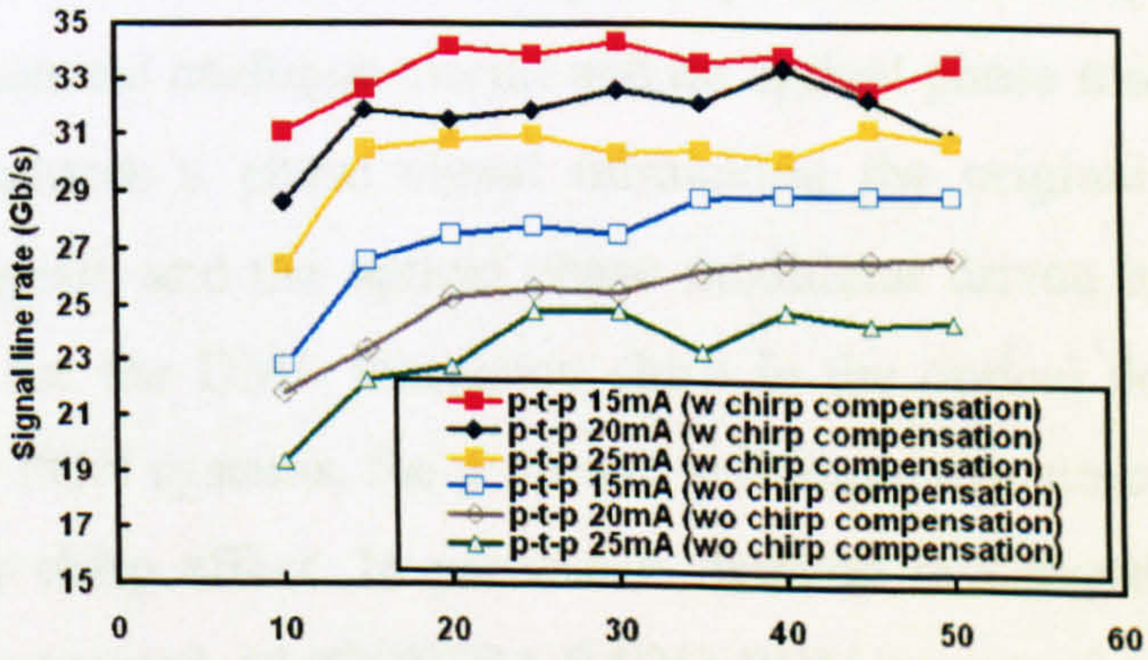

Fig.10.6. Performance sensitivity to DML operating conditions. 60km SSMFs are considered. W: with DML frequency chirp compensation WO: without DML frequency chirp compensation.

It is shown in Fig.10.6 that, for a given peak-to-peak driving current, a broad optimum bias current range occurs, over which maximum signal line rates are observed. For bias currents

below the identified optimum range, the co-existence of the effects of strong DML frequency chirp and DML modulation-induced OFDM signal clipping causes the rapid decay in transmission performance; whilst for bias currents well above the identified optimum range, the reduction in effective SNR plays a dominant role in determining the slight performance degradation. On the other hand, for a fixed bias current, the increase in signal bit rate with decreasing peak-to-peak driving current, as seen in Fig.10.6, is mainly due to the low driving current-induced less amplitude distortions of the AMOOFDM waveforms [6]. Numerical simulations also show that the optimum bias/driving currents are independent of transmission distance.

It can be seen in Fig.10.6 that, over a wide bias (driving) current range of 15mA to 45mA (15mA to 25mA), the DML frequency chirp compensation technique can reduce the signal capacity variation range by a factor of approximately 2, in comparison to those corresponding to the uncompensated cases. This indicates that the present technique can improve the system performance tolerance to variation in DML operation condition, thus leading to enhanced performance robustness.

10.5 Conclusion

A simple and effective DML frequency chirp compensation technique has been proposed, which utilizes an electrical analogue circuit and an optical phase modulator. The electrical analogue circuit produces a phase signal mimicking the original phase of the DML-modulated optical signal, and the optical phase modulator driven by the generated phase signal compensates for the DML frequency chirp in the optical domain. In DML-based AMOOFDM IMDD PON systems, the proposed technique can almost alleviate completely the DML frequency chirp effect. In particular, detailed investigations have shown that, compared to uncompensated AMOOFDM IMDD PON systems incorporating DMLs, the proposed technique can not only improve the transmission capacity by approximately 25% over a wide transmission distance range, but also considerably enhance the system performance robustness to variation in DML operating condition. Optimum electrical analogue circuit design parameters have also been identified, based on which the present technique offers system operating condition-independent transmission performance.

References

[1] N. Suzuki and T. Ozeki, "Simultaneous compensation of laser chirp, Kerr effect, and dispersion in 10-Gb/s long-haul transmission systems," J. Lightw. Technol., vol. 11, no. 9, pp. 1486-1494, Sep. 1993.

[2] M. Tanaka and M. Shigematsu, "Chirp compensation using four-wave mixing and its application to 10-Gb/s directly modulated signal transmission over SMF," IEEE Photon. Technol. Lett., vol. 16, no. 8, pp. 1957-1959, Aug. 2004.

[3] P. A. Yazaki, K. Komori, S. Arai, A. Endo, and Y. Suematsu, "Chirping compensation using a two-section semiconductor laser amplifier," J. Lightw. Technol., vol. 10, no. 9, pp. 1247-1255, Sep. 1992.

[4] J. M. Xie, S. Bouchoule, J-M Lourtioz, E. Brun and D. Lesterlin, "Chirp compensation in mode-locked DFB laser diodes with extended cavity," J. Lightw. Technol., vol. 14, no.2, pp. 179-187, Feb. 1996.

[5] R. Maher, K. Shi, P. M. Anandarajah, A. Kaszubowska, L. P. Barry and Y. L Yu, "Novel frequency chirp compensation scheme for directly modulated SG DBR tunable lasers," IEEE Photon. Technol. Lett., vol. 21, no. 5, pp. 340-342, Mar. 2009.

[6] J. M. Tang and K. A. Shore, "30Gb/s signal transmission over 40-km directly modulated DFB-laser-based single-mode-fiber links without optical amplification and dispersion compensation," J. Lightw. Technol., vol. 24, no. 6, pp. 2318-2327, June. 2006.

[7] J. L. Wei, C. Sánchez, R. P. Giddings, E. Hugues-Salas, and J. M. Tang, " Significant improvements in optical power budgets of real-time optical OFDM PON systems," Opt. Express., vol. 18, no. 20, pp. 20732-20745, Sep. 2010.

[8] X. Zheng, X. Q. Jin, R. P. Giddings, J. L. Wei, E. Hugues-Salas, Y. H. Hong and J. M. Tang, "Negative Power Penalties of Optical OFDM Signal Transmissions in Directly Modulated DFB Laser-Based IMDD Systems Incorporating Negative Dispersion Fibres", IEEE Photonics J., vol. 2, no.4, pp. 532-542, Aug. 2010.

[9] J. L. Wei, X. L. Yang, R. P. Giddings and J. M. Tang, "Colourless adaptively modulated optical OFDM transmitters using SOA as intensity modulator," Opt. Express., vol. 17, no. 11, pp. 9012-9027, May. 2009.

[10] J. M. Tang, P. M. Lane and K. A. Shore, "High-speed transmission of adaptively modulated optical OFDM signals over multimode fibres using directly modulated DFBs," J. Lightw. Technol., vol. 24, no. 1, pp. 429–441, Jan. 2006.

11 Conclusions and Future Work

11.1 Conclusions

With the exponentially increasing end-users' demands for broadband services and the availability of enormous transmission capacities in core networks, existing access networks have become critical bottlenecks for fully utilising the core network bandwidth to provide end-users with desired services. To address such a challenge, great effort has been expended on exploring various techniques to enable cost-effective, flexible and "future-proof" NG-PONs of >10Gb/s. Of those techniques, IMDD OOFDM is a very promising technical solution, due to its inherent and unique advantages including great potential for providing a cost-effective technical solution through fully exploiting the rapid advances in modern DSP technology, considerable reduction in optical network complexity owing to its excellent resistance to linear system impairments, adaptive and efficient utilization of channel spectral characteristics and hybrid dynamic allocation of broadband services among various end-users in both the frequency and time domains.

For practical implementation of IMDD OOFDM in NG-PONs, five technical challenges have to be solved successfully, which originate from inherent OFDM properties and/or IMDD system characteristics. The challenges include: i) insufficient utilization of MMF frequency responses beyond their basebands; ii) improvement in IMDD OOFDM transmission capacity in SMF-based systems; iii) simplification of OOFDM transceiver configurations; iv) the employment of low-cost transceiver components; v) effective compensation of DML-induced positive frequency chirps. These challenges raise significant barriers for practically realizing high-speed and cost-effective OOFDM NG-PON systems. Therefore, the PhD dissertation research work has been dedicated to addressing these challenging issues.

For fully utilizing the system frequency response of a MMF transmission link, an AMOOFDM-SCM has been proposed in Chapter 5, which consists of two AMOOFDM modems in parallel with one operating at the baseband and the other being modulated onto an intermediate RF carrier. Extensive investigations have shown that, compared to

AMOOFDM, AMOOFDM-SCM not only enhances the transmission capacity versus reach performance by a factor of approximately 2, but also considerably improves the system flexibility and performance robustness.

In Chapter 6, use has also been made of the AMOOFDM-SCM technique in SMF-based transmission links, the intermixing effect induced by direct detection in the receiver has been identified to be a dominant factor limiting the maximum achievable AMOOFDM-SCM performance. To maximize the link performance through mitigating the intermixing effect, three AMOOFDM-SCM modem designs of different complexity levels have been proposed by applying SSB modulation and/or spectral gapping in AMOOFDM-SCM. It has been shown that these AMOOFDM-SCM designs can support >60Gb/s signal transmission over at least 20km, which is >1.5 times higher than that supported by the AMOOFDM modems.

In the above-mentioned three AMOOFDM-SCM modems, two IFFT/FFT operations are required in the transmitter/receiver. To reduce the transceiver complexity and system cost, three simplified AMOOFDM-SCM modems have been proposed in Chapter 7, each of which requires a single IFFT/FFT operation. These designs not only significantly simplify the AMOOFDM-SCM modem configurations but also offer extra network features such as input/output reconfigurability without compromising the transmission performance.

To relax the requirements on parameters of key transceiver components such as DACs and ADCs, a reduction in PAPR associated with an OFDM signal is necessary. To achieve such an objective, in Chapter 8, AMOOFDM-PM has been proposed and theoretically explored in IMDD SMF systems. AMOOFDM-PM utilises an electrical OFDM signal to modulate the phase of a RF carrier prior to performing optical intensity modulation. Compared to AMOOFDM, AMOOFDM-PM can considerably reduce the PAPRs of OFDM signals and simultaneously lower the minimum requirements on quantization bits and sampling rates of DACs/ADCs.

To effectively compensate the DML frequency chirp effect, in Chapter 9, detailed investigations of dynamic negative power penalty characteristics of OOFDM signal transmission have been undertaken in DML-based IMDD systems incorporating MetroCor fibres with negative dispersion parameters. Excellent agreement between numerical simulations and real-time experimental measurements has been obtained over a wide

diversity of system conditions. The physical mechanism underpinning the occurrence of negative power penalties is the reduction in subcarrier intermixing impairments due to the compensation between DML positive frequency chirps and MetroCor negative chromatic dispersions. It has also been shown that the negative power penalty is independent of both cyclic prefix and signal modulation format, and, more importantly, controllable when adaptive modulation and/or appropriate adjustments of DML operating conditions are applied.

Finally, for effectively reducing the DML frequency chirp, in DML-based IMDD AMOOFDM PON systems, a simple and effective chirp compensation technique has also been proposed, which utilizes an electrical analogue circuit and an optical phase modulator. The electrical analogue circuit produces a phase signal mimicking the original phase of the DML-modulated optical signal, and the optical phase modulator driven by the generated phase signal compensates for the DML frequency chirp in the optical domain. It has been shown that, the technique can almost completely alleviate the DML frequency chirp effect and simultaneously improve the transmission capacity by approximately 25% for transmission distances in a range of 30-80km. In addition, the technique is also robust to variations in DML operating conditions.

11.2 Future Work

Although extensive research work have been undertaken in the thesis, a number of research topics related to OOFDM-PONs may still be worth exploring in the future. The research work is listed as follows:

1) Practical intensity modulator-enabled intensity modulation of AMOOFDM-SCM signals in SMF-based IMDD PON systems.

   AMOOFDM-SCM has been explored theoretically using ideal intensity modulators in SMF-based IMDD PON systems. In practice, a number of intensity modulators [1] such as SOA intensity modulators and MZMs can be utilized to modulate the AMOOFDM-SCM signals. As mentioned in Chapter 6 and 7, the SOA-based intensity modulator can offer sufficiently wide modulation bandwidth and relatively simplified modem design. In addition, it is also interesting to investigate MZM-enabled intensity modulation in

AMOOFDM-SCM. With the use of MZM, the input electrical signal can be almost linearly converted into optical intensity if the MZM is biased at a current identical to the quadrature point of the MZM [2]. However, nonlinear distortions of both the amplitude and phase of an optical field still exist for such intensity modulation [1], especially for cases where these modulators are not operating at their optimum conditions. Therefore, it is of great importance to identify optimum operating conditions of these intensity modulators to achieve the maximum transmission capacity of AMOOFDM-SCM signals. Furthermore, detailed comparisons can also be made between different intensity modulators in terms of achievable transmission capacity, and tolerance to operating condition variations.

2) AMOOFDM-SCM with PM.

For further reducing the system cost, use may be made of the proposed PM scheme in AMOOFDM-SCM. In such a modem, PM can be utilized in each AMOOFDM modem to offer further relaxed minimum requirements on DACs/ADCs without compromising the transmission performance. Another advantage of the modem is that PM can be implemented with FPGAs, thus the system simplicity can still be maintained.

3) Experimental demonstrations of end-to-end real-time AMOOFDM-SCM transmission in SMF-based IMDD PON systems.

Experimental demonstrations of end-to-end real-time AMOOFDM-SCM transmission are essential not only for evaluating the true potential of the proposed AMOOFDM-SCM technique, but also for identifying the limitations set by practical hardware. Given the fact that AMOOFDM-SCM can double the number of end-users without increasing the split ratio, the technique may offer an effective means of utilizing limited optical power budgets to support more end-users.

It should be noted that the above-mentioned AMOOFDM-SCM technique can also been practically implemented utilizing DMLs, as DMLs with modulation bandwidth as high as >40GHz have been reported [1]. However, at high signal bit rates, the DML frequency chirp effect is expected to be very strong. For mitigating the frequency chirp effect, the feasibility of using the approaches described in Chapter 10 can be explored.

In addition, for further enhancing the transmission capacity to > 100Gb/s, the number of SCM subcarriers in AMOOFDM-SCM may be increased to >4. Further investigations are necessary to solve new challenges associated with the approach. These challenges may include for example the requirements of intensity modulators having broad modulation bandwidths, system complexity and increased intermixing effects.

References

[1] G. P. Agrawal, *Fibre-Optic Communication Systems*, Wiley, 1997.

[2] W. Shieh, I. Djordjevic, *Orthogonal Frequency Division Multiplexing for Optical Communications*, Academic Press, Inc., 2010.

Appendix

Journal Publications

[1] X. Zheng, X. Q. Jin, R. P. Giddings, J. L. Wei, E. Hugues-Salas, *Y. H. Hong and J. M.* Tang, "Negative power penalties of optical OFDM signal transmissions in directly modulated DFB laser-based IMDD systems incorporating negative dispersion fibres," IEEE Photonics J., vol. 2, no. 4, pp. 532-542, Aug. 2010.

[2] X. Zheng, J. L. Wei and J. M. Tang, "Transmission performance of adaptively modulated optical OFDM modems using subcarrier modulation over SMF IMDD links for access and metropolitan area networks," Opt. Express., vol.16, no.25, pp. 20427-20440, Dec. 2008.

[3] X. Zheng, J. M. Tang and P. S. Spencer, "Transmission performance of adaptively modulated optical OFDM modems using subcarrier modulation over worst-case multimode fibre links," IEEE Comm. Lett., vol.12, no.10, pp. 788-790, Oct. 2008.

Conference Presentations

[1] X. Zheng and J.M. Tang, "Phase modulation enabled relaxation of DAC/ADC requirements and optical OFDM performance improvement over SMF-based IMDD systems," presented at ECOC, (Torino, Italy, 2010), Paper P3.08.

[2] X. Zheng, X.Q. Jin, R.P. Giddings, J.L. Wei, E. Hugues-Salas, Y. Hong and J.M. Tang, "Negative power penalty of optical OFDM signal transmission over directly modulated DFB laser-based IMDD systems incorporating negative dispersion fibres," presented in Photonics in Switching (PS) Topical Meeting, (Monterey, Florida, USA, 2010), Paper PWC3.

[3] X. Zheng, J.L. Wei, R.P. Giddings, and J. M. Tang, "Simple adaptively modulated optical OFDM modems using subcarrier modulation with input/output

reconfigurability," presented in Future Network and MobileSummit, (Florence, Italy, 2010), Paper 37.

[4] X. Zheng, J. L. Wei, X. L. Yang, R.P.Giddings, J. M. Tang and K.A.Shore, "Input/output reconfigurable adaptively modulated optical OFDM modems using subcarrier modulation," presented at OECC, (Hongkong, China, 2009), Paper ThLP2.

[5] X. Zheng and J.M. Tang, "Subcarrier modulation enabled improvement in the transmission performance of adaptively modulated optical OFDM signals over multimode fibre links," presented at the International Conference on Communication Technology (ICCT), (Hangzhou, China, 2008), Paper 789-792.

[6] X. Zheng and J.M. Tang, "Adaptively modulated optical OFDM modems using subcarrier modulation for multimode fiber-based transmission links," presented at the Semiconductor and Integrated Opto-Electronics Conf. (IEE/SIOE' 08), (Cardiff, U.K, 2008).

Journal Papers (co-authored)

[1] J. L. Wei, E. Hugues-Salas, R. P. Giddings, X. Q. Jin, X. Zheng, S. Mansoor and J. M. Tang, "Wavelength reused bidirectional transmission of adaptively modulated optical OFDM signals in WDM-PONs incorporating SOA and RSOA intensity modulators," Opt. Express., vol.18, no. 10, pp. 9791-9808, Apr. 2010.

[2] J. L. Wei, A. Hamié, R.P. Gidding, E. Hugues-Salas, X. Zheng, S. Mansoor, and J. M. Tang, "Adaptively modulated optical OFDM modems utilizing RSOAs as intensity modulators in IMDD SMF transmission systems," Opt. Express., vol. 18, no.8, pp. 8556-8573, Apr. 2010.

[3] E. Hugues-Salas, R.P. Giddings, X.Q. Jin, J. L. Wei, X. Zheng, Y. Hong, C. Shu and J.M. Tang, "Real-time experimental demonstration of low-cost VCSEL intensity-modulated 11.25Gb/s optical OFDM signal transmission over 25km PON systems," Opt. Express., vol. 19, no. 4, pp. 2979-2988, Feb. 2011.

Conference Papers (co-authored)

[1] J. L. Wei, E. Hugues-Salas, R. P. Giddings, X. Q. Jin, X. Zheng and J. M. Tang, "Wavelength reused bidirectional adaptively modulated optical OFDM transmission in colourless WDM-PONs," ECOC, (Torino, Italy, 2010), Paper P6.04.

[2] J. L. Wei, E. Hugues-Salas , R. P. Giddings, X. Q. Jin, X. Zheng, J. M. Tang, "Wavelength reused bidirectional transmission of adaptively modulated optical OFDM signals in SOA/RSOA intensity modulator-based WDM-PONs," Future Network and MobileSummit, (Florence, Italy, 2010), Paper 260.

Journal Papers submitted

[1] X. Zheng, C. Sánchez, B.Ortega and J. M. Tang, "Compensation of directly modulated DFB laser frequency chirps in optical OFDM IMDD PON systems," submitted to IEEE Photonics J.

[2] X. Zheng and J. M. Tang, "Phase modulation-enabled optical OFDM transmission performance improvement in IMDD SMF systems incorporating parameter-relaxed DACs/ADCs," submitted to J. Opt. Comm&Netw.

[3] X. Zheng, J. L. Wei, R. P. Giddings and J. M. Tang, "Simplified adaptively modulated optical OFDM modems using subcarrier modulation with added input/output Reconfigurability," submitted to IET Communications.